UNIVERSITÀ DEGLI STUDI DI TRIESTE

XXXV CICLO DEL DOTTORATO DI RICERCA IN

INGEGNERIA INDUSTRIALE E DELL'INFORMAZIONE

EXPERIMENTAL CHARACTERIZATION OF AN INNOVATIVE LOW ENVIRONMENTAL IMPACT POLYMERIC FUEL CELL ELECTRICAL POWER GENERATION PLANT FOR USE ONBOARD CRUISE SHIPS

Settore scientifico-disciplinare: ING-IND/09 SISTEMI PER L'ENERGIA E L'AMBIENTE

DOTTORANDO
ANDREA PIETRA

COORDINATORE DOTTORATO
PROF. ALBERTO TESSAROLO

SUPERVISORE DI TESI
PROF. RODOLFO TACCANI

CO-SUPERVISORE DI TESI
ING. ROBERTO PELASCHIAR

ANNO ACCADEMICO 2021/2022

UNIVERSITÀ DEGLI STUDI DI TRIESTE

UNIVERSITÀ DEGLI STUDI DI TRIESTE

XXXV CICLO DEL DOTTORATO DI RICERCA IN

INGEGNERIA INDUSTRIALE E DELL'INFORMAZIONE

EXPERIMENTAL CHARACTERIZATION OF AN INNOVATIVE LOW ENVIRONMENTAL IMPACT POLYMERIC FUEL CELL ELECTRICAL POWER GENERATION PLANT FOR USE ONBOARD CRUISE SHIPS

Settore scientifico-disciplinare: ING-IND/09 SISTEMI PER L'ENERGIA E L'AMBIENTE

DOTTORANDO
ANDREA PIETRA

COORDINATORE DOTTORATO
PROF. ALBERTO TESSAROLO

SUPERVISORE DI TESI
PROF. RODOLFO TACCANI

CO-SUPERVISORE DI TESI
ING. ROBERTO PELASCHIAR

ANNO ACCADEMICO 2021/2022

Author's Information

Andrea Pietra

Ph.D. Candidate at Università degli Studi di Trieste

Electrical Systems Senior Engineer at Fincantieri S.p.A.

Author's e-mail:

- Academic: *andrea.pietra@phd.units.it*
- Industrial: *andrea.pietra@fincantieri.it*

Author's address:

- *Academic:* Dipartimento di Ingegneria e Architettura, Università degli Studi di Trieste, Piazzale Europa, 1, 34127, Trieste, Italy
- *Industrial:* Fincantieri Merchant Ships Business Unit, Passeggio Sant'Andrea, 6/A, 34123 Trieste, Italy

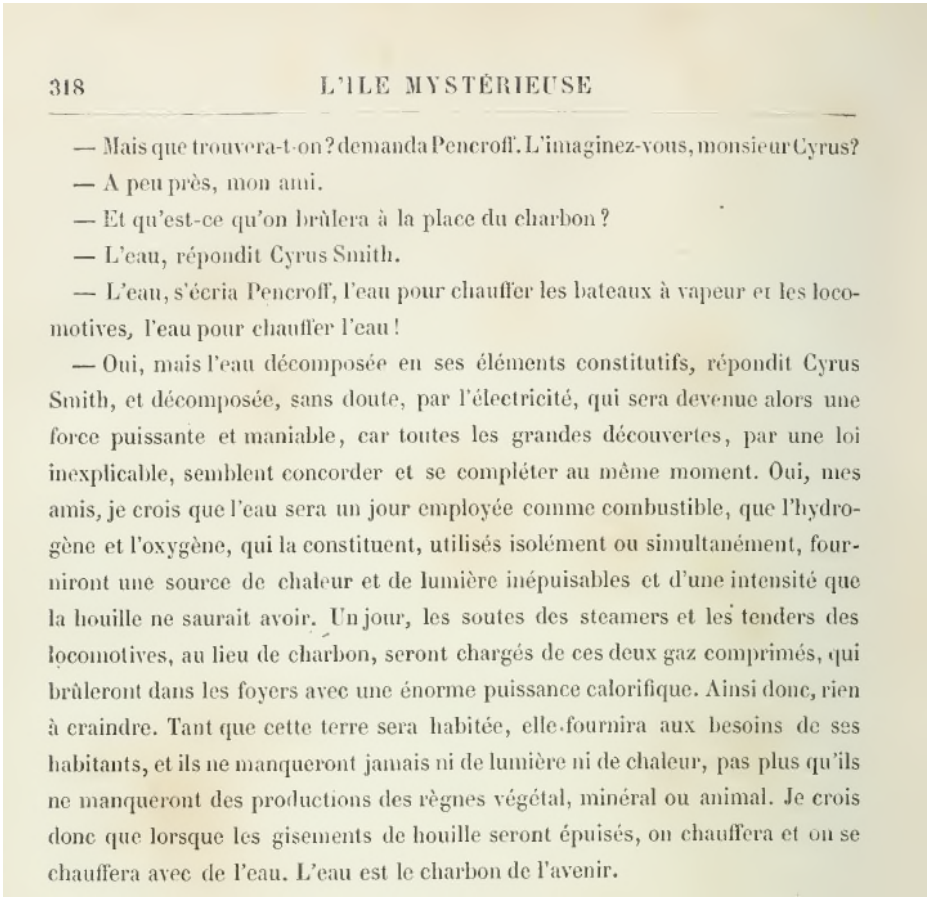

318 L'ILE MYSTÉRIEUSE

— Mais que trouvera-t-on ? demanda Pencroff. L'imaginez-vous, monsieur Cyrus?

— A peu près, mon ami.

— Et qu'est-ce qu'on brûlera à la place du charbon ?

— L'eau, répondit Cyrus Smith.

— L'eau, s'écria Pencroff, l'eau pour chauffer les bateaux à vapeur et les locomotives, l'eau pour chauffer l'eau !

— Oui, mais l'eau décomposée en ses éléments constitutifs, répondit Cyrus Smith, et décomposée, sans doute, par l'électricité, qui sera devenue alors une force puissante et maniable, car toutes les grandes découvertes, par une loi inexplicable, semblent concorder et se compléter au même moment. Oui, mes amis, je crois que l'eau sera un jour employée comme combustible, que l'hydrogène et l'oxygène, qui la constituent, utilisés isolément ou simultanément, fourniront une source de chaleur et de lumière inépuisables et d'une intensité que la houille ne saurait avoir. Un jour, les soutes des steamers et les tenders des locomotives, au lieu de charbon, seront chargés de ces deux gaz comprimés, qui brûleront dans les foyers avec une énorme puissance calorifique. Ainsi donc, rien à craindre. Tant que cette terre sera habitée, elle fournira aux besoins de ses habitants, et ils ne manqueront jamais ni de lumière ni de chaleur, pas plus qu'ils ne manqueront des productions des règnes végétal, minéral ou animal. Je crois donc que lorsque les gisements de houille seront épuisés, on chauffera et on se chauffera avec de l'eau. L'eau est le charbon de l'avenir.

"Yes, my friends, I believe that water will one day be used as fuel, that the hydrogen and oxygen which constitute it, used separately or simultaneously, will provide an inexhaustible source of heat and light of an intensity that coal cannot have. One day, the holds of steamers and the tenders of locomotives, instead of coal, will be charged with these two compressed gases, which will burn in hearths with an enormous calorific power. So, nothing to fear. As long as this earth is inhabited, it will supply the needs of its inhabitants, and they will never lack either light or heat, any more than they will lack the productions of the vegetable, mineral or animal kingdoms. I therefore believe that when the coal deposits are exhausted, we will heat, and we will heat ourselves with water. Water is the coal of the future."

L'ile Mistérieuse, Ch. XI

Jules Verne, 1875

Abstract

International maritime transport has a non-negligible impact on greenhouse gas emissions. It is in fact responsible for about 2-3 % of global greenhouse gas emissions and constitutes about 13% of the emissions due to transport in Europe. Only through the use of innovative high-efficiency technologies and the adoption of carbon-free alternative fuels will it be possible to progressively reduce greenhouse gas emissions from maritime transport to zero by the end of this century as imposed by the International Maritime Organization. This is especially true for the growing cruise ship market whose global CO_2 emissions increased by about 10% between 2013 and 2017.

In this context, this research project had the objective of verifying the suitability of hydrogen-powered polymeric fuel cells for use on board cruise ships through the development of an innovative generator for marine applications based on this technology and the experimental characterization of a prototype unit to evaluate its efficiency and define strategies to extend its lifetime.

The methodological approach adopted for the project involved the analysis of the state of the art of the application of polymeric fuel cells and hydrogen on board ships, the design and construction and experimental characterization of the performance of a land prototype and the installation and testing of the system on board an operational cruise ship.

The test rig developed for the research project consisted of two plants: one for the production of gaseous hydrogen by electrolysis and for its compression in a storage system at 200 bar g; the other for the production of electricity, consisting of a 100-kW polymeric fuel cell generator, a DC/AC converter including a supercapacitor energy storage system and a load bank.

The test rig also included the field instrumentation and the dedicated automation system for the characterization of the plants and of their components. Although difficulties have been encountered in identifying recognized international test standards, dedicated test procedures have been developed for both plants.

As regards the hydrogen production and compression system of the test rig, although the efficiency of the electrolyser was found to be in line with the data declared by the manufacturer and comparable with that of other commercial systems, the overall efficiency of the plant was found to be lower than expected due to the use of an air-driven hydrogen compressor which, while safer than conventional electrically-driven units, was inherently low-efficiency and unable to process the rated flow rate of the electrolyser.

Data from the experimental characterization of the test rig electric power plant demonstrated that the efficiency of the fuel cell generator developed for the research project is comparable to that of other heavy-duty commercial systems. Tests also showed that the dynamic performance of the system is enhanced by the supercapacitors included in the DC/AC converter which, at the same time, guarantee an immediate response to load variations and reduce the stress on the fuel cell generator by smoothening its response time.

The experimental activity made it possible to identify possible system improvements to be implemented on board (e.g., installation of a more efficient electrically driven hydrogen compressor) and optimal operating strategies for the system to increase its overall efficiency and extend its operational life.

The post-processed data was then used to complete the resolution of technical and regulatory issues related to the installation of the system on board a newly built cruise ship through the development of detailed HAZID, HAZOP and CFD studies.

The onboard system, the first ever of its kind to be installed aboard an operating cruise ship, was successfully commissioned in November 2022 to provide alternative power supply to houselighting dimmers serving the main public areas of the vessel.

Sommario

Il trasporto marittimo internazionale ha un impatto non trascurabile sulle emissioni di gas serra. È infatti responsabile di circa il 2-3% delle emissioni globali di gas serra e costituisce circa il 13% delle emissioni dovute ai trasporti in Europa. Solo attraverso l'utilizzo di tecnologie innovative ad alta efficienza e l'adozione di carburanti alternativi carbon free sarà possibile ridurre progressivamente a zero le emissioni di gas serra del trasporto marittimo entro la fine di questo secolo come imposto dall'Organizzazione Marittima Internazionale. Ciò è particolarmente vero per il crescente mercato delle navi da crociera le cui emissioni globali di CO2 sono aumentate di circa il 10% tra il 2013 e il 2017.

In questo contesto, questo progetto di ricerca ha avuto l'obiettivo di verificare l'idoneità di celle a combustibile polimeriche alimentate a idrogeno per l'utilizzo a bordo di navi da crociera attraverso lo sviluppo di un generatore innovativo per applicazioni marine basato su questa tecnologia e la caratterizzazione sperimentale di un'unità prototipale per valutarne l'efficienza e definire strategie per estenderne la durata.

L'approccio metodologico adottato per il progetto ha previsto l'analisi dello stato dell'arte dell'applicazione di celle a combustibile polimeriche e idrogeno a bordo delle navi, la progettazione e costruzione e caratterizzazione sperimentale delle prestazioni di un prototipo terrestre e l'installazione e collaudo del sistema a bordo di una nave da crociera operativa.

Il banco di prova sviluppato per il progetto di ricerca era costituito da due impianti: uno per la produzione di idrogeno gassoso per elettrolisi e per la sua compressione in un sistema di accumulo a 200 bar g; l'altro per la produzione di energia elettrica, costituito da un generatore a celle a combustibile polimeriche da 100 kW, un convertitore DC/AC comprendente un sistema di accumulo di energia a supercondensatori e un banco di carico.

Il banco prova comprendeva anche la strumentazione di campo e il sistema di automazione dedicato per la caratterizzazione degli impianti e dei loro componenti. Sebbene siano state incontrate difficoltà nell'individuare standard di prova internazionali riconosciuti, sono state sviluppate procedure di prova dedicate per entrambi gli impianti.

Per quanto riguarda il sistema di produzione e compressione idrogeno del banco prova, sebbene l'efficienza dell'elettrolizzatore sia risultata in linea con i dati dichiarati dal costruttore e comparabile con quella di altri sistemi commerciali, l'efficienza complessiva dell'impianto è risultata essere inferiore al previsto a causa dell'uso di un compressore di idrogeno azionato ad aria che, sebbene più sicuro delle unità convenzionali ad azionamento elettrico, era intrinsecamente a bassa efficienza e incapace di elaborare la portata nominale dell'elettrolizzatore.

I dati della caratterizzazione sperimentale della centrale elettrica del banco di prova hanno dimostrato che l'efficienza del generatore di celle a combustibile sviluppato per il progetto di ricerca è paragonabile a quella di altri sistemi commerciali pesanti. I test hanno inoltre dimostrato che le prestazioni dinamiche del sistema sono potenziate dai supercondensatori inclusi nel convertitore DC/AC che, allo stesso tempo, garantiscono una risposta immediata alle variazioni di carico e riducono lo stress sul generatore a celle a combustibile attenuandone il tempo di risposta.

L'attività sperimentale ha permesso di identificare possibili migliorie del sistema da implementare a bordo (es. installazione di un più efficiente compressore di idrogeno ad azionamento elettrico) e strategie operative ottimali per il sistema per aumentarne l'efficienza complessiva e prolungarne la vita operativa.

I dati post-elaborati sono stati poi utilizzati per completare la risoluzione dei problemi tecnici e normativi relativi all'installazione del sistema a bordo di una nave da crociera di nuova costruzione attraverso lo sviluppo di dettagliati studi HAZID, HAZOP e CFD. Il sistema di bordo, il primo in assoluto del suo genere ad essere installato a bordo di una nave da crociera in funzione, è stato messo in servizio con successo a novembre 2022 per fornire un'alimentazione alternativa ai dimmer luce delle principali aree pubbliche della nave.

Acknowledgments

In this section of my Ph.D. thesis, I would like to acknowledge some of the people, and institutions, who helped me in the preparation of this work, both directly and indirectly, with their priceless support and commitment.
I would first like to thank my academic, and industrial, supervisors. First of all, to Prof. Rodolfo Taccani of the University of Trieste, who supported me throughout the period of my doctoral studies, actively collaborating in the design, construction and characterization of the experimental power generation plant which is the subject of this work. My gratitude goes to him for having given me the opportunity to get in touch with the world of research, for having passed on to me part of his vast experience and technical knowledge, and for having guided me along my path with valuable advice.
Special thanks also go to Roberto Pelaschiar, a longtime friend and colleague from the Fincantieri electrical office, who agreed to accompany me on this journey as industrial supervisor, constituting not only my direct bureaucratic contact person in the company, but also and above all a reliable technical reference.
Heartfelt thanks also go to the management of the Merchant Ships Business Unit of Fincantieri for being the first to believe in me and in the validity of my research project, for sponsoring my doctorate and for having allocated the necessary fundings for the construction and characterization of the experimental plant.
Thanks to all the colleagues and technicians involved in the development of the test rig and in the installation and commissioning of the onboard demonstrator plant.
Thanks also to all the suppliers for the support and collaboration demonstrated in these years during which the project has evolved from experimental research on hydrogen and PEM fuel cells into the integration of the plant onboard a cruise ship. It has been an exciting and unrepeatable experience! Hopefully the first step of a long journey.
My gratitude also goes to all the authors and co-authors with whom I have had the privilege of collaborating over the years in drafting the articles and conference proceedings which have formed the heart and structure of this thesis.

Finally, I would like to express my appreciation and love to my wife, parents and friends for their support during my studies. Without their tremendous understanding and encouragement over the past few years, it would have been impossible for me to complete this work.

The author,

Andrea Pietra

Contents

Index of Figures

Index of Tables

Nomenclature

V – Volumetric flowrate (Nm^3/h); 128

Δg - Molar enthalpy ($kJ\ mol^{-1}$); 15

a – activity of a chemical species; 17

A – Area (m^2); 20

c – specific heat (kJ/(kg*k)]); 145

E - Cell open circuit voltage (V); 15

e - electron charge ($1.602176634\times10^{-19}$ C); 15

F - Faraday's constant ($96485.3321233100184\ C\cdot mol^{-1}$); 15

i – current flowing though the cell (A); 19

l – lenght (m); 20

N - Avogadro's number (6.022×10^{23}); 15

p – partial pressure; 17

P – Power (kW); 128

q – flowrate (m^3/s); 145

Q – Thermal energy (J); 145

R - Gas constant ($8.314\ JK^{-1}mol^{-1}$); 17

R – Resistance (Ω); 19

T – Absolute temperature (K); 16

t – time (s); 145

V – Voltage or voltage drop (V); 18

Ψ – specific membrane resistivity in open circuit at 30 °C; 20

Acronyms

ABS – American Bureau of Shipping; 60

AC – Alternating Current; 202

AEC – Alkaline Electrolyser Cell; 42

AFC - Alkaline Fuel Cell; 7

AIP - Air Independent Propulsion; 8

ANSI – American National Standards Institute; 201

API – American Petroleum Institute; 195

APU – Auxiliary Power System; 30

ARB - Air Resource Board (California); 2

ASME – American Society of Mechanical Engineers; 195

ATEX– ATmosphere EXplosibles (French Explosive Atmospheres); 200

AUV – Autonomous Underwater Vheicle; 23

BESS – Battery Energy Storage System; 175

BOL – Beginning Of Life; 77

BOP – Balance Of Plant; 77

BV – Bureau Veritas; 60

CCC – Subcommittee fro the Carriage of Cargo and Containers (IMO); 57

CFD – Computational Fluid Dynamics; 167

CGA – Compressed Gas Association; 199

CH_2 – Compressed Hydrogen; 47

CII - Carbon Intensity Indicator; 4

COVID-19 - Corona Virus Disease 2019; 8

CPL – Constant Power Load; 176

CT – Current Transformer; 93

CVM – Cell Voltage Monitoring; 81

DC – Direct Current; 43

DER – Distributed Energy Resources; 171

DG – Decentralized Generation; 171

DMFC - Direct Methanol Fuel Cell; 7

DNV - Det Norske Veritas; 7

ECA - Emission Control Area; 2

ECSA – Electro-Chemically active Surface Area; 156

EEDI - Energy Efficiency Design Index; 3

IPS – Integrated Power System; 174

IR – Infra Red; 36

IRENA – International Renewable energy Agency; 41

JAMSTEC – japan Agency for Marine-Earth Science and Technology; 26

JRC – Joint Research Centre (European Commission); 201

KR – Korean Register; 61

LEL – Lower Explosive Limit; 36

LFL – Lower Flammable limit; 35

LH_2 – Liquified Hydrogen; 47

LHV – Lower Heating Value; 21

LNG – Liquified Natural Gas; 4

LR – Lloyd's Register of Shipping; 61

LV – Low Voltage; 171

LVDC – Low Voltage Direct Current; 172

MARPOL - International Convention for the Prevention of Pollution from Ships; 1

MCFC - Molten Carbonate Fuel Cell; 7

MCR – Maximum Continuous Rating; 78

MEA – Membrane Electrode Assembly; 12

MEPC - Marine Environmental Protection Committe; 2

MSC – Maritime Safety Committe; 55

MVR – Marine Vessel Rules (ABS); 60

NASA - National Aeronautics and Space Administration (USA); 12

NFPA – National Fire Protection Association; 200

NK – Nippon Kaiji Kyokai; 53

OCV – Open Circuit Voltage; 15

OER – Oxygen Evolution Reaction; 43

PAFC - Phopshoric Acid Fuel Cell; 7

PC – Personal Computer; 108

PC – Power Converter; 176

PE - Polyethilene; 13

PEM – Proton Exchange Membrane; 7

PEMFC - Proton Exchange Membrane Fuel Cell; 7

PF – Power Factor; 98

PM - Particulate Matter; 2

PO – Partial Oxydation; 40

PT – Pressure Transmitter; 124

PTFE - Polytetrafluorethylene; 13

P-TR – Power TRansformer; 176

PWM – Pulse Width Modulation; 96

QSCS – Quality System Certification System; 60

Rd – Reading; 125

RES – Renewable Energy Source; 42

RINA – Italian Naval Register; 62

SAE – Society of Automotive Engineers; 51

SEEMP - Ship Energy Efficiency Management Plan; 3

SFOC – Specific Fuel Oil Consumption; 173

SMR – Steam Methane Reforming; 40

SOFC - Solid Oxide Fuel Cell; 7

SOLAS – International Convention for the Safety of Lifa at Sea; 55

SWIFT – Structured What If Technique; 166

SWOT – Strenght Weakness Opportunity and Threat; 43

TC – Technical Committe; 196

TEFC – Total Final Energy Consumption; 42

TEM - Transmission Electron Microscopy; 12

THDV – Total Harmonic Distortion in Voltage; 98

TT – Temperature Transmitter; 124

UEL – Upper explosive Limit; 36

UFL – Upper Flammable Limit; 35

UK - United Kingdom; 30

UN - United Nations; 1

USA - United States of America; 23

UUV – Unmanned Underwater Vehicle; 23

UV – Ultra Violet; 36

VAC – Voltage, Alternating Current; 68

VDC – Voltage, Direct Current; 79

VFD – Variable Frequency Drive; 82

ZEUS – Zero Emission Ultimate Ship; 32

Subscripts and Superscripts

0 - reference state (T=298.15 K, p=1 atm); 16

a – active; 20

act – activation; 18

act,a – activation, anode; 18

act,c – activation, cathode; 18

c – cathode; 19

cell – at cell level; 86

cold start – start without previous warning; 86

conc – concentration; 18

conc,a – concentration, anode; 18

conc,c – concentration, cathode; 18

dur – duration; 145

e - equivalent; 1

el – electrical; 128

el_gross – electrical system, gross; 143

el_net – electrical system, net; 143

elFC – fuel cell electrical output power; 142

elin – electrical in input; 143

elin – electrical, input; 128

elSYS – electrical system; 143

f - formation; 15

fc – fuel cell; 19

FC_gross – fuel cell, gross; 142

FC_net – fuel cell, net; 142

H_2 – relevant to hydrogen; 17

H_2O – relevant to water; 17

HR – heat recovered; 145

in – in input; 142

m – membrane; 19

O_2 – relevant to oxygen; 17

ohmic – related to ohmic dissipation; 18

p – protonic; 19

rated – rated value; 86

rev - reversible; 15

sat – saturation; 19

satate 1 – initial state; 86

satate 2 – final state; 86

stack – at stack level; 86

V – volumetric; 145

warm start – start with previous warming; 86

Greeek symbols

Δ - Variation; 15

η – efficiency; 21

ρ – density (kg/m3); 128

ρ – resistivity (Ωm); 20

List of Publications and Conferences

Peer-Reviewed Journal Articles

1. A. Pietra, M. Gianni, N. Zuliani, S. Malabotti and R. Taccani, "Experimental Characterization of an Alkaline Electrolyser and a Compression System for Hydrogen Production and Storage" in *Energies (https://doi.org/10.3390/en14175347), vol. 14, 2021.*

2. M. Gianni, A. Pietra, A. Coraddu and R. Taccani: "Impact of SOFC power generation plant on Carbon Intensity Index (CII) calculation for cruise ships" in *Journal of Marine Science and Engineering (https://doi.org/10.3390/jmse10101478) vol. 10, 2022.*

Submitted papers

3. Pietra A., Gianni M., Zuliani N., Malabotti S., Taccani R., "Experimental characterization of a PEM fuel cell for marine power generation" for *International Journal of Hydrogen Energy - Special Issue dedicated to EFC21.*

4. M. Luna, G. La Tona, A. Acceta, M. Pucci, A. Pietra, M.C. Di Piazza: "*Optimal Management of Battery and Fuel Cell-Based Decentralized Generation in Hybrid DC/AC Shipboard Microgrids*" for *IEEE Systems Journal.*

Conference Proceedings and Abstracts

5. G. Fiore, D. Negroni, T. Lamberti, P. Gualeni, L. Magistri, F. Silvestro and A. Pietra, "Distributed Energy Resources On-Board Cruise Ships: Integration into the Ship Design Process," in *Technology and Science for the Ships of the Future - Proceedings of NAV 2018: 19th International Conference on Ship & Maritime Technology, Trieste, 2018.*

6. A. Boveri, M. Maggioncalda, D. Rattazzi, P. Gualeni, P. Magistri, L. Magistri, F. Silvestro and A. Pietra, "Innovative Energy Systems: Motivations, Challenges and Possible Solutions in the Cruise Ship Arena," in *Technology and Science for the Ships of the Future - Proceedings of NAV 2018: 19th International Conferrence on Ship & Maritime Technology, Trieste, 2018.*

7. M. C. Di Piazza, M. Luna, G. La Tona, A. Accetta, M. Pucci and A. Pietra, "A mixed DC/AC low voltage electrical distribution architecture for increasing payload on ships." in *Technology and Science for the Ships of the Future - Proceedings of NAV 2018: 19th International Conferrence on Ship & Maritime Technology, Trieste, 2018.*

8. R. Taccani, F. Ustolin, N. Zuliani, S. Pinamonti and A. Pietra, "Fuel Cells and Shipping Emissions Mitigation," in *Technology and Science for the Ships of the Future - Proceedings of NAV 2018: 19th International Conference on Ship & Maritime Research, Trieste, DOI:10.3233/978-1-61499-870-9-885, 2018.*

9. V. Bucci, U. La Monaca, D. Bosich, G. Sulligoi and A. Pietra, "Integrated Ship Design and CSI Modeling: a New Methodology for Comparing Onboard Electrical Distributions in the Early-Stage Design" in *Technology and Science for the Ships of the Future - Proceedings of*

NAV 2018: 19th International Conference on Ship & Maritime Research, Trieste, DOI:10.3233/978-1-61499-870-9-124, 2018

10. M. C. Di Piazza, M. Luna, G. La Tona, A. Pucci and A. Pietra, "A New Method for Selecting the Voltage Level for an Advantageous Transition to DC Distrbution in Ships," in *IEEE International Conference on Electrical Systems for Aircraft, Railway, Ship Propulsion and Road Vehicles & International Transportation Electrification Conference (ESARS-ITEC) (https://doi.org/10.1109/ESARS-ITEC.2018.8607438), Nottingham, UK, 2018.*

11. M. Pucci, A. Accetta, M. C. Di Piazza, M. Luna, G. La Tona and A. Pietra, "Electric Ship Propulsion Improvement by Increasing Efficiency of Adjustable-Speed Motor Drives," in *IEEE International Conference on Environment and Electrical Engineering and 2018 IEEE Industrial and Commercial Power Systems Europe (EEEIC / I&CPS Europe) (DOI: 10.1109/EEEIC.2018.8494207), Palermo, Italy, 2018.*

12. G. La Tona, M. Luna, M. C. Di Piazza and A. Pietra, "Energy Management System for Efficiency Increase in Cruise Ship Microgrids," in *IECON 2019 - 45th Annual Conference of the IEEE Industrial Electronics Society (DOI: 10.1109/IECON.2019.8927314), Lisbon, Portugal, 2019.*

13. M. Gianni, A. Pietra e R. Taccani, "Outlook of future implementation of PEMFC and SOFC onboard cruise ships" in *E3S Web of Conference 238, DOI: 10.1051/e3sconf/202123804004, 2021.*

14. M. C. Di Piazza, M. Luna, G. La Tona, A. Accetta, M. Pucci and A. Pietra, "Shipboard microgrids: comparison of solutions based on LVDC distribution on cruise ships," in *2021 IEEE International Conference on Environment and Electrical Engineering and 2021 IEEE Industrial and Commercial Power Systems Europe (EEEIC / I&CPS Europe), Bari (doi: 10.1109/EEEIC/ICPSEurope51590.2021.9584742), 2021.*

15. A. Pietra, M. Gianni, Z. Nicola e S. Malabotti, "Experimental characterization of a PEM fuel cell for marine power generation" in *ES3 Web Conf. Volume 334 EFC21-European Fuel Cells and Hydrogen Piero Lunghi Conference, DOI: 10.1051/e3sconf/202233405002, 2022*

16. *Roberta R., Micoli L., Coppola T., Pietra A* "Computer simulation of an integrated Solid Oxide Fuel Cell-Heat Recovery System on board a cruise ship" Accepted Abstract for *ICHEAP16 Conference* (*16th International Conference on CHEmical And Process engineering), 21-24 May 2023, Naples, Italy.*

1 Background and motivations

Ships are one of the oldest means of transportation for goods and passengers, as they contributed during history to migrations, commerce, research, defense and humanitarian purposes.
From their beginnings until the 19th century, ships were clean means of transport whose means of propulsion were essentially oars and sails. Only in recent times engines and turbines powered by non-renewable fuels become the most common power generators on-board [1].
Thanks to the technological and engineering progress that has improved the safety and reliability of ships, over the centuries the maritime sector has progressively established itself above all the others to become the backbone of world trade. Today ships do not only handle 80 per cent of global trade by volume, but also provide livelihoods for a wide range of businesses in nearly worldwide [2].
Ships also carry a very significant passenger number on ferries and cruise ships.
The cruise industry started as a niche sector in the early 1970s and has grown significantly since the 1990s. Currently, the cruise industry unquestionably plays a role of primary importance for the tourism industry and has a great influence as a world economic factor. Today the cruise industry represents an excellent example of globalization with new cruise ports distributed all over the world and with passengers from every continent [3].
Over the years, the size and carrying capacity of cruise ships have also progressively increased to exceed 6,000 passengers and nearly 3,000 crew members [4]. This negatively impacted both energy consumption and the carbon footprint of cruise ships.
In 2016 and 2017, for example, two of the largest cruise companies self-reported their carbon emissions. Published data shows that, on average, cruise companies' carbon emissions are continuing to grow steadily with increases of just over 1% per year [3].
Shipping has therefore become one of the sectors responsible for atmospheric pollution along with air, road and rail transport. While shipping is one of the most carbon-efficient transportation systems and although the efficiencies of cruise vessels are still better than decades back, global ship-related pollution has grown rapidly.
The entire transport sector as a whole is currently responsible for 14% of global CO_2e (carbon dioxide equivalent) emissions and, according to the International Maritime Organization (IMO) in 2012, shipping was responsible for about 2.1% of global CO_2e emissions, with approximately 961 million tons of CO_2e released into the atmosphere. Ship emissions were also responsible for an annual average of 15% of global NOx emissions (20.9 million tons) and 13% of global SOx emissions (11.3 million tons) in the 2007-2012 period [1].
In 2015, shipping was responsible for almost 13 % of the total GreenHouse Gases (GHG) emission from transportation in the European Union (EU). According to the fourth IMO GHG Study (2020), emissions have increased of almost 10 % between 2012 and 2018 as a result of the growth in shipping activities. The study also highlights a sharp increase in short-lived climate pollutants, like methane and black carbon. In the next years, shipping is expected to grow and thus its emissions are expected to increase up to 50% by 2050 if no proactive actions will be put in place [5].
The IMO as the supreme council established within the United Nations (UN) responsible for international shipping activities and the prevention of environmental pollution from ships, aims to control maritime activities and keep related environmental pollution ships at standard levels by regularly publishing and updating the relevant regulations to be followed by all Member States.
To prevent the increase in ship emissions and their environmental impact in the future, on 2 November 1973 adopted the first International Convention for the Prevention of Pollution from Ships (MARPOL). Over the years, the text of the original MARPOL Convention has been modified and updated with dedicated Annexes including requirements related to pollution by oil (Annex I), noxious liquid substances in bulk (Annex II), harmful substances carried by sea in packaged form (Annex III), sewage (Annex IV), garbage (Annex V) and finally, with the introduction of Annex VI adopted in

1997, dedicated to atmospheric pollution and emissions from ships. MARPOL Annex VI entered into force on 19 May 2005 [6]. In October 2008, the Marine Environment Protection Committee (MEPC) of the IMO adopted amendments to Annex VI. which entered into force on 1 July 2010. The amendments included significant and progressive limits for Sulfur Oxide (SOx) and Nitrogen Oxide (NOx) emissions from marine engines and for the first time addressed emissions of Particulate Matter (PM).
These limits have become stricter over the years, leading to the introduction of the mandatory global limit of 0.5% (mass on mass) content of SOx in marine fuels starting from 1 January 2020 [1].
The 2008 amendments introduced also two sets of emission and fuel quality requirements: global requirements, and more stringent requirements for SOx and PM, or NOx, or all three types of emissions applicable to ships in specific Emission Control Areas (ECA).
Curently IMO ECA include:

- Baltic Sea (SOx: adopted 1997/entered into force 2005; NOx: 2016/2021);
- North Sea (SOx: 2005/2006; NOx: 2016/2021);
- North America, including most of US and Canadian coast (NOx & SOx: 2010/2012);
- US Caribbean, including Puerto Rico and US Virgin Islands (NOx & SOx: 2011/2014) [7].

In addition to the IMO fuel quality requirements, regional and local regulations have been adopted by the EU, Hong Kong, China and California for seagoing ships. Regarding the European Union, the Sulfur Directive provides for a maximum sulfur content of 0.5% for ships in all EU waters from 1 January 2020 and a limit of 0.1% in ports. Hong Kong currently has a 0.5% sulfur content limit for berthed ships. China, on the other hand, has recently issued regulations requiring a maximum sulfur content of 0.5% in fuel in coastal selected areas. The Air Resources Board (ARB) of California instead introduced a limit of 0.1% on the sulfur content used within 24 nautical miles from the coast. Additional restrictions are also imposed in the EU and California in the use of scrubbers or in the discharge of scrubber water [8].

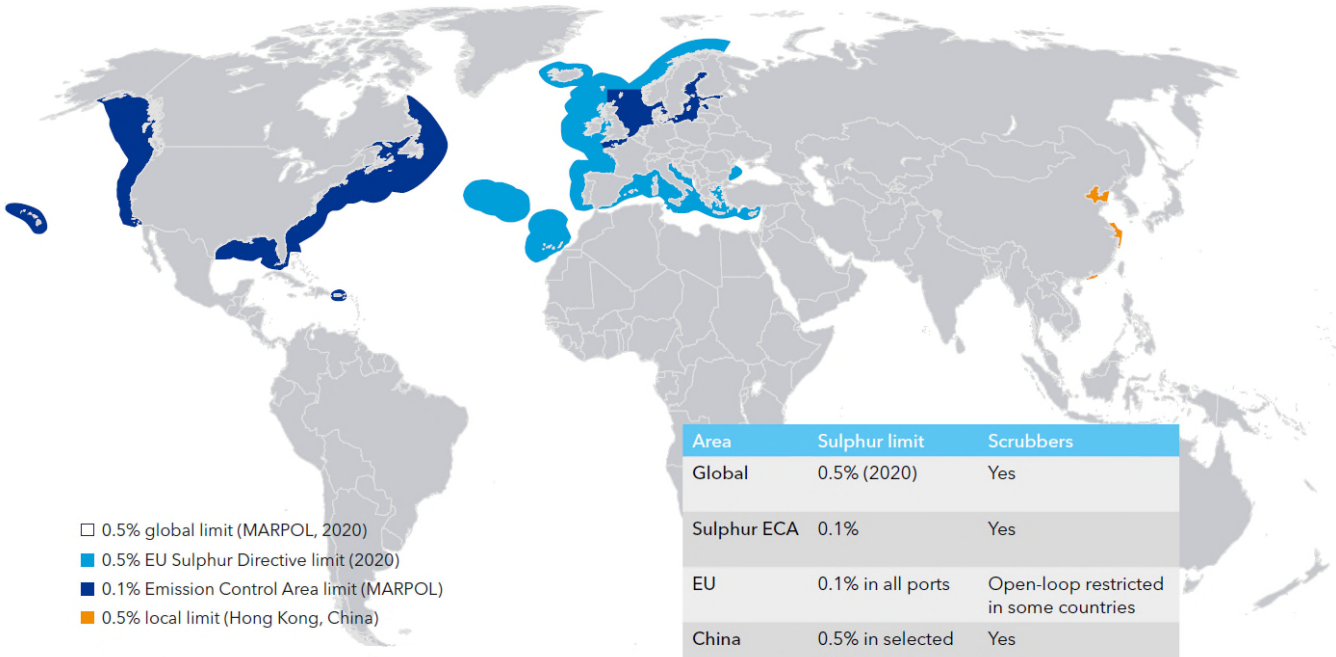

Area	Sulphur limit	Scrubbers
Global	0.5% (2020)	Yes
Sulphur ECA	0.1%	Yes
EU	0.1% in all ports	Open-loop restricted in some countries
China	0.5% in selected areas	Yes
California	0.1% within 24 nm	No, only through research exemption

Figure 1. Map of established Emission Control Areas (ECAs) [8].

In the 62nd MEPC meeting (2011), the IMO further amended the MARPOL Annex VI making it mandatory the calculation of Energy Efficiency Design Index (EEDI) for new ships as well as the adoption of the Ship Energy Efficiency Management Plan (SEEMP) for all ships. The amendment entered into force on 1 January 2013 for ships weighing 400 GT [9].
The EEDI is a performance-based mechanism that requires newly built ships to emit less CO_2 per unit of "transport work", typically expressed in grams of carbon dioxide (CO_2) per tonne mile: the smaller the EEDI, the higher the energy efficiency the ship's design is. For a given ship, the EEDI is calculated using a formula based on technical design parameters, which can be freely chosen by ship designers and shipbuilders. After a preliminary phase (phase 0, 2013-2014) in which the ships were encouraged to start implementation of EE measures, the introduction of the EEDI required ships built between 2015 and 2019 (phase 1) to be 10% above the average efficiency of ships built between 2000 and 2010 taken as the baseline. For ships built between 2020 and 2024 (phase 2), the efficiency gain over the baseline must be 20%. For ships built from 2025 onwards (phase 3) it is mandatory that they are 30% more efficient than the baseline. [7].

Figure 2. EEDI phases, implementation periods and reduction targets [10].

The SEEMP, on the other hand, consists of a set of operational measures aimed at improving the energy efficiency of a ship in a cost-effective way. The SEEMP also provides shipping companies with an approach to increase the efficiency of ships and their fleet over time using (on a voluntary basis) appropriate monitoring tools such as the Energy Efficiency Operational Indicator (EEOI).
The EEOI allows operators to calculate the fuel consumption of a ship in service and to evaluate the effect of any changes aimed at optimizing efficiency and performance, such as the adoption of different cruise profiles, the reduction of the cleaning intervals of the propellers and the hull, the introduction of energy efficiency systems such as recovery plants residual heat or high-performance propellers [11].

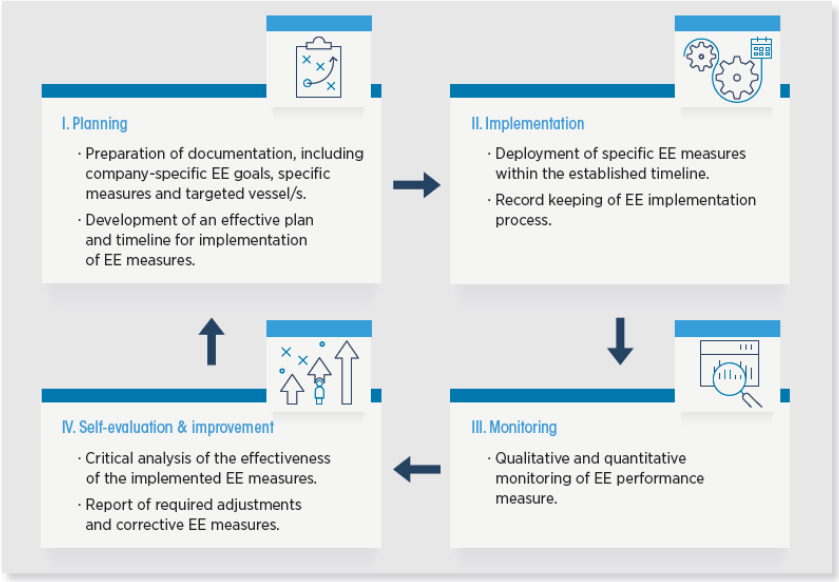

Figure 3. SEEMP cyclical process [10].

At the 70th meeting of the MEPC (2016), a plan was then approved for the development of a roadmap for the implementation by 2023 of a global strategy for the reduction of GHG emissions from ships. The roadmap included short, medium and long-term measures.
At the 72nd meeting of the MEPC (April 2018) the first phase of the planned GHG doadmap was officially approved as an initial strategy of the IMO for the reduction of greenhouse gases from ships and follow-up programs for the implementation of the subsequent phases were organized during the 73rd MEPC meeting (October 2018) [9].
Taking as a reference the average emissions per "transport work" in 2008, the initial strategy outlined by the IMO aims to reduce them by 40% by 2030 and by at least 70% by 2050. In terms of total annual GHG emissions the strategy aims to reduce them by at least 50% by 2050 cmpared to the 2008 values taken as reference and to achieve zero emissions from shipping as soon as possible by the end of the century. The strategy is outlined in Figure 4, where "Total" refers to the absolute amount of GHG emissions from international shipping and "Intensity" indicates the amount of carbon dioxide (CO_2) emitted per tonne-mile.

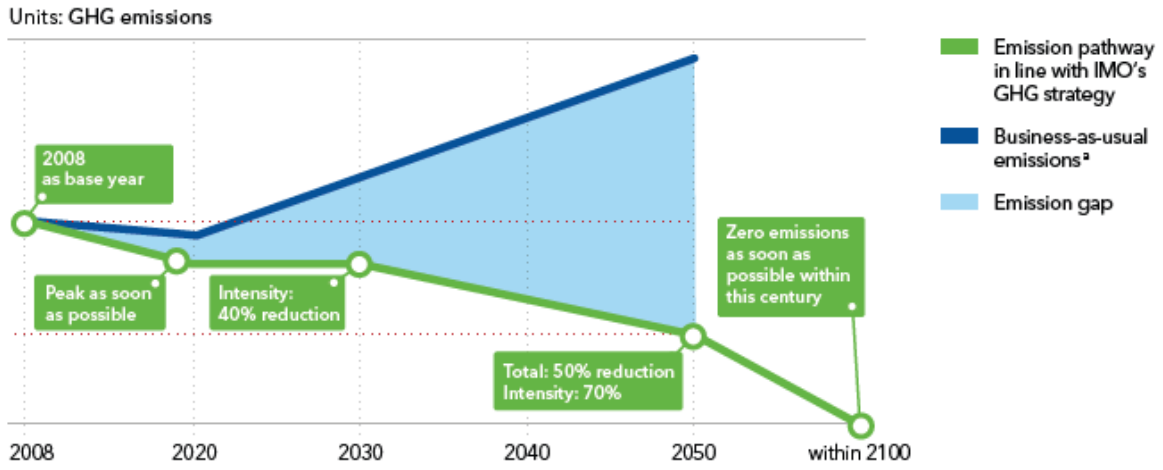

Figure 4. IMO GHG reduction strategy [12].

In the 76th MEPC meeting (June 2021), a new annual performance index was proposed for discussion: the Carbon Intensity Indicator (CII).
According to this proposal, starting from 2023, the CII requirements will take effect for all bulk carriers, gas carriers, tankers, container ships, general cargo ships, refrigerated cargo carriers, combination carriers, Liqified Natural Gas (LNG) carriers, vehicle carriers, Ro-Ro cargo vessels, Ro-Ro passenger vessels and cruise ships above 5,000 Gross Tonnage (GT) and trading internationally. This factor measures how efficiently a ship transports goods or passengers and is given in grams of CO_2 emitted per cargo-carrying capacity and nautical mile on an annual basis [13]. At the moment only the basic calculation method of the annual CII has been developed at MEPC 76. The calculation will be further improved through the adoption of correction factors that will be developed in a separate guideline.

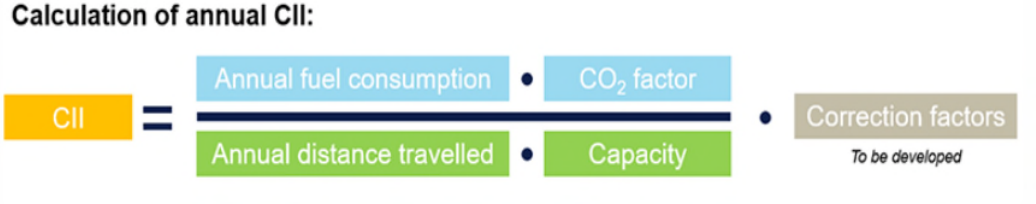

Figure 5. Basic calculation of the annual CII [14].

Based on this indicator, the ships will then receive an assessment of their energy efficiency (A, B, C, D, E - where A is the best), which will be incorporated into their Declaration of Conformity. The rating is assigned based on to the ratio between the attained CII and the required CII: the higher is this ratio, the worse the rating The rating thresholds will become increasingly stringent towards 2030. In case a ship is rated D for three consecutive years or achives an E rating in a single year would have to submit a corrective action plan needs to be developed as part of the SEEMP, to show how the required index (C or above) would be achieved. This need to be included and submitted within one month after reporting the CII [15].
Over the past decade, shipping has become more energy efficient, so total emissions have grown more slowly than the increase in total number of ships, as illustrated by Figure 6 showing the trend in total monthly CO_2 emissions (in million tonnes) by ship type between January 2011 and April 2021 [16].

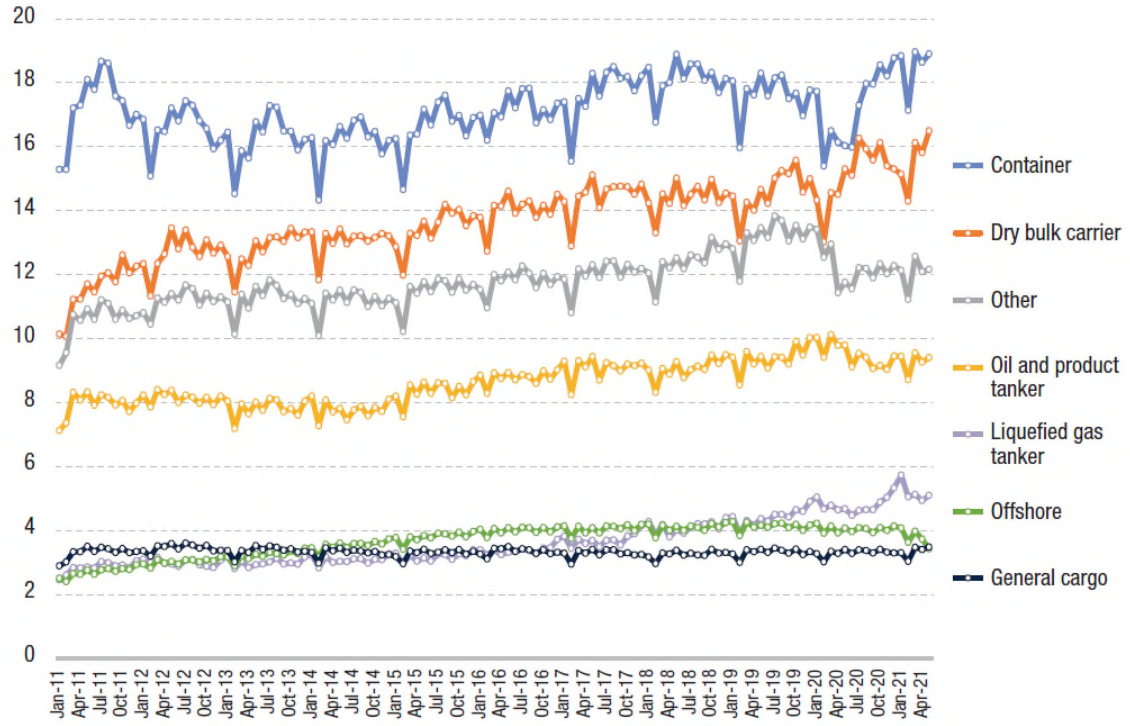

Figure 6. Monthly carbon dioxide emissions by ship type (2011-2021) [16].

However, sector studies show that what has been done to date in shipping in terms of improving efficiency and reducing GHG emissions is still not enough to achieve the objectives set by the IMO strategy [16].
In this context, innovative technologies and carbon-free fuels and efficiency gains will therefore play a key role in the future of the maritime sectoras can be observed in the scheme proposed in

Figure 7 which shows that future carbon-free energy carriers and related enabling technologies represent one of the solutions with the greatest potential for reducing emissions.

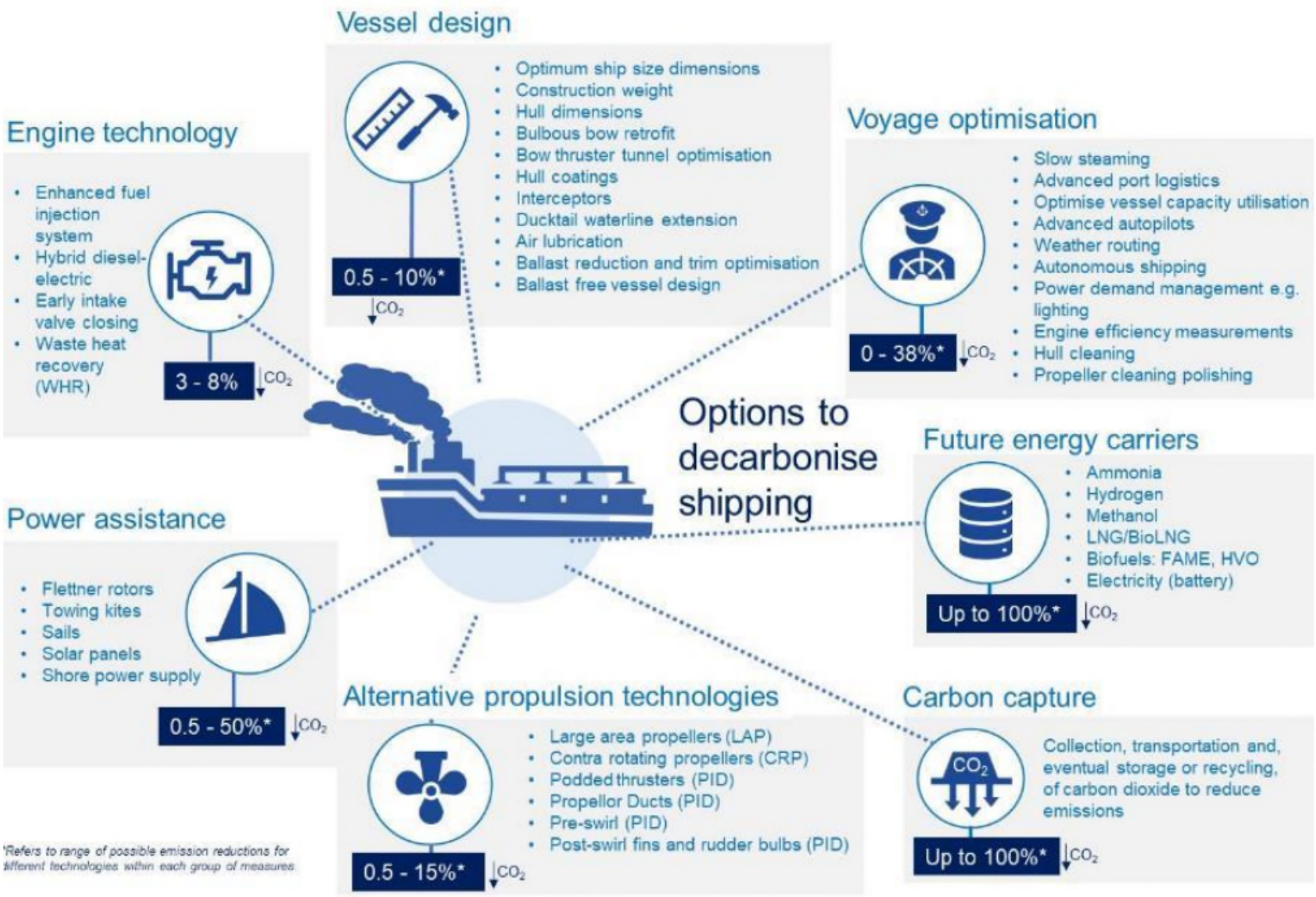

Figure 7. Strategies toreduce fuel consumption and emissions in the marine sector [17].

2 Research Question

Among the potential alternative fuels for the maritime sector in line with the IMO emission reduction strategy, hydrogen (H_2) is one of the most promising in the long term [10].
Like electricity, hydrogen is in fact a carbon-free energy vector. This means that there is no release of CO_2 when hydrogen is burned in Internal Combustion Engines (ICEs) for the production of mechanical power, or electrochemically converted in Fuel Cells (FCs) for the production of electricity [18].
The use of H_2 for powering ICEs is today a less mature technology than FCs and the introduction of hydrogen ICEs in series production has not yet begun. Furthermore, H_2 as a fuel is more efficient when used in FCs. Depending on their technology, FC generators have an average efficiency between 50% and 60%. The FCs operating at high temperatures, in particular, can reach an overall efficiency (electrical plus thermal) of 85% if coupled to heat recovery systems. The use of H_2 in modified ICEs, on the other hand, allows to reach efficiency levels between 40% and 50%. Like conventional ICEs, FC generators are modular by nature, but they are more felxible and can be more easily scaled up or down according to the energy demand.
Currently, H_2 FC has been mainly intended for land transport and the transport sector, both private and public, mainly by car, bus and train. In the shipping sector, on the other hand, the introduction of FCs is still very limited despite various initiatives being developed both directly by shipbuilders and through nationally and internationally funded programs [10]. In 2017 the DNV-GL carried out for the European Maritime Safety Agency (EMSA) a technical assessment on the state of the art of Fuel Cell technology oriented to their specific application in shipping. In the study, the different Fuel Cell technologies were classified on the basis of 11 attributes.

Technology/ Attributes	Relative cost	Module kW levels	Lifetime	Tolerance for cycling	Fuel	Maturity	Size	Sensitivity to fuel impurities	Emissions	Safety Aspects	Efficiency	Total
Weighting	3	2	3	2	3	3	3	3	2	3	3	
Alkaline fuel cell	3	3	2	3	1	2	2	1	3	3	2	
(AFC)	9	6	6	6	3	6	6	3	6	9	6	66
Phosphoric acid fuel cell	2	3	3	2	2	2	1	2	3	2	2	
(PAFC)	6	6	9	4	6	6	3	6	6	6	6	64
Molten carbonate fuel cell	1	3	3	1	3	3	1	3	1	2	3	
(MCFC)	3	6	9	2	9	9	3	9	2	6	9	67
Solid oxide fuel cell	1	3	2	1	3	3	2	3	2	2	3	
(SOFC)	3	6	6	2	9	9	6	9	4	6	9	69
Proton Exchange Membrane	3	3	2	3	1	3	3	2	3	3	2	
(PEMFC)	9	6	6	6	3	9	9	6	6	9	6	75
High Temperature PEMFC	2	2	2	3	2	2	3	3	3	2	3	
(HT-PEMFC)	6	4	6	6	6	6	9	9	6	6	9	73
Direct methanol fuel cell	2	1	2	3	3	1	2	3	1	3	1	
(DMFC)	6	2	6	6	9	3	6	9	2	9	3	61

Table 1. Fuel Cell for shipping application technology rating [19].

In the scoring a weighting and a ranking were used, both based on a scale from 1 to 3 in ascending order of importance.The Proton Exchange Membrane Fuel Cell (PEMFC) was the technology receiving the highest score, followed by the High Temperature PEMFC and the Solid Oxide Fuel Cell (SOFC) [19].
PEMFC generators require high purity hydrogen as a fuel and therefore PEM technology can be considered a key enabling technology for carbon-free fuels. In recent years there have been some niche

applications of PEM fuel cells in the maritime sector, mainly as an underwater air independent propulsion system (AIP) or small demonstration projects, but none have yet been specifically developed for the maritime sector with the most promising growth projections: that of cruise ships [5]. Worldwide, the cruise ship industry experienced an annual passenger growth rate of 6.6% from 1990 to 2019. Although COVID-19 halted the ocean-going passenger cruise industry for about 11 months, the number passenger numbers quickly returned to growth in 2021. It therefore seems quite unlikely that the pandemic will have a permanent impact on the industry's growth projections for the coming decades [20].

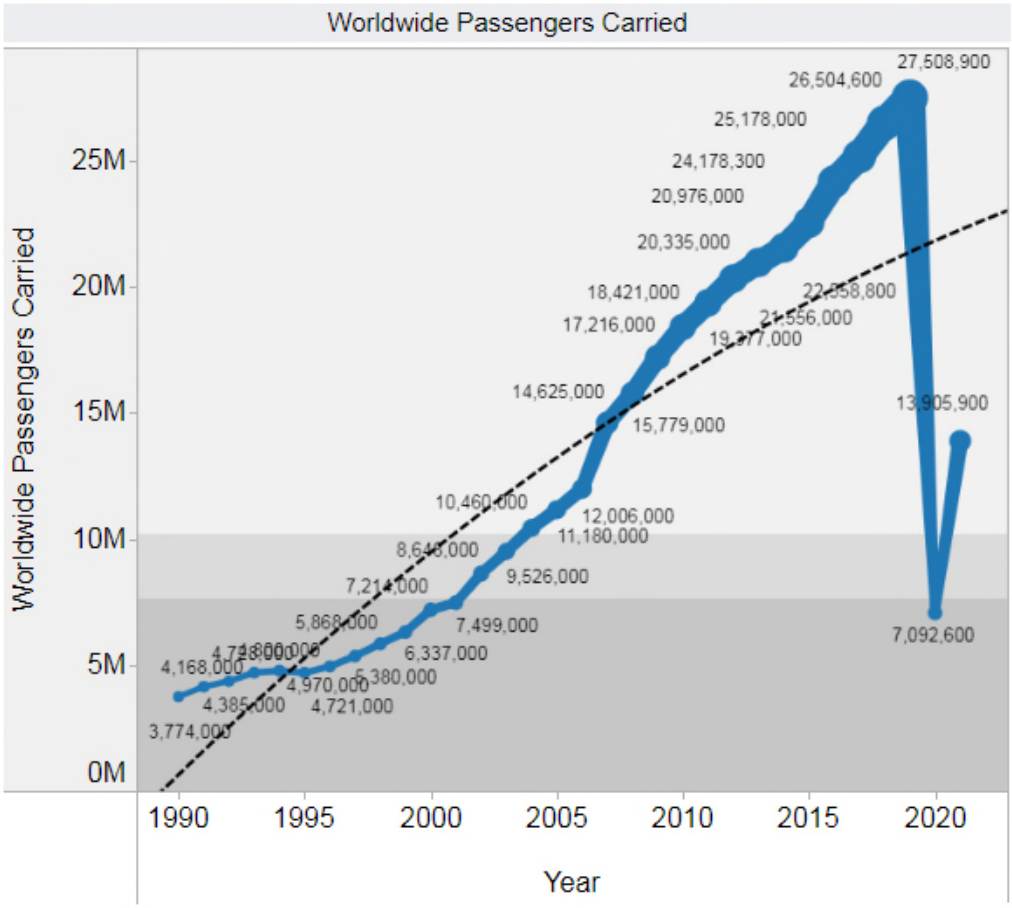

Figure 8. The worldwide development of cruise passenger numbers between 1990 and 2021 [20].

In this context, the research question of the proposed doctoral work can be summarized as follows:

- **Are PEMFCs and hydrogen suitable for use onboard cruise ships?**

The question was addressed through an experimental approach, with the aim of investigating and identifying which are the main problems and the real prospects for the use of hydrogen-fed PEMFC generators on board cruise ships. Specifically, the answer has been investigated trough:

- The developement of an innovative PEMFC generator for marine aplication integrating automation and control systems;
- The identification of a strategy for the use of the generator on board the ship despite the absence of rules and regulations for the use of hydrogen on board ships;
- The experimental characterization of a prototype plant for assessing efficiency and lifetime improvement strategies.

3 Methodology

This section provides a general overview of the contents of the thesis and of the applied methodology applied.
The core of this thesis is contained in the following six main sections which are in turn divided into various sub-parts.
Section four is completely dedicated to PEMFC cell technology and, after illustrating its operating principles, provides a detailed overview of the studies and application experiences of this technology in the maritime sector both on submarines and on surface ships. The section concludes with an analysis of hydrogen as a viable alternative fuel for shipping by highlighting its properties, dangers, advantages and disadvantages compared to other alternative fuels and by assessing the state of the art of its production and storage methods. The section was developed through the analysis of the literature and the consultation of texts, technical articles, scientific journals and websites.
Section five presents an overview of the main regulations, standards and guidelines related to the use of fuel cells and hydrogen on board ships. For the development of this section, the most relevant IMO conventions for the use of hydrogen on board ships were first analyzed and, subsequently, the regulations already in force or under development by the classification societies belonging to the International Association of Classification Societies (IACS) were presented. An examination of the main international standards on hydrogen and fuel cells that could provide useful insights for the development of the regulatory framework for their future use on board ships has been developed through an in-depth analysis of specialist literature and included in Annex A.
Sections six, seven and eight constitute the "heart" of the thesis and summarize the design, testing, installation, and experimental characterization activities of the innovative PEMFC generator for marine applications which integrates an automation and control systems developed for this research project. After a descriptive section in which the P&I diagrams of the experimental bench and the technical specifications of its main components and dedicated automation system are presented, the next two sections illustrate and describe in detail the methodologies, tools, tests and results obtained during the experimental activities.
The development of these three sections was based on the use of all the published material during the research project in the form of journal articles, papers and/or conference proceedings and of the technical documentation accompanying the main components of the experimental plant.
Section nine of this work is divided into two parts: in the first, the design and evaluation activities which were carried out in parallel with the experimental laboratory activities and which allowed the installation of the experimental plant as a demonstrator on aboard an operational cruise ship. In the second, on the other hand, some prospects for the future use of PEM cells and hydrogen on board cruise ships are presented through the examination of a case study.
For the development of this last section, part of the documents used in the design of the demonstrator and the reports of the HAZID, HAZOP and CFD studies developed for the on-board installation were used. As far as the last part is concerned, the case study, the analysis and the results presented were taken from publications presented over the years in the form of conference proceedings.

4 Technology Background

This section is divided into four parts. The first aims to provide a general overview of PEMFC technology. Specific technical details will then be inserted, where required, in the subsequent sections of the document. In the second part, the state of the art of the application of the technology in the maritime sector is presented.
The third part provides an overview of the regulatory framework relating to the use of fuel cells and hydrogen on board ships and the applicable reference standards for the characterization of this type of plant.
The last part is finally dedicated to hydrogen. In this last part, the main chemical-physical characteristics of the element are recalled, and an overview of the technologies used for its industrial production is provided.

4.1 PEMFC technology

PEMFCs, like all fuel cells, are electrochemical conversion devices that generate electricity, pure water and heat by combining a fuel (hydrogen) and an oxidant (oxygen from air), in the absence of combustion.
The schematic structure of a typical PEM cell, with indication of the reagent flows, of the basic chemical reactions and of the electrical charges moved internally and externally to it, is shown in Figure 9.

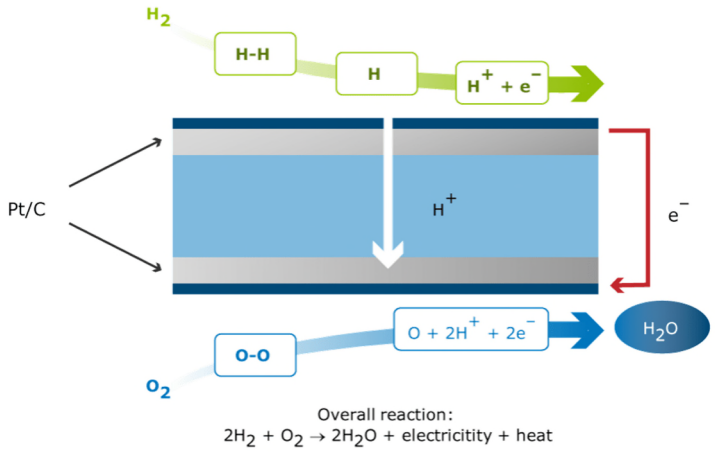

Figure 9. PEMFC working principles [21].

In the figure the blue layers are the Gas Diffusion Layers (GDLs). The GDLs are one of the critical components of a PEMFC as they perform some of the essential functions for its operation. The GDS, in fact:

- evenly distribute the reactant gases on both sides of the cell;
- drain the liquid water produced during the operation of the cell;
- ensure a low resistance conductive path for electrons;
- maintain the correct degree of unification of the inner layers of the cell [22].

The gray layers in Figure 9 are the electrodes: the anode lapped by the hydrogen flow and the cathode by the oxygen flow.The electrodes are porous and have the same design. They are made made up of carbon cloth or carbon fiber paper. On the side of the electrodes facing the inner part of the cell is located a thin layer of catalyst that allows redox chemical reactions that occur on them [23]. The

catalyst typically used for both the anode and the cathode of PEMFCs is platinum (Pt). In the first developed PEMFCs, platinum was distributed on the surface of the electrodes with an area density of approximately 28 mg/cm^2. The latest generation PEMFCs have significantly improved performance although the surface density of platinum on the electrodes has been progressvely reduced to approximately 0.2 mg/cm^2. In the electrodes of PEMFCs, platinum is found in the form of nanoparticles on carbon powders. A Transmission Electron Microscopy (TEM) image of a PEMFC catalyst is given in Figure 10 [24].

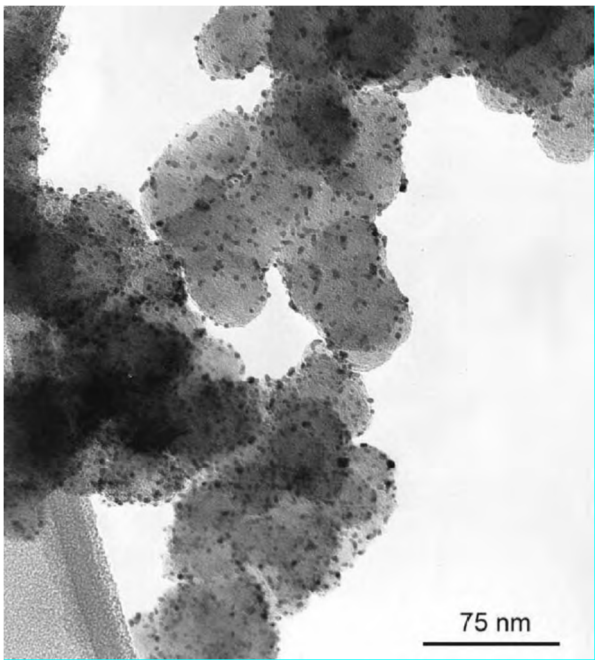

Figure 10. PEMFC catalyst [24].

Between these layers is comprised the solid electrolyte of the cell made from a gas-impermeable but proton-conducting polymer called the Proton Exchange Membrane (PEM).
The anode-electrolyte-cathode assembly is a thin element, which is referred to as a whole by the term Membrane Electrode Assembly (MEA). In some cases the platinum on the carbon catalyst is fixed directly to the electrolyte. In this way, instead of being a separate layer, the electrode becomes an integral part of the membrane [24].
The PEMFCs were first developed in the US in the 1960s by General Electric (GE) for use by NASA on their first manned spacecraft. The first membranes used, manufactured by Grubb and Niedrach of GE, were made with phenol-formaldehyde sulfonic acids produced by the condensation of phenolsulfonic acid and formaldehyde. However, this material hydrolyzed easily and was extremely weak. These first membranes were then followed by others reinforced with a partially sulphonated polystyrene skeleton. However, even the performances of the latter were unsatisfactory, guaranteeing a duration of only 200 hours at 60 °C. The first membranes to have sufficient physical strength were the "D" type membranes, manufactured by the American Machine Foundry. These were made by grafting styrene-divinylbenzene into a fluorocarbon matrix, which was subsequently sulfonated by adding to the molecules a side chain, ending with sulphonic acid HSO_3. The membranes of type "D" guaranteed a duration of 500 hours at 60 °C and were those used in the PEMFCs of all seven Gemini space missions. [25].
The performance and durability of PEMFCs has been significantly improved thanks to the adoption in 1967 of a new polymer membrane made of Nafion® by Dupont. This type of membrane has become and still is the standard for PEMFCs.

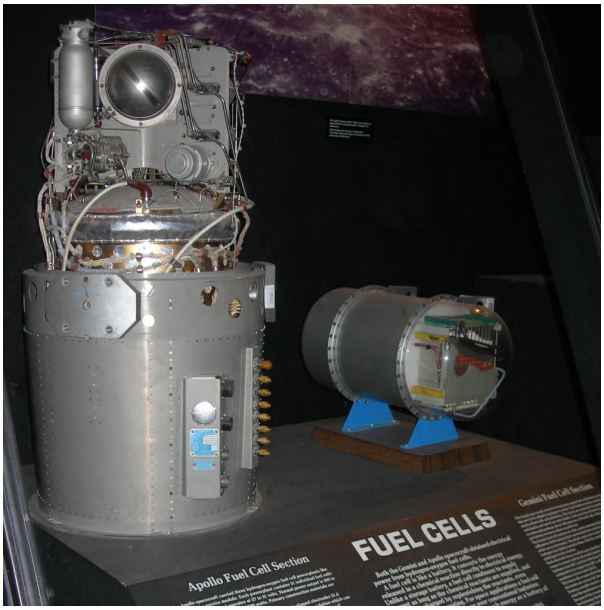

Figure 11. Smithsonian National Air and Space Museum, Washington D.C. Apollo AFC (left) and Gemini PEMFC (right). Photo by the author.

In general, the starting point for the production of a fuel cell membrane is the common polyethylene (PE), ethylene-based polymer with chemical formula $(C_2H_4)_n$. The PE is first of all chemically modified by replacing hydrogen with fluorine in its molecules (perfluorination process). The resulting modified polymer has the chemical formula $(C_2F_4)_n$ and is called polytetrafluoroethylene (PTFE).

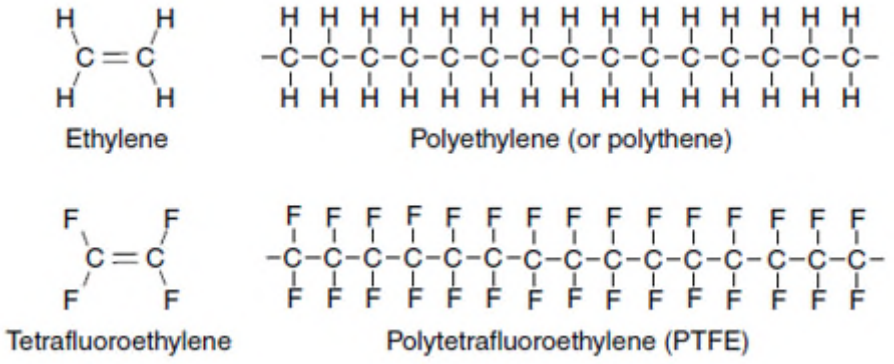

Figure 12. PE and PTFE molecules [24].

The strong bonds between fluorine and carbon make PTFE durable and resistant to chemicals. Another important property of PTFE for its use in PEMFCs is that it is highly hydrophobic. This property makes it particularly suitable for use in fuel cell electrodes to expel the water produced, thus preventing its flooding during its operation.

The next step in the process is the sulphonation of the PTFE. The added HSO_3 group added with the side chain to PTFE is ionically bonded to the molecule, and so the end of the side chain is actually an SO_3^- ion. For this reason, the resulting sulphonated PTFE is called an "ionomer".

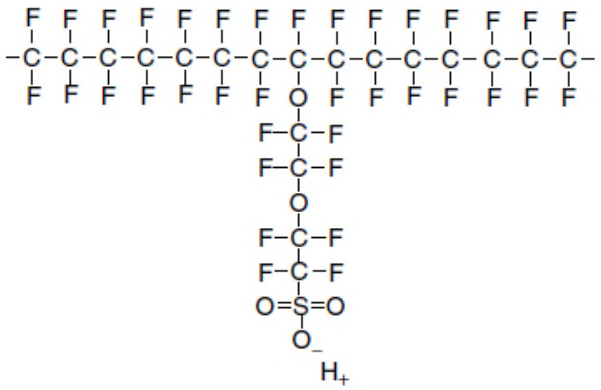

Figure 13. Sulphonated PTFE [24].

The presence of SO_3^- and H^+ ions determines a strong mutual attraction between the ends of the adjacent molecules. The result is that the side chains tend to "cluster" within the overall structure of the material.
In addition, sulfonic acid is a highly hydrophilic substance, i.e. it attracts water molecules.The presence of hydrophilic regions within a generally hydrophobic substance underlies the conductivity of these materials.The hydrophilic regions absorb large amounts of water, increasing their dry weight by up to 50%. Within these hydrated regions, the H^+ ions are relatively weakly attracted to the SO_3^- group and are able to move, giving these areas weakly acidic properties. The resulting material therefore possesses a so called "separate microphase morphology" which includes acidic zones within a strong and resistant hydrophobic structure.
Although the hydrated regions are separated from each other, it is still possible for the H^+ ions to move through the supporting molecule structure. However, for this to happen easily, the hydrated regions must be as extensive as possible. In a well hydrated electrolyte, each SO_3^- in a side chain is surrounded by about 20 water molecules. Typically the conductivity of a well hydrated fluorosulfonated ionomer is about 0.1 S/cm. As the water content decreases, its conductivity also decreases.
Nafion and other fluorosulfonate ionomers are particularly suitable for use in PEMFC cells as:

- they are very resistant to chemicals;
- they have high mechanical resistance and can be produced in very thin films (up to 50μm);
- they include are weakly acidic;
- they can absorb large quantities of water;
- if well hydrated, they have a good proton conductivity [24].

The anode of a PEMFC is the site of an oxidation reaction, or the loss of electrons, according to the half-reaction indicated in (1):

$$H_2 \rightarrow 2H^+ + 2e^- \qquad (1)$$

The H^+ ions (protons) diffuse through the electrode and electrolyte towards the cathode. The negative charges e^- (electrons), on the other hand, are forced to move through the external circuit since, as already mentioned, the intrinsic characteristics of the electrolyte prevent its passage.
The flow of electrons through the circuit outside the cell constitutes the electricity that is consumed by the user. A reduction occurs at the cathode, i.e. the acquisition by oxygen of the electrons coming from the anode according to the half-reaction (2):

$$\frac{1}{2}O_2 + 2H^+ + 2e^- \rightarrow H_2O$$

(2)

The overall cell reaction is the sum of the two half-reactions and is the same that occurs in the combustion of hydrogen:

$$H_2 + \frac{1}{2}O_2 \rightarrow H_2O$$

(3)

As shown above for each water molecule produced and for each hydrogen molecule used, two electrons are moved through the external circuit. In molar terms this means that, for every mole of hydrogen consumed at the anode (or, equivalently, for every mole of water produced at the cathode), 2N electrons travel through the external circuit, where N is Avogadro's number. If $-e$ is the charge of an electron, then the charge flowing in the external circuit is given by (4):

$$-2Ne = -2F$$

(4)

Where F is the Faraday's constant, or the charge on a mole of electrons. Called E_{rev} the fuel cell voltage, the electrical work done by moving this charge in the external circuit is calculated as the product of the displaced charge times the cell voltage.

$$Electrical\ work\ done = -2F \cdot E_{rev}$$

(5)

If there are no losses in the cell, or more properly, if the process is 'reversible', then all the molar Gibbs free energy of formation ($\Delta\bar{g}_f$) for the previous chemical reaction is converted into electrical energy:

$$\Delta\bar{g}_f = -2F \cdot E_{rev}$$

(6)

Thus, the reversible open circuit voltage (OCV) of the cell is given by:

$$E_{rev} = \frac{-\Delta\bar{g}_f}{2F}$$

(7)

The values of $\Delta\bar{g}_f$ at 1 bar pressure are available in tabulated form various temperatures. An example is iven in Table 2.

Form of product water	Temperature [°C]	$\Delta g\bar{f}$ [kJ mol−1]
Liquid	25	-237.2
Liquid	80	-228.2
Gas	80	-226.2
Gas	100	-225.2
Gas	200	-220.4
Gas	400	-201.3
Gas	600	-199.6
Gas	800	-188.6
Gas	1000	-177.4

Table 2. $\Delta g\bar{f}$ for the reaction $H_2+½O_2 \rightarrow H_2O$ at various temperature (p =1 bar) [24].

For a cell operating at ambient temperature (25 °C) at standard atmospheric pressure (1 bar), the reversible open circuit voltage E_{rev} is calculated with the previous formula is equal to $E^0 = 1.229$ V.

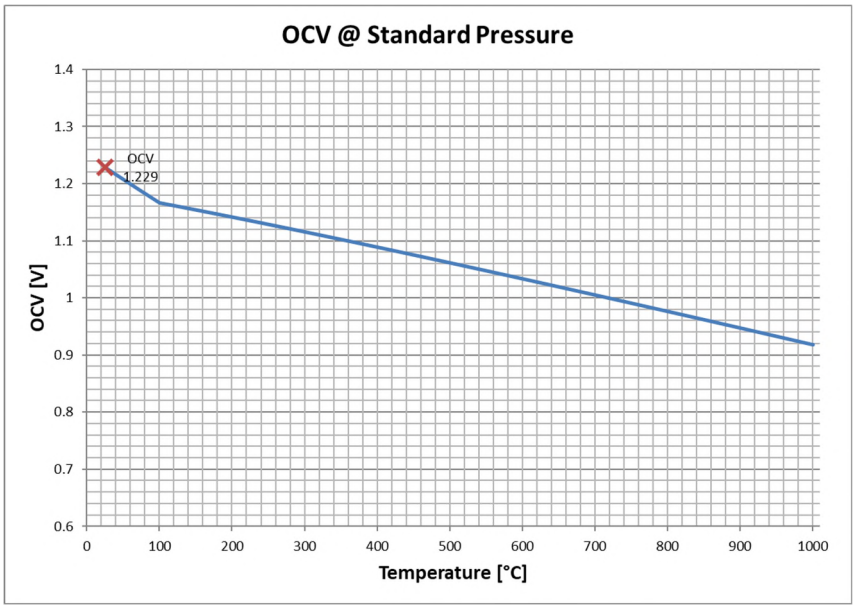

Figure 14. Reversible open circuit voltage OCV variation with temperature.

More complex, is the analysis of the influence on Gibbs free energy of other parameters such as the pressure and concentration of the reactants [26]. Equally important, although more complex, is the analysis of the influence on Gibbs free energy of other parameters such as pressure and concentration of reactants. In this regard, consider a generic reversible chemical reaction expressed by the formula

$$jJ + kK \rightarrow \mathrm{mM} \tag{8}$$

in which the capital letters represent the chemical formulas of the various chemical species and the lower case letters the stoichiometric coefficients. Using thermodynamic arguments it is possuble to demonstrate that it is shown that the following relation applies:

$$\Delta\bar{g}_f = \Delta\bar{g}_f{}^0 - \mathrm{RT}\ln\left(\frac{{a_J}^j \cdot {a_K}^k}{{a_M}^m}\right) \tag{9}$$

When applied to the reaction $H_2+½O_2 \rightarrow H_2O$, the equation becomes:

$$\Delta\bar{g}_f = \Delta\bar{g}_f{}^0 - \mathrm{RT}\ln\left(\frac{a_{H_2}\cdot a_{O_2}{}^{\frac{1}{2}}}{a_{H_2O}}\right) \quad (10)$$

where R indicates the gas constant (R = 8.314 $JK^{-1}mol^{-1}$) and a_x indicates the activity of the chemical species x which is calculated from the ratio between the partial pressure p_x of the reactant and the standard pressure p^0.

$$a_x = \frac{p_x}{p^0} \quad (11)$$

Substituting equations (7) and (11) into equation (10) the Nernst equation is given. This equation allows to calculate the reversible open circuit voltage E_{rev} of a PEMFC add a given temperature, the pressures of the reactants and the state of the water produced and in its operating reaction.

$$E_{rev} = \mathrm{E}^0 + \frac{\mathrm{RT}}{2F}\ln\left(\frac{p_{H_2}\cdot p_{O_2}{}^{\frac{1}{2}}}{p_{H_2O}}\right) \quad (12)$$

When liquid water is produced from the PEMFC, $p_{H_2O} = 1$. From equation (12) it follows also that the higher the pressure of the reagents, the higher is the reversible open circuit voltage E_{rev}. Furhetmore, if diluted reagents are used (for example air instead of pure oxygen), there will be a reduction in the relative partial pressures, as these are proportional to their concentration. This will result in a reduction of the reversible open circuit voltage E_{rev}. [23]
The performance of a PEMFC can be summarized with a graph of its current–voltage characteristics. This graph, known also as “polarization curve”, shows the voltage output of the fuel cell for a given current output.

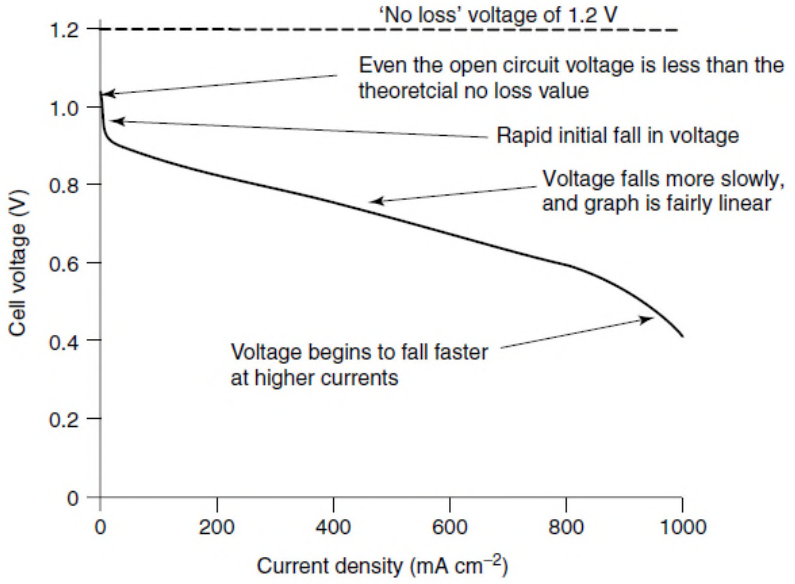

Figure 15. Typical PEMFC polarization curve [24].

Note that in the graph the current has been normalized to the cell surface, i.e. the current density is reported. This approach makes the performance of cells with different surface easily comparable.
An ideal cell is capable of delivering current, while maintaining a constant voltage equal to the theoretical one determined by the laws of thermodynamics.
In reality, however, the operation of a cell is affected by irreversible losses. Its effective output voltage is therfore always lower than the ideal thermodynamically predicted voltage. Also, the higher is the current delivered by a real cell, the greater these losses and the lower the output voltage.
The typical trend of the polarization curve of a real cell can be traced back to three main types of irreversible losses:

1. Activation losses (losses due to electrochemical reaction)
2. Ohmic losses (losses due to ionic and electronic conduction)
3. Losses of concentration (losses due to mass transport)

The activation losses mainly affect the initial part of the polarization curve. These are caused by the limited speed of reactions occurring on the electrode surface. Part of the generated voltage is lost to activate the chemical reactions that transfer electrons to or from the electrode. The voltage drop due to activation losses is highly non-linear.
The ohmic ones are dominant in the central section of the curve. This voltage drop is related to the resistance encountered by the flow of electrons as they pass through the electrode material and the various interconnections, as well as to the resistance encountered by the flow of protons through the electrolyte. This voltage drop for ohmic losses is proportional to the current density and has a typical linear trend.
The concentrarion losses, on the other hand, are the most significant in the operation at high current densities. In this operating condition the cell is unable, due to the hydrodynamic limitations of the hydrogen and oxygen flows, to guarantee the high quantity of reagents required and the elimination of the reaction products. At the limit, all the chemical energy supplied by the reactants is converted only into heat rather than into electrical form [24] [27].
From what above, considering that activation and concentration losses are present at both anode and cathode, the operating voltage of a fuel cell of can be esperssed by the following equation:

$$E = E_{rev} - (V_{act,a} + V_{act,c}) - V_{ohmic} - (V_{conc,a} + V_{conc,c}) \quad (13)$$

Where:

- E is the real output voltage of the cell;
- E_{rev} is the thermodynamically calculated reversible cell opern circuit voltage;
- $V_{act,a}$ and $V_{act,c}$ are the activation losses on the anode and the cathode electrode;
- V_{ohmic} is the cell ohmic loss;
- $V_{conc,a}$ and $V_{conc,c}$ are the concentration losses at the anode end the cathode.

The above equation can be written also in the following format:

$$E = E_{rev} - V_{act} - V_{ohmic} - V_{conc} \quad (14)$$

Where:

- V_{act} are the cell overall cativation losses on anode and the cathode electrode;
- V_{conc} are the cell overall concentration losses at the anode and the cathode.

Leaving aside the theoretical analysis of the individual irreversibility that characterizes a cell and a fuel, which goes beyond the scope of this work and for which reference is made to dedicated texts and

specialized literature, in the following simplified relations for the calculation of the activation, ohmic and concentration losses are given.

Activation losses are connected to the chemical reactions at the anode and cathode and the consequent transfer of electrons . The relationship between the activation losses and the cell current density is described by the Tafel equation which can be expressed as indicated below.

$$V_{act} = v_0 + v_a(1 - e^{-c_1 * i}) \tag{15}$$

where i is the current flowing through the cell, c_1 is a constant ($c_1 = 12$), while the coefficients v_0 and v_a are calculated using the following relations depending on the cell temperature and operating pressures:

$$v_0 = 0{,}279 - 8{,}5 * 10^{-4}(T_{fc} - 298{,}15) + 4{,}308 * 10^{-5} * T_{fc}\left[ln\left(\frac{p_c - p_{sat}}{1{,}01325}\right)\right] + \frac{1}{2} ln\left(\frac{0{,}1137(p_{ca} - p_{sat})}{1{,}01325}\right) \tag{16}$$

$$v_a = (-1.618 * 10^{-5} - 1{,}618 * 10^{-2}) * \left(\frac{p_{O_2}}{0{,}1173} + p_{sat}\right) + \left(1{,}8 * 10^{-4} * T_{fc} - 0{,}166\right) * \left(\frac{p_{O_2}}{0{,}1173} + + p_{sat}\right) + (-5{,}8 * 10^{-4} * T_{fc} + 0{,}5736) \tag{17}$$

Where:

- T_{fc} is the cell average operating temperature in Kelvin;
- p_c is the cathode average operating pressure;
- p_{sat} is the water vapour saturation pressure;
- $p_{O_2}$is the oxygen partial pressure.

In the previous relations only the activation losses at the cathode are considered since the oxidation reaction at the anode of a PEMFC is much faster than the O_2 reduction at the cathode.

The ohmic losses depends on the hydration state of the membrane and the temperature of the cell. It can be calculated with the following relation:

$$V_{ohm} = i * (R_m + R_p) \tag{18}$$

Where:

- i is the current flowing through the cell;
- R_p is the membrane resistance to the passage of protons. It is considered constant and its value can be assumed equal to $3*10^{-3}$ Ω [28];
- R_m is the membrane equivalent resistance, calculated with the following relation :

$$R_m = \frac{\rho_m * l}{A_a}$$

(19)

where ρ_m is the specific resistivity of the membrane to the flow of electrons, A_a is the area of the active cell surface and l is the thickness of the membrane. For membranes made of the Dupont Nafion 117® (one of the most common for the construction of PEMFC) the specific resistivity ρ_m can be calculated using the following expression:

$$\rho_M = \frac{181{,}6 * \left[1 + 0{,}03\left(\frac{i}{A_a}\right) + 0{,}062(\frac{T_{fc}}{303})^2 * (\frac{i}{A_a})^{2{,}5}\right]}{\left[\Psi - 0{,}634 - 3(\frac{i}{A_a})\right] exp\left[4{,}18(\frac{(T_{fc} - 303)}{T_{fc}})\right]}$$

(20)

The term Ψ expresses the specific resistivity in open circuit at 30 °C. It assumes values between 14 and 23 [28] depending on the relative humidity and the stoichiometric ratio of the air to the cathode.

Concentration losses V_{conc} are caused by changes in the concentration of the reactants as they are consumed during the reaction. The voltage reduction for concentration losses can be approximated with the following relation:

$$V_{conc} = i(c_2 \frac{i}{i_{max}})^{c_3}$$

(21)

Where:

- i is the cell current density;
- i_{max} is the limiting current density that causes abrupt voltage drop in tne concentration region.

Parameters c_2, c_3 and i_{max} are calculated using the following expressions whose choice depends on the saturation pressure [29]:

$$\left(\frac{p_{O_2}}{0{,}1173} + p_{sat}\right) < 2\ atm$$

$$c_2 = \left(7{,}16 * 10^{-4} * T_{fc} - 0{,}622\right) * \left(\frac{p_{O_2}}{0{,}1173} + p_{sat}\right) + \left(-1{,}45 * 10^{-3} * T_{fc} + 1{,}68\right)$$

(22)

$$\left(\frac{p_{O_2}}{0{,}1173} + p_{sat}\right) \geq 2\ atm$$

$$c_2 = \left(8{,}66 * 10^{-5} * T_{fc} - 0{,}068\right) * \left(\frac{p_{O_2}}{0{,}1173} + p_{sat}\right) + \left(-1{,}6 * 10^{-4} * T_{fc} + 0{,}54\right)$$

(23)

$$i_{max} = 2{,}2 \tag{24}$$

$$c_3 = 2 \tag{25}$$

The voltage of an operating PEMFC is relatively low (typically 0.7 V). This means that to produce a useful voltage multiple cells must be electrically connected in series to form a "stack".
In a stack, the interconnection between the cells is achieved using a conductive "bipolar plate" which puts the entire surface of a cathode of a cell in electrical contact with that of the anode of the adjacent cell (hence the name "bipolar"). The two faces of the bipolar plate are also equipped with channels that allow the reactants to be distributed to the electrodes between which it is interposed: oxygen at the cathode and hydrogen at the anode.
Typically, the "bipolar plates" are larger than the electrodes and have additional channels running through the stack that feed the reactants from one cell to the next one. This arrangement is called "internal manifolding" [24].

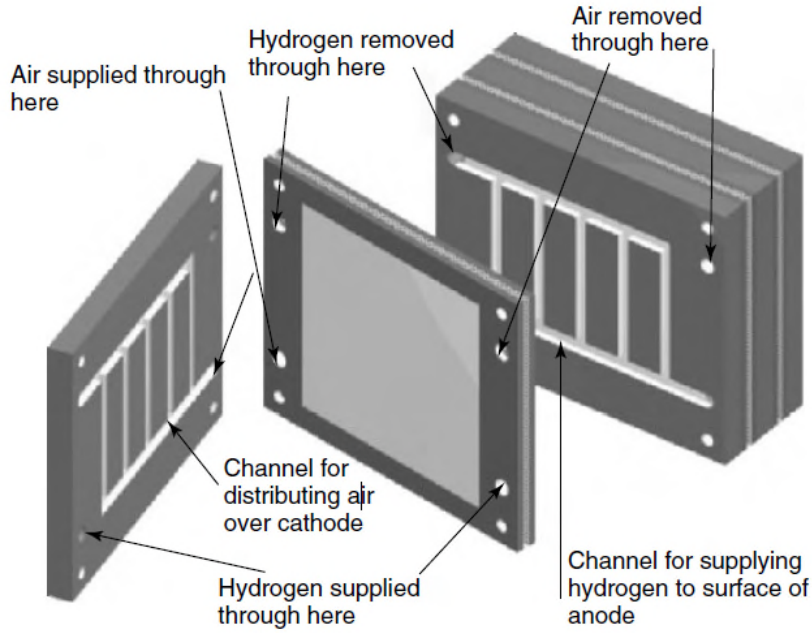

Figure 16 . PEMFC internal manifolding. [24].

The theoretical efficiency of a PEMFC can be calculated, as for all energy conversion devices, as the ratio between useful energy output and energy input.
For the PEMFC, as for all fuel cells, the useful energy is is the electrical energy output, whereas the energy input is the energy reltatef to the fuel (hydrogen) which is normally referret to its Lower Heating Value (LHV). In an ideal cell it can be ssumet that all the Gibbs free energy is cpnverted into electrical power, therefore, with reference to the hydrogen LHV (-242 kJ/mol), the theoretical efficiency of a fuel cell can be calculated in percent with formula
(26) [24].

$$\eta\% = \frac{-\Delta\bar{g}_f}{H_{2LHV}} \times 100 \qquad (26)$$

The values of $\Delta\bar{g}_f$ is influenced by temperature as illustrated in Table 2 (values referred at 1 bar pressure).
In Figure 17 the plot of the maximum theoretical efficiency of a fuel cell calculated with reference to hydrogen LHV is given.

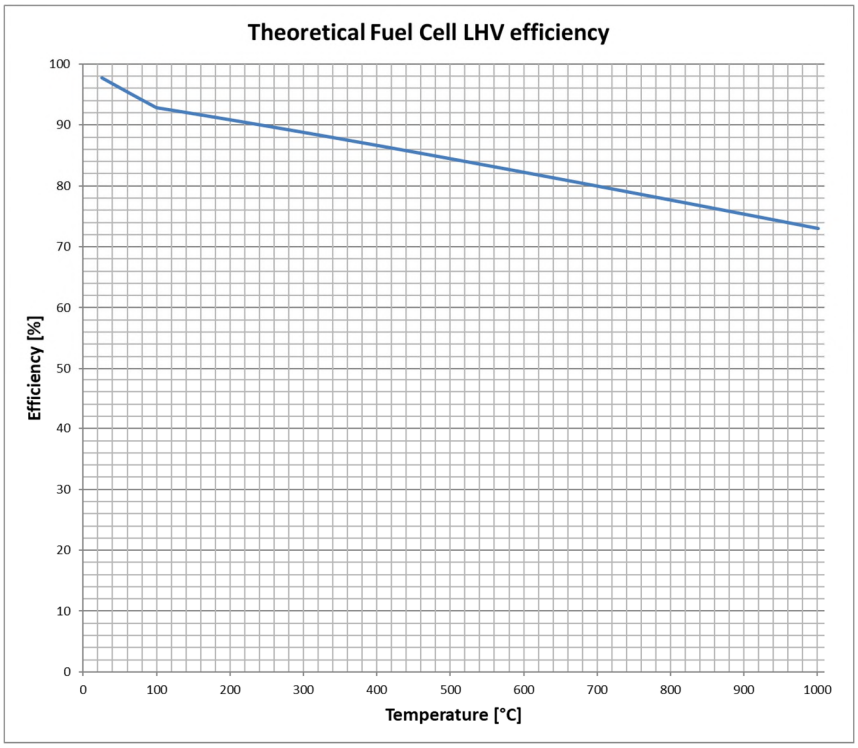

Figure 17. Theoretical hydrogen fuel cell efficiency.

From Figure 17, the following important points should be noted:

- although the graph would suggest that lower temperatures are better, the fuel cell voltage losses due to irreversibilities are always lower at higher temperatures. Therfore, in practice, fuel cell voltages are higher at higher temperatures;
- the waste heat from the higher-temperature cells is more useful than that from lower t emperature cells.

4.2 State of the art of PEMFC application in shipping sector

In the shipping sector, PEMFC have been used for niche applications since the 1960s. The technology was mainly used for the development of air independent propulsion systems (AIPs) for submarines or in small demonstration projects mainly in the military. Civilian applications of the technology did not emerge until this century. In the following paragraphs an overview of the most noticeable applications of PEMFC in submarines and surface ships is provided.

4.2.1 Submarine applications

Starting from 1980s, PEM fuel cell-based AIP fuelled by hydrogen has been tested on board submarines. The nominal power of PEMFC installed installed has progressively increased during the years reaching a maximum of 300 kW on board class U-212A submarines developed for German and Italian Navies since 2002 [5].

Key suppliers	Country	PEMFC Power rating	Date	Vessel name, notes
Non-nuclear submarines/naval ships				
ThyssenKrupp Marine Systems/HDW	Germany	9 × 34 kW fuel cells (in U31) 2× 120 kW fuel cells (later subs)	2005	SiNavy PEMFC from Siemens, first contracted for class **212A** sub in 1996, **U-31** and **U-32** first into service for German Navy, now in service with or ordered by seven countries.
UUV/AUV submersibles				
Perry Technologies/Ballard	USA/Canada	3 kW	1989	PC-14
Atlas Elektronik/ZSW	Germany	160 kW	2002	**DeepC**, prototype with ZSW fuel cell
Mitsubishi Heavy Industries	Japan	4 kW	2004	**Urashima**, 317 km long-distance cruise record at 800 m depth, metal hydride storage

Table 3. Submarine application of PEMFC [30].

The first operational prototype of the class U-212A subamarines (named U-31 Wittenberg) completed the test phase in March 2004 reaching a range of 3000 km underwater at low speed with the onboard fuel cell-battery AIP system. The unit included a diesel propulsion (3.12 MW engine) for surface navigation. The submarine entered active service in the German Navy in mid-2004. In 2005 the Germans put into service a second unit, the U-32 Edenkoben. Submarine U-32 then broke the diving world record by staying 2 weeks underwater.
In the following years other four class U-212A submarines entered into force in the German Navy: U-33 in June 2006, U-34 in June 2007, U-35 in March 2015 and U-36 in October 2016 [31].

Figure 18. The U-36 submarine [31].

In the Italian Navy four U-212A class submarines are currently in operation: Salvatore Todaro (2006), Scirè (2007), Pietro Venuti (2016) and Romeo Romei (2017).

Figure 19. The launch of Salvatore Todaro (2006) [31].

The main charactereistics of the Italian Navy class U2-12A submarines are summarized in Table 4.

Submarine U-212A Todaro Class specifications	
Length overall	57.15 m
Length between perpendiculars	55.90 m
Max breadth	7.00 m
Height overall (mast in)	11.875 m
Surface displacement (ready to dive)	1509 t
Submerged displacement	1720 t
Fuel Cell	9 x 34 kW
Maximum surface speed	12 kn
Range at 8 kn on surface	8000 nm
Maximum submerged speed	>16 kn
Crew	27

Table 4. Italian Navy U-212A Todaro Class [32].

Submarines of Class U-212 A (six in the German Navy and four in the Italian Navy) are equipped with 9 Siemens SINAVY FCM 34 modules, which were developed from 1985 at the request of the German Ministry of Defense. The moduels are supplied with gaseous hydrogen stored in metal hydrides and pure oxygen [33].
Figure 20 shows the main components (bipolar plates and membrane) of the elementary cell used in FCM 34 modules. The external dimension of the cell are 400 x 400 mm.

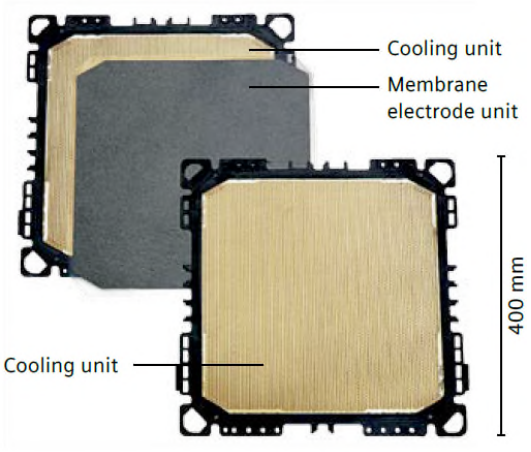

Figure 20. Siemens SINAVY FCM 34 cell [33].

Onboard Class U-212A, the FCM 34 modules, valves, piping, and sensors and the module electronics control and the ancillaries are installed into a single container in order to optimize the use of the limited space available on board. The ancillaries comprise the equipment for supplying H_2, O_2, and N_2, for reactant humidification, for product water and waste heat and residual gas removal.
The container is filled with N_2 inert gas at 3 bar abs. to prevent a release of H_2 and/or O_2 in case of leakages [33].
The FCM 34 modules have a rated current in continuous operation of 650 A. For currents higher than the rated current, operation time is reduced due to the limitations of the thermal dissipation system. The maximum current that can be supplied by the cells for a limited time can in any case reach double the rated current.
At rated output the stack efficiency with respect to the hydrogen LHV is about 59 %. The efficiency of the stack increases at part load, reaching a maximum of approximately 69% when delivering a current equal to 20% of the rated current (approximately 130 A) [33].
The output power/current characteristics for FCM 34 modules and efficeincy curves are shown in Figure 21.
In Figure 21 are also reported the performances of the FCM 120 modules installed on the Class U-214 submarines developerd for the Hellenic Navy, Republic of Korea Navy, Portuguese Navy, and Turkish Navy. Other curves refer to performance of the next generations of FCM modules.

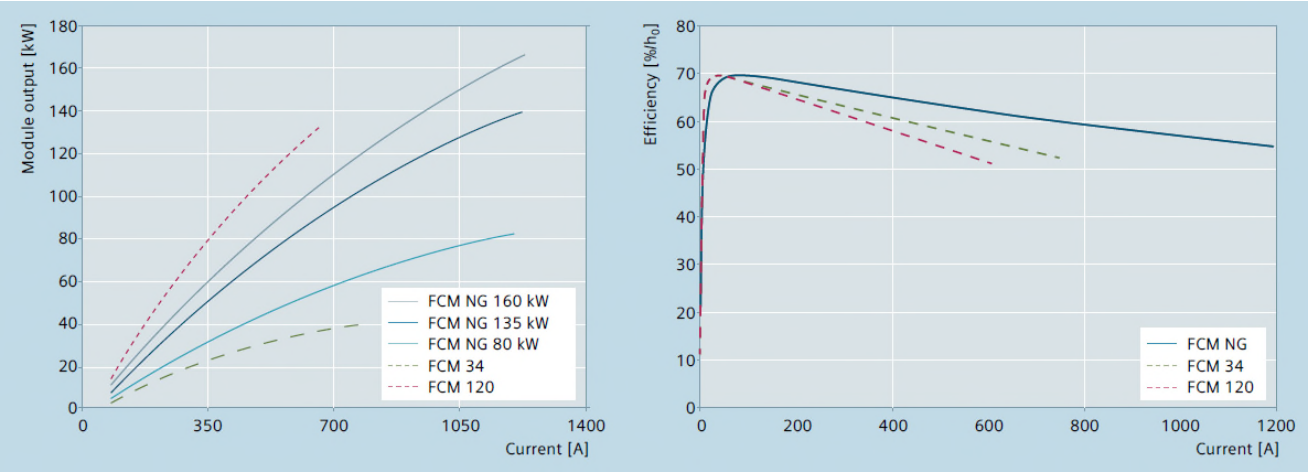

Figure 21. Siemens SINAVY FCM 34 module power/current characteristics and efficiency [33].

For the FCM 34 module, the degradation rate declared by the manufacturer is less than 2 µV/h per cell.

The main technical data of the Siemens SINAVY FCM 34 module are summarized in Table 5.

FCM 34 Technical data	
Rated power	34 kW
Voltage range	50–55 V
Efficiency at rated load, approx.	59 %
Efficiency at 20 % load, approx.	69 %
Operating temperature	75 °C
H_2 pressure	2.3 bar abs.
O_2 pressure	2.6 bar abs.
Dimensions	H = 48 cm W = 48 cm L = 145 cm
Weight (without module electronics)	650 kg

Table 5. Siemens SINAVY FCM 34 module technical data [33].

In 2003, a PEMFC power system has been installed on the Autonomous Underwater Vehicle (AUV) Urashima by the Japan Agency for Marine-Earth Science and Technology (JAMSTEC).
The aim of JAMSTEC the designers was to develop a compact unmanned underwater vehicle, capable of traveling great distances (up to 1000 km) and generating low noise in order not to interfere with the acoustic sensors installed on board.
Lead acid and silver zinc batteries have been widely used as conventional power sources for underwater vehicles however, as the demand for electrical power increases, the volume and weight of the battery also increase, making underwater vehicles large and heavy.
The adoption of fuel cells as the vehicle's main power source made it possible to meet the design requirements in terms of cruising range, low noise emission and slenderness of the vehicle body.

Figure 22. AUV Urashima [31].

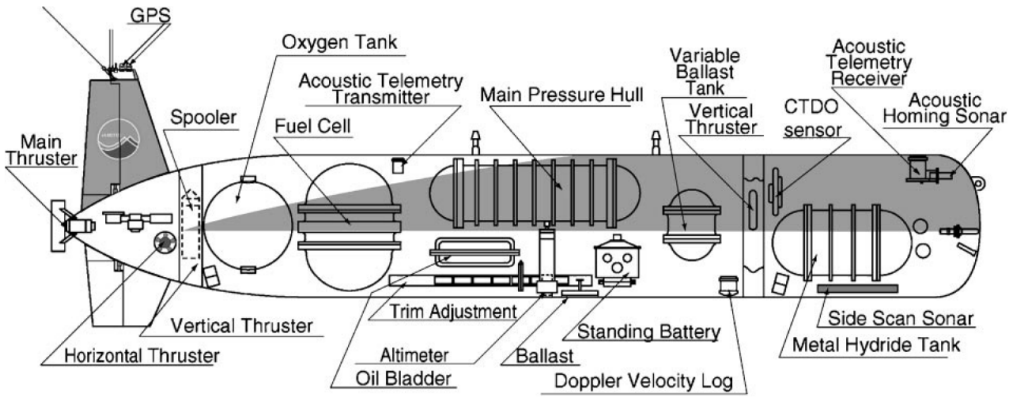

Figure 23. AUV Urashima. General arrangement [34].

The main specifications of the AUV Urashima are summarized in Table 6.

AUV Urashima specificaitons	
Dimensions	L = 10 m W = 1.3 m H = 1.5 mm
Weight (in air)	10 ton
Operation depth (max)	3500 m
Cruiseing range	300 km
Cruising speed	Aprox. 3 kt

Table 6. AUV Urashima specifications [34] [35].

The PEM fuel cell power installed as main source of power on Urashima consisted of two stacks in series with a reated outpit of 120 V, 4 kW and was integrated with a lithium-ion 130 V, 300 Ah rechargeable battery storage system [35] [36].
JAMSTEC began to develop fuel cells in 1991, and had developed a prototype of a closed cycle fuel cell using a PEMFC. It developed 1.5 kW rated power in 1993, and reached 4 kW capacity only in 1998 [34]. The fuel cell installed onboard Urashima was enclosed in a dedicated titanium alloy canister locatedmin the aft part of the AUV as indicated in the general arrangement of the AUV provided in Figure 23. The closed cycle fuel cell block diagram and overview of tits titanium canister are shown in Figure 24.

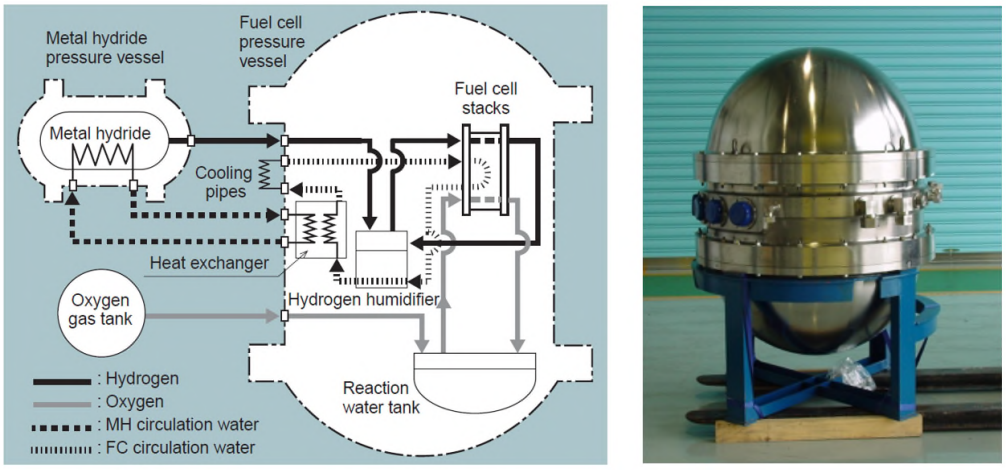

Figure 24. AUV Urashima. Block diagram of fuel cell system and its titanium alloy canister [35] [36].

After the preliminary tests in stationary conditions, the PEMFC installed on board Urashima was tested on a specific test device (Figure 25) designed in order to verify its performance in the presence of oscillations and vibrations.

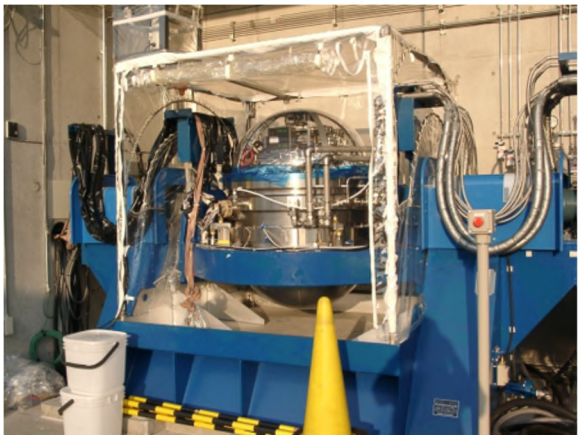

Figure 25. AUV Urashima. PEMFC on the swing test machine [36].

Oxygen gas is supplied from a high-pressure (14.7 MPa) oxygen gas tank, and he hydrogen was stored in an AB5-type Mn-Co-Misch metal hydride alloy [31] [35].

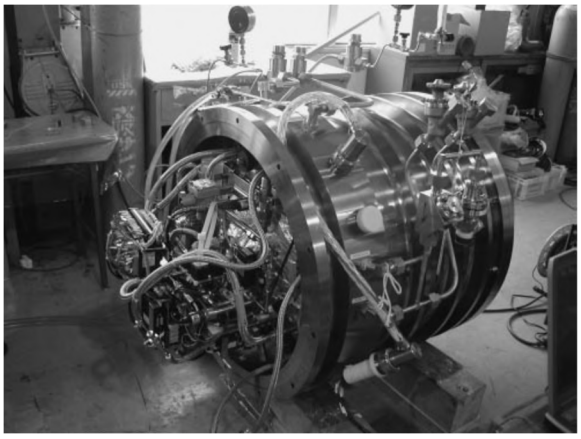

Figure 26. AUV Urashima. Titanium alloy canister for the metal hydride hydrogen storage system [34].

The AB5-type metal hydride absorbs hydrogen under 0 °C, stores it at about 25 °C, and discharges it at temperatures of over 50 °C, in atmospheric pressure. Since the temperature at which the AB5-type metal hydride discharges the hydrogen is higher than the temperature of the water in the deep sea, it was necessary to heat the AB5 during the dive to ensure the supply of the fuel cells. For this purpose, the vehicle was equipped with a heat exchange system that used heated water from the fuel cells as a vector of thermal energy for the metal hydride [34].
Launched in December 2000, In Suruga Bay, in September 2003, Urashima carried out a seagoing trial and achieved the first autonomous cruise powered by a fuel cell. The vehicle cruised for six hours, covering 21 km in total. The amount of hydrogen consumption in this trial was 10.9 Nm^3, about 10% of stored capacity [34].
The vehicle powered only by the Li-ion battery had a 100 km cruising range with the contribution of the power generated by the fuel cell, the cruising range increased to 300 km. In February 2005 Urashima successfully completed a diving course of 317 km at a diving depth of 800 m in 56 hours [31]. The maximum depth reached by the vehicle was 3500 m.

4.2.2 Surface applications

Small but successful applications of PEMFC powered surface boats have been developed starting from the beginning of the 21st century. Since 2000 more than 40 projects have been developed worldwide, in which PEMFCs have been applied to different types of inland and seagoing ships:

- Sailboats;
- Research vessels;
- Water taxies and ferries;
- Recreational boars.

Despite the large number of projects, the official technical documentation available in publications and articles is very scarce. The documentation available on the web is also often limited or provides only general information. Given the limited availability of information, providing a detailed description of each of the projects developed to date in this maritime sector is very difficult and is, however, beyond the scope of this work.
The most noticeable "operative" projects (i.e. projects in which the ship/pilot plant has successfully operated at sea at least once or where the ship is currently under construction) related to the application of PEMFC in surface ships are listed and described in Table 7.
Other projects have been developed in more recent years but either they have not yet moved from the design phase to the experimental phase or they have not yet completed the test program in operational conditions. We will refer to these projects as "non-operative" projects. The main main "non-opertive" projects implementing PEMFC are listed in Table 8.

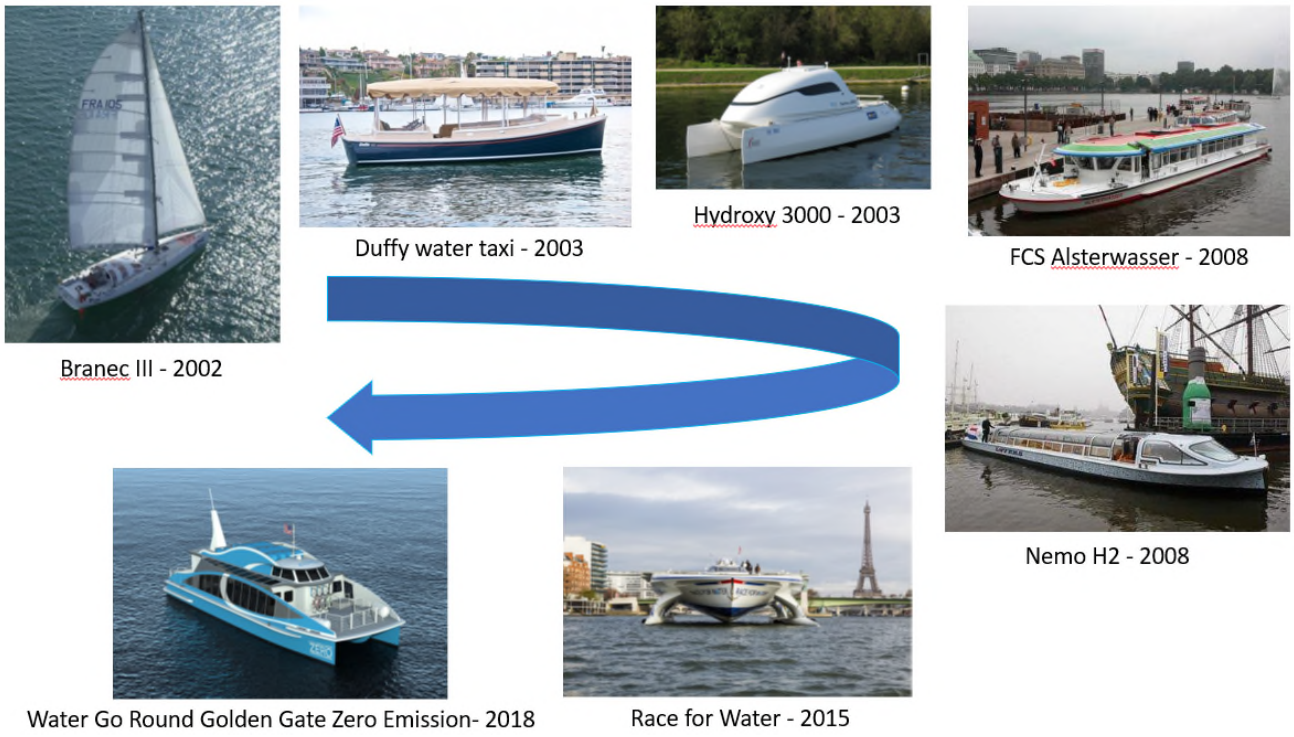

Figure 27. Surface applications of PEMFC. Some of the "operative" projects [31] [37] [38] [39].

Table 7. List of international "operative" PEMFC demonstrators in shipping [30] [40] [41, 42] [43] [44] [45].

Key suppliers	Country	PEMFC Power rating	Date	Vessel name, notes
Yachts/sailboats				
IESE–EIVD	Switzerland	300 W	2002	**Branec III** used PEMFC as APU in 6600 km transatlantic Route de Rhum race
MTU CFC Solutions/Ballard	Germany/Canada	4.8 kW	2003	**No. 1**, 12 m yacht, CoolCell PEMFC in hybrid system with batteries as APU
Voller Energy	UK	5 kW	2007	**Emerald** Beneteau 411, 12 m long, in 3000 nm ARC transatlantic rally, running on reformed LPG
CEA-Liten	France	25 kW	2009	CEA Liten **Zero CO_2** 12m hybrid electric sailboat with 30 kW PEM Fuel Cell system and 14.8 kWh Li-ion battery
Research vessels				
Icelandic New Energy/Ballard	Iceland/Canada	10 kW	2009	**SMART H_2**, 125-tonne whale watching ship with hybrid PEMFC/battery APU, part of Smart H_2 Program
CEA-Liten	France	20 kW	2015	**Energy Observer**, lightweight ex-racing catamaran (30.5m length) using wind and solar power with on-board electrolysis to fuel a fuel cell.
Water taxis/ferries				
Duffy Electric Boat Co/Anuvu/Millennium Cell	USA	3 kW	2003	**Duffy water taxi** for 18 passengers, sodium borohydride Hydrogen on Demand® system
Proton Motor	Germany	6–20 kW	2008	**FCS Alsterwasser**, 100 passengers, Zemships Project, primary propulsion with lead gel battery
Fuel Cell Boat BV	Netherlands	60–70 kW	2009	**Nemo H_2**, 22 m long, 82 passenger capacity, hybrid with batteries for main propulsion
CMR Prototech	Norway	12 kW	2010	**MF Vågen**, small passenger ship in the harbour of Bergen
Auriga Energy	UK	12 kW	2014	**Hydrogenesys**, small passenger ship in Bristol
Golden Gate Zero EmissionMarine; Hydrogenics	USA	360 kW	2018	**Water Go Round Golden Gate Zero Emission.** Speed ferry length 21 m. Batteries in hulls to provide boost power to reach peak speed of 22 knots.
Recreational boats				
IESE–EIVD/ZeTek Power	Switzerland/UK	3 kW	2003	**Hydroxy 3000** catamaran, two earlier Hydroxy craft
University of Birmingham	UK	5 kW	2007	**Ross Barlow** waterway maintenance boat, student project, metal hydride
Horizon Fuel Cell/Plug Power	Singapore/USA	300 W	2007	Trolling boat propelled by electric motors
Zebotec	Germany	24 kW	2007	**Cobalt 233 Zet.** Small sport boat. Originally only batteries, then partially replaced by fuel cells.
Fronius International/Bitter GmbH	Austria	4 kW	2009	**Riviera 600** motorboat (16 m long), H_2 in high-pressure cartridges, part of Future Project Hydrogen
Tropical Green Technologies	Greece	1 kW	2009	Testing RFC-1000 unit on motorboat, H_2 from reformed LPG
Rensselaer Polytechnic Institute	USA	4.4 kW	2009	**New Clermont**, 6.7 m Bristol 22 sailboat outfitted as student project with two Plug Power fuel cells
Ecofys	Netherland	1.2 kW	2009	**Xperiance NX Hydrogen**, 12-person boat with a 1.2 kW PEM fuel cell propulsion system; designed to travel 2-3 days without refuelling, funded by the Province of Friesland and the Dutch Ministry of Economic Affairs
Yanmar Co Ltd, National Maritime Research Institute, Japan Ship Technology Research Association	Japan	60 kW	2015	**Kamine boat.** Small size boat, 16.5 m long, 17 tons, 50 kW installed for propulsion; boat was successfully tested under maritime loads and conditions. 60 kWh Li-ion battery and CH_2
Breguet, Plastic Omnium, Etia Ecotechnologies, Skysails Yacht	Switzerland	60 kW	2015	**Race for water.** Catamaran. Length 30 m, breadth 16 m. PV panels (512 m^2) charge batteries and power a desalination unit that produces water to obtain H_2 through an electrolyser (50 bar), then compressed to 350 bar. Self-piloting kite (41 m^2) enhances the propulsion.
-	South Korea	35 kW	2016	**Busan tourist boat.** Tourist boat, length 20 m.

Table 8. List of "non-operative" PEMFC projects in shipping. [45] [46] [47].

Project	Country	Period	PEMFC Power [Kw]	Application	Partners and funding	Note
Aero 42	Norway	End in 2023	2800	Pax Ferry	Wstcon Automation, Boreal, Arena Ocean Hyway Cluster, Brodene Aa	Includes 672 kWh Li-ion battery. CH_2 612 kg, 250 bar.
Future Proof Shipping	Netherland /Belgium	2021-	635	Inland container vessel	CCNR, Holland shipyards Group, Future Proof Shipping, Interreg Northsea, Kwr Allied Waters	Includes 300 kWh Li-ion battery. CH_2 1160 kg, 300 bar.
Norled-Ryfylke	Norway	2021-	400	Cars and pax ferry	Linde, Ballard, Norled, Westcon Power and Automation, Open Bridge Partner, Sintef, Lloyd Register	LH_2 150 kg daily consumption. Criogenic tanks: multilayer-vacuum (10 bar, 3.8 tons). Holding time 115 days.
GKP7H2-MoSEEZ program	Norway	2019-	120	High speed ferry	Norwegian R&D Institution Ife	CH_2 250 bar
Zeff (part of Pilot E scheme)	Norway	2018-	2200	Fast ferry	Selfa Artic, Lmg Marin, Hyon, Norled, Servogear	50 kWh ESS and CH_2
FCSHIP	Norway	2002-2004	400	River ferry RoPax	Norwegian Shipowner Association, Ansaldo Fuel Cells	PEMFC/SOFC/MCFC. CH_2 for River Ferry, Low sulphur diesel oil, LNG or LH_2 for RoPax
FLAGSHIPS (France)	Norway /France	2019-	400	River push boat	Lmg Marin, Norled, Ada Shipyard for Building No Ships, ABB, Kongsberg Marine, Greenstat, Weston Power & Automation, Protech, Nce Marine Technology, Ballard Europe, Pers-Ee.	ESS and CH_2
FLAGSHIPS (Norway)	Norway /France	2019-	600	Cars and pax ferry	Lmg Marin, Norled, Ada Shipyard for Building No Ships, ABB, Kongsberg Marine, Greenstat, Weston Power & Automation, Protech, Nce Marine Technology, Ballard Europe, Pers-Ee.	500 kWh ESS and CH_2 460 kg 250 bar
Ulstein SX190 Zero Emission DP2	Norway	2019-	2000	Offshore vessel	Ulstein Design and Solutions, DNV, Nedstack	CH_2
Free CO2ast (part of Pilot E scheme)	Norway	2018-	3200	RoRo ferry	Havyard Group, Powercell, Linde, Havila Kystruten, Norwegian Control Systems, Sintef	LH_2 total capacity 3500 kg
Hyseas III	Scotland	2018-	700	RoRo ferry	Ferguson Marine, Ballard, University of St. Andrews, Kingsberg, McPhy, DLR, Interferry, Orkney Ferries.	Li-ion battery, H_2 2000 kg (no data if liquid or compressed)
MARANDA	Finland	2017-	165	Research Vessel	Teknologian Tutkimuskeskus Vit Oy, Powercell Sweden, ABB Oy, Omb Saleri, Pers-Ee, Suomen Ymparistokeskus, Swiss Hydrogen Sa.	CH_2 83 kg, 350 bar
Rødne E-Maran sluttraport	Norway	2019-	1500 2625 3750	1130 Pax 24 m 2145 Pax 24 m 3190 Pax 28 m	Maran, Achandia Marine, Fjellstrand, Scalesia, Maran Utvikling	Lithium Titanate Cellls ESS, no data on capacity
Elektra and Elektra 2 (e4ships consortium)	Germany	2017	300	Push boat	TU Berlin, Ballard	2.5 kWh Li-Mn_Co battery, . CH_2 750 kg
Hynovar	France	2016	480	200 Pax	Hyseas Energy, Bateliers De La Cote Azur, Engie Cofely, Cci Var	CH_2 260 kg 350 bar
Hornblower-Hybrid	USA	2012-	32	Pax Ferry	Hornblower	Hybrid ferry with diesel generator, batteries, PV, wind and fuel cell and CH_2
SFBreeze	USA	2015-	4920	Pax Ferry	Sandia National Laboratory, Hydrogenics, Gardner Cryogenics	Feasibility study of a highspeed hydrogen fuel cell passenger ferry and LH_2 (1200 Kg) hydrogen refueling station in San Francisco Bay area
Zero-V	USA	2017-	1800	Research Vessel	Sandia National Laboratory, Glosten, The Scripps Institution of Oceanography San Diego, DNV	Feasibility study of a liquid hydrogen fuelled coastal research vessel. LH_2 (1100 Kg)
ZEUS (Zero Emission Ultimate Ship)	Italy	2018-	140	Experimantal ship	Fincantieri	Zero-emission 25-meter, 70-ton hybrid experimental ship with diesel generator, PEMFC fed with hydrogen (50 kg) stored in metal hydrides and batteries.

Figure 28. Fincantieri Zero Emissions Ultimate Ship (ZEUS) [48].

A recent study analyzed the "operative" and "non-operative" projects of maritime and inland navigation vessels equipped with fuel cell generators and developed since 2000. The search was limited to projects for which the information was freely accessible in English on the web and for which at least two of the following data were available: FC technology, FC rating and fuel type.
The study identified 44 projects and analyzed 40 in detail. Sailboats and 4 "non-operational" projects (feasibility studies) were not included. The analysis of the identified projects has shown that those in which the FCs are used as the main power generation system on board are related to small boats or small passenger ferries, while on ships of greater tonnage FC are generally used as Auxiliary Power Units (APUs) [45].
The share of each type of fuel cell used in the considered porjects is summarized in the pie diagram of Figure 29. From the chart it emerges that, thanks to the high level of technological maturity they have reached, PEMFCs are currently the most widely used fuel cell technology in in porjects and studies for the shipping sector [45].

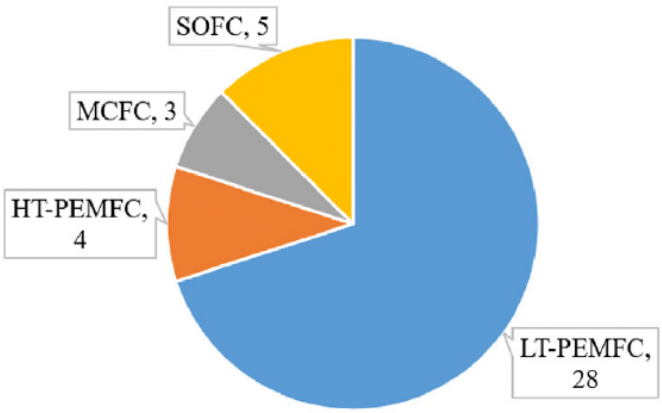

Figure 29. Fuel cell types in surface ships "operative" projects developed since 2000 [45].

4.3 Hydrogen as an alternative fuel in shipping

For the maritime sector, drop-in fuels (synthetic and fully interchangeable substitute for traditional petroleum-derived hydrocarbons) represent a viable alternative especially on older ships and on all those for which retrofitting is not economically convenient.
For refurbished or newer ships, the use of biomethane or methanol in dual-fuel engines represents a promising prospect yet to be explored, in which methanol appears to be particularly suitable for retrofit projects.
In the long term, however, zero-carbon energy carriers such as ammonia and, above all, hydrogen are certainly the most promising for low- or zero-carbon shipping [49].
Comparing the zero-carbon energy carriers with batteries, it can certainly be said that there is a complementarity between the two technologies. But the shorter refueling times and higher energy density give hydrogen an advantage over battery-only solutions in many applications, including freight and passenger transport [50].

4.3.1.1 Hydrogen properties

Although hydrogen is the most abundant element in the universe, gaseous hydrogen is not readily available on Earth.
Hydrogen is an odorless, colorless and tasteless gas and at atmospheric pressure it has a very low density: about fourteen times lower than air.
Thanks to its low density, hydrogen rises and diffuses very quickly in the air.
Hydrogen has a very high gravimetric energy density (33.3 kWh/kg), but due to its very low density, its volumetric energy density is only 3 kWh/m3 (at normal temperature and pressure).
By compressing hydrogen, its volumetric energy density increases: at 350 bar it increases to 776 kWh/m3 and reaches 1309 kWh/m3 at 700 bar.
The maximum volumetric energy density of hydrogen (2363 kWh/m3) is achievable only by liquefaction at a temperature of 20 K (-253 °C).
Cryo-compressed storage i.e. storing liquid hydrogen in an insulated pressure vessel designed for up to 350 bar combines the benefits of both compressed and liquefied hydrogen: high storage density and reduced boil-off-losses losses [51].
A comparison of the energy density of different energy carriers can be found in Table 9 and Figure 30. Energy density of different energy carriers..

Fuel	Volumetric Energy Density (kWh/m^3)	Gravimetric Energy Density (kWh/kg)	Density (kg/m^3)
Diesel	10044	12.0	837
Heavy Fuel Oil	10938	10.8	1010
Liquified Natural Gas (111 K)	6165	13.9	443.5
Liquified Ammonia (10 bar or 239 K)	3528	5.2	678.5
Hydrogen (350 bar)	766	33.3	23.3
Hydrogen (700 bar)	1309	33.3	39.3
Liquified Hydrogen (20 K)	2363	33.3	70.96
Methanol	4424	5.6	790
Liqiod Organic Hydrogen Carrier (Dibenzyltoluene)	1886	2.1	913.4
Metallhydride (MgH_2)	3672	2.5	1450

Table 9. Comparison of the energy density of different energy carriers [51].

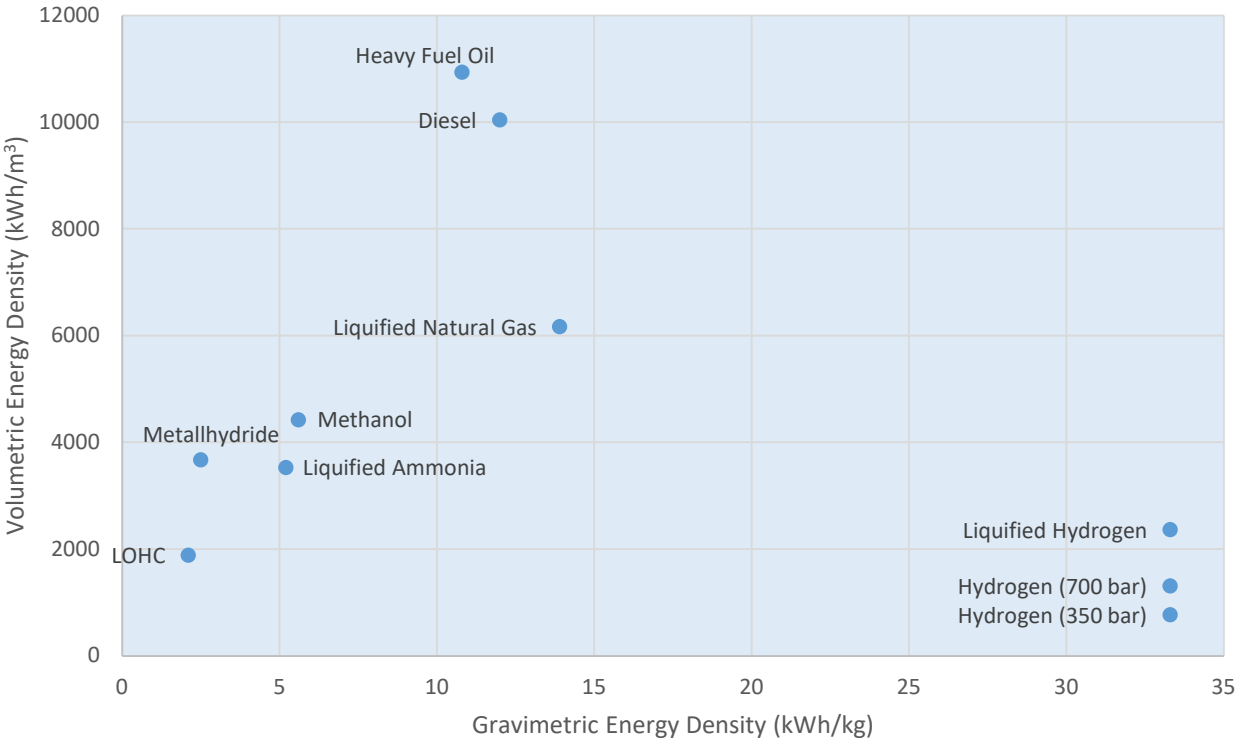

Figure 30. Energy density of different energy carriers.

At normal pressure hydrogen has a boiling point of 20 K and its melting point is 14 K, both of which are pressure dependent. The triple point, i.e. the one in which all three phases coexist, has a temperature of 13.8 K and a pressure of 7.2 kPa (72 mbar).
The increase in pressure above the critical point characterized by a temperature of 33 K and 1296 MPa (12.96 bar) has no further influence on the boiling point [51].
These points are represented in the hydrogen phase-diagram of Figure 31.

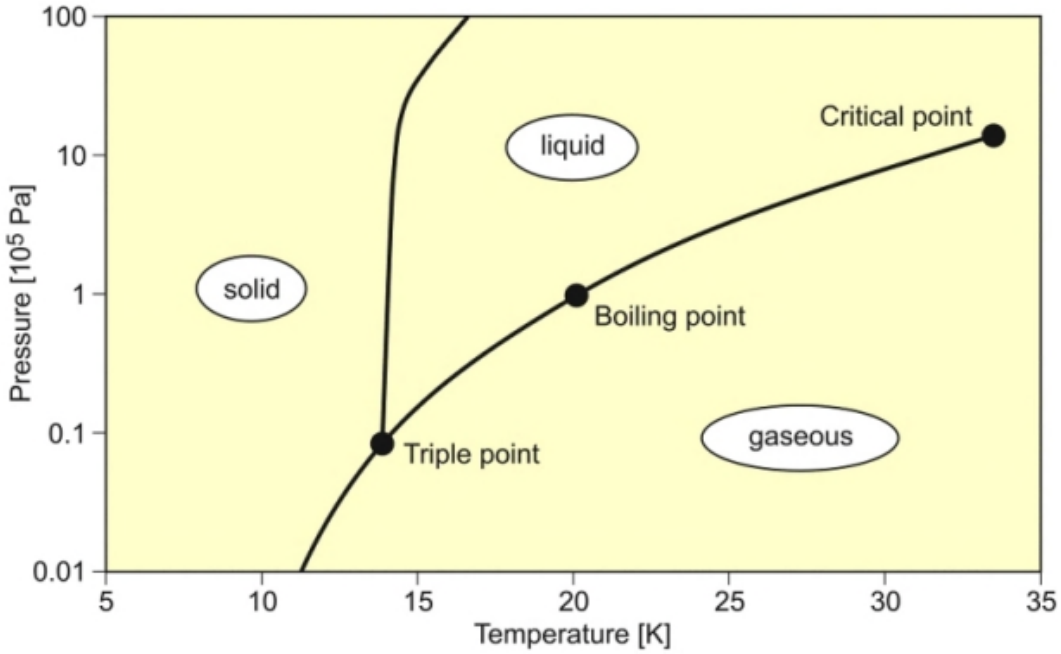

Figure 31. Hydrogen phase diagram [52].

Hydrogen has a very high high self-ignition temperature (858 K), but has a minimum ignition energy of only 0.02 mJ at the stoichiometric mixture of 29.5% in air. Mixed with air, hydrogen is flammable in concentrations ranging from 4% to 75%.
Depending on the mixture, a hydrogen flame can reach a temperature of 2318 K, but emits very little radiation. Its flame is therefore invisible and the radiated heat is very limited.
With a laminar burning rate that can reach 3.46 m/s the flame front speed of hydrogen flame can reach 24 m/s. However, since most flames are not laminar but turbulent, in a real case of hydrogen fire the flames can reach speeds of several hundreds of meters per second.
The detonation speed of hydrogen can reach 2000 m/s. Although the occurrence of a detonation is favored by the high speed of the flame, this is however only possible for concentrations between 18.3 and 59.0% in volume [51].

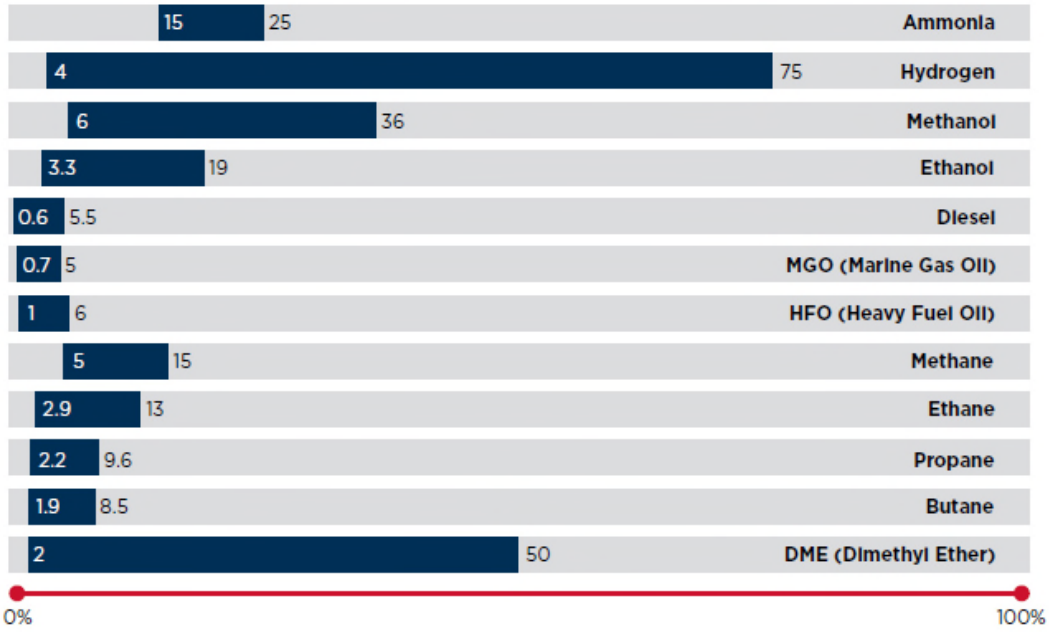

Figure 32. Typical Gas Flammability Ranges in % Volume with Air [53].

4.3.1.2 Hazards arising from the use of hydrogen in shipping

This section lists the main risks related to the use of hydrogen on board ships, comparing them, where applicable, with those of LNG.

Flammability limits:
With its high range of flammable concentrations (4–75%), hydrogen is often considered more dangerous than natural gas, which is already widely used in shipping. About 30% of all new ship orders, in fact, foresee liquefied natural gas (LNG) as a fuel [51].
Compared to the flammability limits of the main component of LNG, that is methane (5.3-15%), hydrogen has a much wider flammability range and, therefore, potentially more dangerous but, actually in the definition of the potential level of dangerousness of a gaseous substance the parameter that has greater relevance is not so much its Upper Flammable Limit (UFL) but its Lower Flammable Limit (LFL).
In a real scenario, in fact, the gas will escape from the system into the surrounding air due to the overpressure in the gas system. On the other hand, fotr the same reason, it is extremely unlikely that

the opposite will occur, that is, it is unlikely that air will penetrate the system. The gas from the leak will then rapidly diffuse into the environment and its concentration will increase until the LFL is reached. All onboard safety systems, such as gas detection and ventilation, are designed to prevent the atmosphere from reaching the LFL. The LFL of hydrogen of 4% is very close to the LFL of methane of (5.3%), therefore their ignition risk is similar [51].

Ignition energy:
Hydrogen has a self-ignition temperature of 858 K and a minimum ignition energy of 0.02 mJ, while methane has a self-ignition temperature of 813 K and a minimum ignition energy of 0.29 mJ. The self-ignition temperatures are very similar, but the minimum ignition energy is significantly lower for hydrogen.
Even in this case, however, the difference in the level of danger of the two substances appears less marked if we consider that a weak ignition source such as the electrostatic discharge generated by a human body contains about 10 mJ, s and is therefore already able to ignite both gases [51].

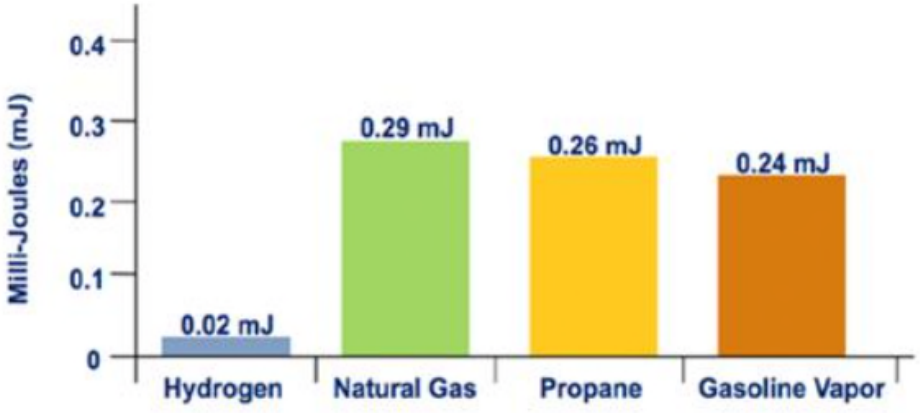

Figure 33. Self ignition energy [54].

Fire detection systems:
As already mentioned, the hydrogen flame emits little radiation and is therefore invisible. This makes it difficult to choose the components suitable for the realization of on-board fire detection systems. Usually, infrared (IR) flame detectors are used in these safety systems. Since hydrogen flames emit mainly ultra-violet (UV) radiation, IR sensors cannot be used to detect a hydrogen flame. However, even pure UV sensors are not equally suitable for detecting the hydrogen flame, as it is potentially subject to false alarms from other UV sources, such as the sun. To prevent false alarms, multi-spectrum infrared (MIR) sensors are typically used which use a combination of software analysis and IR filters to detect hydrogen flames [51].

Explosive limits:
Another risk related to the use of gaseous fuels on board is that of "explosions" (with the generic term "explosions" we mean both explosions and detonations). Similarly to what happens for flammability, the concentrations in which a gas can explode are given in a range between its Lower Explosive Limit (LEL) and its Upper Explosive Limit (UEL). Again, the lower limit is the most relevant, because safety systems are designed to prevent the atmosphere from reaching the lower limit. At room temperature hydrogen is explosive in the range of 18.3 to 59.0% by volume, while methane has a range of 6.3 to 13.5% by volume [55]. Again, hydrogen has a wider risk range, due to its wider explosion limit. However, methane reaches its LEL much earlier than hydrogen, thus posing a greater danger when an explosive atmosphere builds up in the air.

Hydrogen embrittlement:

Due to their small size, hydrogen molecules can easily diffuse into other materials. In particular, contact with hydrogen and ferritic steels constitutes a danger to be considered for its use on board ship. The hydrogen permeating the ferritic steel will cause the so-called hydrogen embrittlement. The different behavior of brittle and ductile materials is shown in the stress-strain diagram of Figure 34.

In engineering, it is usually preferable for a material to have a ductile behavior, because in this way a component undergoes a plastic deformation before breaking. The onset of plastic deformation in a component can be identified visually or as a result of the onset of vibrations or friction. This offers the possibility of intervening before a complete failure occurs. A fragile component, on the other hand, suddenly fails, without the possibility of preventing a failure. Austenitic steels, copper and aluminum are not subject to hydrogen embrittlement [51].

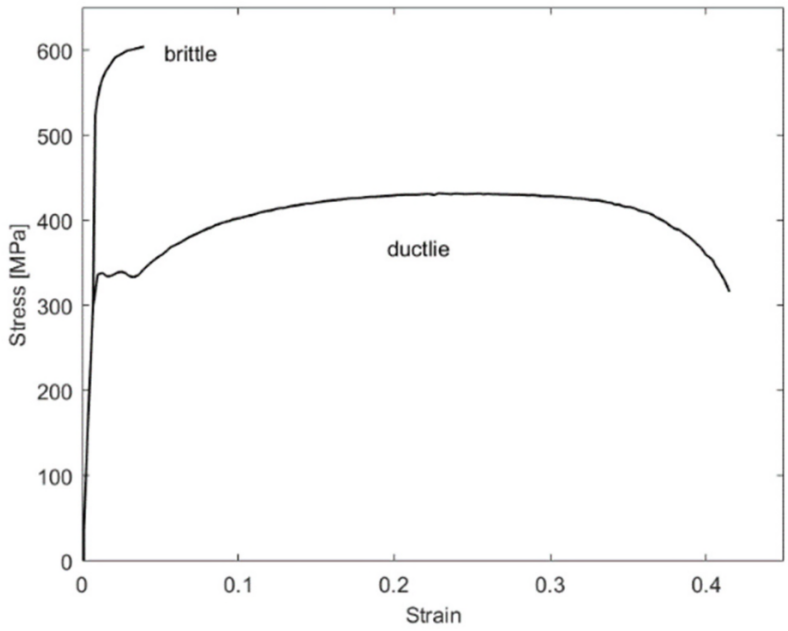

Figure 34. Brittle vs. ductile behavior in materials [51],

Buoyancy:

Being 14 times lighter than air, hydrogen rises rapidly into the air. If a leak occurs in an open space, this high level of buoyancy is an important safety feature: the hydrogen will rapidly disperse and dilute below the LFL.

Within confined spaces, the high buoyancy of hydrogen must be considered when designing safety systems. The sensors must be positioned above possible leak points or at the highest point of the room if it is a confined space.

The ceiling of the spaces containing hydrogen must be designed in such a way as to avoid its accumulation (for example by slightly sloping the ceiling), and the ventilation exhaust ducts/outlets should be always placed in the highest point in the room. Natural gas, on the other hand, is 8 times heavier than hydrogen, but still 2 times lighter than air, so in the event of a leak it will tend to rise and disperse too, but it will take longer than hydrogen to diluite below its LEL [51].

Toxicity:
Pure hydrogen is not toxic. At very high concentrations in air, hydrogen is a asphyxiant gas because of its ability to displace oxygen and cause hypoxia. Hydrogen-induced asphyxiation may occur at lower hydrogen concentrations when oxygen concentrations are also reduced as onboard a submarine [56]. When the oxygen concentration in the air falls below 16%, the first effects of hypoxia begin to be noticed, such as an increase in respiratory rate. Oxygen concentrations below 7% lead to death.
However, hydrogen concentrations needed to induce hypoxia even in a low-oxygen environment would far exceed the explosive limit of the gas. Thus, occupational exposure standards are set on the basis of the explosivity of hydrogen rather than its toxicity [56].
Although hydrogen is an odorless, colorless, and tasteless gas, high concentrations can be detected by the voice becoming high-pitched and shrill, such as from inhaling helium [51].
No carcinogenic effects from hydrogen are known.

Gas detection:
There are several types of hydrogen sensors available. Most of the sensors currently available on the market are of the electrochemical type.
For a specific application, the correct hydrogen sensor must be chosen based on the following performance parameters:

- sensitivity;
- ambient conditions;
- aging;
- drift;
- response time;
- reliability.

The combination of different types of sensors allows to compensate the limits of the single instruments. Other factors that should be considered when choosing sensors are: power consumption, physical size and cost.
The cross-sensitivity of some types of sensors should also be considered. Electrochemical hydrogen sensors, for example, usually have cross-sensitivity to carbon monoxide.
To mitigate the risks deriving from the gas and make it easily detectable by the human senses, natural gas is mixed with odors (odorization). Odorization allows natural gas to be detected in the air before it reaches dangerous levels, enabling countermeasures to be initiated, such as cutting off the gas supply, venting and evacuation of the affected area.
For hydrogen, however, this type of approach is not applicable. Fuel cells, especially those of the proton exchange membrane type, require very pure hydrogen and the odor could "poison" the fuel cell. Furthermore, the odorant molecules normally used are significantly larger than the hydrogen molecule. In some cases there may be leaks from small cracks, sufficient for the passage of hydrogen but too small for the passage of odor. Therefore, if not detected, a dangerous hydrogen atmosphere could still form [51].

4.3.1.3 Hydrogen for transport and shipping: advantages and drawbacks

Hydrogen as a future energy carrier for transport and shipping has numerous advantages. One of the main is that it can be produced from a variety of primary resources, many of which are easily accessible and available almost anywhere in the world. Another important advantage of hydrogen over other fuels is that it does not produce CO_2 or other GHG: its only oxidation product is water [57].
The main industrial technologies used for the production of hydrogen will be examined in 4.3.2 with particular focus on the production of hydrogen by electrolysis.

The main disadvantage of using hydrogen as a transport fuel is the volume occupied by the on-board storage tanks, which are necessary due to its very low density.
Hydrogen can be stored on board a vehicle or ship as a compressed gas, as a liquid in cryogenic containers or adsorbed in metal hydrides. However, due to the low density, compressed hydrogen for the same volume will not be able to provide autonomy comparable to that of traditional fossil fuels. Hydrogen reaches its highest volumetric energy density when adsorbed in metal hydrides, but the weight of the latter makes this solution not viable on heavy vehicles or ships.
To make clearer the energy differences, Table 10 provide as an example a comparison between various forms of hydrogen and diesel fuel.

Energy content of:	is equivalent to:
1·Nm^3 of gaseous hydrogen	0.30 liters of diesel
1 liter of liquid hydrogen	0.24 liters of diesel
1 kg of hydrogen	2.79 kg of diesel fuel

Table 10. Comparison of hydrogen and diesel fuel energy densities [58].

Comparing liquid hydrogen with diesel, the advantage of liquid hydrogen is that it stores approximately 2.8 times more energy per unit mass than diesel (Table 9), meaning that liquid hydrogen is more energy efficient than gasoline.The disadvantage is that it needs an estimated 4 times more volume than diesel to store the same amount of energy.
The most widespread technologies to date for the storage of hydrogen on board ships will be examined in 4.3.3.

4.3.2 Hydrogen production

Hydrogen can be produced by different processes: thermochemical, electrochemical, photochemical, photocatalytic or photoelectrochemical.
Figure 35 shows the main alternative methods of hydrogen production from energy sources.

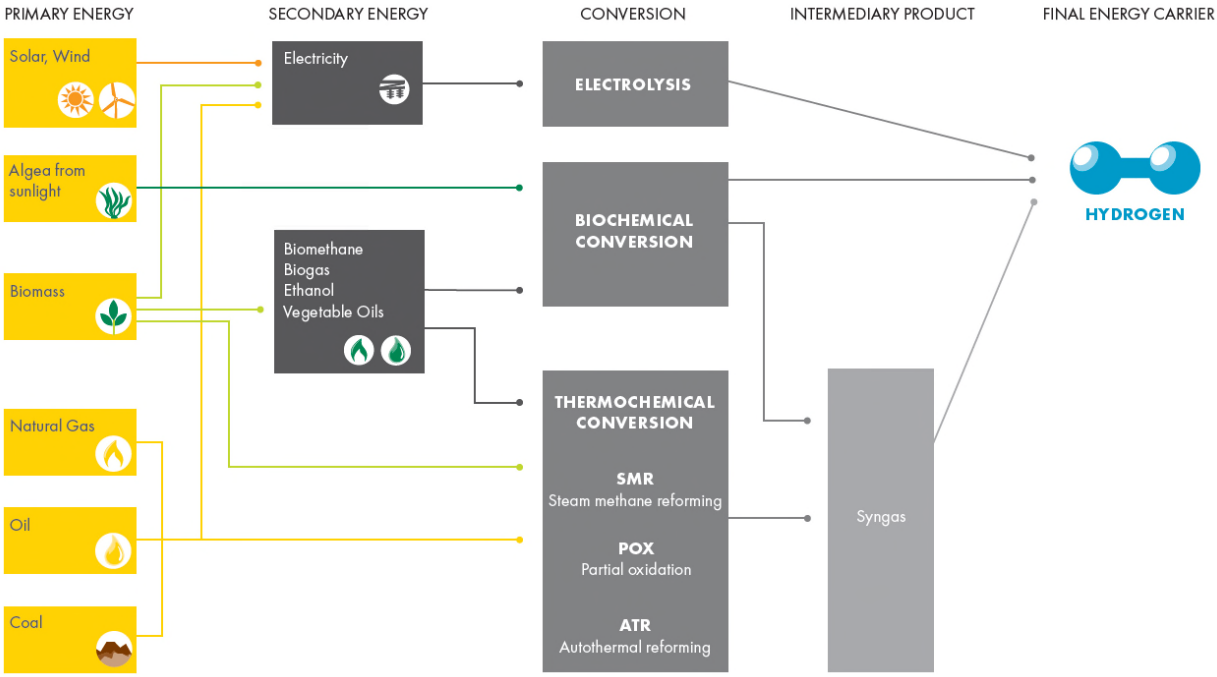

Figure 35. Processes for hydrogen production. [59]

More than 95% of the current production of hydrogen is based on the use of fossil fuels [60]. Today, hydrogen is mainly produced by two thermochemical processes: the Steam Reforming of Methane (SMR) and the Partial Oxidation (POX) of hydrocarbons. Among these two processes, the most widespread worldwide is SMR [57].
In an SMR reactor, methane is reacted reacting with steam in the presence of a catalyst. The gaseous flow leaving the reactor is mainly composed of hydrogen, carbon monoxide and carbon dioxide. Then, by means of a reaction called "water-gas shift reaction", the carbon monoxide leaving the SMR reactor is reacted with more steam in the presence of a catalyst to produce additional hydrogen and carbon dioxide. In the final stage of the process, the streams of carbon dioxide and gaseous hydrogen are separated. [61].

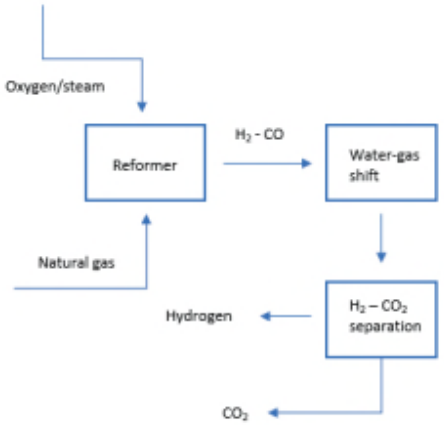

Figure 36. Hydrogen by gas reformation. [61]

The POX process is similar to the SMR process but uses pure oxygen instead of steam as an oxidant.
In a recent study on the possible introduction of hydrogen into the British gas distribution network, Auto Thermal Reforming (ATR), which uses a mix of steam and oxygen as an oxidizer, was considered a better solution than SMR, both in terms of investment costs, both in terms of size and ability to capture CO_2 [61].
The gasification of oil and coal are still widely used in some geographical areas, especially in China and Australia but, anyway, to a much lesser extent than in the SMR [60].
From a purely technical-economic point of view, thermochemical processes are advantageous compared to all the others as they are those that boast the highest overall efficiency (about 52% from thermal to hydrogen) and the lowest production cost [57].
As regards GHG emissions, on the other hand, the data reported in the literature relating to CO_2 emissions per kilo of hydrogen from an SMR plant vary in the range of 7-9 $kgCO_2/ kgH_2$.
To these must be added also the emissions deriving from the production of natural gas which, based on the data of US gas production, vary in the range 1-5 $kgCO_2/ kgH_2$ [61].
The largest share of hydrogen demand comes, globally, from the chemical sector where it is mainly used for the production and refining of ammonia and for hydrocracking and desulfurization of fuels. Other industrial sectors, such as steel, glass, electronics, and the production of special or bulk chemicals, also use hydrogen but their overall share is negligible compared to global demand.
Currently hydrogen produced by electrolysis, mainly with chlor-alkali processes, does not exceed about 4% of the global supply [60].

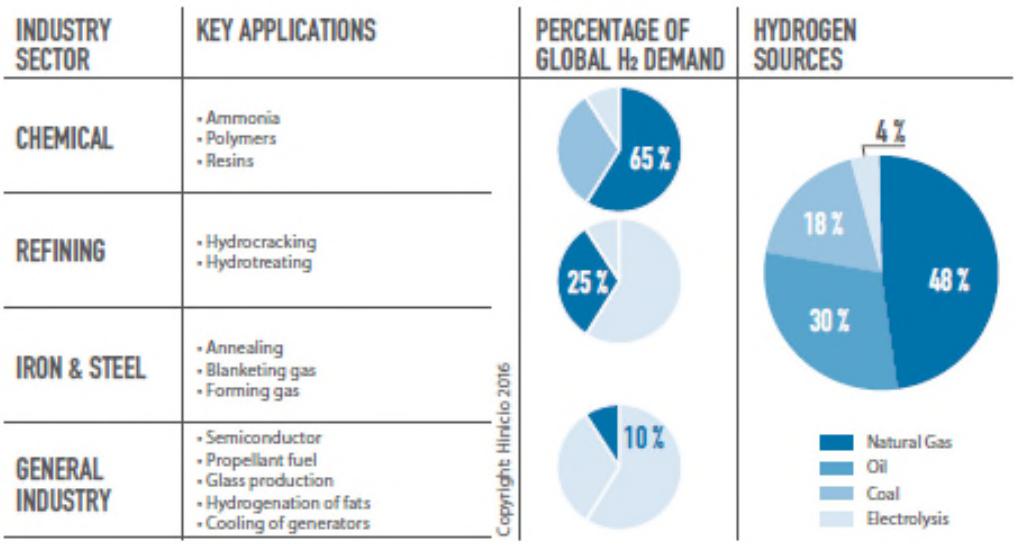

Figure 37. Global hydrogen demand and production sources. [60]

The transition from traditional carbon-based non-renewable energy sources to renewable ones is one of the most discussed and urgent themes of our times.
To achieve the goals of the Paris Agreement, the global energy system will have to undergo a radical transformation from the current polluting system based on fossil fuels to a more efficient and renewable low-carbon one.
According to the results of a recent analysis conducted by the International Renewable Energy Agency (IRENA), over 90% of the global reductions necessary to achieve the objective of reducing CO_2 emissions could derive from the transition to this new energy system.
In the analysis, IRENA, taking as a Reference Case the path traced by current plans and policies, defines a new roadmap (REmap) to rapidly increase renewable energies in the coming decades. The

study predicts that renewable energy alone will contribute 41% to the required reduction in emissions and an additional 13% of reduction can be achieved through electrification [60].
To achieve this, the renewable energy share of Total Final Energy Consumption (TEFC) will need to grow from the current 18% to around 65% by 2050. The results are summarized in Figure 38 which compares the share of renewable in TFEC for transport, industry and building and electricity under the Reference Case and REmap.

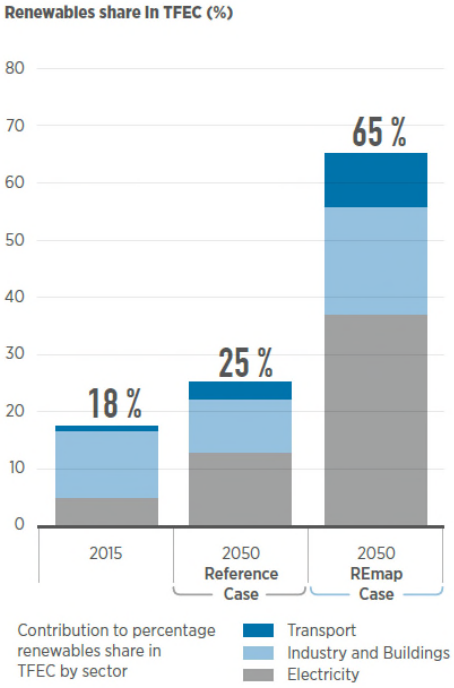

Figure 38. Share of renewables in total final energy consumption under the Reference Case and REmap. [60]

Renewable energy installed power capacity in 2019 grew more than 200 GW, establishing a record for the largest increase of capacity deployed in a year. Although over a five-year span Renewable Energy Sources (RES) represented less than one-third of the global energy growth, their installation rate was anyway higher than fossil fuel-based plants and nuclear ones. [62]
While renewable energy sources are progressing in the power generation sector, the transportation and industrial sectors continue to depend highly on traditional carbon-based fuels.
One of the main reasons for the difficulty of penetration of RES in these sectors is the fact that most of them, such as solar or wind, are not entirely and directly dispatchable as they are intermittent and therefore unable to meet load requirements, especially if highly variable. To overcome these obstacles, Energy Storage Systems (ESS) must be employed. Among the different energy storage systems, storing renewable energy in chemicals, like hydrogen, can bring numerous benefits like high energy density, seasonal storability, possible cost reduction of the final product, and the potential to expand renewable power exploitation. In the last years, the production of this gas from renewable energy sources via electrolysis has grown its reputation as one feasible solution to satisfy future zero-emission energy demand. This production process is often called Power-to-Gas and is considered the most cost-efficient solution for long-term energy storage. It is beneficial because it can connect electrical power and gas networks and can help the diffusion of zero-emission energy sources in sectors like heat production, transportation, and heavy industries [62].
In this context, water electrolysis can be the key enabling technology for this type of energy storage. Alkaline, Proton Exchange Membrane (PEM), and the latest solid oxide electrolysers are the main commercially accessible technologies today on the market. Alkaline Electrolyser Cells (AEC) have been in commercial use in industrial application since the 1920s and can be considered as the most mature electrolyser technology available today [62].

4.3.2.1 Alkaline Electrolysis

Like fuel cells, alkaline electrolysers are provided with stacks of cells, each composed of two electrodes, an anode and a cathode, separated by an electrolyte [63]. An alkaline solution of sodium hydroxide (NaOH) or potassium hydroxide (KOH) in water is used as electrolyte while electrodes are in most cases manufactured of steel covered with a nickel coat. AEC is a mature technology and these types of electrolysers have been working even for decades. Alkaline electrolysers with kilowatt scale have been integrated to get up to megawatt capacities, letting them be considered as the main option to produce large quantities of hydrogen. Their working principle is illustrated in Figure 39.

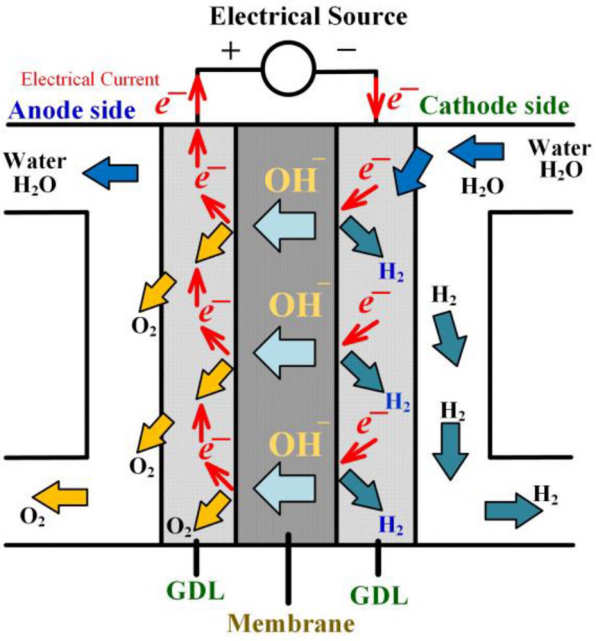

Figure 39. Alkaline Electrolyser Cell (AEC) working principle. [63]

When a DC voltage is applied between the two electrodes of an AEC (typically between 1.8–2.0 V), water molecules in contact with the cathode acquire electrons to form hydroxide (OH^-) ions and release H_2 molecules according to the Hydrogen Evolution Reaction (HER):

$$2\,H_2O + 2e^- \rightarrow H_2 + 2\,OH^- \quad (27)$$

The OH^- ions migrate through the electrolyte to the anode where, with the release of electrons, H_2O and O_2 are produced according to the Oxygen Evolution Reaction (OER):

$$2\,OH^- \rightarrow \frac{1}{2}\,O_2 + H_2O + 2e^- \quad (28)$$

In the AEC, the recombination of the hydrogen and oxygen produced at the electrodes is avoided by a separator (typically made of ceramic material), placed between the two electrodes. Typical hydrogen output pressure is between 1 bar g and 30 bar g [62].
To highlight the strength, weakness, opportunity, and threat of alkaline technology, the results of a (SWOT) analysis performed on AEC are presented in [63]. The outcome of the analysis is summarized in Table 11.

AEC Electrolysers SWOT analysys
Strenght
Low cost (due to cheaper materials such as Nickel (Ni)).
High lifetime and gas purity.
High hydrogen production capacity (up to 3880 Nm^3h^{-1})
Low specific energy consumption
Weakness
Limited current density (0.2-0.7 Acm^{-2})
Frequent maintenance (due t the use of a liquid electrolyte solution)
Limited production capacity dynamic range (15-100%)
Opportunities
Increase in the use of non-precious materials (Co, Fe, Mn, Cr, Cu and Zn) conbined with Ni to enhance performance.
Designin spacing electrodes to optimize hydrogen production.
Dissemination of low carbon footprint by hydrogen production plants supplied by renewable and nuclear sources.
Threats
Growing development of PEM water electrolysis technology due to its benefit (high current density and efficiency, large production capacity and dynamic range, low maintenece)
Lackof hydrogen refueling stations close to the hydrogen production units.

Table 11. AEC Electrolysers SWOT analysis. [63]

Although alkaline technology has numerous strengths, it nevertheless has several weaknesses such as limited current density, frequent maintenance and limited dynamic range of hydrogen production. In any case, the study [63] highlights that there are still opportunities to improve the performance of the technology such as: the use of new materials and the implementation of an improvement in the stacks design.

Among the factors that most influence the efficiency of AEC electrolysers, one of the most important is the chemical formulation of the electrolyte. This, in fact, significantly affects the electrical resistance of the electrolysis cell. Furthermore, by using an electrolyte with a high degree of purity it is also possible to prevent unwanted side reactions [64].

Another factor that influences the efficiency is the temperature at which the chemical reactions occur in the cell. Experimental results show that with increasing temperature the AECs exhibit a lower splitting reaction potential, a reduced electrical resistance of the electrolyte, a greater activity of the electrode surface and, ultimately, a higher efficiency [64].

Pressure also affects the efficiency of AECs. The increase of the process pressure increases the cell efficiency thanks to the reduction of the volume of the gas bubbles generated at the electrodes. This reduction in the size of the bubbles increases the effective contact area between the electrodes and the electrolyte thus reducing the ohmic resistance and the voltage required by the cell for its operation [64].

The physical configuration of the electrolysis cell is certainly a further key factor that influences the behavior of the process and the efficiency of an AEC.

The physical parameters that have the greatest influence on cell performance are the distance between the electrodes, their size, their alignment and their shape.

Cells with large-area and parallel-arranged electrodes dissipate less power and are more efficient. However, for this type of cells there are optimal distance values and the height of the electrodes that must be respected to guarantee the best performance [64].

Innovative technologies and materials also play a key role in improving the electrochemical activity of the electrodes and reducing the ion and mass transfer resistance of the separator plate.

Regarding electrolyser's efficiency, report [42] specifies the state-of-the-art values of large-scale alkaline electrolysers and the future targets set by the European Community Fuel Cells and Hydrogen 2 Joint Undertaking (FCH 2JU). These values are shown in Table 12 and Table 13 respectively.

Electricity Consumption @ Nominal Capacity [kwh/kgH_2]	
State-of-the-Art	
2012	2017
57	51

Table 12. Large-scale alkaline electrolysers electrical energy consumption per each kilogram of hydrogen produced at nominal capacity. State of the art. [42]

Electricity Consumption @ Nominal Capacity [kwh/kgH_2]		
FCH 2JU Target		
2020	2024	2030
50	49	48

Table 13. Large-scale alkaline electrolysers electrical energy consumption per each kilogram of hydrogen produced at nominal capacity. EU targets. [42]

The key performance metrics of different alkaline electrolysers models available on the market is reported in Table 14.
With reference to Table 14, the average specific energy consumption is 57.6 kWh/kgH_2. The data reported in Table 14 therefore confirm the values presented in Table 12 and Table 13 and extend their field of applicability also to medium and small size electrolysers.

Table 14. List of electrolysers available on the market (not exhaustive) with key performance metrics [62]

Company	Country	Type	Model	Capacity [Nm^3/h]	H_2 Output Pressure [bar g]	H_2 Purity [%]	Electrical Consumption [kWh/kgH_2]	HHV Efficiency [%]
Acta	Italy	AEM	EL1000	1	29	99.94	53.2	74%
Angstrom Advanced	USA	PEM	HGH170000	10	4	99 to 99.9999	64.5 [1]	61.4% [2]
Elogen (ex AREVA H_2 Gen)	France	PEM	ELYTE 10	10	30	99.999	47.8–60.0 [1]	65.6%–82.4% [4]
Enapter (ex Acta)	Italy	AEM	EL 2.1	0.5	35	99.9	53.3 [1]	73.9% [4]
Erredue	Italy	PEM	SIRIO 200	2	15 (Opt. 30)	99.99	53.3 [1]	73.9% [4]
GreenHydrogen	Denmark	PEM	HyProvide P1	1	50	>99.995	61.2 [1]	64.9% [2]
H-TEC SYSTEMS	Germany	PEM	EL30/144	3.6	29	N/A	55.4	71.1%
Idroenergy	Italy	Alkaline	mod. 8.0	5.33	4	>99.5	62.5 [3]	63.0% [4]
ITM Power	UK	PEM	HGAS3SP	3.2	N/A	99.999	N/A	N/A
Nel Hydrogen	Norway	PEM	H6	6	15 (Opt. 30)	99.9995	75.5 [1]	52.2% [4]
Pure Energy Centre	UK	Alkaline	4Nm^3	4	Up to 12	>99.3	62	63% [4]
Sagim	France	Alkaline	M5000	5	7	99.9	55.6 [1]	70.8% [2]
Teledyne Energy Systems	USA	Alkaline	NH–450	450	10	N/A	65.6 [1]	60.2% [2]

[1] Data obtained by conversion from kWh/Nm^3 to kWh/kg using a hydrogen density of 0.09 kg/Nm^3.

[2] Data obtained by conversion from an efficiency given on a hydrogen Lower Heating Value (LHV) basis.

[3] Data calculated by authors from production rates and maximum electrical consumption stated in data sheets.

[4] Data calculated by authors from the electrical consumption.

4.3.3 Hydrogen storage technologies for the shipping sector

The most widespread and tested hydrogen storage methods to date both in the industrial and transport sectors are essentially "physical storage" methods based on the compression of hydrogen on its cooling or on a combination of both processes. Many other new hydrogen storage technologies are also currently under study or research. These technologies can be grouped under the name of a collective of "material-based storage" technologies which involve the chemical storage of hydrogen by absorption in solids and liquids or its adsorption on surfaces.

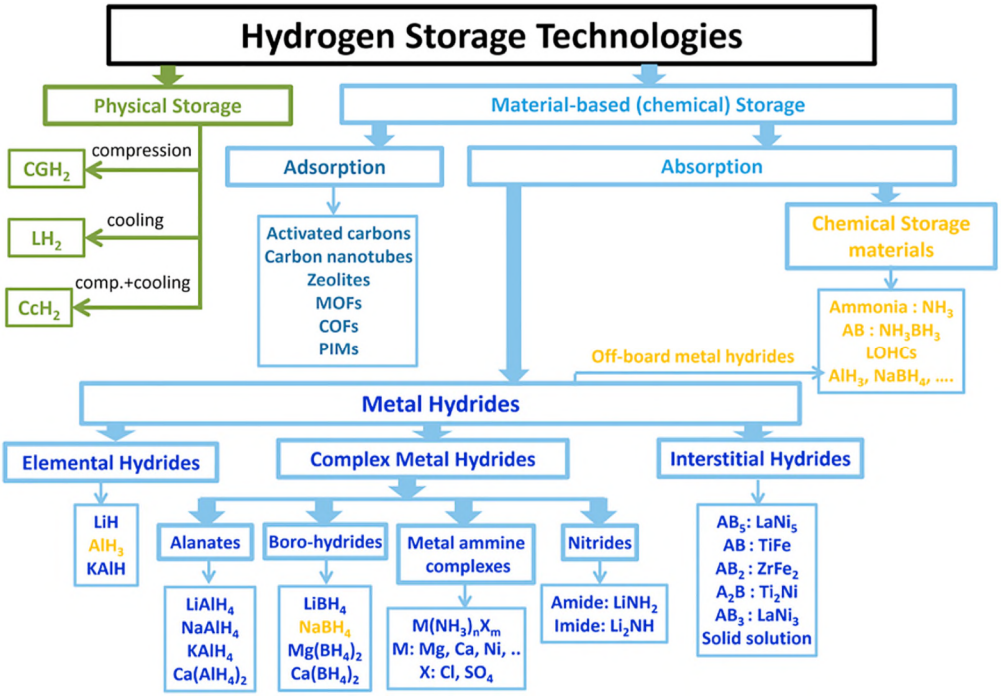

Figure 40. Hydrogen storage technologies. [65]

The "physical storage" of hydrogen is also the most used in the maritime transport sector. If we analyze all the "operative" projects (i.e. projects in which the ship/pilot plant has successfully operated at sea at least once or where the ship is currently under construction) and "non-operative" projects (projects not yet moved from the design phase to the experimental phase or those that have not yet completed the test program) developed from 2000 onwards [45], it can also be noted that the systems of the most widespread "physical storage" of hydrogen are essentially two: compression (CH_2) and liquefaction (LH_2).

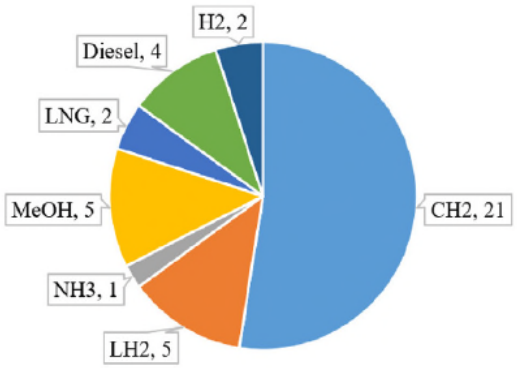

Figure 41. Fuels and hydrogen storage technologies used in the fuel cell surface ships "operative" projects developed since 2000 [45]

4.3.3.1 Compressed hydrogen

The mechanical compression of gaseous hydrogen is mainly based on the use of reciprocating compressors. Reciprocating compressors are best suited for plants characterized by moderate flows and high pressures and can bring to high efficiencies particularly when a multi-stage configuration is employed. In addition, they offer good flexibility in size and capacity. Oil-free reciprocating compressors are preferred because they can bring good performances and high-purity compressed gas [62].

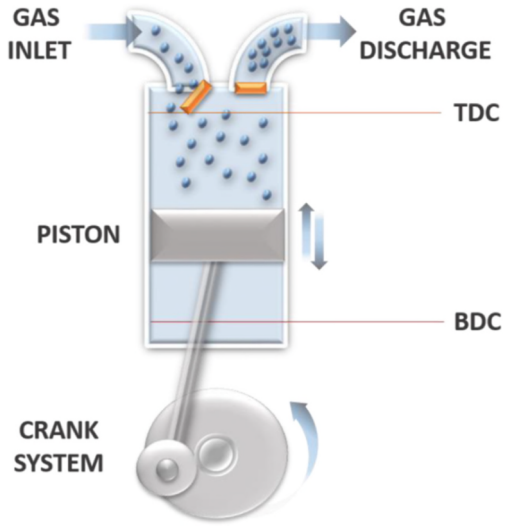

Figure 42. Single stage reciprocating piston compressr (TDC = Top Dead Centre, BDC = Bottom Dead Centre). [66]

In literature, different works deal with hydrogen production, compression, and storage systems, especially when considering hydrogen refueling stations. In [67], in order to study the effect of combining different renewable energy sources with energy storage on grid stability, the characterization of a hydrogen production and storage system composed of a 1.33 Nm^3/h ,2.5 bar outlet pressure alkaline electrolyser and an air-driven reciprocating compressor is presented. The study focuses, in particular, on the system control strategy.
The development of a hydrogen refueling station design tool is described in [68]: a Simulink model is created consisting of an electrolyser, a compressor, a storage tank, a dispensing unit, and a vehicle that consumes the hydrogen fuel. Simulation results in terms of time predictions to refill storage tanks and station operational cost are compared with three different existing hydrogen refueling stations. In [69], a data collection and analysis on different existing hydrogen refuelling stations is presented. Amongst the different presented data, average electrolyser and hydrogen compression performances are shown. However, no data is available regarding hydrogen refueling station design in terms of electrolyser and compressor technology. In [70], the compression section of a hydrogen refueling station has been studied: experimental data from over 20000 compression cycles were used to build a simulation tool of an air-driven hydrogen booster. This equipment is used to increase the hydrogen pressure from 200 to 500 bar g. Some interesting data on compressor-specific energy consumption are presented. In [71], a hydrogen compression system powered by renewable energy sources is described. The system has a specific energy consumption that varies from 4.4 to 9.3 kWh/kgH_2. However, compression ratios considered are different from the study presented in this article because the hydrogen compression system described in [71] is characterized by an inlet pressure decreasing from 200 to 120 bar g, and outlet pressure of the storage of 450 bar g.
Report [72] is focused on compressor's efficiency in hydrogen refueling stations.
The report highlights a specific energy consumption of about 10 kWh/kgH_2 for the considered pressure range (4.6 to 200 bar g).

Five different types of tanks have been developed and are currentely used to store hydrogen in a pressure range from 100‑200 bar g (10-20 MPa) up to to 700 bar g (70 MPa).
The different types of tanks are indicated with progressive Roman numerals (I, II, III, IV and V) corresponding to an increasing level of complexity of the tank design.

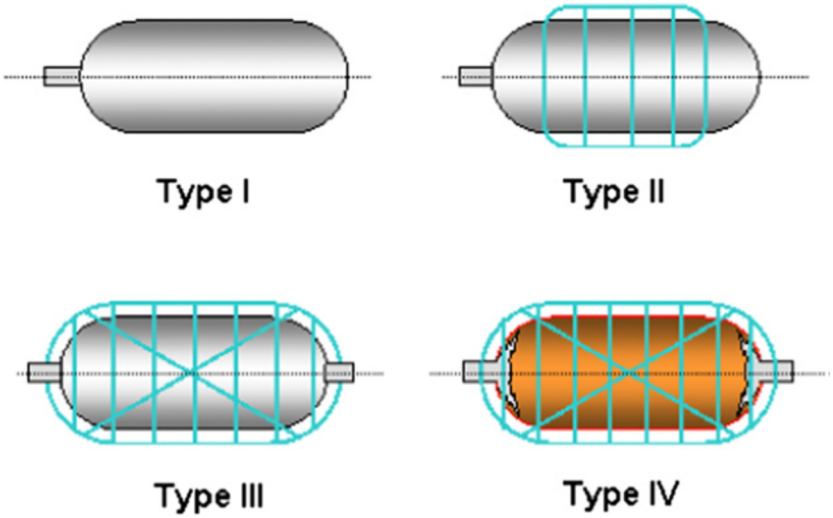

Figure 43. Schematic representation of hydrogen tanks types I, II, III and IV. [73]

- Type I pressure vessels are full metallic;
- Type II are based on the Type I vessels, but are provided with a polymer liner wrapped around a metallic tank, but with the polymer liner wrapped around the cylindrical part of the vessel only;
- Type III are based on the type II vessels with the metallic liner fully wrapped with the composite fibre for support:
- Type IV pressure vessels consist of a polymeric liner fully wrapped with composite fibres;
- Type V pressure vessels are made only with composite fibers without any liner (Figure 44).

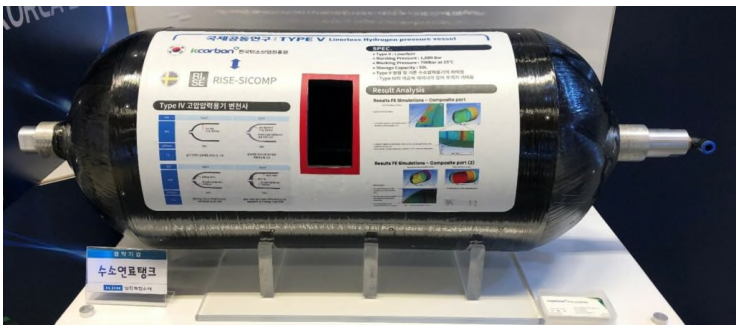

Figure 44. Type V linerless hydrogen tank prototype. [74]

The most common types of pressure vessels for hydrogen storage (or gas storage in general) in the pressure range 20‑30 MPa are the type I metallic pressure vessels.
Type II tanks are lighter than type I tanks and can withstand only pressure up to 20 MPa. The gravimetric storage capacity (hydrogen storage mass per tank weight) of a type II tank is anyway higher than for type I, 2.1 wt% vs. 1.7 wt%. Type III, IV and V are desigend for higher pressures: up to 70 MPa for type III and IV and above (up to 80 MPa) for type V.
The type IV storage vessels have reported gravimetric capacities of 5.7 wt% and are currently used to store hydrogen in fuel cell-powered cars such as the Toyota Mirai [75]. This higher storage capacity

for hydrogen is translated into an almost ten times increase in cost per kilogram of hydrogen stored when compared to cheaper low pressure vessels [76].

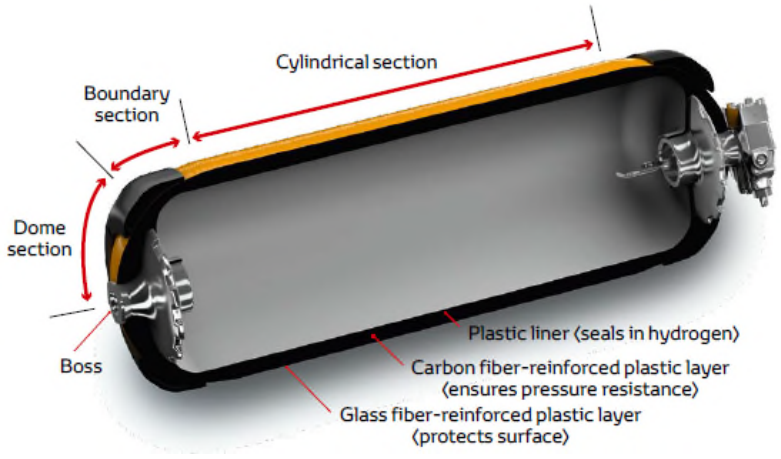

Nominal working pressure	70 MPa (700 bar)
Tank storage density	5.7 wt%
Tank internal volume	122.4 L (front tank: 60.0 L, rear tank: 62.4 L)
Hydrogen storage mass	Approx. 5.0 kg

Figure 45. Toyota Mirai Type IV storage tank specifications. [75]

The main features of the various types of hydrogen tanks are summarized in Figure 46.

<table>
<tr><td colspan="3">Type</td><td>I</td><td>II</td><td>III</td><td>IV</td><td>V</td></tr>
<tr><td colspan="3">Schematic</td><td></td><td></td><td></td><td></td><td></td></tr>
<tr><td rowspan="6">Components and related failures</td><td rowspan="2">Metallic</td><td>part</td><td>Fully metallic</td><td>Metallic enclosure</td><td>Metallic liner</td><td>Boss</td><td rowspan="2">-</td></tr>
<tr><td>Failure</td><td colspan="4">- Hydrogen Embrittlement, mechanical properties degradation and premature cracks.
- Premature failure for fatigue for metal liner and liner damage[α].
Reason: contact between metal and Hydrogen, surface impact[α].</td></tr>
<tr><td rowspan="2">Composite</td><td>part</td><td rowspan="2">Not applicable</td><td>Some fibre over-wrap</td><td colspan="2">Full composite over-wrap</td><td>Fully composite</td></tr>
<tr><td>failure</td><td colspan="4">Fibber breaks, delamination and matrix cracking, composite thickness decrease.
Reason : accidental mechanical impacts and subsequent pressure loads.</td></tr>
<tr><td rowspan="2">Polymer</td><td>part</td><td colspan="3" rowspan="2">not applicable</td><td>Polymer liner</td><td rowspan="5">Under consideration</td></tr>
<tr><td>failure</td><td>Permeation, leakage
Reason : contact between polymer and H_2 charge/discharge conditions</td></tr>
<tr><td colspan="3">Pressure limit</td><td>≤ 50 MPa</td><td>Not limited</td><td>≤ 45 MPa</td><td>≤ 100 MPa</td></tr>
<tr><td colspan="3">Vessel price</td><td>++</td><td>+</td><td>-</td><td>-</td></tr>
<tr><td colspan="3">Gravimetric capacity wt. % or tank mass</td><td>-</td><td>±</td><td>+</td><td>++</td></tr>
<tr><td colspan="3">Popularity & maturity</td><td>****</td><td>**</td><td>*</td><td>*</td></tr>
</table>

Figure 46. Tanks for compressed hydrogen. Main features summary. [65]

A fundamental aspect to consider when choosing the fuel of the future for shipping is the ease with which it can be embarked and managed on board.
With compressed hydrogen the storage difficulties are twofold. As already seen, cylinder storage has a limited gravimetric storage capacity. Therefore, on-board arrangement of the hydrogen storage system will require large volumes on the decks or in the hold of the dedicated cylinder store.
Another problem that cannot be overlooked is the slow bunkering time resulting from the transfer of a low-density gas [76].
For the automotive industry, a specific gas supply protocol has been developed by the Society of Automotive Engineers (SAE) for refueling hydrogen at 70 MPa (SAE J2601 protocol). The protocol stipulates that the hydrogen is first cooled to -40 ° C and that the feed rate is limited to approximately 1 kg of hydrogen per minute. For safety reasons, in fact, with type IV polymeric tanks the gas temperature must not exceed 70 ° C. It is therefore necessary that the bunkering is carried out slowly and with refrigerated gas. This protocol is well suited for operations in the automotive industry were 1 kg of hydrogen corresponds to a driving range of around 100 km. [76]. For a standard 70 MPa Fuel Cell Electric Vehicle (FCEV), the SAE J2601 refueling protocol ensures that a state of charge equal to 90-100% of the vehicle's nominal storage capacity (defined at nominal operating pressure and 15 ° C) is reached in approximately 3 min refueling at a T40 filling station (hydrogen pre-cooled to -40 ° C) [77].

Parameter	Limit
Minimum gas temperature	-40 °C
Maximum gas temperature	85 °C
Minimum dispenser pressure	0.5 MPa
Maximum dispenser pressure (70 MPa Nominal)	87.5 MPa
Maximum flowrate	60 g/s

Table 15. SAE J2601 performance and safety limits for hydrogen vehicle tank fueling. [77]

For the Oakney Island ferries, a compressed hydrogen bunkering system has been described and assessed for safety in [78]. This project opted for the storage of hydrogen at 35 MPa instead of 700 MPa. The total bunkering plant was sized at 2 MW or 800 kgH_2 per day.

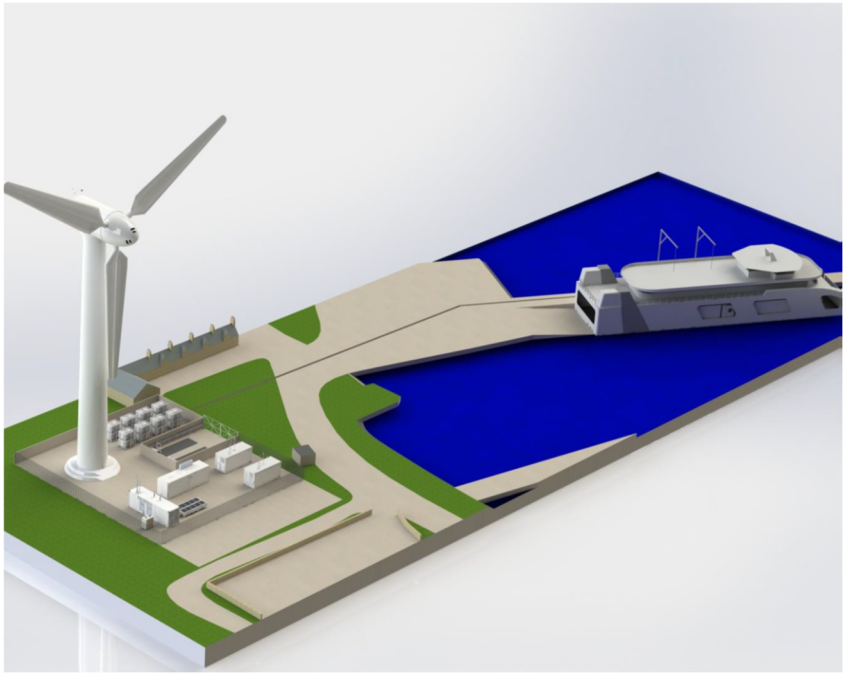

Figure 47. Layout of the site containing the site for the hydrogen equipment, pipeline and dispensing equipment on the harbour. [78]

A large seagoing vessel will require several hundred tons of hydrogen for its operation. If its refueling were conducted at peak performance of the plant described in the study, this would require several weeks or more plants operating simultaneously. From a technical, economic and safety point of view, this approach does not therefore seem to be applicable to large ships.
A different approach to compressed hydrogen bunkering is that which involves the use of hydrogen tanks installed in standard 20 or 40 foot containers, which can be loaded onto a ship and disembarked once used.
However, this solution also seems suitable only for small or medium-sized vessels such as ferries. For large ships, however, the time required to load and unload all these containers would drastically lengthen the time spent in port [76].

4.3.3.2 Liquid hydrogen

The maritime sector is gaining experience with cryogenic fuels thanks to the now widespread use on board of LNG. However, the use of liquid hydrogen in shipping is technically much more challenging than LNG as liquid hydrogen is about 90 °C colder than LNG, furthermore its density and specific heat capacity are lower than those of LNG.
Despite the different physical properties between the two cryogenic fluids, what has been learned and developed for the use of LNG on board the ship will in any case constitute the basis of the know-how for the potential future use of liquid hydrogen.
Liquid hydrogen management has also been developed in other sectors, such as aerospace, where liquid hydrogen is commonly used as a fuel [76].
After cooling, the hydrogen must be stored at temperatures below the boiling point (-253 °C). For this purpose, tanks made with super insulating materials and spherical in shape are used in order to minimize the surface/volume ratio of the tank. Despite this, NASA's largest liquid hydrogen tank currently in operation, located at the Kennedy Space Center and with a capacity of 3218m^3 (21 m diameter), loses over 730 m^3 [79] of hydrogen per year due to evaporative losses. NASA engineers also designed a cooling system with a liquid helium heat exchanger for a 125 m^3 hydrogen tank. They demonstrated that to achieve zero boil-off losses in the liquid hydrogen tank, the heat exchanger had to be switched on and off regularly with a 50% duty cycle (50% on time, 50% off time) [76].

Figure 48. Kennedy Space Center hydrogen tank. [79]

The automotive industry has also experimented with liquid hydrogen. Two models of hydrogen-powered cars with liquid hydrogen storage have been marketed: one is the GM HydroGen3 (2001-2006) equipped with a 4.6 kg cryogenic hydrogen tank, the other is the BMW Hydrogen 7 (2006-2008), with dual-fuel engine (petrol and hydrogen) and a 170-liter tank capable of storing about 8 kg of liquid hydrogen [76].

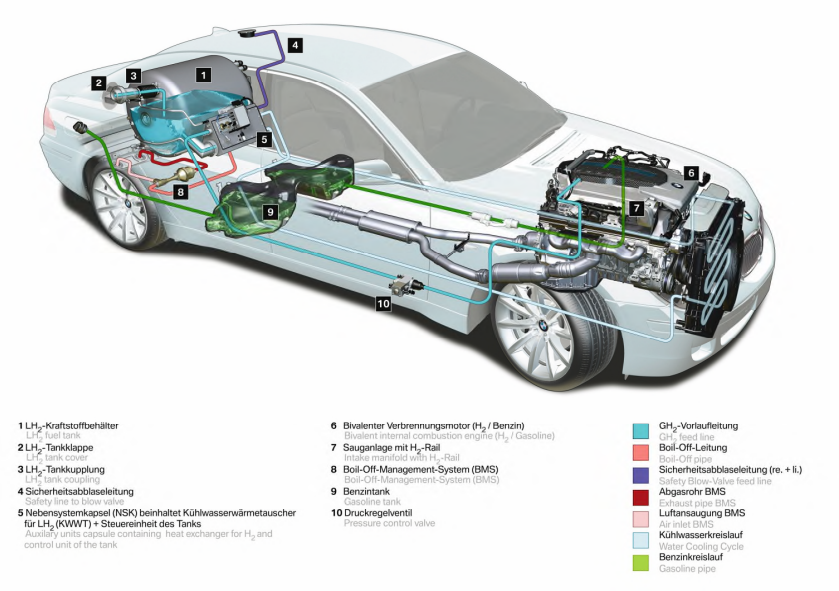

Figure 49. BMW Hydrogen 7. [80]

Liquid hydrogen has not proved to be the best storage method for the automotive sector, one of the reasons being the high energy requirement for the liquefaction of hydrogen, the other being the boil-off losses. Even using super insulated tanks, liquid hydrogen cannot be stored for more than 5 days. For hydrogen-powered ships, the boil-off phenomenon is less of a concern than stationary applications. Just like LNG carriers, ships with propulsion fueled by liquid hydrogen could also be designed to use boil-off gas as well [76]. At present, the maritime sector does not manage large-scale shipments of liquid hydrogen: liquid hydrogen is not a commodity shipped globally. There have been attempts in the past to investigate the transfer of renewable energy across the oceans in the form of liquid hydrogen which, however, never made it to the implementation stage. Recently, a first pilot LH_2 tanker ship (Suiso Frontier, IMO 9860154) has been launched by Kawasaki Heavy Industries. On December 3, 2021, Suiso Frontier became the worlds first vessel to be officially classified as a liquefied hydrogen carrier, after being registered by the General Incorporated Association Nippon Kaiji Kyokai (ClassNK). [76] [81]

Figure 50. Kawasaki Heavy Industries Suiso Frontier (IMO9860154). [81]

Suiso Frontier (IMO9860154) specifications	
Length overall	116.0 m
Length between perpendiculars	109.0 m
Molded breadth	19.0 m
Molded depth	10.6 m
Molded draft	4.5 m
Gross tonnage	Approx. 8,000 t
Tank cargo capacity	Approx. 1250 m^3
Propulsion system	Diesel electric propulsion
Sea speed	Approx. 13.0 kn
Capacity	25 persons
Classification	Nippon Kaiji Kyokai (ClassNK)
Country of registration	Japan
Ship owner	CO_2-free Hydrogen Energy Supply-chain Technology Research Association (HySTRA)

Table 16. Kawasaki Heavy Industries Suiso Frontier (IMO9860154) specifications. [82]

Most of the research relating to the use and storage of liquid hydrogen on board ships is based on the experience gained in the aerospace sector which, to date, is the only non-industrial sector in which liquid hydrogen is most used.
As previously highlighted, the main obstacles correlated with the use of liquid hydrogen in the transport sector and in particular, given the volumes managed, in the maritime one are represented by the low temperature at which the transfer and bunkering process must take place and by the evaporation of hydrogen liquid from the storage system. To solve both problems the only technically applicable solution consists in the use of specific insulating materials to minimize the technical dissipations both from the supply systems and from the on-board storage system.
The data provided by NASA on liquid hydrogen used in the space shuttle launches confirm the critical issues just highlighted. In each launch, 45% of the allocated liquid hydrogen was lost in the management process (storage, transport and refueling), even before reaching the space carrier's fuel tank. Specifically, 12.6% of the losses occurred during the transfer by truck from the production site to the large storage tank of the Kennedy Space Center, 20.6% of the losses occurred in the transfer of hydrogen from the ground storage tank to that of the Space Shuttle, the remaining losses were due to evaporation from the ground storage tank. [76].
Since the hydrogen liquefaction process is highly energy-intensive, liquid hydrogen losses must be minimized to keep the overall energy efficiency of the process as high as possible. Before ports are able to supply ships with the massive quantities of liquid hydrogen they need, the inland supply infrastructure which, to date, does not yet exist, will first have to be developed [76].
As anticipated at the beginning of the paragraph, for the management of liquid hydrogen on board and in port, it will be possible to take advantage of the experience already gained in the use of LNG as a fuel.
As regards the use of liquid hydrogen on board ships, similarly to what is currently done for LNG, naval designers are oriented towards creating a storage system for LH_2 divided into several tanks. However, this type of approach poses technical problems that have not yet been fully studied and overcome. Each of the tanks will in fact be subject to non-uniform evaporative phenomena due to the different volume, shape and arrangement on board. The sloshing of liquid hydrogen in partially full tanks, if not appropriately limited or avoided, could compromise the stability of the ship [76].

5 Regulatory framework for hydrogen as maritime fuel

This chapter is intended to provide an overview of currently applicable regulations, directive standards and guidelines regarding the use of fuel cells and hydrogen on board ships. Regulations, codes and directives are legal requirements imposed by legislative bodies and, therefore, are mandatory. Directives, on the other hand, are implemented at EU level and are not used as a tool by the IMO. On the other hand, standards, guidelines and codes of practice are voluntary documents unless required by regulations [83]. Maritime regulations and rules exist on three levels:

- International regulations developed by IMO;
- National regulations;
- Class rules.

Other international codes and standards can assist in supporting the approval process for hydrogen-powered ships. The use of some of these standards may be required by a class corporation and / or the Flag State, and some may be required as part of the approval process for specific components and/or subsystems [83]. An examination of the main international standards on hydrogen and fuel cells that could provide useful insights for the development of the regulatory framework for their future use on board ships is included in Annex A.

5.1 IMO's regularory framework for hydrogen and fuel cells

To date, the IMO has adopted approximately 50 conventions and has published more than 1000 codes and recommendations.

5.1.1 The SOLAS convention

The "International Convention for the Safety of Life at Sea" (SOLAS) was first convention adopted by IMO. It was introduced in 1914 after the sinking of the Titanic.
It is applicable to all ships engaged in international voyages except for warships and merchant ships of less than 500 gross tonnage. The 1974 version of SOLAS is still in effect but has been updated with amendments several times over the years. The latest SOLAS update was adopted during the 104th session of the Maritime Safety Committee (MSC104) in October 2021.
The SOLAS Convention consists of 14 chapters which define the minimum standards that must be adopted to ensure the safety of the construction, equipment and operation of the ships to which it is applicable.
SOLAS Chapters II and VII are the most relevant for hydrogen applications, although specific prescriptive rules and regulations for the use of hydrogen as a marine fuel have not yet been addressed directly:

- Chapter II defines the rules for building a ship and refers to the International Code of Safety for Ships Using Gas or Other Low Flash Point Fuels (IGF Code) for details on ships using this type of fuel;
- Chapter VII, on the other hand, deals with the transport of dangerous goods and refers to various codes, containing prescriptions for the different types of such goods. For hydrogen applications, the International Code for the Construction and Equipment of Ships Carrying Liquefied Gases in Bulk (IGC Code) applies [51].

SOLAS Chapter II-1/55 describes the approval process for "alternative designs and arrangements". If a project deviates from the current requirements of SOLAS or other IMO document, a detailed

engineering analysis must be performed. If this analysis demonstrates that the ship's design provides an equivalent level of safety and fulfills the purpose of the regulation from which the design deviates, the Flag State administration can still approve it.
An overview of the alternative design process for preliminary and final design according to the Alternative Design approach, describing the roles of the Administration (Flag State) and the submitter (Project Owner) are provided in Figure 51 and Figure 52.

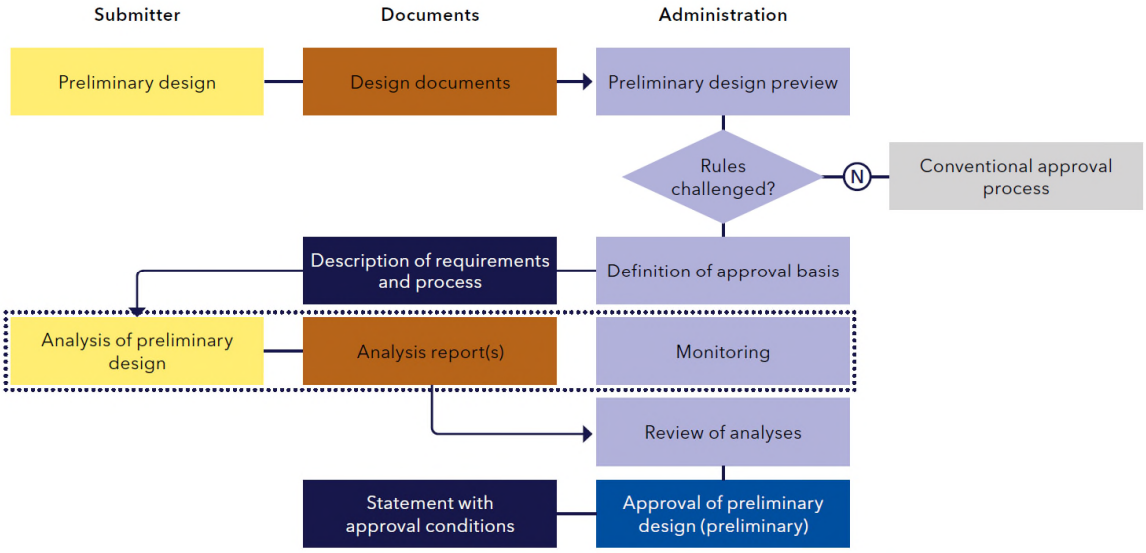

Figure 51. Approval procedure for preliminary design according to the Alternative Design approach. [83]

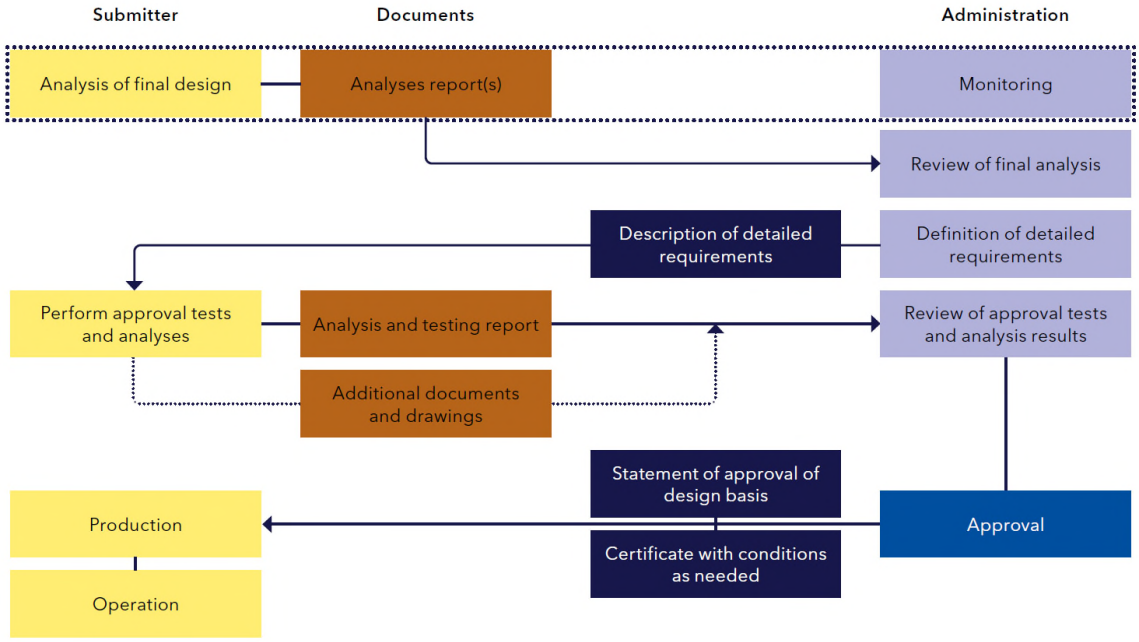

Figure 52. Approval procedure for final design according to the Alternative Design approach. [83]

More details on this process are provided in the following MSC circulars:

- MSC.1 / Circ.1212 / Rev.1 for deviations from SOLAS;
- MSC.1 / Circ.1455 for deviations from other IMO documents [51].

5.1.2 The IGF code

The "International Code for the Safety of Ships Using Gases or Other Low Flash Point Fuels" (IGF Code) was adopted by IMO with resolution MSC.391 (95) in June 2015 and entered into force in 2017. The IGF Code is based on a goal-based approach, defined in MSC.1 / Circ.1394. Its main objective is to ensure a safe ship design. From this derive specific functional objectives or functional requirements such as, for example, ensuring that a single failure does not lead the ship to operate in an unsafe mode. From the functional requirements then derive the specific detailed rules that must be respected and applied in the design.
The IGF code applies to all ships built after 2017, with the exception of gas carriers, which use part of their cargo or other low-flash point gaseous fuels and must comply with the IGC code, and to government-owned or operated ships performing non-commercial service. Currently, the IGF code only covers natural gas as a fuel. For other low flash point fuels (including hydrogen) it still allows the use of the "alternative design approach" defined in SOLAS Chapter II-1/55 [51].
The IMO's activities are assigned to committees and several internal sub-committees. Within the IMO Maritime Safety Committee (MSC), the Subcommittee for the Carriage of Cargo and Containers (CCC) is responsible for the development and updating of the IGF code [83].
Work has begun to include fuel cells (FCs) in the IGF code which in the future should include a new part dedicated to them. Until then, FCs will be covered by provisional guidelines. The aim is to gain more experience with FCs before the next revision of the IGF Code is issued.
During the 7th meeting of the Subcommittee for the Carriage of Cargo and Containers (CCC7 - September 2021) the draft interim guidelines for the safety of ships using fuel cell power installations was finalized. The approval of the Interim Guidelines has been considered as an urgent action item from CCC7 at MSC105 (April 2022) [84].
The final fuel cell requirements will be included in Chapter E of the IGF Code as an amendment to it. Chapter E is expected to formally enter into force as a new part of the IGF Code in 2028 [83].

5.1.3 The IGC code

Ships carrying liquefied gases as cargo, such as LNG, are covered by the "International Code for the Construction and Equipment of Ships Carrying Liquefied Gases in Bulk" (IGC Code). it is applicable to all ships carrying the products listed in its Chapter 19, including those of less than 500 gross tonnage. The code does not apply to Floating Production, Storage and Offloading (FPSO) units. Hydrogen is not currently covered by Chapter 19 of the Code [51].
The code classifies LNG tanks according to their structural characteristics and ships according to the risks of the products they transport.
The code categorizes independent LNG tanks into three categories: A, B and C:

- Type A: these tanks are designed using the traditional method of ship structural design. Only LNG at near-atmospheric conditions or LNG can be carried in these tanks: their design pressure is less than 700 mbar. Such tanks are provided with a full secondary barrier.
- Type B: the concept behind the design of such tanks is to have such a structure in which a crack can be detected long before the actual failure. This allows a time margin before the actual failure occurs. The methods used for design of such tanks include determination of stress levels at various temperatures and pressures by first principle analyses, determination of fatigue life of tank structure, and study of crack propagation characteristics. Their design pressure is the same as for Type A tanks. The enhanced design of Type B tanks requires a partial secondary barrier. The most common shapes for these tanks are spherical and prismatic.
- Type C: these tanks are designed as cryogenic pressure vessels, using conventional pressure vessel codes, and the dominant design criteria is the vapour pressure. The design pressure for

these tanks is in ranges above 2000 mbar. The most common shapes for these tanks are cylindrical and bilobe.

The IGC code also covers membrane tanks and tanks forming a structural part of the hull, so-called integrated tanks. The use of cargo as a fuel is also regulated by the IGC Code in Chapter 16. The IGF Code allows only methane (LNG) to be used as a fuel. Other fuels, except for toxic products, might be permitted, if an equivalent level of safety can be ensured [51]. A summary of the ICG code classification of LNG vessels is provided in Figure 53.

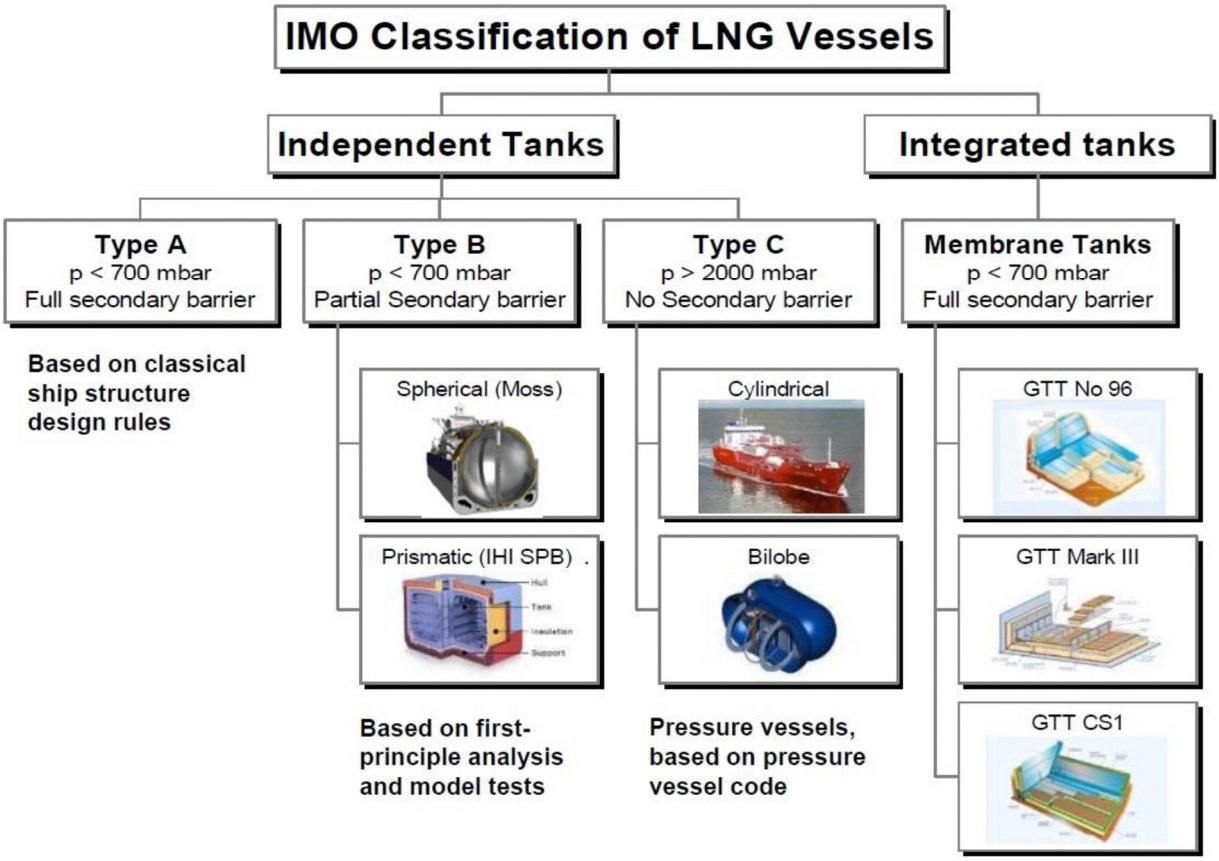

Figure 53. IMO classification of LNG vessels. [85]

The IGC code classifies ships into four categories; 1G, 2G, 2PG and 3G. Type 1G ships carry the most dangerous products and have the most stringent requirements. Ships carrying less hazardous products that need only moderate measures to prevent escape are classified as 3G type ships. Type 2G is an intermediate classification with hazards and preventive measures between 1G and 3G. Type 2PG vessels carry products classified for 2G vessels but are less than 150m in length and use Type C tanks with design pressure above 7 bar and design temperatures above -55 ° C [51].

5.1.4 The IMDG code

According to the requirements of the IMO, the transport of dangerous goods in packaged form must comply with the relevant provisions of the International Maritime Dangerous Goods (IMDG) code which is considered an extension of the provisions of chapter VII of SOLAS.
The Code, initially adopted in 1965 as a recommendation tool, was formally adopted by IMO General Assembly at its seventeenth session with resolution A.716(17) on 6 November 1991 [86]. The IMDG Code obtained a mandatory status from 1 January 2004. Some parts of the IMGD code are however still recommendatory.
The IMDG code covers hydrogen and other dangerous goods, but only as packaged goods. Transportation of such goods in ship's cargo tanks is not included. The code provides requirements for CH_2 and LH_2, which are comparable to those for compressed natural gas and LNG.
According to the IMDG provisions, CH_2 and LH_2 as cargo cannot be carried by cargo or passenger ships carrying more than 25 passengers or 1 passenger for 3 m overall length. LH_2 cannot be stowed below deck [83].

5.1.5 The Interim Recommendations for Carriage of Liquefied Hydrogen in Bulk

For the carriage of liquefied hydrogen as cargo, the Interim Recommendations for Carriage of Liquefied Hydrogen in Bulk, the Maritime Safety Committee (MSC) Resolution MSC.420(97) adopted on 25 November 2016 is the only IMO instrument available that may be applicable to ships carrying a cargo of liquefied hydrogen.
Such ships are expected to fall under the scope of the International Code of the Construction and Equipment of Ships Carrying Liquefied Gases in Bulk (IGC Code). However, the Interim Recommendations were initiated by and developed for a liquid hydrogen supply pilot project, and as such may be limited in application to that project [53].
The Interim Recommendations classify hydrogen carriers as 2G-type ships and specify 29 additional requirements that hydrogen carriers will have to fulfil. One requirement is, for example, that helium or a mixture of hydrogen and nitrogen should be used for the tightness tests. These requirements are then explained in detail and linked to the related hazard [51].
The IMO recognizes that information from this developing pilot project, and other Member State experiences, are required prior to amending the IGC Code to include requirements for the carriage of liquefied hydrogen [53].

5.2 Class rules on hydrogen and fuel cell

This paragraph describes the regulations in force or under development by the classification societies belonging to the International Association of Classification Societies (IACS).
The IACS is a non-profit organization of classification societies that establishes the minimum technical standards and requirements relating to maritime safety and environmental protection and ensures their consistent application.
The association carries out this activity through its committees, expert groups and project teams and provides a Quality System Certification System (QSCS) to which its members adhere, as a guarantee of professional integrity and maintenance of high professional standards. IACS is recognized as the IMO's Lead Technical Advisor.
More than 90% of the world's freight tonnage is covered by the design, construction and through-life compliance rules and standards established by the eleven member societies of the IACS [87].

IACS List of Members		
Acronym	**Name**	**Date of joining**
ABS	American Bureau of Shupping	11 Sept 1968
BV	Bureau Veritas	11 Sept 1968
CCS	China Classification Society	31 May 1988
CRS	Croatian Register of Shipping	3 May 2011
DNV	Det Norske Veritas	17 Dec, 2013
IRS	Indian Register of Shipping	22 June 2010
KR	Korean Register	31 May 1988
LR	Lloyd's Register	11 Sept 1968
NK	Nippon Kaiji Kyokai	11 Sept 1968
PRS	Polish register of shipping	3 June 2011
RINA	Italian Naval Register	11 Sept 1968

Table 17. IACS List of members. [88]

5.2.1 American Bureau of Shipping (ABS)

The ABS standard currently in force for fuel cells is the Guide for Fuel Cell Power Systems for Marine and Offshore Applications, published in November 2019 with references to Marine Vessel Rules (MVR) Part 5C, Chapter 13 for ships using gas or other low flash point fuels. The Guide for Fuel Cell Power Systems takes into consideration the draft IMO Interim Guidelines for the Safety of Ships Using Fuel Cell Power Installations and will be updated upon completion of the interim guidelines.
The Guide focuses primarily on fuel cell design requirements, but also includes provisions for hydrogen as a fuel, including fuel containment system, materials and general piping systems, fire safety, electrical systems and control, monitoring and safety systems. Parts of this guide specific to hydrogen storage and supply systems may also apply to internal combustion engines using hydrogen [53].

5.2.2 Bureau Veritas (BV)

In January 2022, BV officially issued the Rule Note NR547.
This provides the requirements for the arrangement and installation of fuel cell power systems on board ships used for the supply of electricity and / or heat. The Rule Note is applicable to fuel cell power systems used as auxiliary or primary electrical power systems on board ships. It includes requirements for the design and installation of fuel cell power systems and the spaces that contain such installations [89].

5.2.3 Det Norske Veritas (DNV)

The DNV Class Rules for FC installations are included in Part 6, Chapter 2, Section 3 of the “Rules for Classification of Ships (Additional class notations for Propulsion, power generation and auxiliary systems) [83].
The section provides requirements to ensure that fuel cell power plants can operate safely and with a defined level of availability and includes requirements for the design and layout of fuel cell power systems and the spaces that contain them. This section covers all aspects of the installation, from the primary fuel supply up to and including the exhaust gas system [90].
Additionally, the following is covered:

- reformers used to convert liquid or gaseous primary fuels to reformed hydrogen rich gas;
- control, monitoring and safety systems;
- manufacture, workmanship and testing.

The DNV Class Rrules for FC installations do not cover the remaining installation arrangements for the use of hydrogen as fuel, i.e., the hydrogen fuel storage, and preparation and distribution of hydrogen [83].

5.2.4 Korean Register KR

In 2015, KR published the Guidance for Fuel Cell Systems on Board of Ships.
The Guidance applies to fuel cell systems on board ships and used as an auxiliary or main power source. In the Guidance, only gaseous fuels lighter than air in ambient conditions, as well as liquid fuels with a flash point below 60 ℃ (such as natural gas, methanol, hydrogen or diesel fuels) are considered as "FC fuel" According to as prescribed in the Guide, the gas can be stored in a gaseous or liquid state [91].

5.2.5 Lloyd’s Register (LR)

LR is currently revising the document "Proposal Rules for fuel cell installation" issued in 2021.
This document contains the draft amendment proposal to Part 5 of the “Rules and Regulations for the Classification of Ships”, with the addition of the new chapter 26 entirely dedicated to fuel cells.
This amendment proposal aims to address, for fuel cell systems to be installed on board ship, the design, layout, materials, electrical monitoring, control, alarms and equipment and components of safety systems, as well as their testing.
The new chapter of Part 5 will be applicable to the most popular fuel cell technologies, generally classified according to their chemistry or operating temperature or both. The new regulation will apply to the following types of fuel cells:

- Solid Oxide (high temperature);
- Molten Carbonate (high temperature);
- Proton Exchange Membrane, also known as Polymer Electrolyte (low temperature);
- Alkaline (low temperature);
- Phosphoric Acid (intermediate temperature).

The goal of the proposed amendment is to provide rules for a safe and reliable supply of electrical and/or heat energy through the use of fuel cell technology [92].

5.2.6 Italian Naval Register (RINA)

RINA has introduced specific changes to Parts A, C and F of the “Rules for the Classification of Ships "dealing with the use of fuel cells on board ship. The changes compared to the previous edition of the Rules are described below. The changes entered into force from 1 October 2021.

Part A, Chapter 1, Section 2: Par. [6.14.57] (NEW), Par. [6.14.58] (NEW) and Table 3;
Introduction of additional class notations H2 FUELLED (assigned to ships using hydrogen as fuel, complying with the design and constructional requirements of Pt C, Ch 1, App 14.) and H2 FUELLED READY (X1,X2 and X3) assigned to ships whose design is in compliance with Pt C, Ch 1, App 14, and the relevant systems and arrangement are partially installed on board, thus easing a future ship conversion into a H2 FUELLED ship. The requirements for the assignment of this additional class notation are given in Pt F, Ch 13, Sec 38 [93].

Part C, Chapter 1, Section 1: Par. [2.9.1] and Appendix 14 (NEW);
The provisions of this Appendix apply to the arrangement, installation, control and monitoring of machinery, equipment and systems of ships using hydrogen as fuel (hereinafter named "hydrogen fuelled ships") [93].

Part F, Chapter 13, Section 38: (NEW SECTION);
The additional class notation H2 FUELLED READY (X1, X2, X3) is assigned, in accordance with Pt A, Ch 1, Sec 2, [6.14.58], to ships fulfilling the requirements of this section. A Statement of Compliance may be issued to ships not classed with the Society, fulfilling the requirements of this section [93].

6 Experimental test rig description

In order to verify the suitability of PEM cell technology for use on board cruise ships and develop a system capable of operating on board in complete autonomy despite the current absence of IMO guidelines and regulations on bunkering and handling of hydrogen tanks on board ships, an innovative 100kWe PEM fuel cell generator for marine application has been designed.
The plant, equipped with a fixed storage system for gaseous hydrogen (200 bar g storage pressure) is provided with and an autonomous hydrogen generation and compression system consisting of an electrolyser and an auxiliary compressor for hydrogen. The system is interfaced with the ship's electrical distribution system by means of a dedicated DC/AC power converter and is provided with dedicated automation and control systems.
To validate the design of the system to be installed on board, a full-scale test rig has been set up and tested at the Basovizza Area Science Park technology center.

Figure 54. Overview of Basovizza Area Science Park technology center (left) and external view of the test rig building (right). [94]

The plant design integrates standard industrial components suitable for marine applications that include the technologies with the highest degree of maturity currently available on the market. The fuel cell generator and power converter have been specifically designed by manufacturers to fit the specific plant needs. The key features of the plant that make it particularly suitable for installation on board a cruise ship are:

- self-sufficiency: the plant independently produces hydrogen to feed the fuel cell;
- simplicity of integration: the system needs only to be connected to the available onboard distribution systems of potable water, compressed air, electrical power and to the gray water collection system;
- independence: the plant is equipped with completely independent cooling and ventilation systems without any impact on the plants serving the machinery spaces;
- cleanliness: the electrical power produced by the system is generated at zero emissions.

The test rig consists of thwo plants:

- a hydrogen production and compression plant;
- an electrical power production plant.

A schematic representation of the two plants with their block diagrams is given in Figure 55.

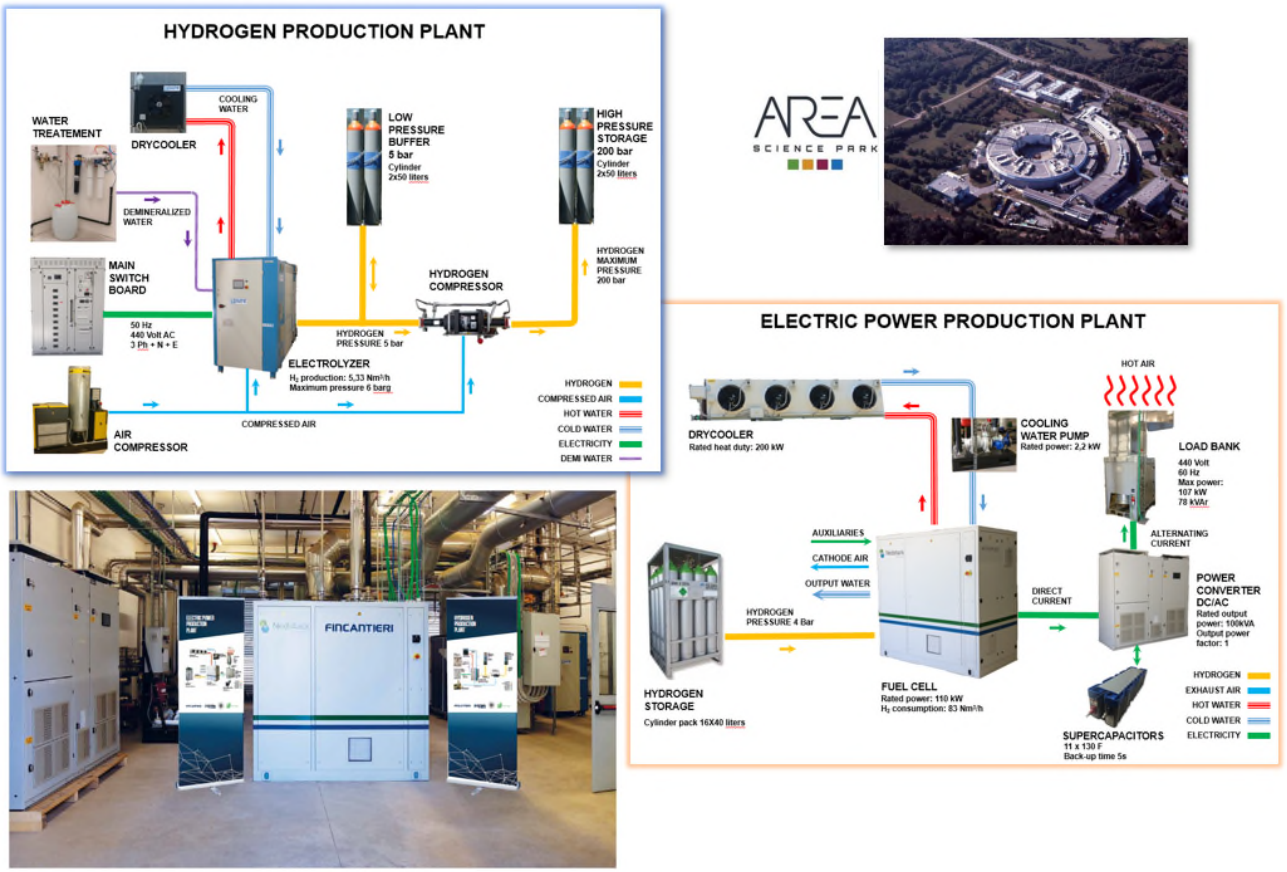

Figure 55. Test rig plants block diagrams. [95]

Detailed P&I diagrams of the experimental rig and detailed layout of the test rig site are provided respectively in Annex B and Annex C of this document.
The two plants and the dedicaed automation and control systems will be described in the next paragraphs of this chapter. The test rig automation plant functional diagram is included in Annex D.
The description of the tests performed for the experimental characterization of the hydrogen production and compression plant and of the electrical power power production plant are given in following Chapters 7 and 8.

6.1 Hydrogen production and compression plant

The description of the hydrogen production and storage plant below refers to the simplified diagram shown in Figure 57.The process flow of the test facility can be summarized as follows:

- Water is treated and appropriately demineralized using a water treatment system (FZ/001DE) in order to reduce its conductivity below the limit imposed by the electrolyser manufacturer;
- Demineralized water goes then to the electrolyser (FZ/001EL) where is converted into hydrogen and oxygen. The electrolyser hydrogen production internal pressure is precisely controlled and limited by an external back-pressure regulator (H2/001BP);
- The produced hydrogen fills a set of buffer cylinders (FZ/001HBA), with a geometric volume of 50 l, interposed between the electrolyser and an air-driven hydrogen booster (FZ/001HC). The buffer cylinders (FZ/001HBA) are filled at a pressure of about 5 bar g. The purpose of these "low-pressure" buffer systems is to ensure smooth and continuous operation of the electrolyser and of the hydrogen booster;
- The oxygen produced in the electrolysis reaction, which for the purpose of the project is considered a by-product, is suitably vented to the atmosphere in a safe location;
- Hydrogen pressure is then raised up to 200 bar g by an air-driven hydrogen reciprocating compressor (FZ/001HC). The compressed air needed to drive the hydrogen booster is produced by the air compressor (FZ/001AC);
- Flow of compressed hydrogen is then stored in high-pressure cylinders with a geometric volume of 50 l (FZ/001HBB). [62]

The electrolyser is equipped with H_2 and O_2 emergency vent and with two drain pipes for the recovery of O_2 and H_2 condensates: The unit is cooled by means of the dry cooler (FZ/001RF).
The internal valves of the electrolyser are operated with compressed air also coming from the air compressor (FZ/001AC). A nitrogen cylinder is also connected to the generator, necessary for startup operations and for any maintenance operations.

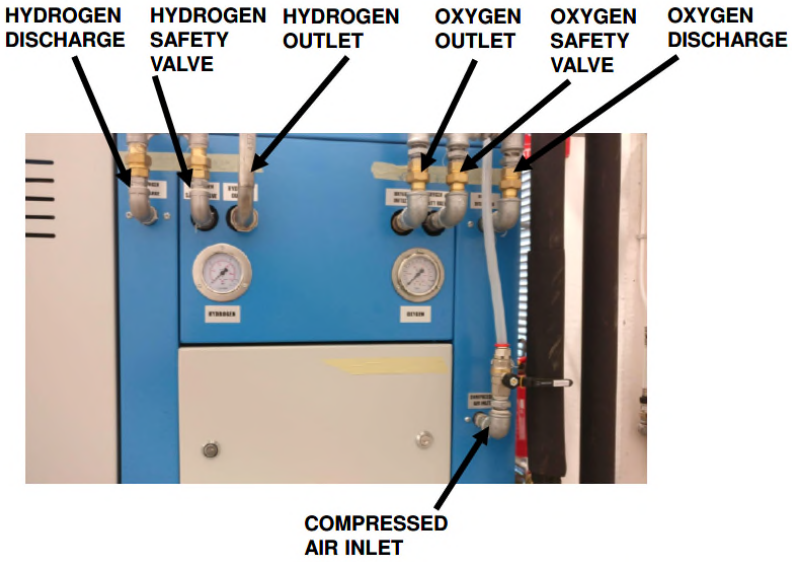

Figure 56. Alkaline electrolyser. Gas piping connections. [94]

In the following, technical information and data sheets of the main components of the hydrogen production and compression plant are provided.

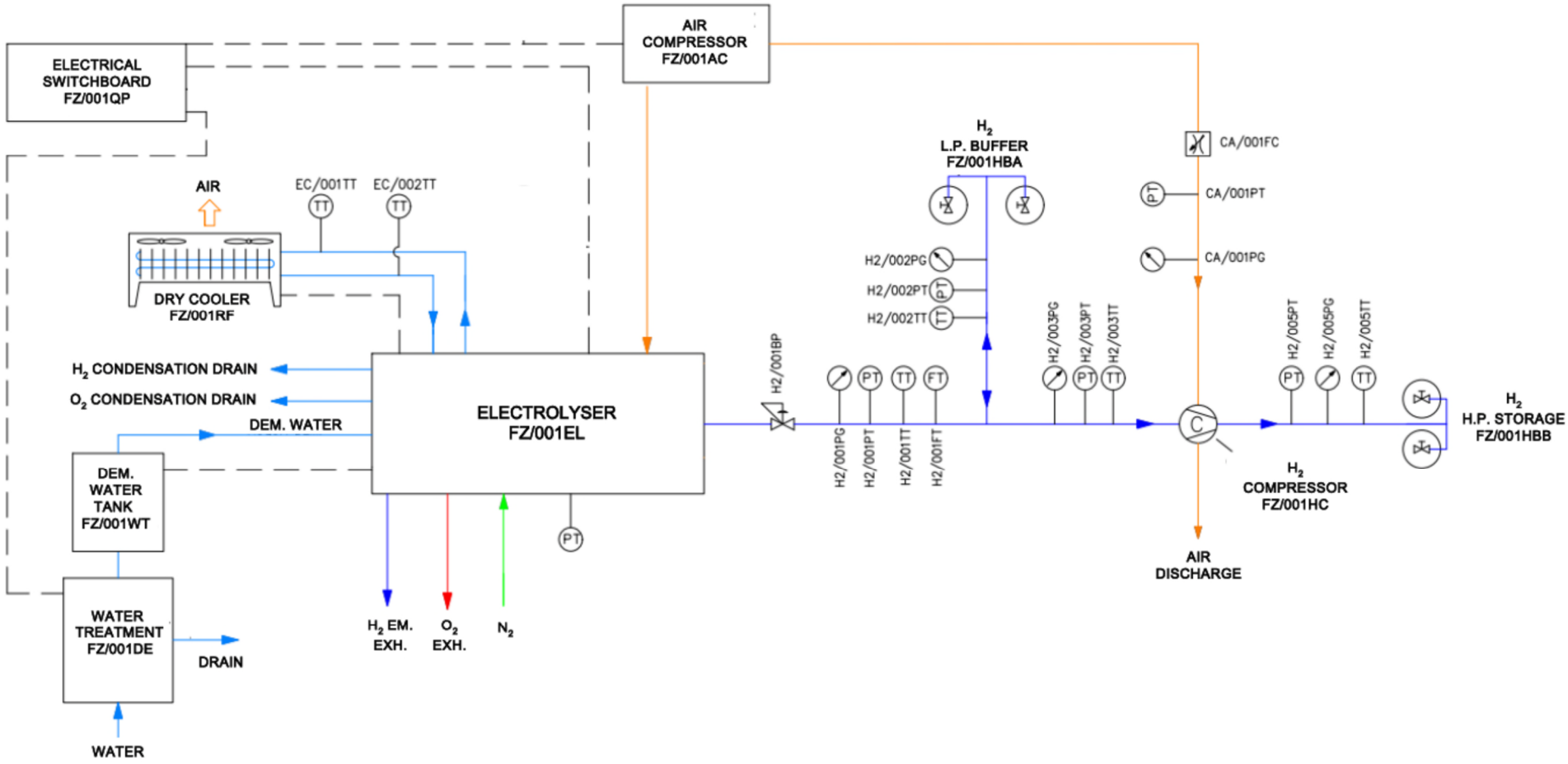

Figure 57. Hydrogen production and compression plant simplified diagram [62]

6.1.1 Alkaline Electrolyser technical specification

The industrial electrolyser used in the testing facility (FZ/001EL) is a Pure H2-5 Alkaline Electrolyser (N_aOH electrolyte) manufactured by Pure Energy Centre.
The unit is provided with a built-in electrical power system which, at the same time, supplies the generator balance of the plant and converts from AC to DC the electrical power required for the operation of two alkaline stacks into which demineralised is converted into gaseous oxygen (anode side) and hydrogen (cathode side). [62]
The PEC H2-5 Alkaline Electrolyser is provided with an external water treatment system (FZ/001DE) designed to convert ordinary tap feeding water into demineralised water required for the process. Demineralised water is collected in an external reservoir tank (FZ/001WT) with a geometric volume 50 l. A schematic layout of the water treatment system FZ/001DE is provided in Figure 58.

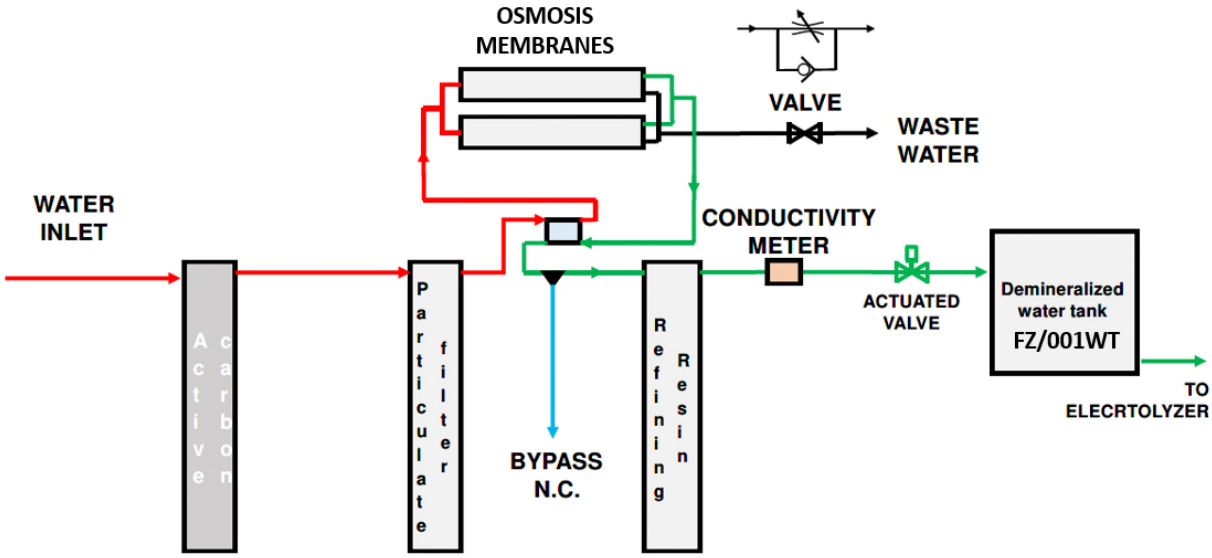

Figure 58. Alkaline electrolyser water treatment system. [94]

The multi-stage water filtration system consists of four purification stages:

- acrive carbon filtration for the removal of organic contaminants;
- sediment micro-filtering;
- reverse osmosis;
- final polishing trough mixed bed resin filter.

An integrated PLC-based process control system provides local monitoring of the hydrogen production process and controls the correct operation of the generator and of the water pumps that extract process water from the reservoir tank (FZ/001WT), pressurize it, and distribute it to the stacks.
The hydrogen output section of the unit includes a zeolites-based gas purification system for removing any traces of unwanted reactant from the hydrogen stream. Hydrogen generated by the unit reaches the purity of 99.999% (grade 5.0 according to ISO 14687-2) and is therefore suitable for high purity applications, such as PEMFC feeding Downstream the gas purification a drying unit reduces and controls the humidity content of the hydrogen outlet flow. [62]
The maximum guaranteed concentrations of contaminants in the produced hydrogen are:

- $O_2 < 0.05\%$
- N_aOH <0.1ppm
- $N_2 < 0.05\%$
- $CO+CO_2 < 1$ppm

The hydrogen purification system uses regenerative cartridges for reducing the maintenance activity on the system. The system automatically regenerates the cartridges when required and without any disruption on the H_2 production and without any major reduction in the H_2 flow rate. In fact, only a small stream of H_2 produced by the generator is used to regenerate the purifier cartridges.
The Pure H2-5 Alkaline Electrolyser is also provided with a built-in oxygen separator designed to separate electrolyte from oxygen produced at the anode of the stacks. The recovered electrolyte is then fed again into the stacks.
The main data of the Pure H2-5 Alkaline Electrolyser are summarized in Table 18.

Pure H2-5 Alkaline Electrolyser			
Electrical supply			
Power supply	3 Phase 400 VAC + Neutral + PE		
Frequency	50 Hz		
Rated power	32 kW		
Rated current	50 A		
Gas production – Hydrogen			
Maximum flow	5.33 Nm3/h		
Pressure*	6 Bar		
Gas purity	< 5 ppm		
Humidity	< -70 °C		
Gas production – Oxygen			
Maximum flow	2.66 Nm3/h		
Pressure	6 Bar		
Gas purity	98.5% - 99.5%		
Humidity (dew point)	about -20 °C		
Environmental condition			
Temperature (within these value)	5 – 35 °C		
Relative humidity (within these value)	20 - 80%		
Max altitude (for std. Performance)	1000 m AMSL		
Noise (emission)	<78 dBA		
Dimension & weights			
Main unit W x H x D (cm)	95x200x200		
Weight (kg)	1550		
Air ext. exchanger W x H x D (cm)	100x70x50		
Weight (Kg)	100		
Additional service connections			
De-ionized water	Max Conductivity	µS/cm	5
	Max Consumption	Lt/h	4.7
Compressed air	Max flow	Nmc/h	2
	Pressure	Bar	5-8
Nitrogen for regeneration (if used)	Flow rate	Nmc/h	1
	Pressure	Bar	2-5
Fluid content			
Electrolytic solution, Caustic soda (NaOH)	Density a 25°C	g/ml (Bè)	1.2 (24)
	Quantity	Lt	70
Freon R404A	Quantity	Kg	2.2
	High pressure	Barg	16
Cooling liquid, water glycol at 50%	Low pressure	Barg	3
	Quantity	Lt	10

Pure H2-5 Alkaline Electrolyser	
Pressure Safety Valves (PSV) - Hydrogen	
Pressure	10 Bar
Min discharge setting value	100 Nm3/h
Medium	Hydrogen
Pressure Safety Valves (PSV) - Oxygen	
Pressure	10 Bar
Min discharge setting value	100 Nm3/h
Medium	Oxygen
Water treatment unit	
Maximum hourly production	6 - 8 Lt/h
Daily production	Max 200 Lt
Min inlet pressure	2.5 bar
Max pressure	5.5 bar
Water supply temperature	3 – 35 °C
Ports connections: IN	Tube 10/8
Ports connections: OUT	Tube 6/4
Ports connections: DRAIN	Tube 6/4
Power supply	220 VAC
Water to be treated	
Max TDS (total dissolved solids)	500 mg/lt
Max total hardness	30 °F
Max Iron	0.1 mg/lt
Max Manganese	0.005 mg/lt
Max Chlorine	0.2 mg/lt
Sdi (silt density index)	< 5

Table 18. Pure H2-5 Alkaline Electrolyser main data [96]

Figure 59. Alkaline Electrolyser and water treatment. Photo by the author.

The alkaline electrolyser is provided with a built-in closed-loop cooling system with water/glycol mixture circulation. The cooling system includes a dry cooler (FZ/001RF) and an active air fan.

Figure 60. Pure H2-5 Alkaline Electrolyser dry cooler. Photo by the author.

The PEC Pure H2-5 Alkaline Electrolyser is provided with a built-in Process Control System for the local monitoring of the process and control of the correct operation of the plant and local front panel touch screen for control and monitoring the hydrogen production process.
For safety reasons, only operative parameters are directly accessible to the final user from the electrolyser Human-Machine Interface (HMI). All the critical and factory setting parameters are password protected.
The unit is suitable for marine environment application, System components are designed to assure the rated performance while operating within the physical and electrical limits and tolerances stated in the International Association of Classification Societies (IACS) "Test specification for Type Approval" document [97].
For this purpose, the unit manufactured for the test rig has been subjected to vibration and inclination tests, following the procedures described in the IACS document, and listed in Table 19.

Pure H2-5 Alkaline Electrolyser			
Test #	**Test description**	**Notes**	**Test parameters**
E10-7	Vibration.	Procedure according to IEC 60068-2-6 Test Fc.	• From 2.0 to 13.2 Hz amplitude = 1mm • From 13.2 to 100Hz acceleration = 0.7 g
E10-8	Inclination.	Procedure according to IEC 60092-504 on both long and short sides	• Static = 22.5° • Dynamic = 22.5° Period 10 s

Table 19. Pure H2-5 Alkaline Electrolyser test list [98]

During the vibration test performed according to the specifications, the following mechanical damages were recorded:

- unscrewing of the doors hinges on the rear of the cabinet, with consequent opening of the doors;
- opening of the locking locks of the side panels of the structure, with slight movement of the closing panels of the cabinet;
- loosening of the inlet gasket of the electrolyte exchanger, with consequent leakage of electrolyte solution and shutdown of the generator.

Based on the result of the test, the following corrective actions have been taken:

- all the fixing nuts of the hinges have been replaced with self-locking nuts, to avoid loosening due to vibrations;
- All the locking system of the panels was based on rotating pin type. They have been replaced with equivalent keylock type;
- Anti-vibration gasket has been added on the frame of the cabinet to reduce vibration of the side panels;
- The loss of electrolyte solution from the Heat exchanger was due to damage of the inlet gasket. This was caused by the vibration of the inlet pipe. An additional supporting bracket has been installed to reduce vibration of the pipe.

After the above modifications, a new set of vibration tests have been performed and have passed successfully [99].
During both static and dynamic inclination tests performed according to the specification, the machine was running and fully pressurized. All the internal parameters were checked, and the machine remained operational with no warnings or alarms [98].

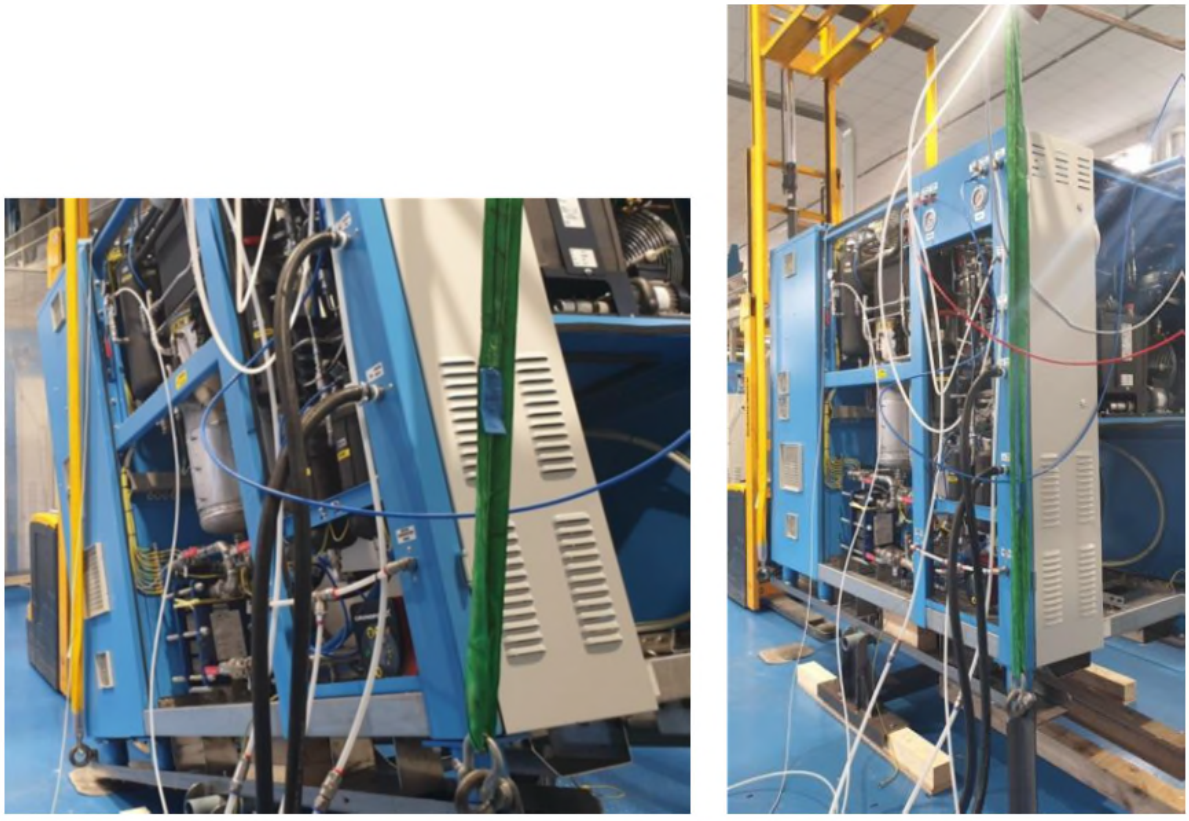

Figure 61. Alcaline Electrolyser on tilting plane during test. [98]

6.1.2 Hydrogen booster technical specification

The industrial hydrogen booster used in the testing facility (FZ/001HC) is an AGT-7/30H2 pneumatic hydrogen booster manufactured by Haskel.
The unit is suitable for marine environment application and built with materials suitable to resist the effects of hydrogen embrittlement at the expected operating conditions.

The main data of the AGT-7/30H2 pneumatic hydrogen booster are summarized in Table 20.

AGT-7/30H2 pneumatic hydrogen booster	
Model	AGT - 7/30
Type	Air driven non-lubricated gas booster
Compression stages	2
Min inlet pressure	1.7 bar
Max outlet pressure	172 bar
Max outlet pressure	620 bar
Max outlet stall pressure	30 Pa + 4 Ps
Max compression ratio	100:1
Max dirve ari pressure	10.3 bar
Weight	19 kg

Table 20. AGT-7/30H2 pneumatic hydrogen booster main data. [100]

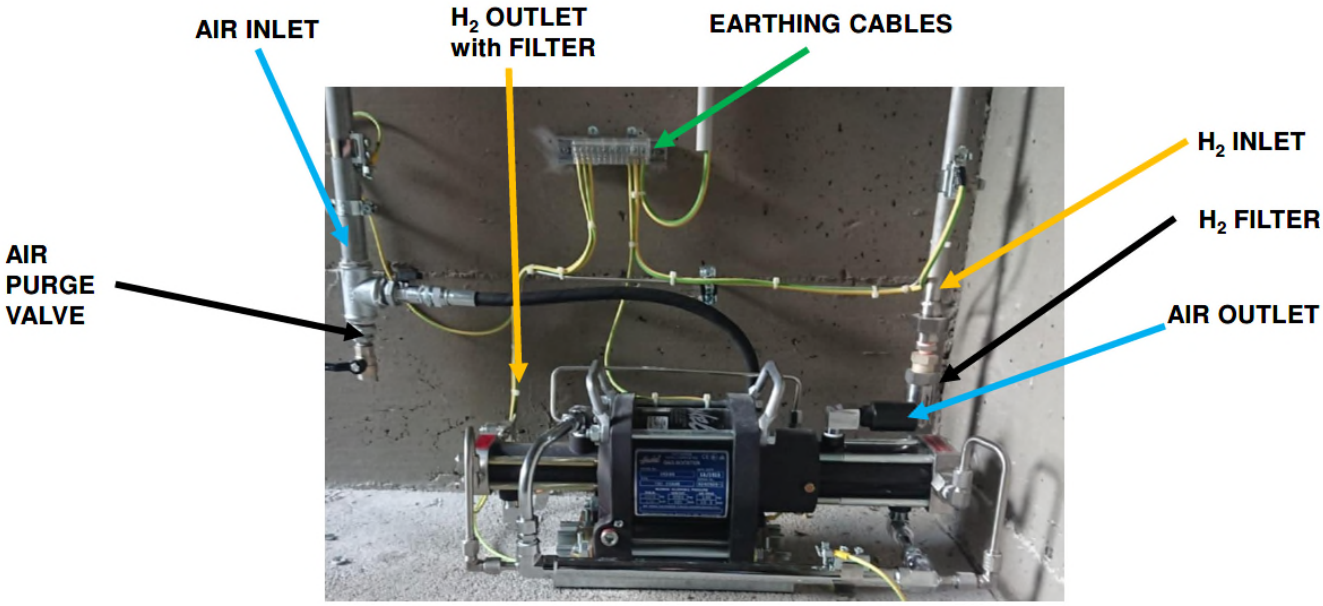

Figure 62. an AGT-7/30H2 pneumatic hydrogen booster in the test rig. [94]

6.1.3 Compressed air package technical specification

The compressed air package used in the test rig consist of the following components:

- Air compressor (FZ/001AC – Kaeser SK 19);
- Air dryer (Kaeser TCH 22);
- Storage tank;
- Automatic condensate drain;
- Line filters.

The main data of the Kaeser SK 19 air compressor are summarized in Table 21.

Kaeser SK 19 air compressor	
Compressor	
Max operating pressure	10 bar
Operating temperature*	75 -100 °C
Weight	270 kg
* Dependent on maximum operating pressure and atmospheric conditions, such as humidity and ambient temperature	
Sound pressure level	
Compressor operating status	At full load. The compressor operates with the following characteristics: rated speed, rated pressure, rated capacity.
Measurement conditions	Open field measurement
Reference standard	CAGI/PNEUROP PN8 NTC 2.3
Sound pressure level	67 dB(A)
Electric motor	
Rated power	11 kW
Rated speed	3000 min^{-1}
Ingress Protection rating	IP 54
Electrical supply	
Power supply	400 ± 10% V 3~/PE
Frequency	50 Hz
Rated current	23 A
Safety valve setpoint	
Set pressure	11.5 bar
Environmental condition	
Max altitude	1000 m AMSL
Min ambient temperature	3 °C
Max ambient temperature	40 °C
Min air intake / cooling air temperature	3 °C
Max air intake / cooling air temperature	40 °C
Room ventilation opening area	0.3 m2
Oil quantity	
Total volume of oil	12 l

Table 21. Kaeser SK 19 air compressor main data. [101]

The main data of the Kaeser TCH 22 air dryer are summarized inTable 22.

Kaeser TCH 22 air dryer	
Nameplate data	
Refrigerant gas	R134a
Refigerant gas quantity	0.65 kg
Max working pressure (refrigeration system)	18 bar
Max working pressure (air system)	16 bar
Rated voltage	230 V/1/50 Hz
Rated current	4.33 A
Ambient temperature	+3 °C / +45 °C
Weight	
Weight	55 kg
Environmental condition	
Max altitude	1000 m AMSL
Ambient temperature	+3 °C / +45 °C
Air intake / cooling air temperature	+3 °C / +45 °C
Compressed air system	
Pressure drop	0.21 bar
Flow rate	2.2 m^3/min
Max operating pressure	16 bar
Dew point	3 °C
Performance data compliant with the reference conditions DIN / ISO 7183 option A: ambient temperature 25 °C, compressed air inlet temperature 35 °C, working pressure 7 bar.	
Sound pressure level	
Operating status	Nominal flow and nominal pressure
Measurement conditions	Measurement in open field according to CAGI / PNEUROP PN8 NTC 2,3 at 1 m distance.
Sound pressure level	< 70 dB(A)

Table 22. Kaeser TCH 22 air compressor main data. [102]

The compressed air package is equipped with a 500l vertical storage tank with a geometric volume of 500 l, equipped with automatic condensate drain. Before being sent to the hydrogen booster, the compressed air is treated with a filtering system in order to comply with quality level 4 of the ISO 8573.1 standard “Compressed air - Part 1: Contaminants and purity classes”.

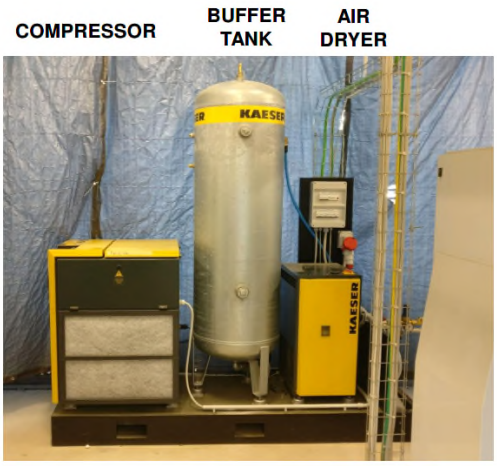

Figure 63. Test rig compressed air package. [94]

6.2 Electrical power production plant

The description of the electrical power production plant below refers to the simplified diagram shown in Figure 65.The process flow of the test facility can be summarized as follows:

- The hydrogen stored in the storage system at 200 bar g (FZ/001HPS), is depressurized by means of a two-stage pressure regulator up to about 4 bar g;
- The hydrogen thus depressurized feeds the PEM type fuel cell generator (FZ/001FC);
- The fuel cell transforms the energy contained in the input hydrogen into DC electrical power;
- Downstream of the fuel cell generator, a DC/AC converter (FZ/001CO) transforms the direct current output of the fuel cell into three-phase alternating electric current with a nominal voltage of 440 V and a frequency of 60 Hz;
- An ohmic / inductive load bank (FZ/001RL) is connected downstream of the converter, which allows to simulate stationary loads and load profiles that vary over time.

To limit sudden load variations on the fuel cell, an accumulation system consisting of supercapacitors has been integrated into the power converter.
The fuel cell is cooled by means of a dedicated dry cooler (FZ/002RF) equipped with active fans. The fuel cell external closed-loop cooling circuit is equipped with a dedicated external circulation pump. The fuel cell generator is equipped with venting pipes for anode (hydrogen) and cathode (air) exhaust. The water produced by the cell during opreation is collected in a process tank inside the generator and is used for humidifying the air and process hydrogen. To prevent possible hydrogen accumulation, this tank is provided with a dedicated venting pipe. The excess water is evacuated through a dedicated drain pipe.

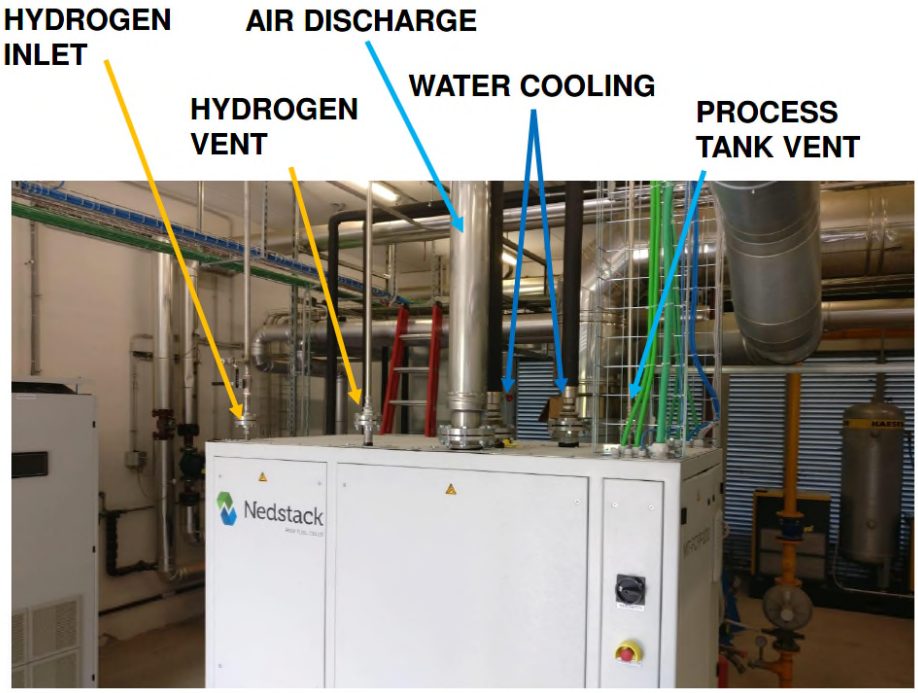

Figure 64. Test rig. Fuel cell generator piping connections on top of the unit. [94]

In the following, technical information and data sheets of the main components of the electrical power production plant are provided. For the fuel cell and for the converter, the preformance tests carried out before their installation in the test rig are also summarized.

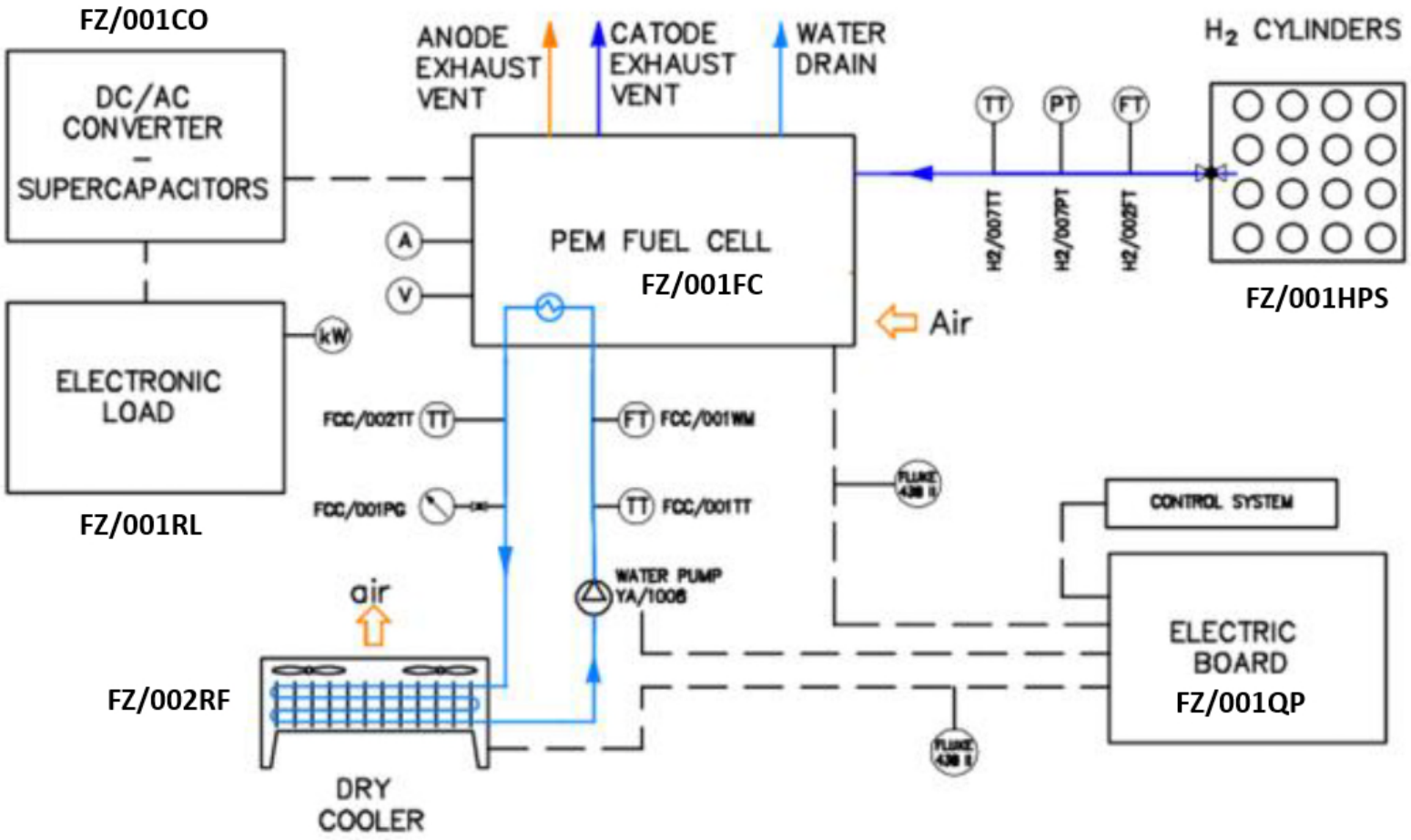

Figure 65. Electrical power production plant simplified diagram.

6.2.1 Fuel cell generator technical specification

The fuel cell generator used in the testing facility (FZ/001EL) is a 100 kWe Nedstack MT-FCPP-100 Maritime Fuel Cell Power-Plant system, based on low temperature PEM (Proton Exchange Membrane) liquid cooled fuel cells, suitable for marine environment application.
The following figure is a simplified block diagram of the fuel cell generator with indication of interfaces to the Balance Of Plant (BOP) and external subsystems.

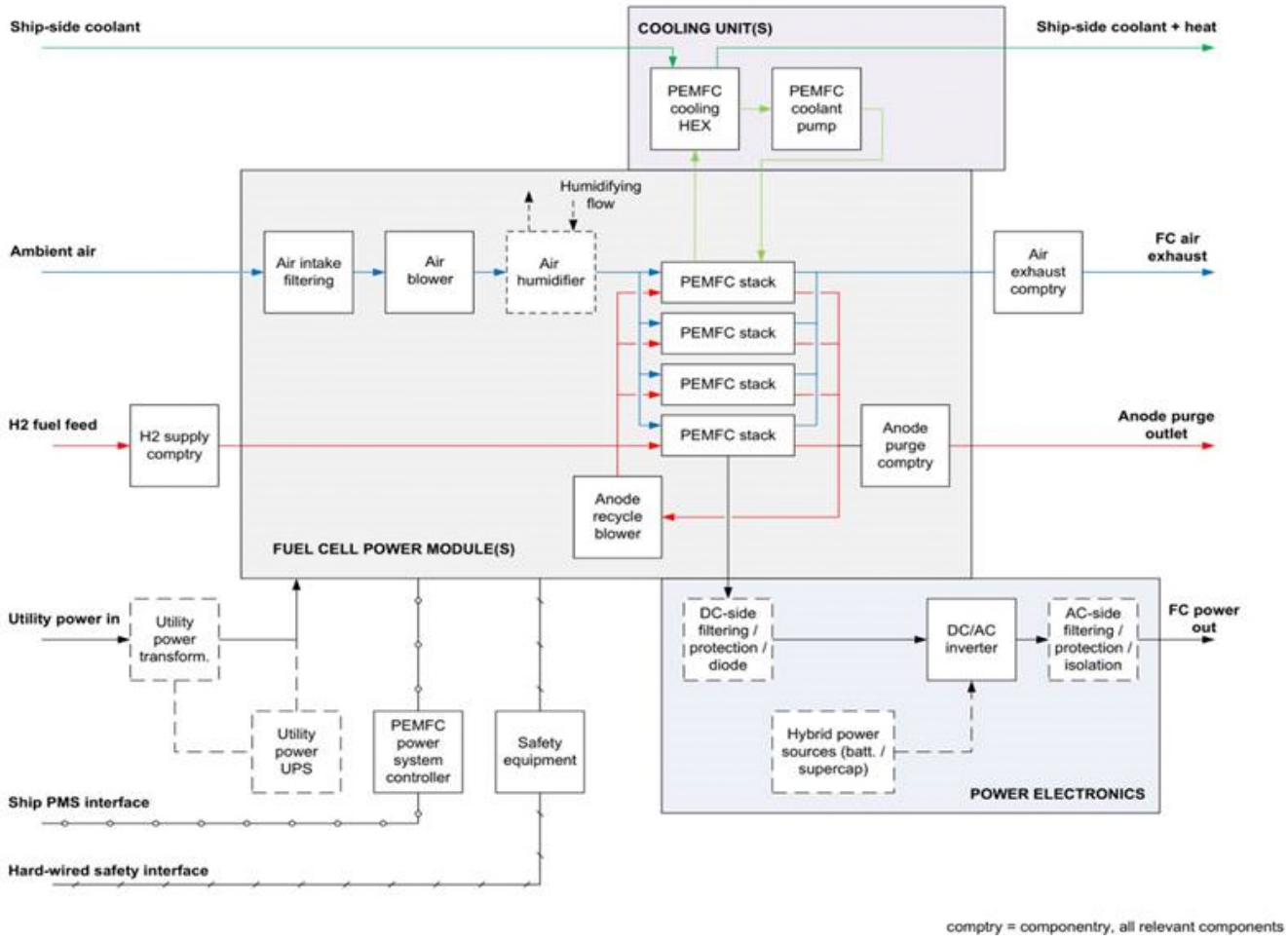

Figure 66. Fuel Cell generator block diagram. [103]

The fuel cell generator is equipped with 12 Nedstack FCS13-XXL [104] stacks arranged in two strings in parallel, each consisting of 6 stacks in series. Each stack consists of 96 cells.
A power diode is placed behind each individual strings of stacks to protect the fuel cell against a reverse current. The manufacturer's main data for the fuel cell stack arrangement are indicated in Table 23 and refer to either Beginning of Life (BOL) or End Of Life (EOL) of the stacks.
End Of Life is defined as 10% decay in performance due to the presence of contaminants in fuel and oxidant. In general, at stack level, refurbishment is foreseen by manufacturer every 24000 running hours.

MT-FCPP-100 Fuel Cell system data	
Performance	
Rated Electrical Power (MCR @ EOL)	100 kWe
Number of stacks	12
Number of stacks in series	6
Number of strings in parallel	2
Nominal current (per string)	120 A
Open Circuit Voltage (OCV)	616 V
Operating voltage maximum (40 A @ BOL)	462 V
Operating voltage nominal (120 A @ BOL)	412 V
Operating voltage minimum (200 A @ EOL)	313 V
Efficiency @ rated power (BOL)	55 %
Efficiency @ rated power (EOL)	34 %
Time from Off mode to Idle	< 60 s
Time from Idle to Rated Power @ cold start	5-10 min
Fuel system requirements	
Gaseous Hydrogen purity	> grade 2.5
CO	< 0.2 ppm
Sulphur (total)	< 0.004 ppm
Hydrocarbons (total)	as per ISO 14687-2
Supply pressure	5 barg
Stack operating pressure	300 mbar
Consumption @ rated current (BOL)	5.4 kg/h
Hydrogen temperature	< 60 °C

Table 23. Fuel Cell generator stack data. [103]

The efficiency values indicated in table Table 23 are those relating to the "gross" efficiency of the fulel cell generator defined as the ratio between the electrical power produced by the fuel cell and the power related toe hydrogen inlet to the fuel cell (referred to its LHV). The value declared by the manufacturer was verified during the performance tests carried at the manufacturer's premises before installation in the test rig (see paragraph 6.2.3) and were further verified with a dedicated test as par of the experimental characterization of the electrical power production plant (see paragraph 8.2.1). The polarization curve provided by the manufacturer at the time of the development of the technical specification for the purchase of the component is reported in at the time of the development of the technical specification for the purchase of the components is reported in Figure 67. The data provided by the manufacturer were used for the sizing of the test rig and, especially, in the design of the DC/AC power converter (FZ/001CO) connected downstream of the fuel cell generator. The actual polarization curve of the generator was detected with a dedicated test (see paragraph 8.2.3) in the experimental characterization of the electrical power production plant.

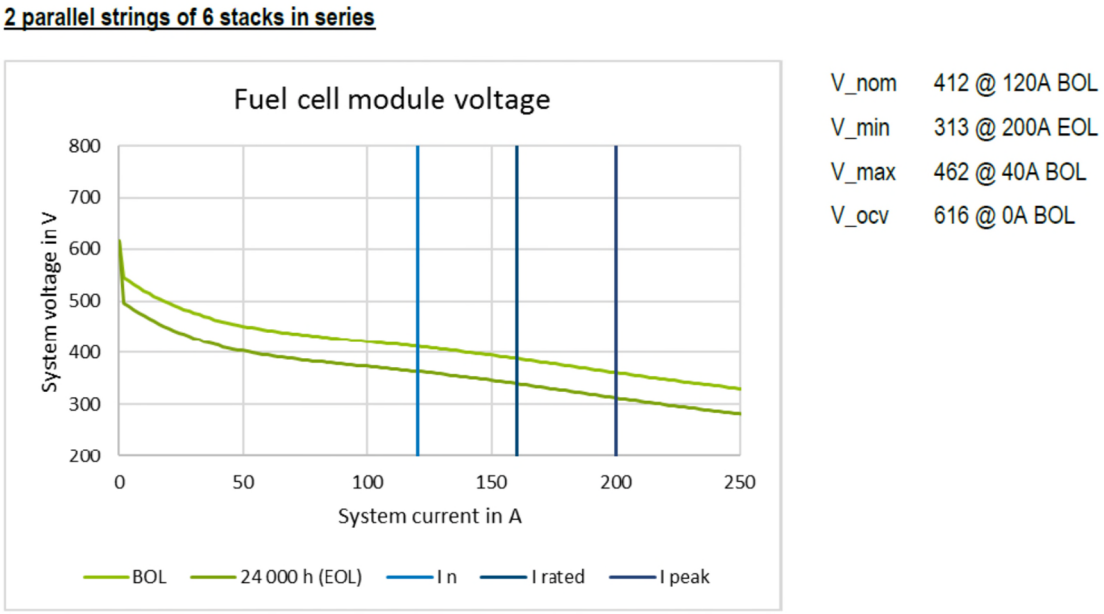

Figure 67. Fuel cell generator BOL and EOL polarization curves porvided by manufacturer. [105]

From the plots reported in Figure 67, it can be seen that the the fuel cell generator FZ/001CO provides an output voltage which spans from a maximum of 616 VDC at no load (OCV – Open Circuit Voltage @ BOL) to a minimum 313VDC at peak load current per string (200A @ EOL). The fuel cell system is designed to provide about 412VDC operating voltage with a string current of 120A @ BOL.
The main subsystems included in the BOP of the Nedstack MT-FCPP-100 fuel cell system are hereinafter described.

Internal thermal management subsystem:
The fuel cell generator is cooled by demi-water. The system is provided with a built-in close-circuit coolant subsystem whose main components are:

- Demi-water expansion tank,
- Pump,
- Filter,
- Heat exchanger.

The following table summarizes the main data provided by the manufacturer on the internal thermal management subsystem for both BOL and EOL of the MT-FCPP-100 Fuel Cell system.

MT-FCPP-100 Thermal Management subsystem data				
	BOL		**EOL**	
	kW	l/min (*)	kW	l/min (*)
Idle @ 40A	30	90	35	105
Nominal @ 120 A	105	310	120	435
Maximum (200 A @ BOL)	200	580	215	795
(*) coolant flow rate				

Table 24. Fuel cell gernator thermal management system data. [103]

Oxidant management subsystem:
The fuel cell generator is provided with a built-in oxidant (air) management subsystem designed to deliver air at a prescribed flow rate to support the Fuel Cells electrochemical reactions.
The built-in air management subsystem main components are:

- Air filter,
- Humidifier,
- Blower.

The following table summarizes the main specifications of the Oxidant Management subsystem.

MT-FCPP-100 Oxidant management subsystem data	
Air filtration	Included
CO	< 25 ppm
Total Sulphur	< 0.01 ppm
Nitrogen dioxide	< 0.3 ppm
Ammonia	< 0.1 ppm
Indicative air flow rate requirements	
Idle @ 40A	120 Nm^3/h
Nominal @120A	360 Nm^3/h
Maximum @200A	600 Nm^3/h

Table 25. Fuel cell oxidant management subsystem data. [103] [105]

As the fuel system operates at ambient pressure, the air system should only compensate for the pressure difference over the fuel cell plates. A blower is used to deliver the required flow at a pressure of approximately 150 mbar. The supply air is humidified using the excess water produced in the fuel cell stack.

Figure 68. Fuel cell generator in the test rig. Photo by the author.

Power plant control system:

The fuel cell generator system is provided with a built-in control system for the local monitoring of the process and control of the correct operation of the plant based on maritime type approved and commercially available components.

The unit is provided with a touch screen installed on a separate cabinet for control and monitoring the of overerall system and of all the subsystem of the unit. In detail, the HMI of the unit is provided with dedicated pages for:

- System Overview (main page);
- Oxidant subsystem;
- Hydrogen management;
- Thermal management sybsystem;
- Power output monitoring.

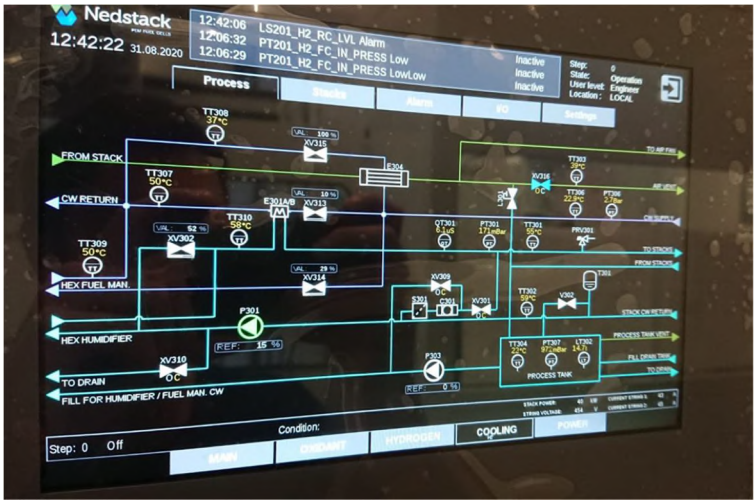

Figure 69. Fuel cell generator. Thermal management sybsystem overview on the HMI. Photo by the author.

For safety reasons, only operative parameters are directly accessible to the final user from the HMI. All the critical and factory setting parameters are password-protected.

Furthermore, each stack is equipped with a Cell Voltage Monitoring (CVM) unit, measuring each individual cell. The voltages measured by the CVM system are displayed on the HMI

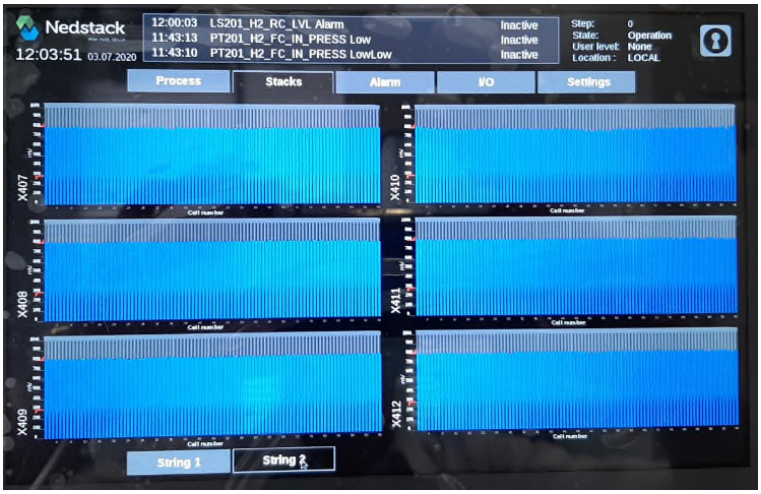

Figure 70. Fuel cell generator. Overview of string 1 individual cell voltage on the HMI. Photo by the author.

Safety:
The fuel cell gereator system complies with the following the following international standards:

- IEC 62282-2 – Fuel cell technologies – Part 2: Fuel cell modules
- IEC 62282-3 – Fuel cell technologies – Part 3: Stationary fuel cell systems - Safety
- IEC 60079 – Electrical apparatus for explosive gas atmospheres
- IEC 60092 – Electrical installations in ships

6.2.2 Fuel cell generator external circulation pump and dry cooler

The closed-loop external cooling circuit of the fuel cell is schematized in Figure 71.
The circuit consists of two main elements:

- a skid containing the circulation pump (YA/1008), accessories and the electric starter of the pump equipped with VFD;
- the dry cooler FZ/002RF.

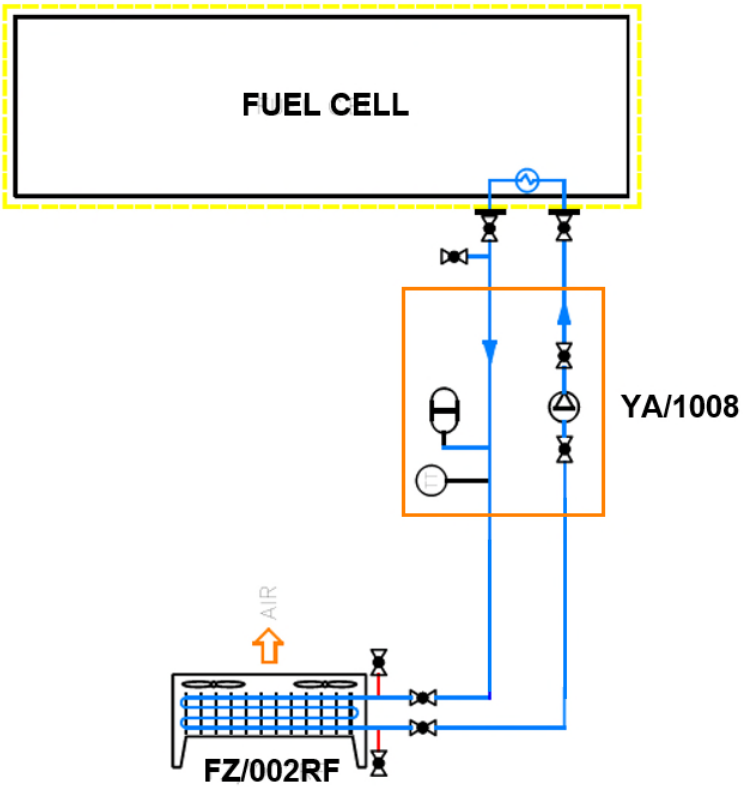

Figure 71. Fuel cell closed loop external cooling circuit.

A detailed description of the equipment einstalled in the circulation pump skid is provided in Figure 72, And a detailed equipment lis is given in Table 26.

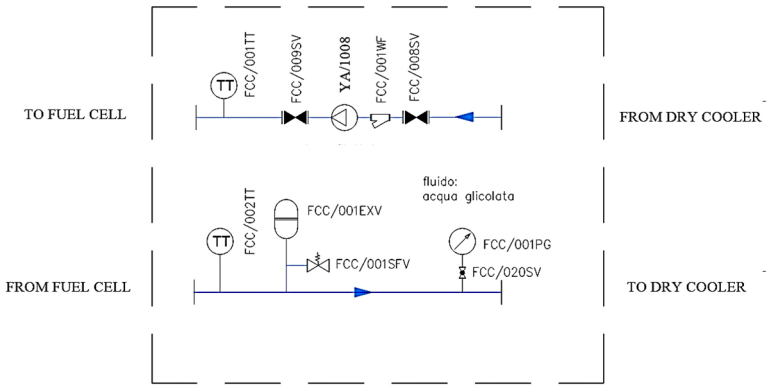

Figure 72. Fuel cell closed loop external cooling circuit pump skid. [106]

Component	Description
FCC/008SV	Shut-off valve
FCC/009SV	Shut-off valve
FCC/020SV	Shut-off valve
FCC/001SFV	Safety valve
FCC/001EX	Expansion vessel
FCC/001FW	Water filter
FCC/001TT	Temperature sensor Pt100
FCC/002TT	Temperature sensor Pt100
FCC/001PG	Pressure gauge
YA/1008	Circulation pump
YE/1008	Circulation pump starter

Table 26. Fuel cell closed loop external cooling circuit pump skid equipment list. [106]

The main data of the circulation pump are summarized in Table 27.

Description	Unit	Value
Type	-	Centrifugal
Fluid	-	Water + 30% Glycol
Casing	-	Cast iron
Impeller	-	Ni-Al Bronze
Shaft	-	AISI 316L
Motor power	kW	2.2 kW
Motor speed	rpm	2900
Power supply	V/Hz/ph	400 VAC/50 Hz – 3 ph

Table 27 Fuel cell closed loop external cooling circuit. Circulation pump main data. [106] [107]

The head7flow chart of the circulation pump, referred to liquid clean water without solid content is reported in Figure 73.

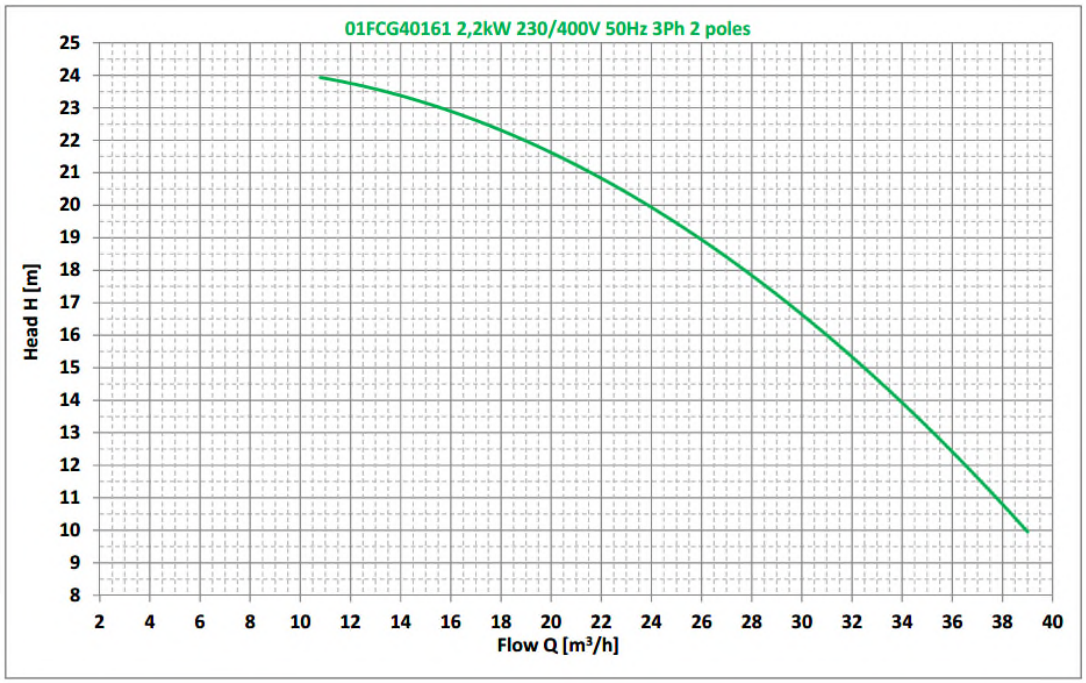

Figure 73. Fuel cell closed loop external cooling circuit. Circulation pump head/flow chart. [108]

Figure 74. Fuel cell external cooling circuit pump skid installed in the test rig. Photo by the author.

The main data of the dry cooler FZ/002RF are summarized in Table 28.

Description	Unit	Value
Type	-	Dry Cooler
Coolant	-	Glycol/Water (Eth.glycol 30.0%)
Installation	-	Horizontal airflow
Dissipated thermal power	kW	115
Coolant flowrate	m^3/h	12.0
Inlet coolant temperature	°C	50
Outled collant temperature	°C	41.0
Pipes material	-	Copper
Fins material	-	Copper
Inlet connection (*)	-	1”1/2 threaded
Outlet connection (*)	-	1”1/2 threaded
Power supply	V/Hz/ph	400 VAC/50 Hz – 3 ph
Fans speed control	-	0-10 V
Inlet and otlet connection on same side		

Table 28. Fuel cell dry cooler main data. [109]

Figure 75. Fuel cell dry cooler installed in the test rig. Photo by the author.

6.2.3 Performance and safety tests carried out on the fuel cell generator

Being a prototype unit, before being installed in the test rig, the fuel cell generator was subject to a program of checks and performance tests conducted at the manufacturer's premises to verify the compliance of the generator with the technical specification requirements, its response times and the presence and correct operation of all required safety devices.
Tests and are listed in Table 29 which also include a summary of the requirements for each test.

Test description	**Requirement**
System build checks	
Leakage test	• < 50-70 mbar pressure drop after 2 minutes
System performance	
Cold startup time	• $T_{stack} = T_{ambient}$ • $t_{cold\ start} \leq 10$ min from command to P_{rated} (110 kWe ± 2 %)
Electrical power response test down transient	• $I_{state\ 1} = 120$ A/string • $I_{state\ 2} = 80$ A/string • $T_{stack} = 55 \pm 3$ °C
Electrical power response test up transient	• $I_{state\ 1} = 80$ A/string • $I_{state\ 2} = 120$ A/string $T_{stack} = 55 \pm 3$ °C
Shutdown time (from rated power to OFF state)	• $P_{rated} = 110$ kWe ± 2 %
Hot startup	• $P_{min} = 120$ A/string • $T_{stack} = 55 \pm 3$ °C • $T_{warm\ start} \leq 5$ s from command to P_{rated} (110 kWe ± 2%)
Steady state P_{rated}	• $P_{rated} = 110$ kWe ± 2 % • $T_{stack} = 55 \pm 3$ °C • $\Delta T_{stack} \leq 5$ °C • Current distribution between strings < 10 A • $U_{cell} > 500 < 950$ mV consistently distributed over the cells • U_{cell} relative > 0,95 with an absolute limit @ 0,9 • $pH_2 = 200 \pm 50$ mbar • No warnings/ errors • No accumulation of water hindering normal functionality
Stability test	
Black-out test	• After power reconnect, system shall remain in OFF state

Emergency shut down (ESD) test	• System shall reach safe state:
	  ○ H_2 inlet valve and purge valve closed
	  ○ DC contactors open
	  ○ Power sources disconnected form equipment

System restart after ESD	• $T_{stack} = 30$ °C • $I_{state\ 1} = 0$ A/string • $I_{state\ 2} = 100$ A/string • No water accumulation issue
Internal H_2 sensor test	• Internal H_2 detector triggers system shutdown at 20% LEL

Table 29. Tests performed on fuel cell generator. [110]

Figure 76. Overview of system test setup. [110]

In the test rig the unit was not cooled by means of a closed-circuit cooling circuit but by using the cooling water distribution system available at the manufacturer's workshop where water from a nearby watercourse circulated in open circuit.
The load bank used for unit testing was of the manually controlled brine tank type with with limited speed of lifting and lowering of the resistances.
Hereinafter a description of the tests performed, and the results obtained is given. All the quantities reported in the plots were monitored and recorded thtrough the sistem's embedded monitoring and control system. In not otherwise stated in the test desctiption, time scale for the plots over time is given in seconds.

Leakage test:
To check the correct tightness of the hydrogen pipes inside the unit, N_2 was applied to the anodic subsystem until its nominal pressure of 340 mbar was reached. The subsystem inlet and outlet valves were then closed, and its pressure recorded after 2 minutes. The pressure recorded in the anodic subsystem at the end of the test was 333 mbar. The pressure drop in the anode subsystem was therefore contained to 7 mbar, well below the maximum limit set by the test requirements.

Cold startup time evalutation test:
The system was cold started with stack temperature of 25 ºC. The load was then set to 60 A per string until the stack was heated to 55 ºC.
The load was then increased to 140 A per string to obtain the system's rated power P_{rated} of 110 kWe. However, this increase in load from 60 A to 140 A could not be achieved in a quick step due to limitation in speed of he manually controlled load bank.
Furthermore, the water in the load bank tank was not conductive enough to step up to 140 A which required addition of salt. Therefore, several steps of load increase can be seen in the graphs below reporting the plot over time of the system output power (Figure 77) and the combined current of the two stack strings (Figure 78).

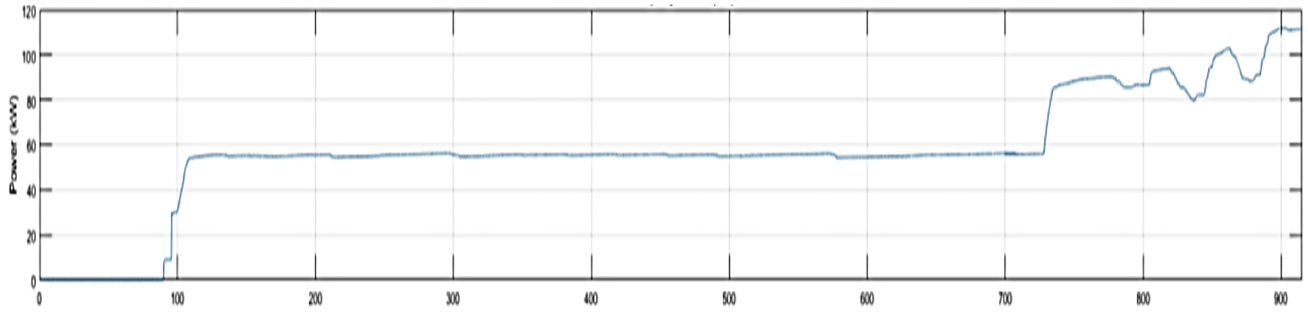

Figure 77. System cold startup: system output power. [110]

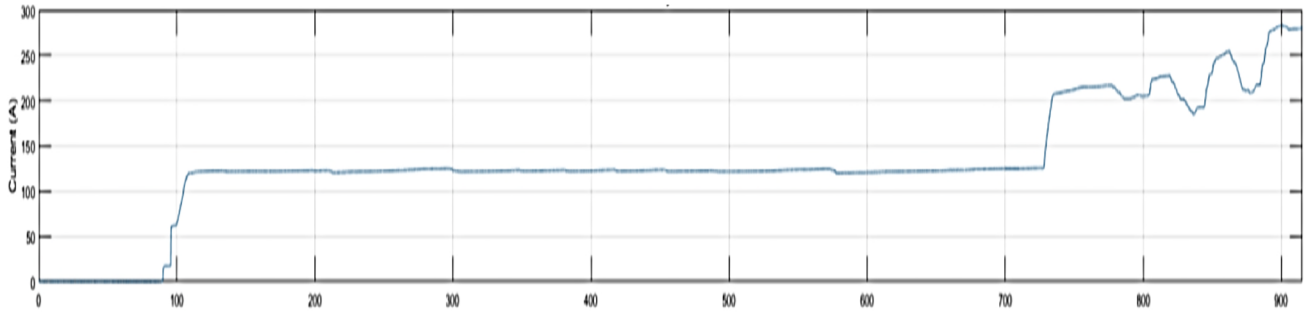

Figure 78. System cold startup: combined current of the two stack strings. [110]

During the test, the temperature of the stack raised from 25 ºC to about 55 °C. The plot over time of the stack temperature recorded during the test is reported in Figure 79.

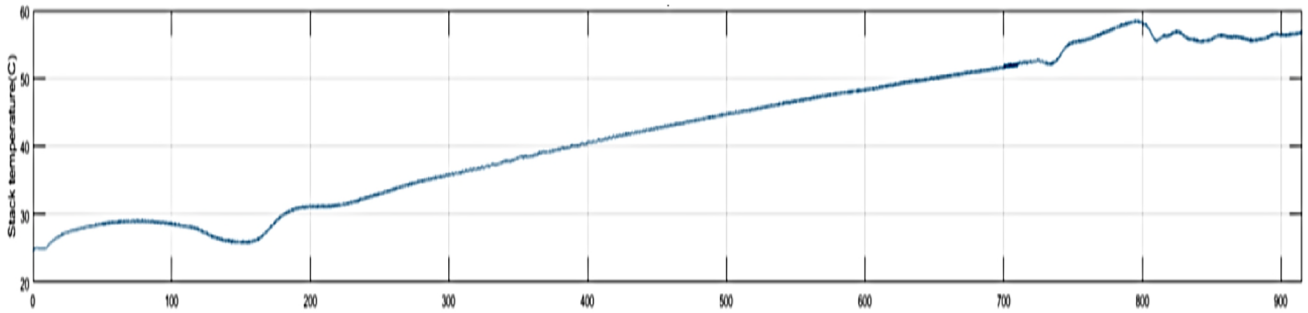

Figure 79. System cold startup: stack temperature. [110]

Due to the issue with the load bank, the duration of this complete process was about 15 min.

Electrical power response test – down transient:
During the test, the system output current was ramped down from 120 A per string to 80 A per string. The two graphs below, respectively report the plot over time of the system output power (Figure 80) and of the combined current of the two stack strings (Figure 81).

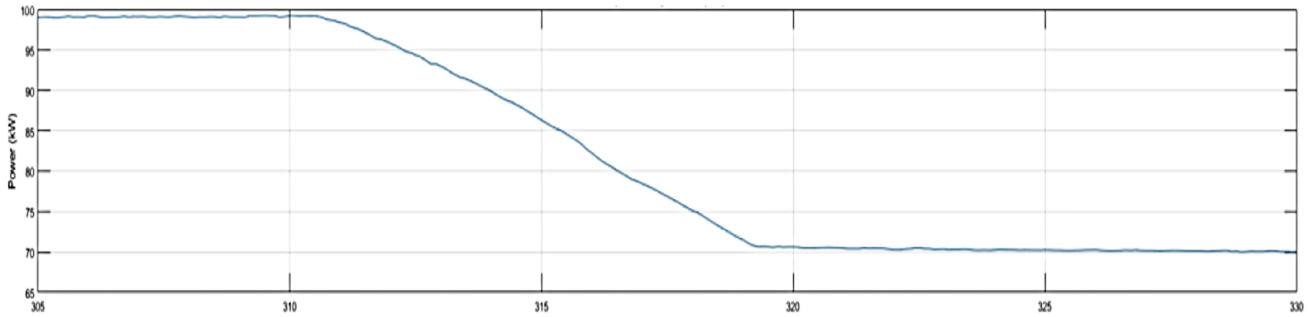

Figure 80. Down transient test: system output power. [110]

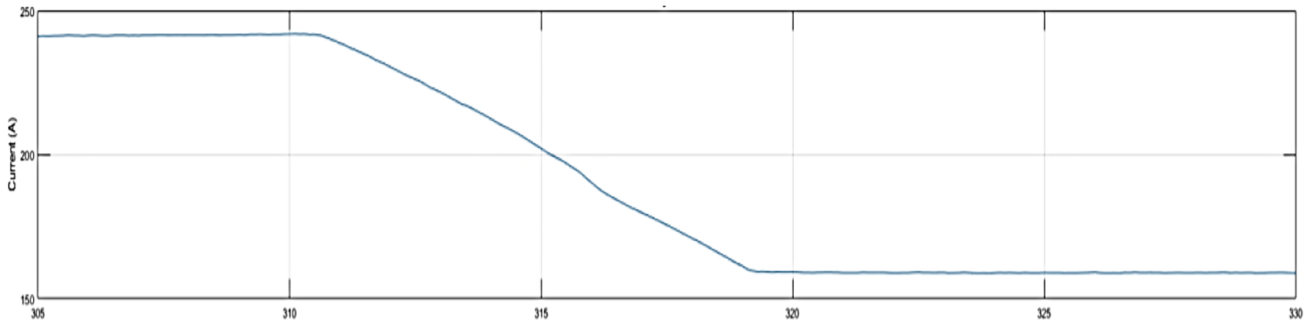

Figure 81. Down transient test: combined current of the two stack strings. [110]

Despite the limitation in speed of he manually controlled load bank used during the test, the time recorded was less than 10 seconds.
During the ramp down the system was stable in terms of performance and temperature control, with stack temperature maintained within the stated in test reqirement (T_{stack} = 55 ± 3 °C).
The plot over time of the stack temperature recorded during the test is reported in Figure 82.

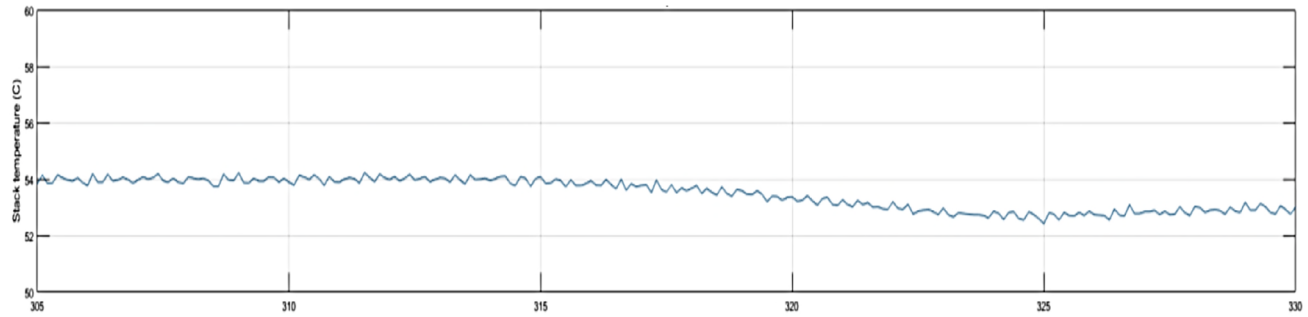

Figure 82. Down transient test: stack temperature. [110]

Electrical power response test – up transient:
During the test, the system output current was ramped up from 80 A per string to 120 A per string.
The plot over time of the system output power and of the combined current of the two stack strings is reported respectively in Figure 83 and Figure 84.

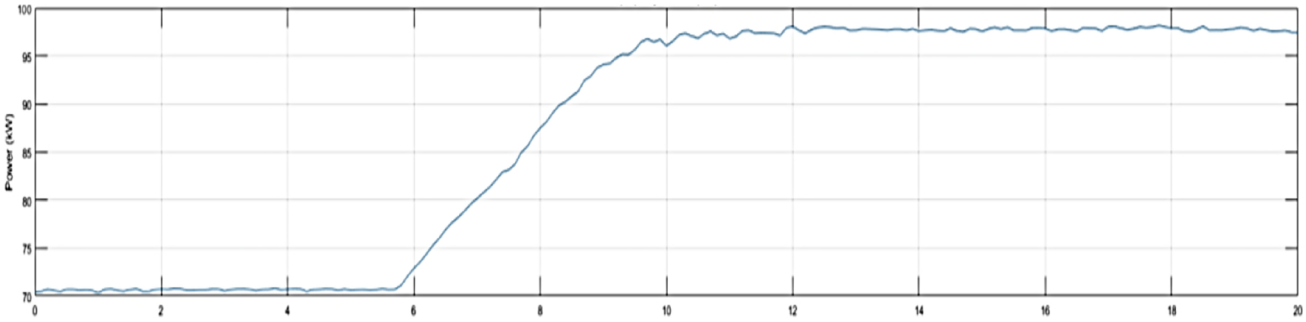

Figure 83. Up transient test: system output power. [110]

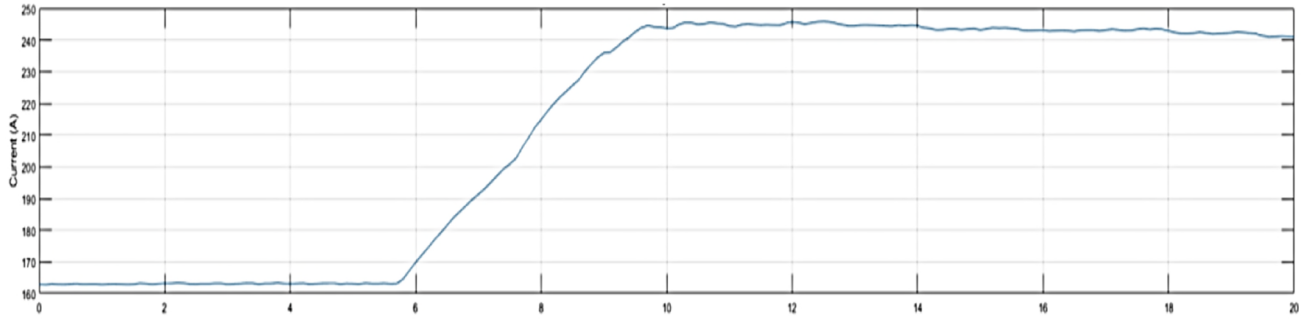

Figure 84. Up transient test: combined current of the two stack strings. [110]

The system response time recorded was of about 6 seconds.
During the ramp up, the system was stable in terms of performance and temperature control, with stack temperature maintained within the stated in test reqirement (T_{stack} = 55 ± 3 °C).
The plot over time of the stack temperature recorded during the test is reported in Figure 85.

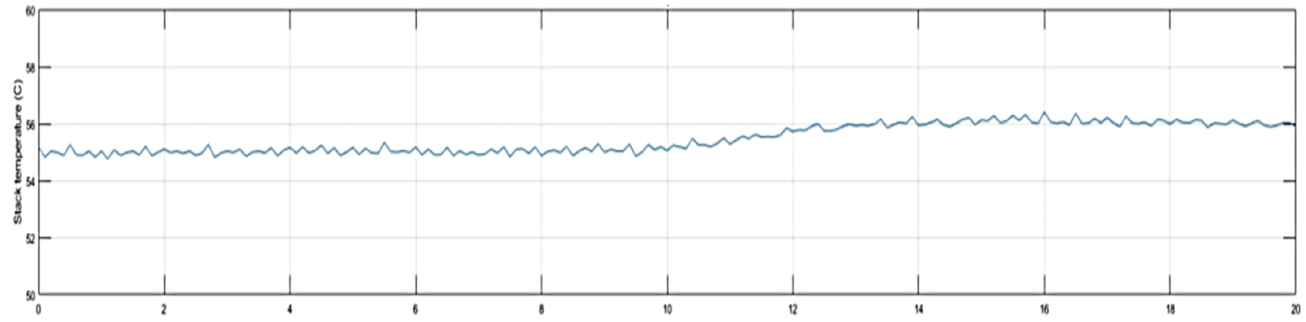

Figure 85. Up transient test: stack temperature. [110]

Shutdown time evalutation test:
At the end of the tp reansient test, the system was given the 'Stop' command from operation at 120 A per string. The plot over time of the system output power and of the combined current of the two stack strings is reported respectively in Figure 86 and Figure 87.

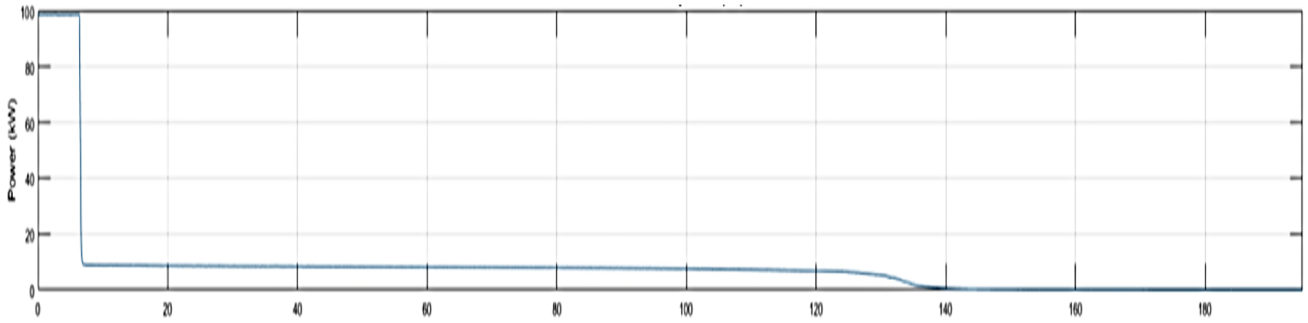

Figure 86. Shutdown test: system output power. [110]

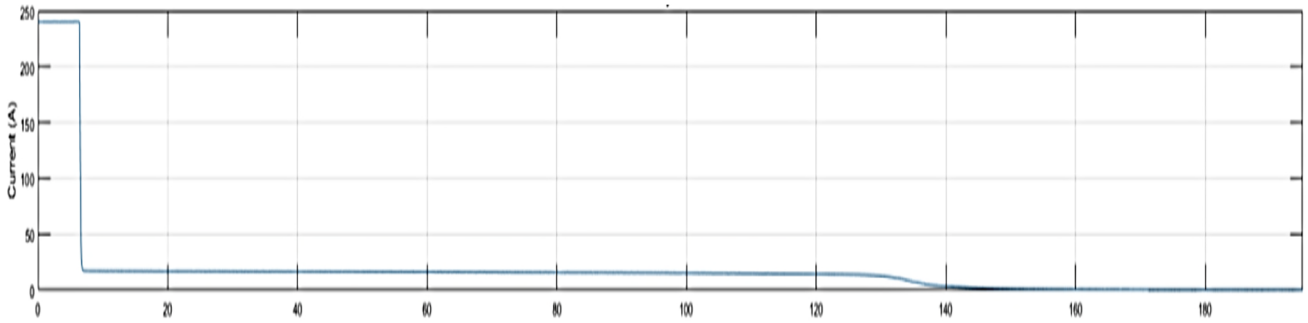

Figure 87. Shu down test: combined current of the two stack strings. [110]

The time taken by the system from receiving the command to reaching the OFF state was 3 min.
The recorded time included the system's embedded stack oxygen depletion procedure which is automatically performed by the system. A recirculation loop on the stack cathode side enables the reaction of residual oxygen to achieve an inert system containing only N_2 and H_2 in the OFF state.
The plot over time of the stack temperature recorded during the test is reported in Figure 88.

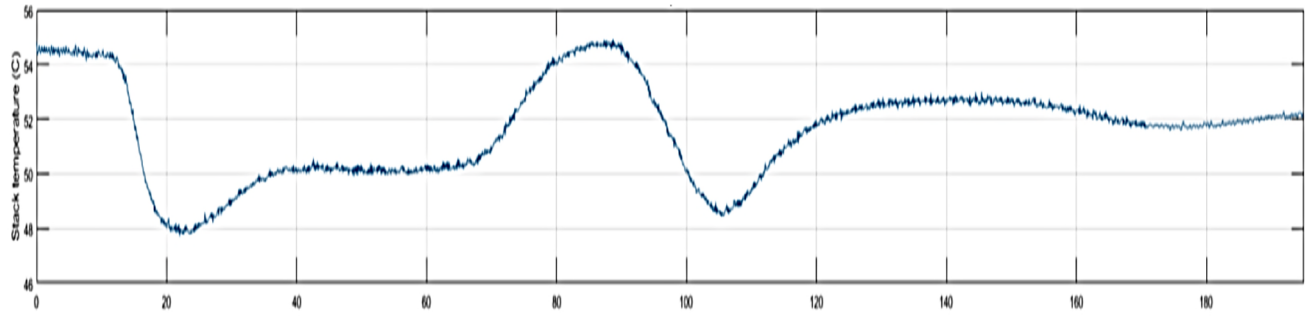

Figure 88. Shut down test: stack temperature. [110]

Hot startup test:
In the test, the system was started from the OFF state with stacks at temperature of 52 ºC and to the operation state at 120 A per string. In the test the rated oytput current per sting was reached by applying a step load of 120 A directly after startup.
The plot over time of the system output power and of the combined current of the two stack strings is reported respectively in Figure 89 and Figure 90.

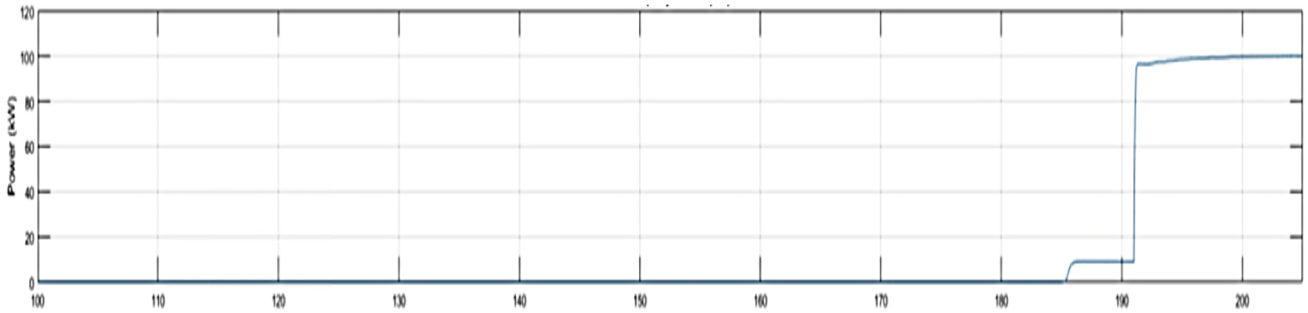

Figure 89. Hot startup test: system output power. [110]

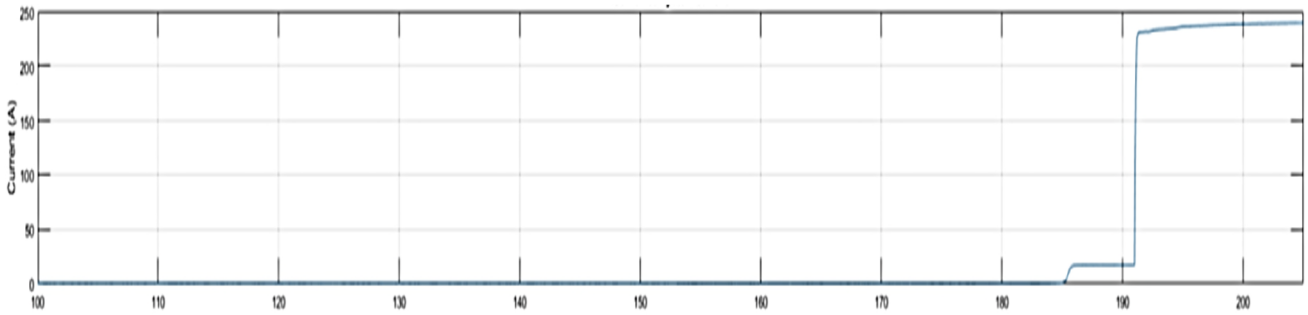

Figure 90. Hot startup test: combined current of the two stack strings. [110]

The hot startup from OFF state to operation at 120 A per string took about 1.5 minutes, for the startup procedure and 3 seconds for ramp-up to 120A per string.
The plot over time of the stack temperature recorded during the test is reported in Figure 91.

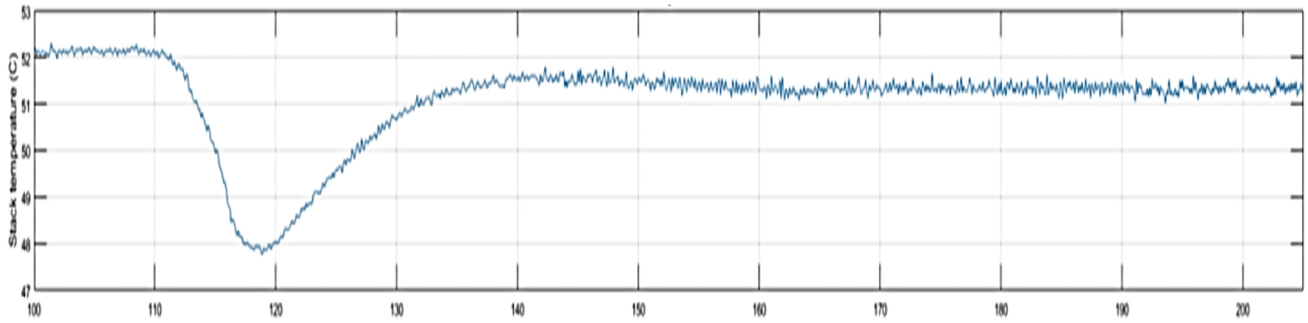

Figure 91. Hot startup test: stack temperature. [110]

An enlargement of the plot over time of the system output power step load is given in Figure 92.

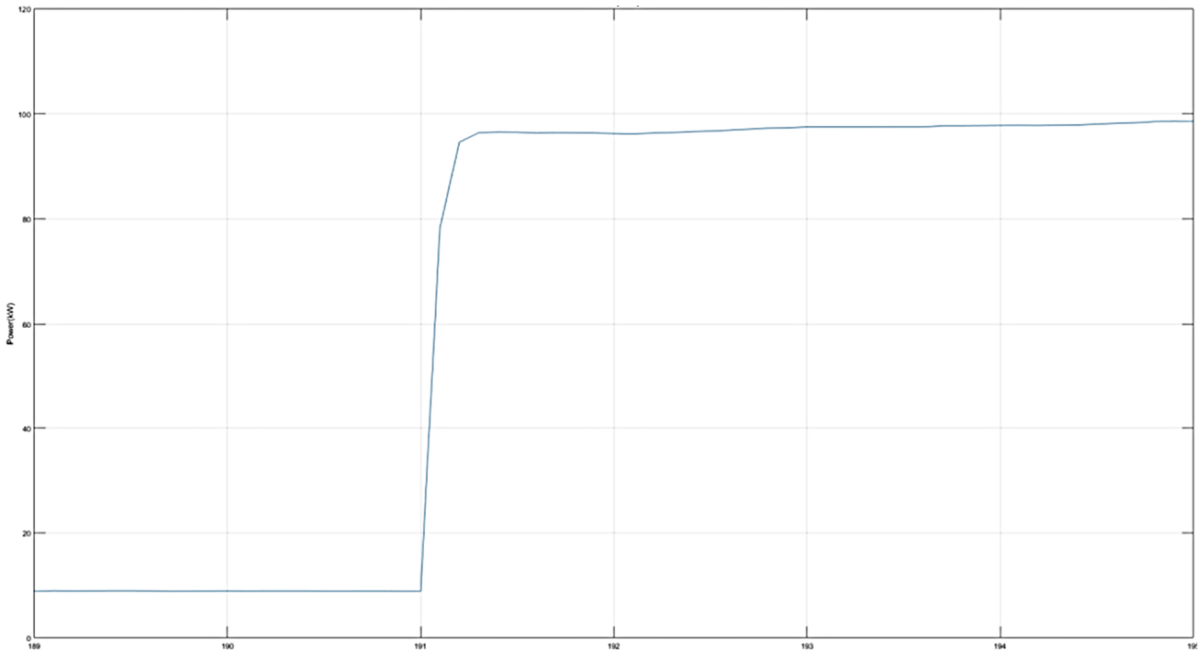

Figure 92. Hot startup test: output power step load. [110]

Steady state operation and stability tests:

In the test the system was kept operational at 140 A per string corresponding to the system's rated output of of 110 kWe for more than 2 hours. The system's performance very stable as can be seen from the power & current plots over time (in minutes) of Figure 93 and Figure 94.

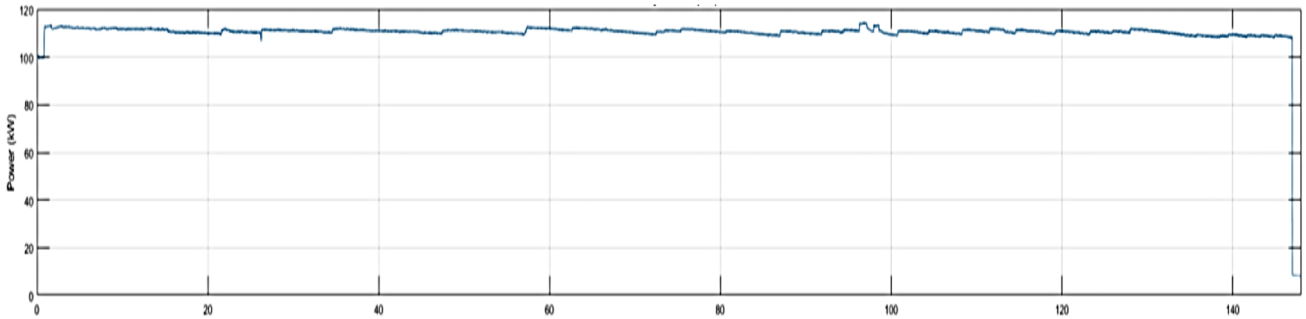

Figure 93. Steady state operation and stability test: system output power. [110]

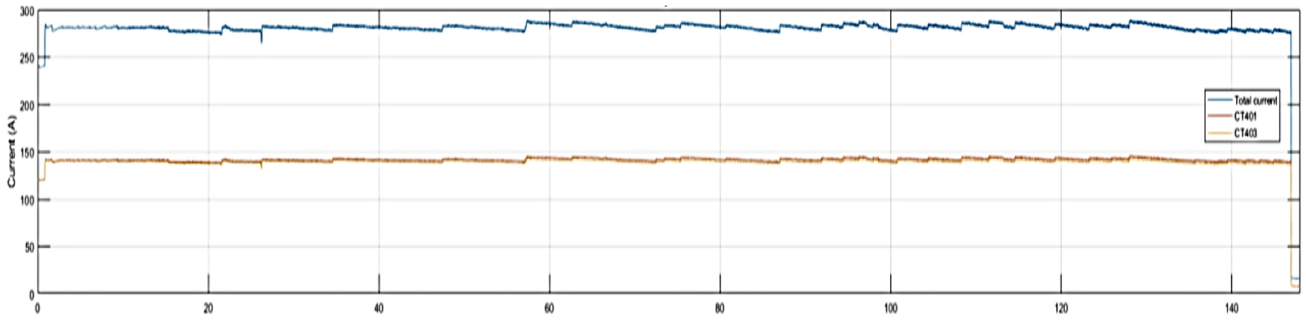

Figure 94. Steady state operation and stability test: string currents and combined current of the two stack strings. [110]

Figure 94 reports both the string currents recorded through currente transformers (CT401 and CT403) and the total output current of the system.

Small disturbances were recorded in the current trends due to manual control of the load bank.
For the entire duration of the test, no warning or error messages were triggered.
During the test the system was stable in terms of performance and temperature control, with stack temperature maintained within the stated in test reqirement ($\Delta T_{stack} \leq 5$ °C) as shown in the plot over time (in minutes) of Figure 95.

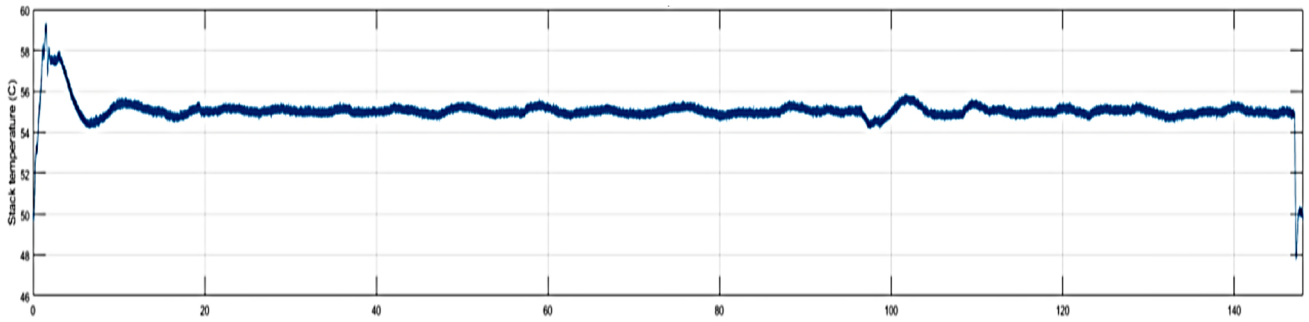

Figure 95. Steady state operation and stability test: stack temperature. [110]

The cell performance was consistently distributed, with average cell voltage ranging between 660 mV and 690 mV. The plot over time (in minutes) of the average cell voltage is reported in Figure 96.

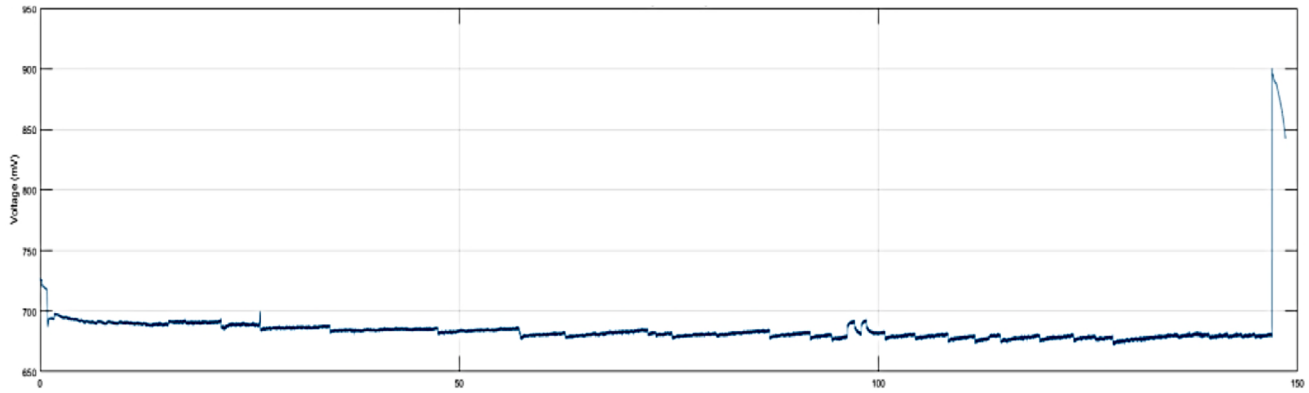

Figure 96. Steady state operation and stability test: average cell voltage. [110]

The difference in current distribution between the 2 strings was less than 3.5 A as reported in Figure 97 which reports the plot over time (in minutes) of the current difference between the two stack strings.

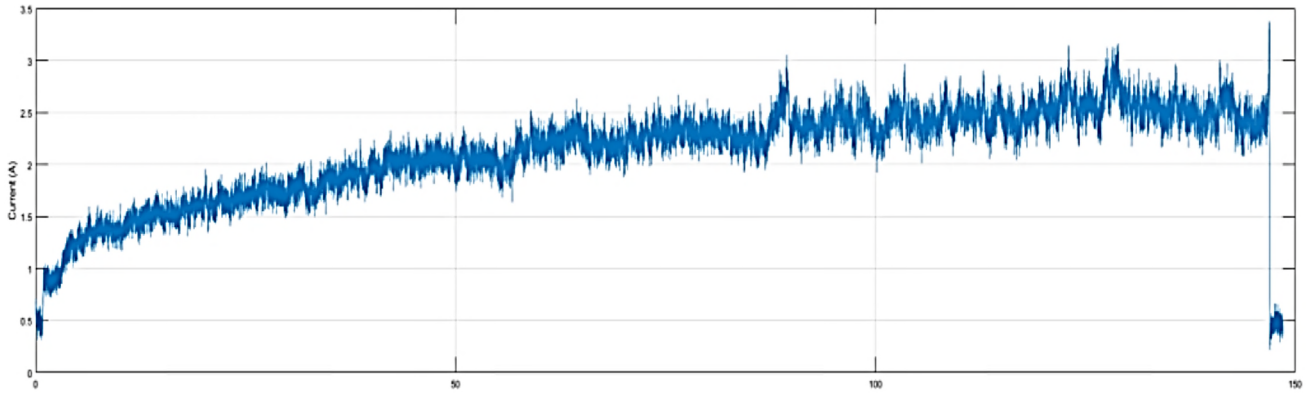

Figure 97. Steady state operation and stability test: current difference between stack strings. [110]

During the test, the stack efficiency referred to hydrogen LHV was calculated as well. The average alculated stack efficiency was 55 %, in line with the data decalred in the technical specification.

Black-out test:
The power supply was switched off while the system was operational at 30 A per string. The system went to OFF state immediately and remained in the OFF state when switching the power supply back on.

Emergency shut down (ESD) test:
The ESD button on the system panel was pressed while the system was in operation at 30 A per string. The system was completely off and reached the defined safe state:

- H_2 inlet valve and purge valve closed;
- DC contactors open;
- power sources disconnected from equipment.

The system is completely powered off with only the H_2 sensor remaining active.

System restart after ESD:
At the end of the ESD procedure, the system was kept in the OFF state for 30 minutes. During this time, the stack cooling system was manually started in "Service" mode to reduce the stack temperature to 30ºC. The system was then given the "Start" command and, after the warming phase, it was brought to deliver 100 A per string. System performance was stable, with no evidence of water accumulation problems within the system.

Internal H_2 sensor test:
The aim of the test was to demonstrate the proper functionality of the H_2 sensor in the system. For this purpose, an internal hydrogen leak event was simulated by manually releasing a forming gas composed of a mixture of H_2 and N_2 inside the system to raise the internal H_2 concentration. The rising H_2 concentration could be seen on the test rig monitoring screen and, as soon as the 20 % LEL was reaches, the system automatically activated the emergency shutdown procedure.

6.2.4 Power converter technical specification

A schematic block diagram of the power converter FZ/001CO installed in the test rig is represented in Figure 98.

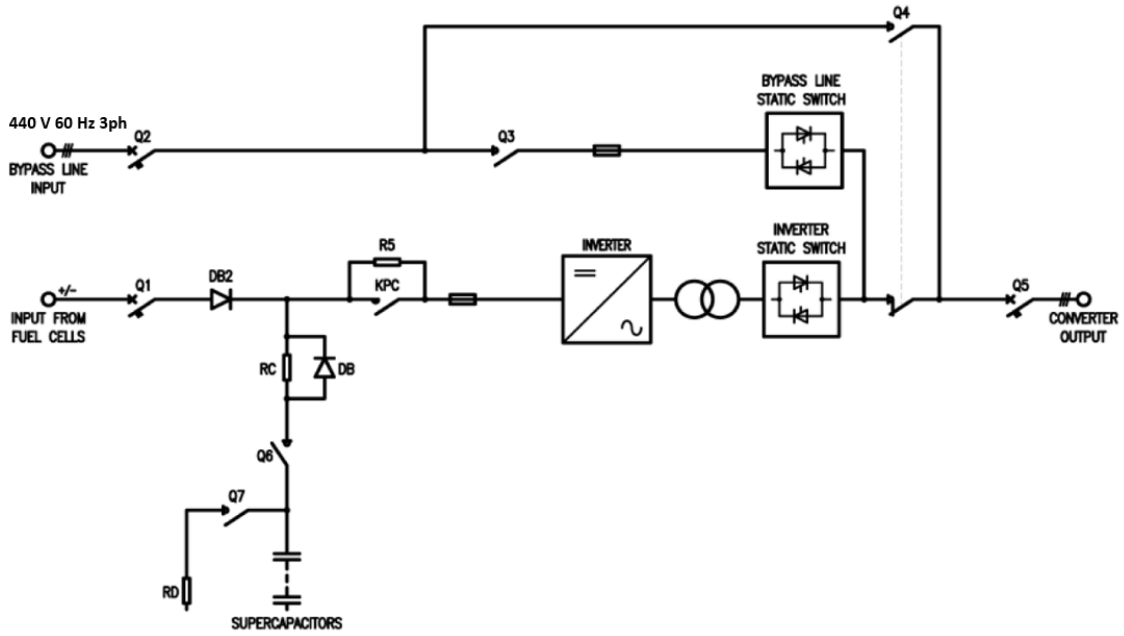

Figure 98. Power converter block diagram. [111]

The equipment is provided with two three phase (3ph) 440 V 60 Hz supply branches feeding the output load:

- Inverter/static transfer switch branch (downstream the test rig fuel cell generator);
- Bypass/static transfer switch branch (mains power supply).

The incoming and outgoing feeder lines are protected by means of automatic circuit breakers.
In normal operating condition (Figure 99), the 3ph 440 V 60 Hz power converter output to the load is fed through the inverter/static transfer switch branch. With reference to Figure 98, the other main components of the system are, from left to right:

- backup unit (Supercapacitors);
- inverter (DC/AC Converter) with isolation transformer;
- static transfer switch;
- bypass line with maintenance manual bypass switch.

The backup unit is composed of supercapacitors and is designed to guarantee continuity of supply to the inverter for 5 seconds (without contribution form the fuel cell) starting from a voltage of 462 VDC. The backup unit is equipped with capacitors pre-charge resistor circuit to limit the current drawn by the fuel cell system during startup. The DC current from the fuel cell enters the 3ph inverter which, with a total controlled sequential turning on of IGBTs, produces a PWM alternated voltage, converted then into 3ph sinusoidal voltage 440 V 60 Hz output to the load. The inverter control logic guarantees three phase constant output and protects inverter from overload. The inverter is equipped with an automatic capacitors pre-charge circuit to charge the inverter input capacitors during system startup [111].

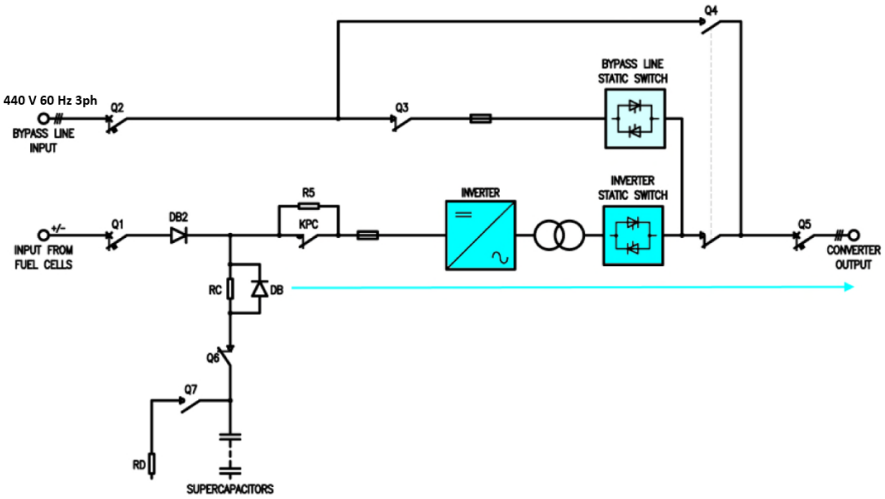

Figure 99. Power converter normal operation. [111]

The static transfer switch has two incoming voltages: one from ship's mains, the other generated by the inverter. Internal control logic provides incoming voltages synchronization. Current on load side of the static transfer switch is monitored to protect it from overload. As previously described, during normal operation the load is fed through the inverter/static switch branch.
The static transfer switch control logic automatically commutates to the bypass/static transfer switch branch in the following cases:

- the inverter output voltage is out of range;
- the inverter is overloaded (e.g., by a short circuit on the downstream distribution system);
- the fuel fell system is turned off.

Commutation occurs without any interruption, being the static transfer switch incoming voltages always synchronized.

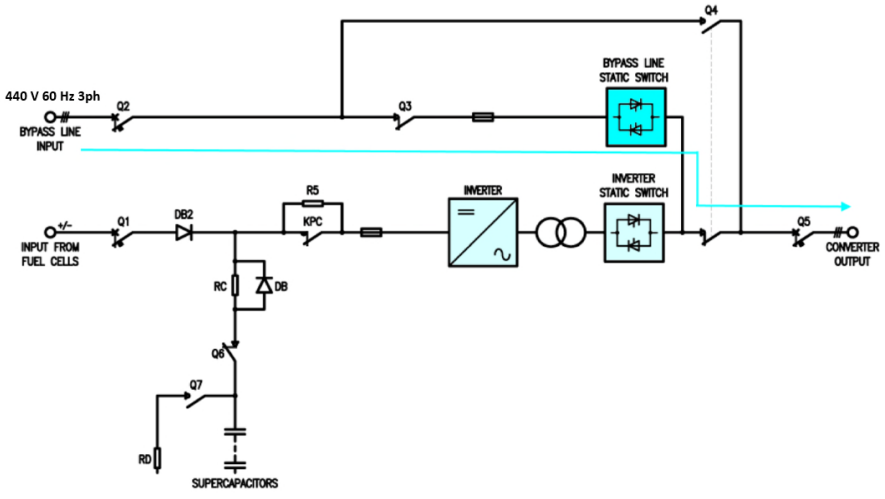

Figure 100. Power converter bypass operation. [111]

In addition, a manual by-pass to be operated only in case the DC/AC Inverter is put out of order for maintenance is provided. Manual operation of the bypass switch does not cause any interruption of the power supply to the electrical load [111].

The power converter and supercapacitors main data are summarized in Table 30 and Table 31.

Power converter main data	
Backup Unit	
Backup time	5 sec. @ full load starting from 462 VDC
Inverter	
Rated power	100 kVA PF1
Input voltage range	300 – 620 VDC
Output voltage	440 VAC 60Hz 3Ph
Output voltage Static Stability	±2%
Output dynamic response	± 10% (0 – 100%; 100%-0% load) recovery time within 100 ms
Output THDV	< 3% with linear load
Bypass Line	
Input voltage	440 VAC 60 Hz 3Ph
Input voltage range	± 10 %
Input frequency range	± 5 %
Commutation time	≤ 1ms
Manual bypass type	Make before brake
Enclosure/Other features	
Cubicle type	“dead front” with doors
IP protection degree (closed doors)	IP 22
IP protection degree (open doors)	IP 20
Cooling	Forced ventilation
Cable penetration	From bottom or top
Cable connection	Insulated screw terminal blocks
HMI (Human Machine Interface)	Display colored touch screen
Communication	Modbus RTU (via RS485)
Dimensions	2190x900x2100mm
Weight	about 2000 kg

Table 30. Power converter main data. [112]

Figure 101. Power converter installed in the test rig. Photo by the author.

Power converter supercapacitors main data	
Description	**Data**
Manufacturer/model	Eaton XLM-62R1137A-R
Maximum working voltage (Single module)	62.1 V
Nominal capacity (Single module)	130 F
Number of modules in series	11
Total bank max voltage	683 V (62.1 V x 11)
Total bank capacity	11.8 F
Backup time	5 s (After an inverter output load step to 100%, with inverter input voltage starting from 462 VDC and considering the final voltage 290 VDC)

Table 31. Power converter supercapacitors main data. [111]

Figure 102. ower converter supercapaciors. Photo by the author.

6.2.5 Performance and safety tests carried out on the power converter

Although based on industrial inverters for marine applications, the power converter for the test bed including the supercapacitor-based energy storage system was a prototype unit.
Similarly to what was done on the fuel cell generator, before being installed in the test rig, the power converter was subjected to a program of performance tests conducted at the manufacturer's premises to verify the compliance of the generator with the technical specification requirements and its response times. In particular, the tests focused on verifying the quality and voltage supplied by the equipment, on the correct activation of the inverter in the expected DC power supply range and on verifying the autonomy guaranteed by the supercapacitor storage system.
The most noteworthy results of the tests performed are hereinafter reported.

Figure 103. Power converter under test. Photo by the author.

Total armonic distortion of voltage (THDV) on AC output:
The purpose of the test was to verify that the harmonic distortion level of the converter output voltage respected the performance limits set by the technical specification.
For this purpose, the converter has been tested with linear resistive inductive and capacitive loads, balanced and unbalanced for different values of DC power supply voltage of the inverter included in the possible operation range of the fuel cell. Test results confirmed that output distortion met the technical specification requirement (THDV < 3% with linear load). A summary of the results of the most the significant test performed is given in Table 32.

Input VDC	Outputvoltage			Output current			power factor	Load %	THDV %
	L1-N	L2-N	L3-N	L1	L2	L3			
300	253	253.6	255.1	131	131	131	1	100	1.3
450	254.5	254.4	255.5	33	33	33	1	25	1.6
450	254.3	254.1	255.5	66	66	66	1	50	1.2
450	253.1	253.6	255	131	131	131	1	100	1.4
620	254.1	253.9	255.4	131	131	131	1	100	1.7
300	256.2	255	254.5	0	0	131	1	100	1.4
450	255.4	255.2	255.6	0	0	33	1	25	1.4
450	255.7	255.1	255.1	0	0	66	1	50	1.4
450	256.1	255.1	254.5	0	0	131	1	100	1.4
620	256.1	255.1	254	0	0	131	1	100	1.4
300	253.9	253.8	255.2	131	131	131	0.8 inductive	100	1.3
450	254.6	254.4	255.8	33	33	33	0.8 inductive	25	1.1
450	254.5	254.2	255.6	66	66	66	0.8 inductive	50	1.1
450	254	253.8	255.2	131	131	131	0.8 inductive	100	1.1
620	254.1	253.9	255.3	131	131	131	0.8 inductive	100	1.4
300	255.9	255.4	254.2	0	0	131	0.8 inductive	100	1.4
450	255.5	255.5	255.6	0	0	33	0.8 inductive	25	1.3
450	255.5	255.5	255.2	0	0	66	0.8 inductive	50	1.4
450	255.9	255.8	254.2	0	0	131	0.8 inductive	100	1.4
620	256.1	255.8	254.2	0	0	131	0.8 inductive	100	1.5
300	254.2	254	255.8	131	131	131	0.8 capacitive	100	1
450	254.7	254.6	256	33	33	33	0.8 capacitive	25	1.2
450	254.6	254.4	255.8	66	66	66	0.8 capacitive	50	1.2
450	254.2	254	255.5	131	131	131	0.8 capacitive	100	1
620	254.3	254	255.6	131	131	131	0.8 capacitive	100	1.2
300	256	254.5	255.1	0	0	131	0.8 capacitive	100	1.7
450	255.3	255.1	256.2	0	0	33	0.8 capacitive	25	1.3
450	255.5	254.7	256.2	0	0	66	0.8 capacitive	50	1.2
450	255.5	254.5	255.1	0	0	131	0.8 capacitive	100	1.4
620	256	254.2	255.1	0	0	131	0.8 capacitive	100	1.6

Table 32. Power converter THDV on linear load. [113]

Inverter turn on test:

The purpose of the test was to verify the correct turning on of the inverter when supplied with a DC voltage variable in the range of possible operation of the fuel cell. For this purpose, the inverter was first supplied with a voltage of 300 VDC, then with a voltage of 450 VDC and finally. with a voltage of 600 VDC. In all cases the inverter switched on and steadily supplied the rated output voltage in less than 30 ms as shown in the upper part of the following oscillographic recordings where trends over time (time scale 10 ms/div in all graphs) of the phase-to-phase voltages at the converter output are reported.

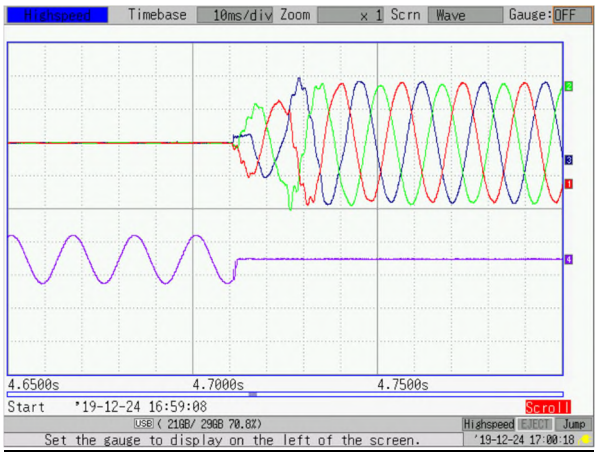

Figure 104. Inverter turning on. Input voltage 300 VDC. [113]

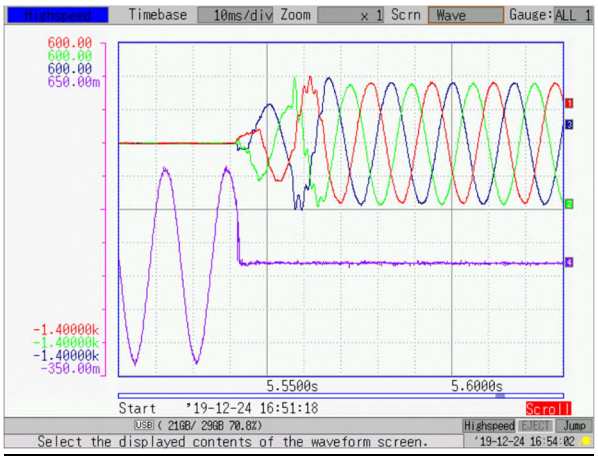

Figure 105. Inverter turning on. Input voltage 450 VDC. [113]

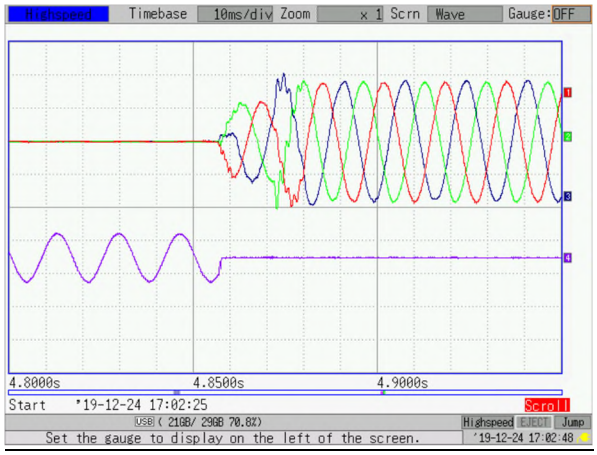

Figure 106. Inverter turning on. Input voltage 600 VDC. [113]

Inverter sudden load variation test

The purpose of the test was to verify compliance with the technical specification requirement relating to the converter response times following instantaneous load variations. for this purpose, the converter was subjected to a sudden 0-100% load increase and, subsequently, a sudden 100-0% load disconnection. The oscillographic recordings of the two tests are placed respectively in Figure 107 and Figure 108 in which are reported (with an appropriate offset) the trends over time of the phase-to-phase voltages at the converter output. In all the graphs the time scale is 10 ms/div. In both tests the voltage undershoot/overshoot recovery time was of the order of 20 ms, well below the technical specification requirement (recovery time within 100 ms).

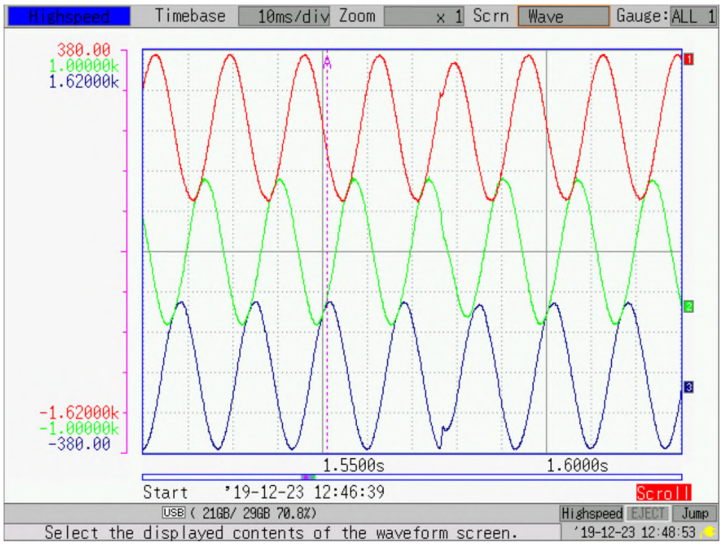

Figure 107. Converter output voltage undershoot recovery following 0-100 % sudden load variation. [113]

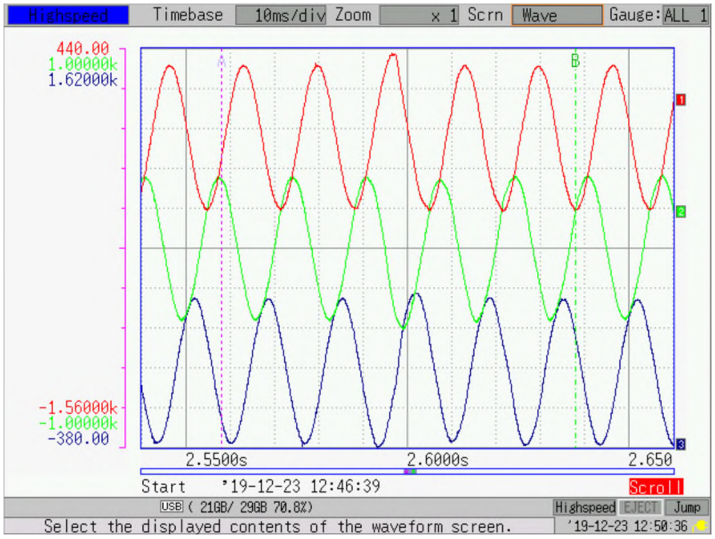

Figure 108. Converter output voltage overshoot recovery following 100-0 % sudden load variation. [113]

Supercapacitor storage system backup time evaluation test:

The purpose of the test was to verify that the supercapacitor bank had been correctly sized and guaranteed power supply to the rated load of the power converter for a time equal to or greater than that indicated in the technical specification.

The supercapacitor bank was therefore initially charged at different DC voltages in the range of possible operation of the fuel cell and was discharged to a minimum voltage of 290 VDC (below which the inverter is switched off) while the converter fed its nominal load of 100 kWe.

For each of the discharge tests, the trends of the voltage and current of the capacitor bank and the duration of the discharge until reaching the final voltage of 290 VDC were recorded. Tests confirmed the technical specification requirement i.e., a backup time of at least 5 seconds with supercapacitors loaded at 462 VDC.

The oscillographic recordings made with supercapacitors loaded at 462 VDC are reported in Figure 109.

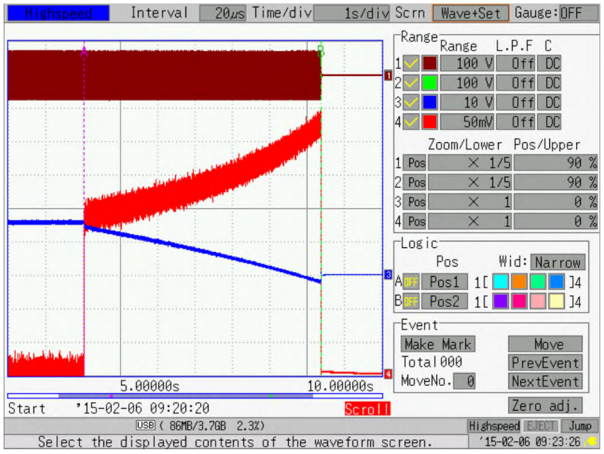

Figure 109. Supercapacitor discharge: from 462 VDC to 290 VDC with converter feeding 100 KWe. [113]

In the recordings the scale of the time axis is equal to 1s/div. The trend over time of the capacitor discharge voltage curve is shown in blue (voltage scale 100V/div), while the trend of the current delivered by the consendstores is shown in red (current scale 50A/div).

As shown in Figure 110, capacitor discharge started at the instant A (t=4.04 sec) and ended at the instant B (t=10.38 sec). The capacitor total discharge time with converter delivering the power of 100 kWe was 6.34 sec, higher than the technical requirement.

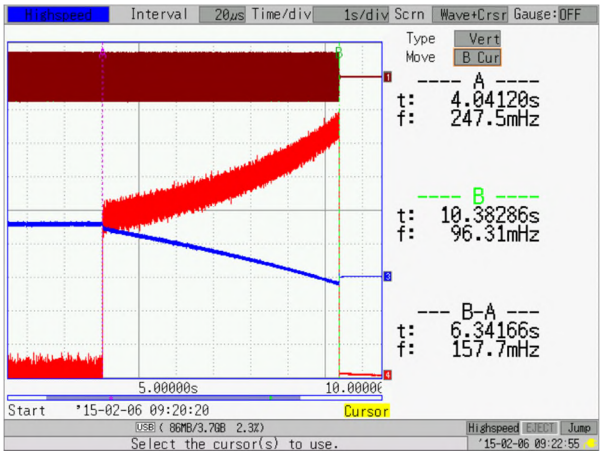

Figure 110. Supercapacitors discharge: from 462 VDC to 290 VDC. Discharge time evaluation with converter feeding 100 kWe. [113]

Additional tests were performerd on order to evaluate the converter rated load backup time guaranteed by the supercapacitors loaded at a voltage higher or lower than the technical specification value. With supercapactors loaded at 520 VDC, the recorded back-up time was 10.78 sec as shown in Figure 111.

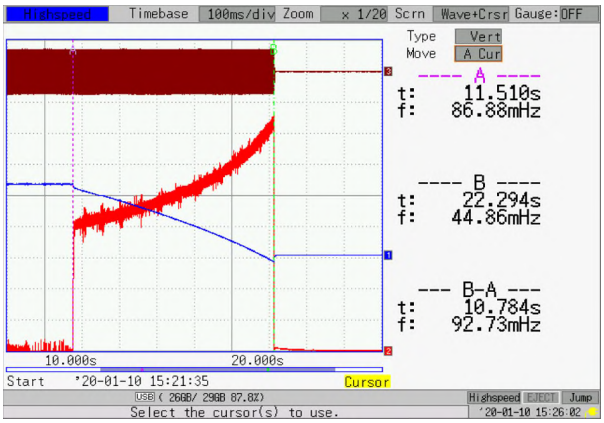

Figure 111. Supercapacitors discharge: from 520 VDC to 290 VDC. Discharge time evaluation with converter feeding 100 kWe. [113]

With supercapactors loaded at 370 VDC, the recorded back-up time was about 2 seconds.

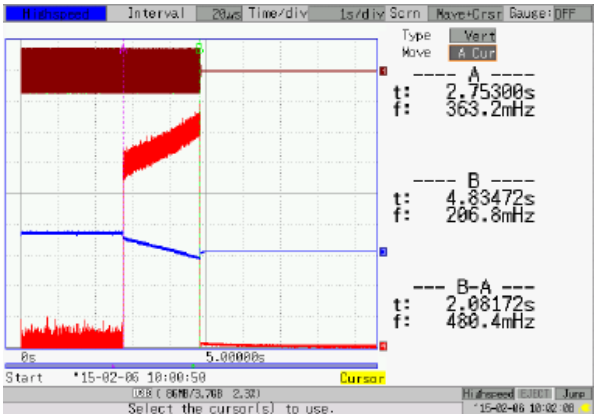

Figure 112. Supercapacitors discharge: from 370 VDC to 290 VDC. Discharge time evaluation with converter feeding 100 kWe. [113]

With supercapactors loaded at 310 VDC, the recorded back-up time was 860 milli seconds.

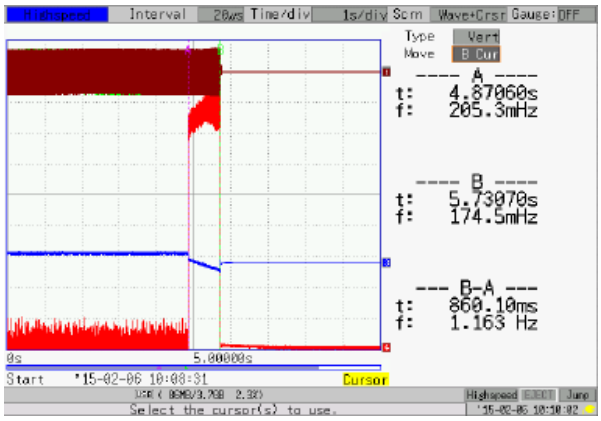

Figure 113. Supercapacitors discharge: from 310 VDC to 290 VDC. Discharge time evaluation with converter feeding 100 kWe. [113]

6.3 Load bank technical specification

The load bench installed in the test rig is a commecial unit ASCO 6045 of the electronic homic/inductive type.

Figure 114. The load bank installed in the test rig (left). Hand-held and software-based control systems (right). [94]

The main data of the load bank asre summarized in the following table:

Load bank main data	
Rated power	100 kVA
Voltage	440 V
Frequency	60 Hz
IP	54 (for outdoor installation)
Cooling systen	Forced ventilation
Noise level	69 ±3 dBA
Resistive load step	1 kW
Indictive load step	1 kVAR

Table 33. Load bank main data. [114]

The load bank is provided with hand-held and software-based monitoring and control systems which allow the parameters of the connected load to be manually modified in terms of:

- kVA and power factor;
- power% and power factor;
- current and power fcator.

The software-based control also implements an automatic control mode that allows the execution of test programs and load cycles carried out by means of a dedicated program editor.

6.4 Safety systems

The terst rig is equipped with dedicated hydrogen and fire detection systems end emergency shutdown pushbuttons. If a safety system is triggered, the solenoid valve for the hydrogen supply to the Fuel Cell is immediately closed and the general shutdown of the equipment is activated.

6.4.1 Hydrogen detection system

Two hydrogen detectors are placed in correspondence with the Fuel Cell and the Electrolyser and connected to a gas detection control unit provided with optical acoustic alarms located inside and outside the test rig room.

Figure 115. Test rig. Hydrogen detection system. [94]

6.4.2 Fire detection system

Fire detectors are arranged to cover the entire surface of the laboratory and connected to a dedicated fire detection control unit provided with optical acoustic alarms located inside and outside the test rig room.

Figure 116. Test rig. Fire detection system. [94]

6.5 Automation plant

The automation plant used in the characterization of the test rig is based on the National Instrument CompactRIO (NI cRIO) controller including a real-time processor, a Field Programmable Gate Array (FPGA), and I/O modules. The I/O modules are directly connected to field instrumentation, and the controller itself is then connected to a host PC on which the user interface has been developed in the National Instrument LabView environment. Both controller and host PC can be connected to the internet for remote system monitoring. Figure 117 below describes the architecture of the monitoring and control system based on the NI cRIO controller.

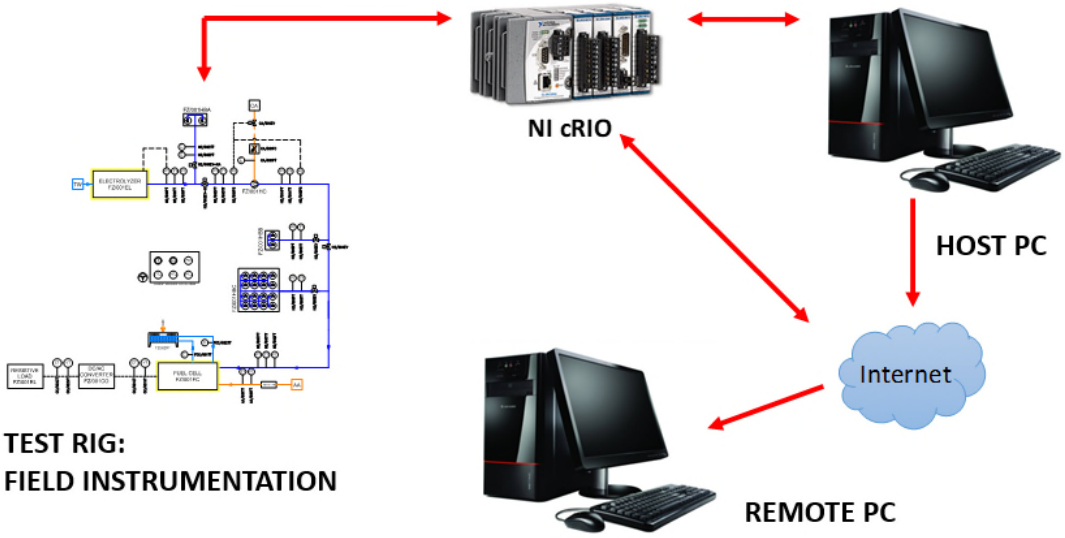

Figure 117. Test rig automation plant. Block diagram.

6.5.1 Automation plant abstract of functions

The I/O modules connected to the compactRIO controller are electrically connected to the sensors and devices present on the test rig lines and to the components of the hydrogen and electrical power production plants. With reference to the plants P&I diagrams (Annex B) and to the automation plant functional diagram (Annex D), Table 34 reports the description of the signals provided from field sensors/devices installed on:

- hydrogen pipes;
- compressed air pipes;
- electrolyser cooling circuit pipes;
- fuel cell cooling circuit pipes;
- converter cooling air outlet;
- load bank cooling air outlet.

The table shows the piece mark of the sensor/device to which the signal refers, the measured quantity or the check carried out, the type of sensor/device and the type of signal.
In the table the field sensors/devices installed on hydrogen pipes are grouped into 5 piping ramps: ramp 1 corresond to the fuel cell generator hydrogen feeding line, whereas ramps 2 to 5 correspond to the various branches of the hydrogen piping od the hydrogen production plant. The location of the various piping ramps is indicated in Figure 118 and Figure 119 with numbered red boxes.

Sensor/ device Piece mark	Measure quantity Or check carried out	Sensor/device type	Signal type
Piping ramp 2			
H2/001PT	H_2 pressure	Pressure transmitter	Analog input 4...20 mA
H2/001TT	H_2 temperature	Temperature sensor	PT 100
H2/001FT	H_2 flowrate	Flowmeter	Analog input 4...20 mA
Piping ramp 3			
H2/001RCV	Open/close	Solenoid valve	Digital output
H2/002TT	H_2 temperature	Temperature sensor	PT 100
H2/002PT	H_2 pressure	Pressure transmitter	Analog input 4...20 mA
Piping ramp 4			
H2/002RCV	Open/close	Solenoid valve	Digital output
H2/003PT	H_2 pressure	Pressure transmitter	Analog input 4...20 mA
H2/003TT	H_2 temperature	Temperature sensor	PT 100
H2/001PS	Status check	Pressure switch	Digital input
Piping ramp 5			
H2/002PS	Status check	Pressure switch	Digital input
H2/005TT	H_2 temperature	Temperature sensor	PT 100
H2/005PT	H_2 pressure	Pressure transmitter	Analog input 4...20 mA
Compressed air circuit			
CA/003PS	Status check	Pressure switch	Digital input
CA/001RCV	Open/close	Solenoid valve	Digital output
CA/001FC	Compressed air flowrate	Controller/flowmeter	Analog input 4...20 mA Output analogico 4...20 mA
CA/001PT	Compressed air pressure	Pressure transmitter	Analog input 4...20 mA
Electrolyser cooling circuit			
EC/001TT	Cooling water temperature	Temperature sensor	PT 100
EC/002TT	Cooling water temperature	Temperature sensor	PT 100
Piping ramp 1			
H2/004RCV	Open/close	Solenoid valve	Digital output
H2/002FT	H_2 flowrate	Flowmeter	Analog input 4...20 mA
H2/007TT	H_2 temperature	Temperature sensor	PT 100
H2/007PT	H_2 pressure	Pressure transmitter	Analog input 4...20 mA
Fuel cell cooling circuit			
FCC/001TT	Cooling water temperature	Temperature sensor	PT 100
FCC/002TT	Cooling water temperature	Temperature sensor	PT 100
FCC/001WM	Cooling water flowrate	Flowmeter	Analog input 4...20 mA
YE/1008_CTR	Circulation pump inverter control	Circulation pump inverter status	Output analogico 4...20 mA
YE1008_PO	Circulation pump inverter power output	Circulation pump inverter status	Analog input 4...20 mA
YE1008_RUN	Circulation pump inverter running	Circulation pump inverter status	Digital input
YE1008_FAIL	Circulation pump inverter failure	Circulation pump inverter status	Digital input
FCC/001DC	Fuel cell dry cooler fans speed	Controllo dry cooler	Analog output 4...20 mA converted in 0-10 V signal through signal converter installed iside automation cabinet
FCC/001DC_S	Fuel cell dry cooler fans CBs status	Fuel cell dry cooler power circuit stats	Digital input
Converter cooling air			
CNV/001TT	Converter cooling air outlet temperature	Temperature sensor	PT 100
Load bank cooling air			
EL/001TT	Load bank cooling air outlet temperature	Temperature sensor	PT 100

Table 34. Test rig automation plant. Field sensors/devices list.

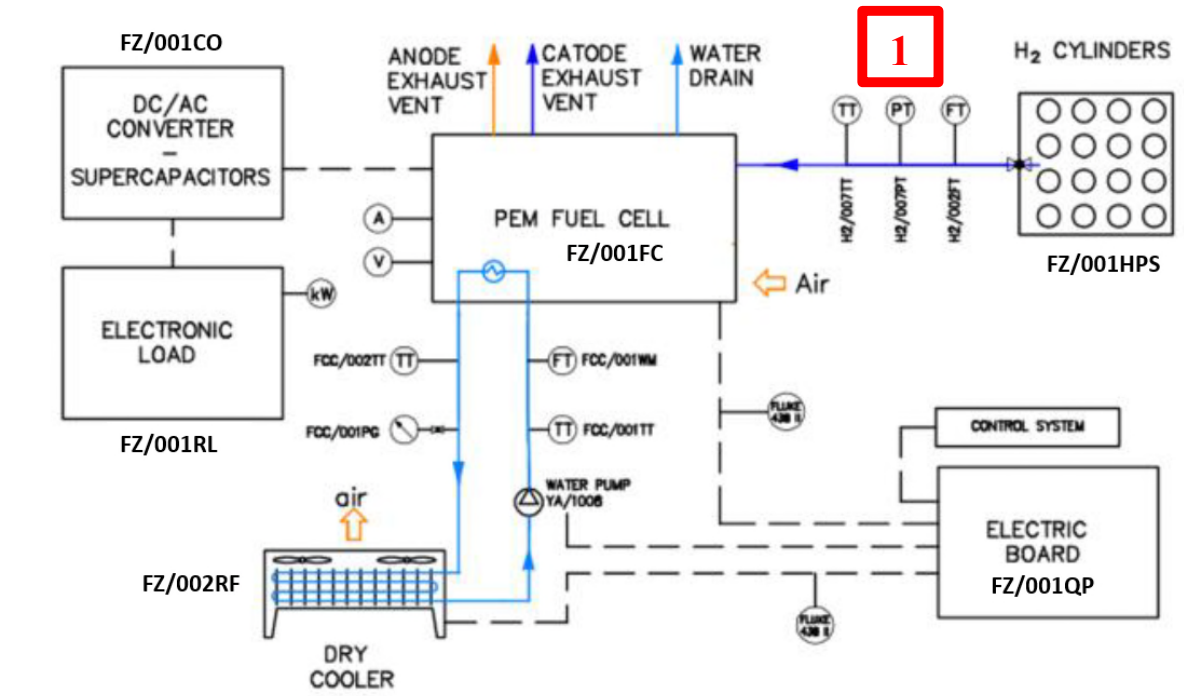

Figure 118. Electric power production plant. Hydrogen piping ramp location.

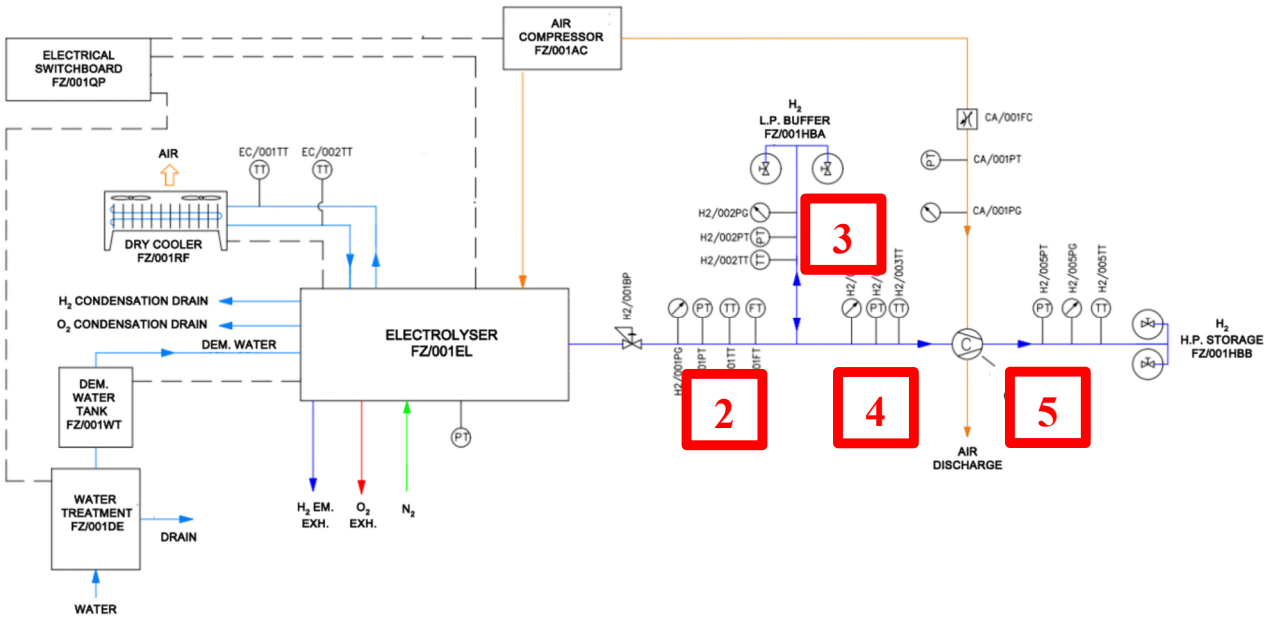

Figure 119. Hydrogen production plant piping ramps location.

In Table 35 are reported the signals coming or supplied to the test rig main components: the electrolyser (FZ/001EL), the fuel cell (FZ/001FC) and the power converter FZ/001CO.

Component Piece mark	Measure quantity Or check carried out	Signal type
Electrolyser		
FZ/001EL	Remote start stop	Digital output.
	Remote reset	Digital output.
	Running	Digital input
	Allarm	Digital input
	Pre-allarm	Digital input
	Power on	Digital input
Fuel Cell		
FZ/001FC	FC running	Digital input
	FC allarm	Digital input
	System start	Digital output
	External emergency stop	Digital output
	External fire allarm	Digital output
	Fuel cell stack voltage	Analog input 4...20 mA
	Fuel cell stack current	Analog input 4...20 mA
Converter		
FZ/001CO	Converter running	Digital input
	Converter allarm	Digital input

Table 35. Test rig automation plant. Signals exchanged with plants main components.

Table 36 summarizes the total number and type of signals managed by the automation system.

Signal type	Total
Analog input 4...20 mA	13
Analog output 4...20 mA	3
Digital input	14
Digital outpi	9
Analog input PT 100	11

Table 36. Test rig automation plant. Total signals managed, by type.

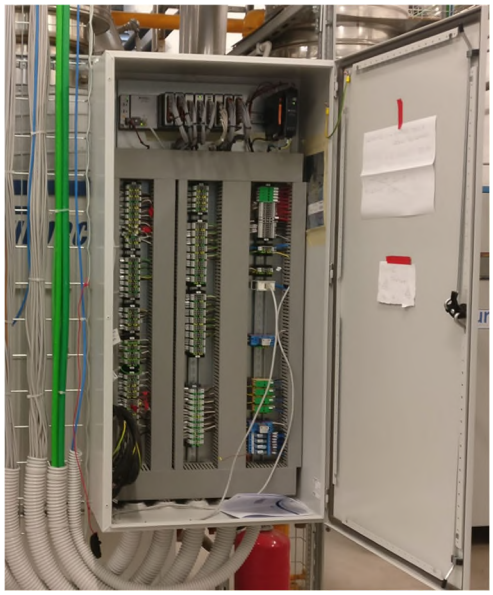

Figure 120. Test rig automation cabinet with compactRIO controller. Photo by the author.

6.5.2 Automation plant operating modes and control logics

The plant has four operating modes:

1. Stand by
2. Hydrogen production
3. Electrical power production
4. System shutdown

The operating modes are initiated and managed by the monitoring and control system which allows the automatic execution of various operations. However, some actions must be performed manually by the operator. The monitoring and control system therefore:

- operate devices such as, for example, remotely operated valves and flow controllers, following a control logic defined according to the state of the system;
- notify the operator of any manual actions to be performed on the system to allow the completion of a certain operating mode;
- check that the status of the connected devices and the value of the monitored quantities are compatible with the expected operating mode and, if not, report it to the operator or initiate corrective actions;
- displays and records the data from the system.

The operating modes listed above are described in the following paragraphs.

6.5.2.1 Stand by mode

The “stand by” mode is activated:

- when starting the acquisition software;
- at the end of the “hydrogen production” mode or the “electrical power production” mode.

In “stand by” mode, the automation plant:

- checks the status of the remote-controlled valves indicated in Table 37, closing them if open:

Valve Piece mark	**Status**
H2/001RCV	Closed
H2/002RCV	Closed
H2/004RCV	Closed

Table 37. “Stand by mode”: controlled valves.

- displays the values of all measured quantities and the status of all remotely controlled devices on the graphical interface;
- records in a specific log file:
    - the values of all the transducer sizes and the status of all remotely controlled devices of the system;
    - the set point values defined in the specific configuration page of the user interface.
- waits for the operator to decide whether to start the hydrogen production plant or the electrical power production plant.

Figure 121 shows an example of the test rig automation plant graphical interface. The page refers to the hydrogen production and compression plant with synoptic representation of the plant. Buttons for the activation of the different operating modes are provided in the lower part of the page.

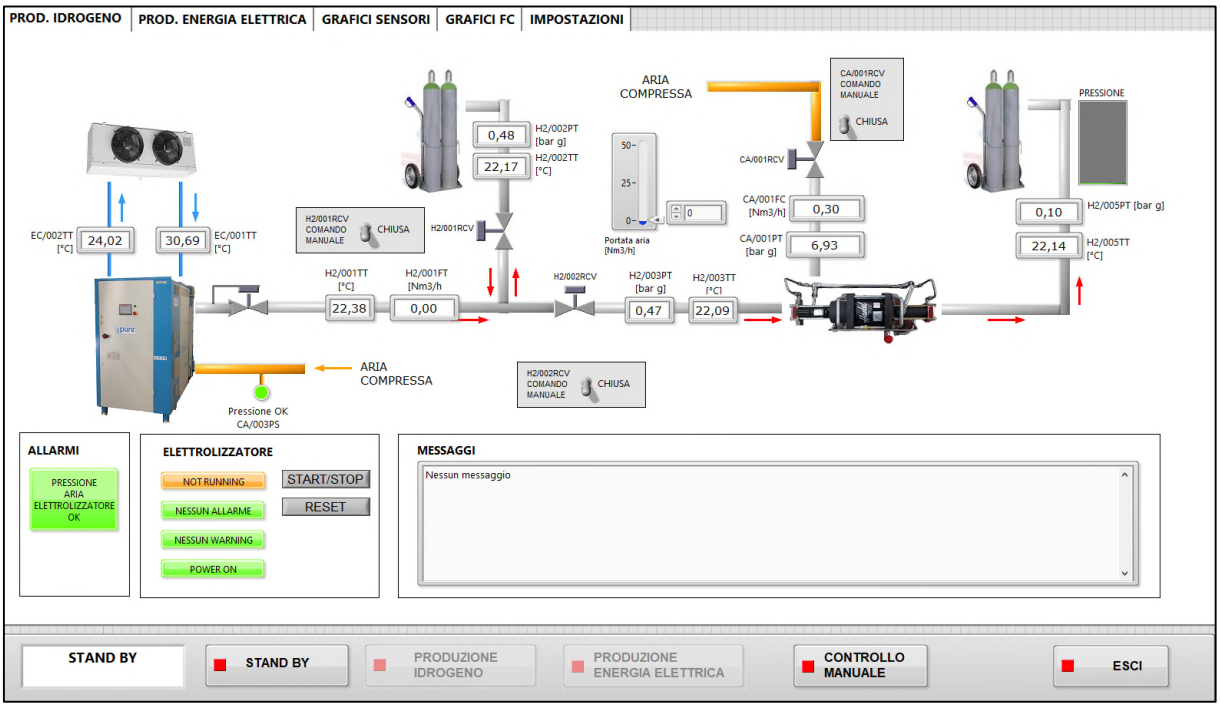

Figure 121. Test rig automation plant. Graphical interface.

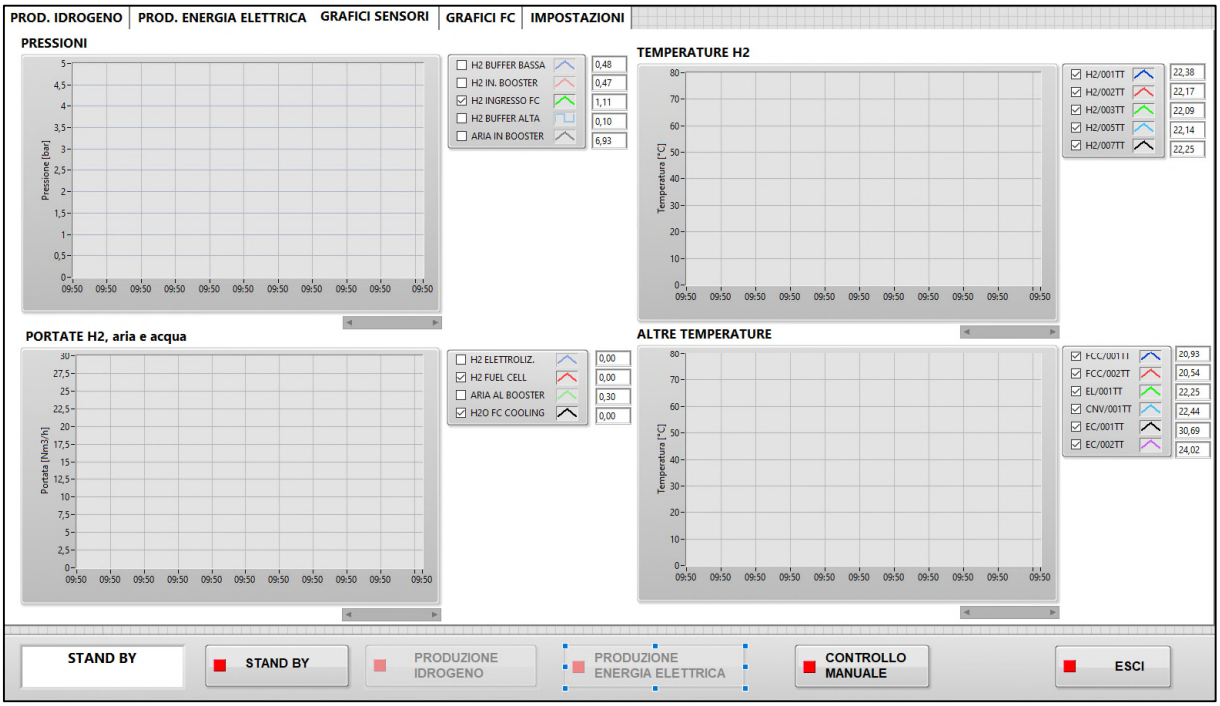

Figure 122. Test rig automation plant. Trends page.

6.5.2.2 Hydrogen production mode

The “hydrogen production” mode is started by the operator who acts on the graphic interface. To access the “hydrogen production” mode, the system must be in “stand by” mode.
Direct access to the “hydrogen production” mode from the “electrical power production” mode is not permitted, nor the other way around: the monitoring and control system does not allow the two modes to operate simultaneously.
In “hydrogen production” mode the control system is programmed as a state machine. The following states are defined:

- plant startup;
- low-pressure buffer filling;
- high-pressure buffer filling.

In this operating mode, the automation system:

- starts and stops the hydrogen production and storage process;
- displays and records in log files the values of all the quantities (pressure, temperatures, flow rates, etc.) measured on the system;
- signals any alarm conditions coming from the electrolyser, the compression system or the hydrogen storage system;
- regulates the compressed air flow to the compressor.

Figure 123 shows the automation page for the control and monitoring of the hydrogen production and storage plant. Figure 124 shows the automation page dedicated to graphs of the trend over time of the values of the following monitored quantities:

- Pressures:
    - Hydrogen in low-pressure buffer (H2/002PT);
    - Hydrogen on hydrogen booster suction side (H2/003PT);
    - Hydrogen in high-pressure buffer (H2/005PT);
    - Compressed air at hydrogen booster input (CA/001PT).
- Hydrogen temperatures:
    - At electrolyser output (H2/001TT);
    - In low-pressure buffer (H2/002TT);
    - On hydrogen booster suction side (H2/003TT);
    - In high-pressure buffer (H2/005TT).
- Hydrogen flowrate at electrolyser output (H2/001FT);
- Compressed ar flowrate at hydrogen booster input (CA/001FC);
- Cooling water temperatures:
    - Electrolyser cooling water outlet temperature (EC/002TT);
    - Electrolyser cooling water inlet temperature (EC/001TT).

In addition to the plant automation system, the electrolyser is equipped with its own graphic interface that makes the data of the main quantities measured inside the generator available to the operator and allows him to access and modify the main operating parameters.

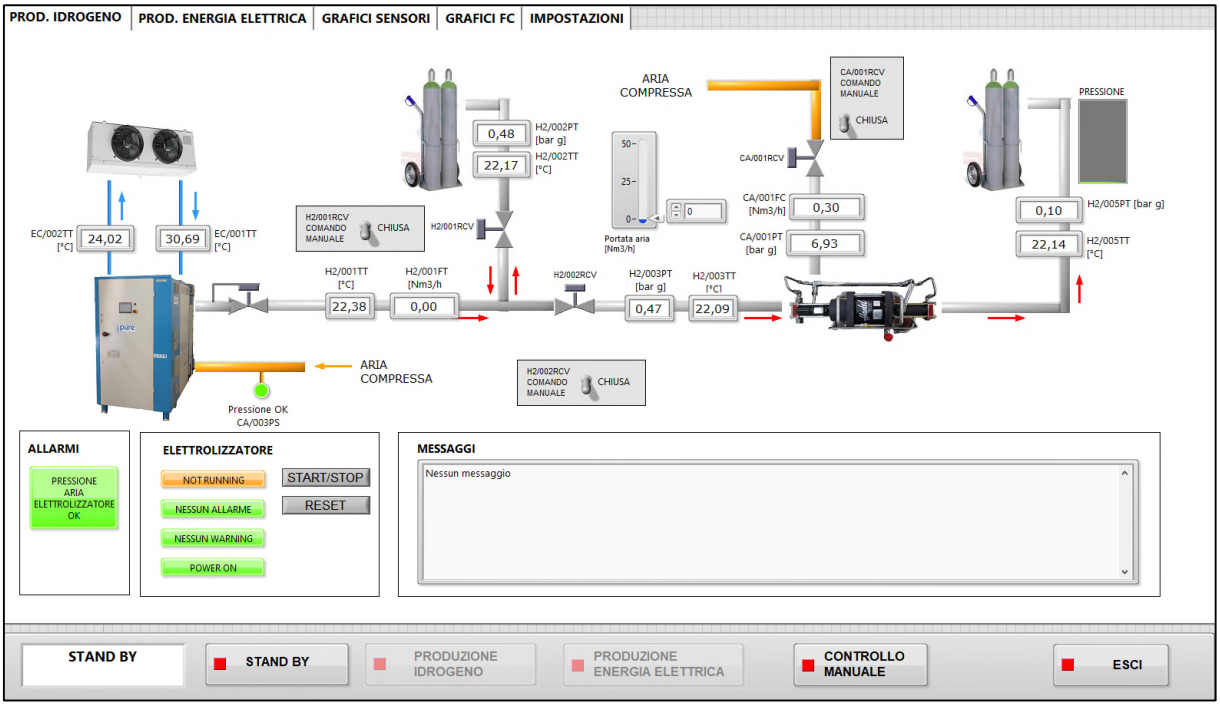

Figure 123. Test rig automation plant. Hydrogen production plant page.

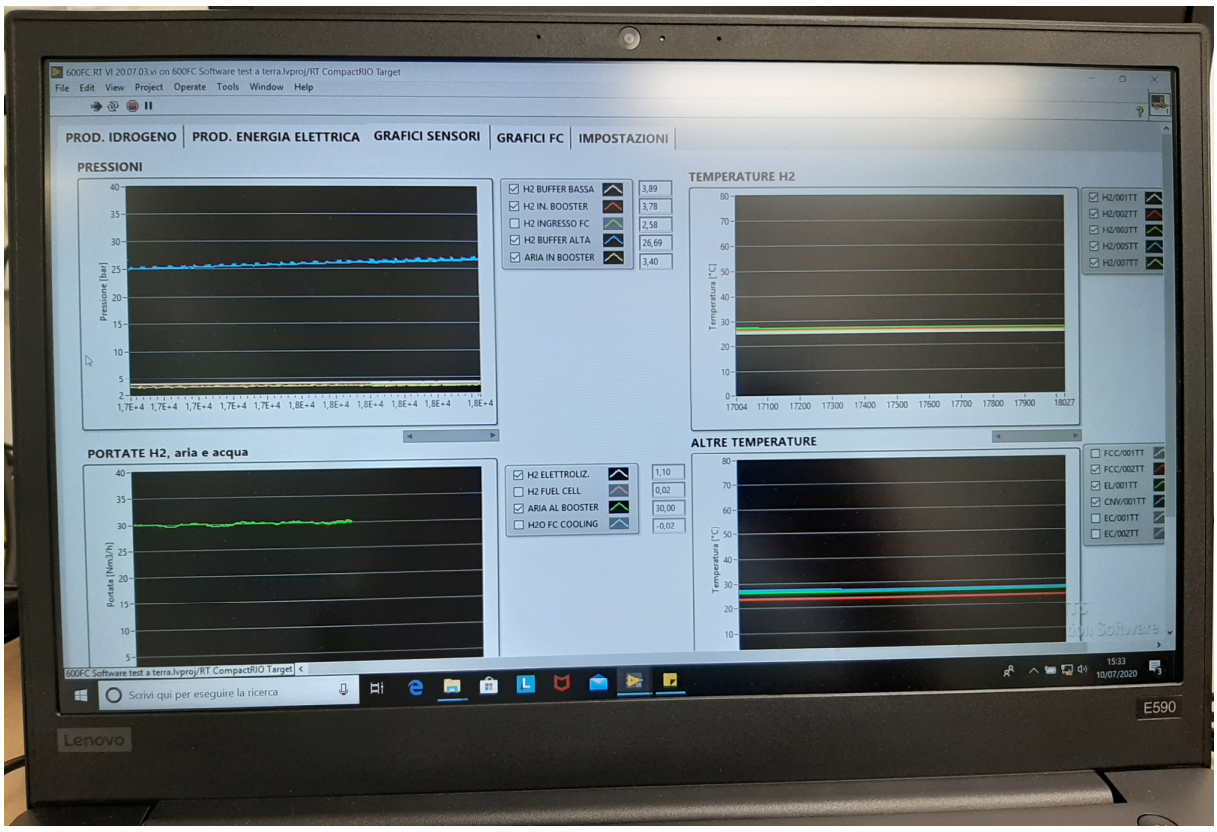

Figure 124. Test rig automation plant. Hydrogen production plant trends page. Photo by the author.

At system startup, the control system verifies that the pressure in the high-pressure buffer is below the minimum value of the pre-established tolerance band defined for its set point value. If this condition is not verified, the system shows a warning message and automatically returns to "stand by" mode. The control system displays on the screen the following list of checks and activities that must be carried out and confirmed by the operator before being able to continue with the system startup:

- check that the alarm system and environmental sensors are turned on and in operation;
- check that the electrical power production plant is off and, if necessary, proceed with the shutdown procedure;
- check that the manual valves of the system are configured as described in Table 38.

Piece mark	Status
N2/004SV	Closed
H2/001SV	Closed
H2/030SV	Closed
H2/031SV	Open
H2/032SV	Aperta
H2/033SV	Closed
H2/020SV	Open
H2/006SV	Closed
H2/011SV	Closed
EC/001SV	Closed
EC/002SV	Closed
TW/001SV	Open
TW/002SV	Open
CA/001SV	Open
CA/002SV	Open
CA/004SV	Open

Table 38. Hydrogen production plant. Status of the valves at startup.

- turn on the air compressor and wait for the pressure inside the tank to reach the expected set point value.

The system then starts the electrolyser and waits to receive the running signal from it.
The running confirmation from the electrolyser allows the software to proceed to the next state "low-pressure buffer filling". The low-pressure buffer filling is carried out according to the control logics based on the low-pressure buffer pressure (monitored through H2/002PT) hereinafter described.

With H2/002PT < set point value for hydrogen booster starting, the control system:

- sets valve H2/001RCV to open;
- sets valve H2/002RCV to closed;
- the system remains in the state of "low pressure buffer filling".

With H2/002PT ≥ set point value for hydrogen booster starting, the control system:

- sets the H2/002RCV valve to open;
- sets the H2/001RCV valve to open;
- waits for a previously defined time, then switches to the "high- pressure buffer filling" state.

The high-pressure buffer filling is carried out according to the control logic hereinafter described.
The hydrogen booster is equipped with two safety pressure switches named H2/001PS and H2/002PS placed respectively upstream and downstream of it. The two pressure switches are calibrated to intervene if the hydrogen pressure on the suction side of the booster drops below the minimum operating pressure or if the maximum delivery pressure is exceeded.

If none of the pressure switches is triggered, the control system energizes and opens the CA/001RV valve downstream of the air compressor. The hydrogen booster is started, and the hydrogen compression begins.
In case the pressure upstream of the hydrogen booster (monitored through H2/003PT) falls below the set pointfor hydrogen booster stopping:

- the system de-energizes the CA/001RCV valve circuit:
- the system returns to the “low pressure buffer filling” state.

When the pressure in the high-pressure buffer (monitored through H2/005PT) is higher than the set point value, the system warns the operator with a message and switches to the “stand by” state, otherwise it remains in the “high pressure buffer filling” state. The low-pressure and high-pressure buffers filling control logics are summarized in the flow chart of Figure 125.

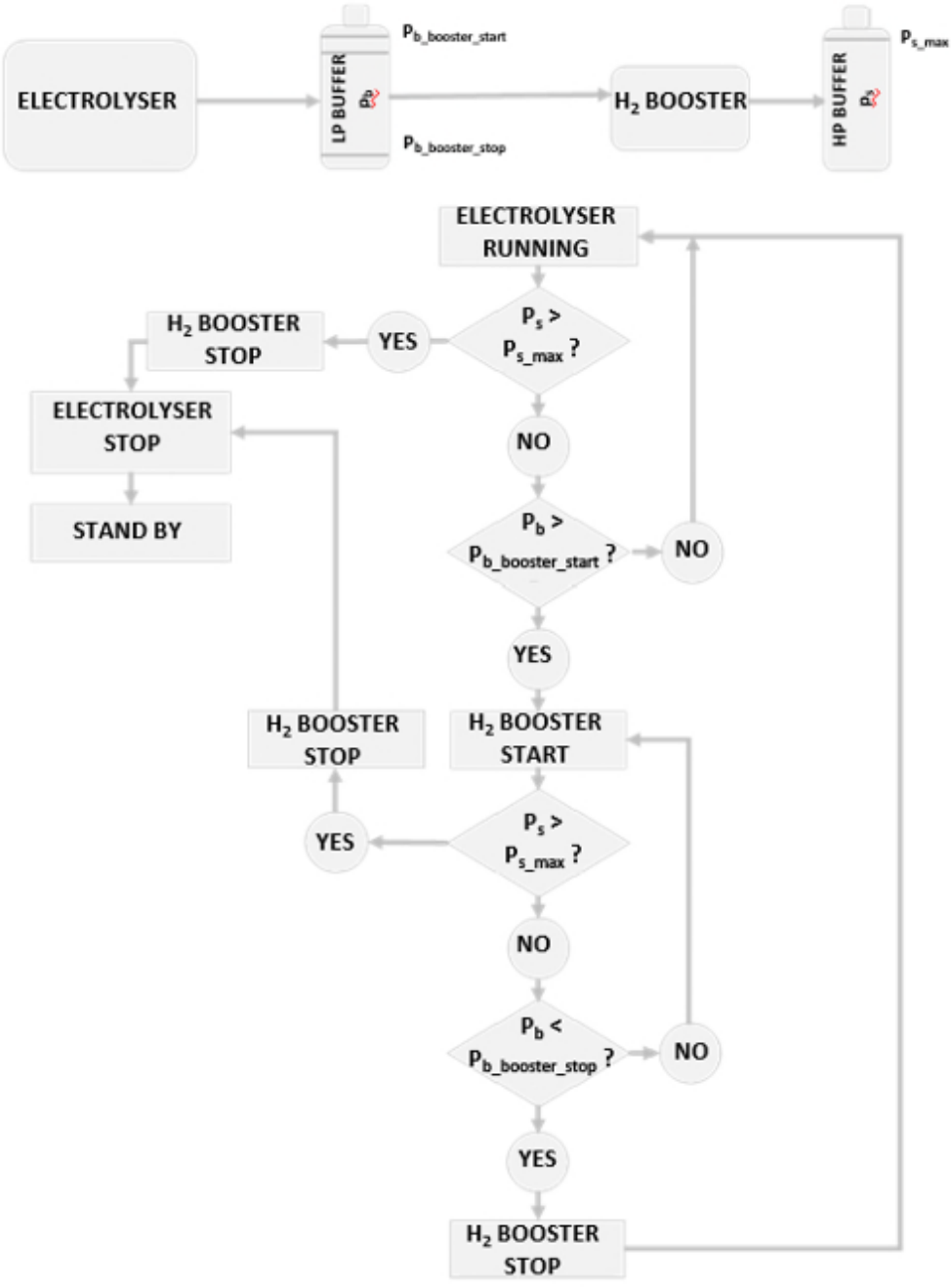

Figure 125. Low-pressure and high-pressure buffers filling control logics flowchart.

In case of activation of H2/002PS or H2/002Ps, the following automatic operations are performed by the control system:

- if the H2/001PS pressure switch ia activated (minimum pressure on booster suction side)
  - the valve CA/001RCV is closed, thus stopping the hydrogen booster;
  - the system returns to the "low pressure buffer filling" state.
- If the H2/002PS pressure switch ia activated (maximum pressure on booster delivery side)
  - the valve CA/001RCV is closed, thus stopping the hydrogen booster;
  - the system returns to "stand by" mode.

The normal shutdown of the system is carried out by the operator by acting on a dedicated button on the graphic interface. With the plant in the "hydrogen production" operating mode, the control and monitoring system carries out the following operations:

- sends the shutdown signal to the electrolyser;
- closes the CA/001RCV valve;
- closes the H2/001RCV valve;
- closes the H2/002RCV valve;
- warns the operator that the status of the manual valves must be that reported in Table 39;

Piece mark	Status
N2/004SV	Closed
H2/001SV	Closed
H2/030SV	Closed
H2/031SV	Closed
H2/032SV	Closed
H2/033SV	Closed
H2/020SV	Closed
H2/006SV	Closed

Table 39. Hydrogen production plant. Status of the valves at shutdown.

- brings the system to "stand by" mode.

In case of activation of one of the safety systems of the test rig (emergency stop button, fire detection or hydrogen detection), the electreolyser activates the "emergency stop" procedure and at the same time the shutdown sequence of the electric power production plant is automatically initiated.

Figure 126. Test rig. Control room overview. [94]

6.5.2.3 Electric power production mode

The “electrical power production” mode is started by the operator by acting on the dedicate button on the graphic interface. To access the “electrical power production” mode, the system must be in “stand by” mode. Direct access to the “hydrogen production” mode from the “electrical power production” mode is not permitted, nor the other way around: the monitoring and control system does not allow the simultaneous operation of the “hydrogen production” and “electrical power production” modes.
In “electrical power production” mode the control system is programmed as a state machine. The following states are defined:

- plant startup;
- electrical power production.

In “electrical power production” mode, the automation plant:

- displays and record in log files the values of all quantities (pressure, voltages, currents, temperatures, etc.) measured on the system;
- reports any alarm conditions from the fuel cell, inverter, dry cooler, converter, circulation pump inverter or hydrogen storage system;
- operates the shut-off valve for the introduction of hydrogen to the fuel cell;
- adjusts the rotation speed of the circulation pump of the fuel cell cooling circuit;
- adjusts the rotation speed of the dry cooler fans.

Figure 127 shows the automation page dedicated to the control and monitoring of the electricity production plant, On the automation system trends page (Figure 122) the graphs describing the variation over time of the following monitored quantities are available:

- Hydrogen pressure at fuel cell inlet (H2/007PT);
- Hydrogen temperature at fuel cell inlet (H2/007FT);
- Hydrogen flowrate at fuel cell inlet (H2/002FT);
- Cooling water temperatures:
    - Fuel cell cooling water outlet temperature (FCC/001TT);
    - Fuel cell cooling water inlet temperature (FCC/002TT).
- Fuel cell output:
    - Fuel cell voltage (from fuel cell generator);
    - Fuel Cell current (from fuel cell generaror).
- Converter cooling air outlet temperature (CNV/001TT);
- Load bank cooling air outlet temperature (EL/001TT).

In addition to the plant automation system, the fuel cell and the converter each have their own user interface from which display the values of the measured quantities and allow the operator to access and modify main operating parameters.

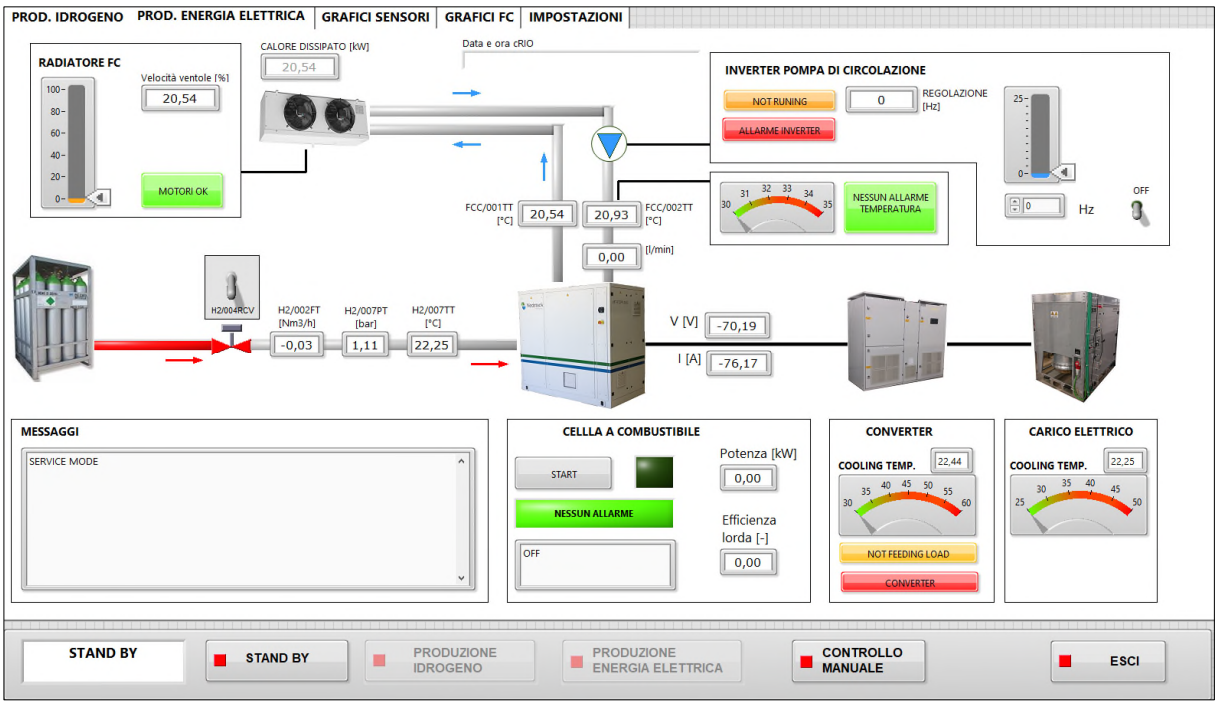

Figure 127. Test rig automation plant. Electric power production plant page.

The control system displays on the screen the following list of checks and activities that must be carried out and confirmed by the operator before being able to continue with the system startup:

- check that the alarm system and environmental sensors are turned on and in operation;
- check that the hydrogen production plant is turned off and, if necessary, proceed with the shutdown procedure;
- check that the manual valves are configured as shown in Table 40.

Piece mark	Status
H2/034SV	Closed
H2/036SV	Closed
H2/019SV	Open
H2/017SV	Closed
H2/018SV	Open
H2/035SV	Open
H2/015SV	Closed
H2/016SV	Open
FCC/001SV	Open
FCC/002SV	Open
FCC/004SV	Open
FCC/005SV	Open
FCC/008SV	Open
FCC/009SV	Open
FCC/003SV	Closed
FCC/006SV	Closed
FCC/007SV	Closed

Table 40. Electric power production plant. Status of the valves at startup.

Upon activation of the "electric power production" status, the automation plant:

- opens valve H2/004RCV;
- commands the switching on of the cell cooling circuit pump;
- commands the ignition of the dry cooler FZ/002RF;
- commands the ignition of the fuel cell and waits for the running status.

The system displays on the screen that it is possible to supply the load to the fuel cell.
The shutdown of the system is carried out by the operator by acting on a dedicated button on the graphic interface. The control and monitoring system carry out the following operations:

- sends the shutdown signal to the fuel cell, recognizes its shutdown status and indicates it on the screen;
- sets the power supply frequency of the fuel cell external circulation pump to a pre-established set point value for the “shutdown” condition;
- sets the rotation speed of the fuel cell dry cooler fans to a pre-established set point value for the “shutdown” condition;
- waits for the fuel cell to complete the shutdown phase, for it to go to the “Off” state and displays on the screen the completion of the sequence;
- switches off the fuel cell circulation pump;
- brings the rotation speed of the dry cooler fans to 0%;
- closes the H2/004RCV valve;
- brings the system to “stand by” mode.

In case of activation of one of the safety systems of the test rig (emergency stop button, fire detection or hydrogen detection), the fuel cell activates the “emergency stop” procedure, the emergency solenoid valve FZ/007RCV is de-energized to cut off the hydrogen supply to the fuel cell and, at the same, time the shutdown sequence of the electric power production plant is automatically activated.

Figure 128. Piping ramps 1(the highest one) and 2 (the lower one) in the test rig. Photo by the author.

7 Experimental characterization of the hydrogen production and compression plant

This chapter summarizes the tests carried out for the experimental characterization of the test rig hydrogen production and compression plant. The aim of the characterization activity was to assess the energy performance of the electrolyser and the compression system to evaluate the overall system energy efficiency in terms of specific energy consumption. The goal was to increase the experimental data available about hydrogen production and storage plants of this capacity. This size of plants in the future could be attractive from a commercial point of view; enabling for household application and small or medium industries the possibility to store the renewable energy that they produce when not immediately used [62].
The characterization tests performed on the plant are listed in Table 41.

Test	Scope
Hydrogen production efficiency characterization	Electrolyser efficiency evaluation in different operating conditions
Hydrogen production and storage plant overall characterization	Characterization of the performance of the whole test plant in terms of specific energy consumption
Electrolyser pirge gas (nitrogen) consumption evaluation	Evaluation of electrolyser nitrogen consumption diring operational phases (startup, hydrogen production and shutdown)
Electrolyser demineralized water consumption evaluation	Evaluation of electrolyser demineralized water consumption diring operation

Table 41. Hydrogen production and compression plant. Experimental characterization test list.

7.1 Field instrumentation

The characterization of the plant was carried out using part of the instrumentation part of the field instrumentation installed on the test rig and described in the prvious chapter (paragraph 6.5).
The electrical power measurements required for plant characterization were made with a portable network analyser.

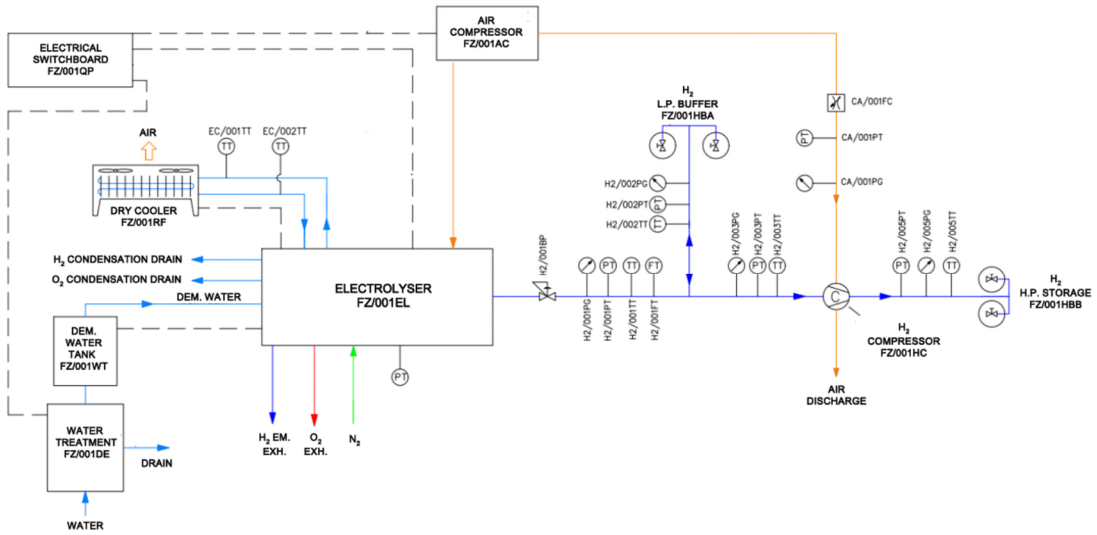

Figure 129. Overview of the field instrumentation for the experimental characterization of the hydrogen production and compression plant. [62]

Detailed description of the filed instrumentation involved in the experimental test (type, location and metrological characteristics) are provided in the following paragraphs.

7.1.1 Instrumentation on hydrogen lines

Instrumentation providing analog input to the automation system controller is installed on the four branches that make up the hydrogen piping system:

1. Between the electrolyser and the low-pressure buffer (piping ramp 2);
2. Upstream the low-pressure buffer (piping ramp 3);
3. Upstream the hydrogen booster (piping ramp 4);
4. Hydrogen booster delivery side, upstream the high-pressure storage (piping ramp 5).

On each branch, hydrogen pressure and temperature are monitored through dedicated transmitters. These instruments are indicated respectively with suffix PT (Pressure Transmitter) and TT (Temperature Transmitter–IEC751 class A Pt100 sensors) in the P&I diagram of Figure 129.
Hydrogen flowrate from the electrolyser is then monitored by the automation system through a dedicated flowmeter (H2/001FT) installed downstream the back-pressure regulator (H2/001BP).

7.1.2 Instrumentation on compressed air lines

Compressed air line between the compressed air package and the hydrogen booster is interfaced with the automation system for pressure monitoring via the pressure transmitter CA/001PT, and for monitoring and regulating the flow via the controller CA/001FC.

7.1.3 Instrumentation metrological characteristics

Table 42 summarizes the list of the field instruments used in the characterization of the plant with indication of their location on the hydrogen lines (ramps) and on the compressed air lines.

Sensor/ device Piece mark	**Measure quantity Or check carried out**	**Sensor/device type**	**Signal type**
Piping ramp 2			
H2/001PT	H_2 pressure	Pressure transmitter	Analog input 4...20 mA
H2/001TT	H_2 temperature	Temperature sensor	PT 100
H2/001FT	H_2 flowrate	Flowmeter	Analog input 4...20 mA
Piping ramp 3			
H2/002TT	H_2 temperature	Temperature sensor	PT 100
H2/002PT	H_2 pressure	Pressure transmitter	Analog input 4...20 mA
On piping ramp 4			
H2/003PT	H_2 pressure	Pressure transmitter	Analog input 4...20 mA
H2/003TT	H_2 temperature	Temperature sensor	PT 100
Piping ramp 5			
H2/005TT	H_2 temperature	Temperature sensor	PT 100
H2/005PT	H_2 pressure	Pressure transmitter	Analog input 4...20 mA
Compressed air circuit			
CA/001FC	Compressed air flowrate	Controller/flowmeter	Analog input 4...20 mA Output analogico 4...20 mA
CA/001PT	Compressed air pressure	Pressure transmitter	Analog input 4...20 mA

Table 42. Hydrogen production plant characterization. Field sensors/devices list.

The accuracy of the main instruments (fixed and portable) used is plant characterization presented in Table 43.

Component	Feature	Value
Hydrogen flowmeter (H2/001FT),	Accuracy Repeatability	±0.5% Rd plus ± 0.1% FS <0.2% Rd
Hydrogen pressure transmitter (H2/001PT, H2/002PT, H2/003PT, H2/005PT)	Accuracy Repeatability	±0.50% FS <0.1% FS
Compressed air pressure transmitter (CA/001PT)	Linearity error Repeatability	≤±0.5% FS ≤±0.1% FS
Compressed air flowmeter/controller (CA/001FC)	Accuracy	± (0.5% Rd plus 0.5% FS)
Portable network analyzer	Voltage accuracy Ampere accuracy	0.1% of V_{nom} ± (0.5% Rd plus 5% counts)

Table 43. Hydrogen production plant characterization. Main metrological characteristics of the instrumentation. [62]

During the tests, the environmental parameters (ambient temperature and pressure) were monitored by means of a dedicated weather station installed in the test rig room. The speed of the hydrogen booster (cycles/minute) was checked by means of a stopwatch.

Figure 130. electrolyser during the experimental characterization tests. Photo by the author

7.2 Hydrogen production efficiency characterization

The tests aimed at evaluating the electrolyser efficiency at two hydrogen flow rates: the full flow rate and a reduced flow rate. The original test schedule included evaluating the electrolyser efficiency at three different hydrogen output pressures: nominal (4.6 bar g), intermediate and minimum operating (4.2 bar g). However, the tests have shown that even minimal reductions (a few tenths of a bar) of the outlet pressure with respect to the nominal value, always brought the electrolyser to a condition of maximum deliverable flow rate.
The test has been therefore carried out setting the back-pressure regulator H2/001BP was set at two values only: 4.6 bar g and 4.2 bar g, respectively.

7.2.1 Test Procedure

Once the electrolyser has been started and the heating phase completed in accordance with the procedures described in its operating manual, the hydrogen production was started, and the data listed in Table 44 were recorded.

Quantity	Unit	Instrument	P&I Reference
Electrolyser H_2 outlet flow rate	[Nm^3/h]	Flow meter	H2/001FT
Electrolyser H_2 outlet pressure	[bar g]	Electrolyser display	PT
Electrolyser power consumption	[kW]	Power analyzer	-
Ambient temperature	[°C]	Weather station	-
Ambient pressure	[hPa]	Weather station	-

Table 44. Quantities measured during the hydrogen production efficiency test with unit of measurement, instrument used for the survey and P&I diagram reference.

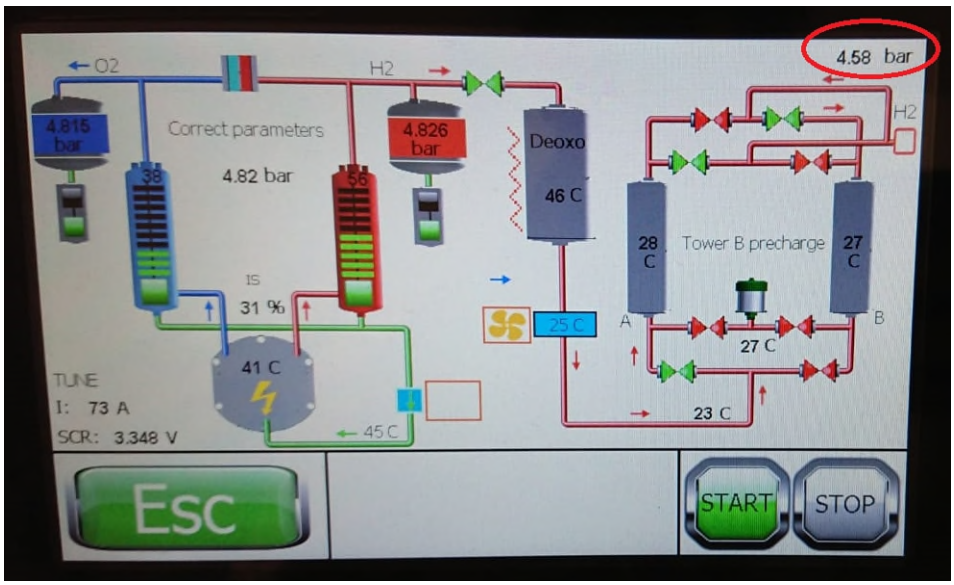

Figure 131. Electrolyser HMI main page with indication of working pressure (4.6 bar g). Photo by the author.

The plots over time of the hydrogen flow rate (in blue) and of the electrical power absorbed by the electrolyser (in orange) during the tests performed at 4.6 and 4.2 bar g output pressure are shown in Figure 132 and Figure 133.

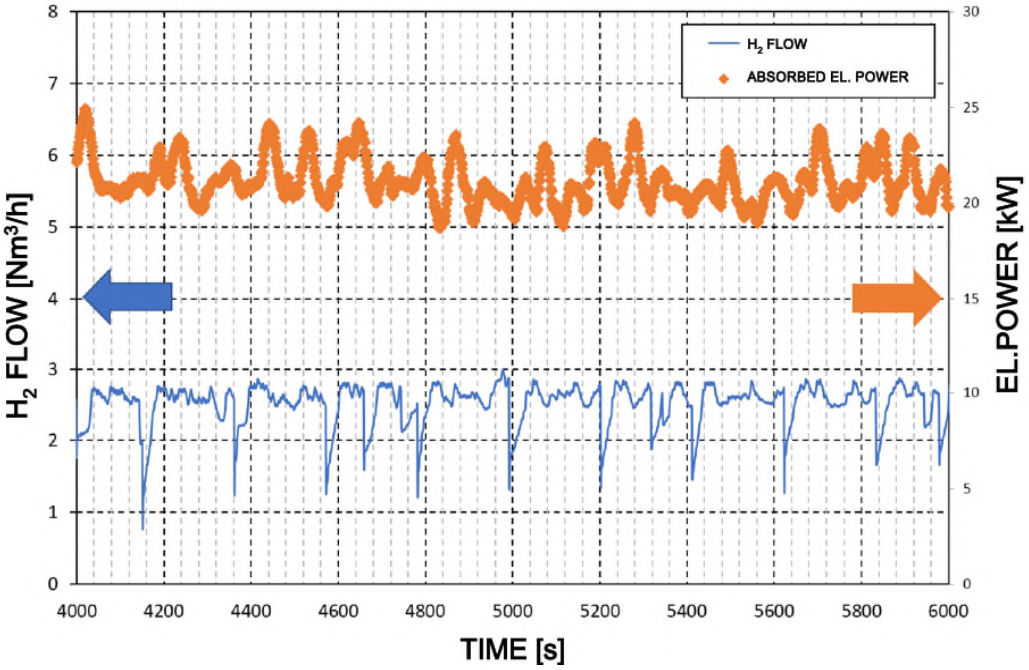

Figure 132. Plot over time of the electrical power absorbed and of the hydrogen outlet flowrate during test 4.6 bar g. [62]

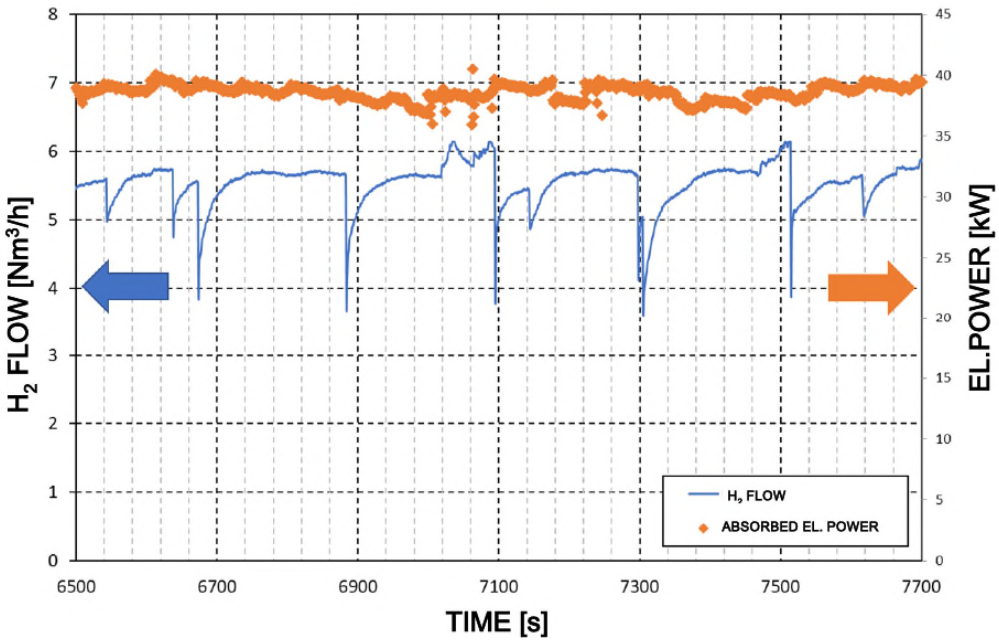

Figure 133. Plot over time of the electrical power absorbed and of the hydrogen outlet flowrate during test 4.2 bar g. [62]

The two figures show trends recorded by the automation system during the tests for a duration of about 30 min. It is possible to observe as, in both tests, sudden changes in flow rate occur for a few seconds at intervals of about three minutes. This phenomenon is related to the electrolyser internal hydrogen purification system which, as anticipated in paragraph 6.1.1, uses a part of the hydrogen produced to periodically regenerate the filter cartridges.

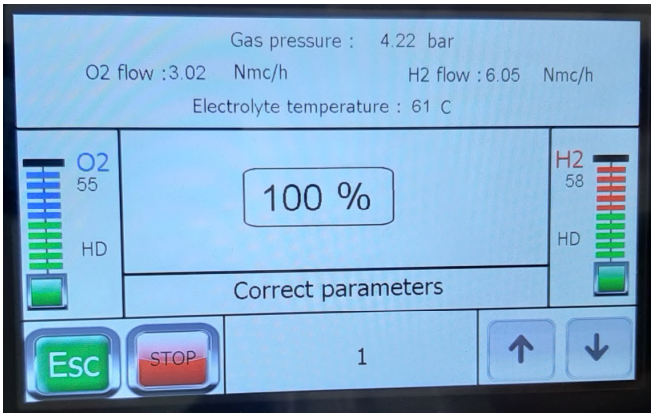

Figure 134. Electrolyser HMI summary page with indication of working pressure (4.2 bar g), gas flows and electrolyte temperature. Photo by the author.

7.2.2 Electrolyser efficiency calculation

The electrolyser efficiency (in percentage) is evaluated with equation (29) as the ratio between the power available in the produced hydrogen flow (referred to hydrogen LHV, Lower Heating Value) and the electrical power absorbed by the electrolyser [62]:

$$\eta_{el} = \frac{P_{H2}}{P_{elin}} \times 100 \quad [\%] \tag{29}$$

The average power associated with the hydrogen flow produced by the electrolyser (P_{H_2}) is calculated with equation (30) [62]:

$$P_{H_2} = \rho_{H_2} \times \frac{\dot{V}}{3600} \times LHV \times 1000 \quad [\text{kW}] \tag{30}$$

The meaning of the quantities shown in the above formulas, the corresponding unit of measurement, and the methodology used to calculate them are summarized in Table 45.

Table 45. Quantities used for the calculation of the electrolyser production efficiency, unit of measurement and methodology used for the calculation. [62]

Quantity	Unit	Formula, Calculation Method or Value
P_{H_2}	[kW]	Power associated with hydrogen flow. Equation (30)
LHV	[MJ/kg]	120 [1]
$\dot{V}$	[Nm³/h]	Flow rate measured by the H2/001FT flowmeter referred to normal conditions: 101.325 Pa, 0 °C
ρ_{H_2}	[kg/m³]	0.0899 [2]
P_{elin}	[kW]	The average electrical input power in the electrolyser, obtained as the average of the input power values recorded with the portable network analyzer

[1] IEC 62282-3-200–Stationary fuel cell power systems–Performance test method. [115]
[2] National Institute for Standards and Technology (NIST)–Reference Fluid Thermodynamic and Transport properties Database (REFPROP). [116]

7.2.3 Test results: Hydrogen production efficiency

The results of the tests performed with the electrolyser operating at 4.6 and 4.2 bar g output pressure are summarized in Table 46.

Table 46. Test results for tests with electrolyser operating at 4.6 and 4.2 bar g output pressure. [62]

Quantity	Unit	Average @ 4.6 Bar g	Average @ 4.2 Bar g
Electrolyser H_2 outlet flow rate	[Nm^3/h]	2.52	5.53
Electrolyser H_2 outlet pressure	[bar g]	4.6	4.2
Electrolyser power consumption	[kW]	21.2	38.6
Ambient temperature	[°C]	25	25
Ambient pressure	[hPa]	1017	1017
Electrolyser efficiency[1]	[%]	36	43
Specific Energy Consumption[1]	[kWh/kg]	93	77

[1] Including hydrogen used for filter cartridges regeneration.

Moving from part load operation (2.52 Nm3/h) to design load operation (design flow rate) the electrolyser efficiency is increased from 36% to 43%.
It should also be noted that, for the unit under test, the calculated specific energy consumption, id est the kW per hour needed to make one kg of hydrogen available at the electrolyser output, is in line with the data reported in the manufacturer's technical specification and is also higher than the available data referred to large scale alkaline electrolysers considering both the state-of-the-art of this technology and the future targets set by the European Community shown in Table 12 and Table 13.
The test result can be compared with different electrolysers available on the market, as per data given in Table 14.
When the average value of the specific energy consumption for alkaline electrolysers listed in Table 14 (57.6 kWh/kgH2) is compared to the experimental data recorded with electrolyser delivering the rated flow (77 kWh/kgH_2) it is evident that the tested system has, even in this case, a lower efficiency. As already mentioned, part of the hydrogen is used for the regeneration of the cartridge of the hydrogen purification system and so this flow is lost and brings to a decrease in efficiency. Therefore, we can conclude that the experimental value of the efficiency is at least in line with one of the models presented in Table 14.

7.3 Hydrogen production and storage plant overall characterization

The purpose of this test is to characterize the performance of the whole test plant in terms of specific energy consumption. After having characterized the hydrogen production system in 7.2, in this test hydrogen is produced at 4.6 bar g and then compressed at 200 bar g. For the purpose of the test, both the low-pressure buffer and the high-pressure storage system consisted of a single cylinder with a geometric volume of 50 l.
The test was carried out with the electrolyser operating at the nominal output pressure of 4.6 bar g because this condition is the one that assures the best performance of the hydrogen booster. The test has been carried out with the air-driven hydrogen booster operating at rated speed first (44 cycles per minute), and then and at a reduced speed of 35 cycles per minute to compare the influence of the booster's speed on the specific energy consumption [62].

7.3.1 Test Procedure

The same set-up procedure described in paragraph 7.2.1 is carried out to collect the data for the hydrogen production and storage analysis. Table 47 shows the quantities measured during the test.

Quantity	Unit	Instrument	P&I Reference
Electrolyser H_2 outlet flow rate	[Nm^3/h]	Flow meter	H2/001FT
Electrolyser H_2 outlet pressure	[bar g]	Electrolyser display	PT
Electrolyser power consumption	[kW]	Network analyzer	-
Air compr. power consumption	[kW]	Network analyzer	-
H_2 compr. driving air flow rate	[Nm^3/h]	Flow controller	CA/001FC
H_2 compr. speed	[Cycles/min]	Stopwatch	-
H_2 buffer pressure	[bar g]	Pressure transmitter	H2/002PT
H_2 storage pressure	[bar g]	Pressure transmitter	H2/005PT
Ambient temperature	[°C]	Weather station	-
Ambient pressure	[hPa]	Weather station	-

Table 47. Quantities measured during the hydrogen production and storage overall charactherization test with unit of measurement, instrument used for the survey and P&I diagram reference.

7.3.2 Test Results: Booster Hydrogen and Driving-Air Flow Rate Variation with Time and Booster Specific Energy Consumption

The test has been divided into two steps. In the first step, the hydrogen storage pressure was raised from 10 to 100 bar g and, in the second step from 100 to 200 bar g. The overall filling time was about 5 h.

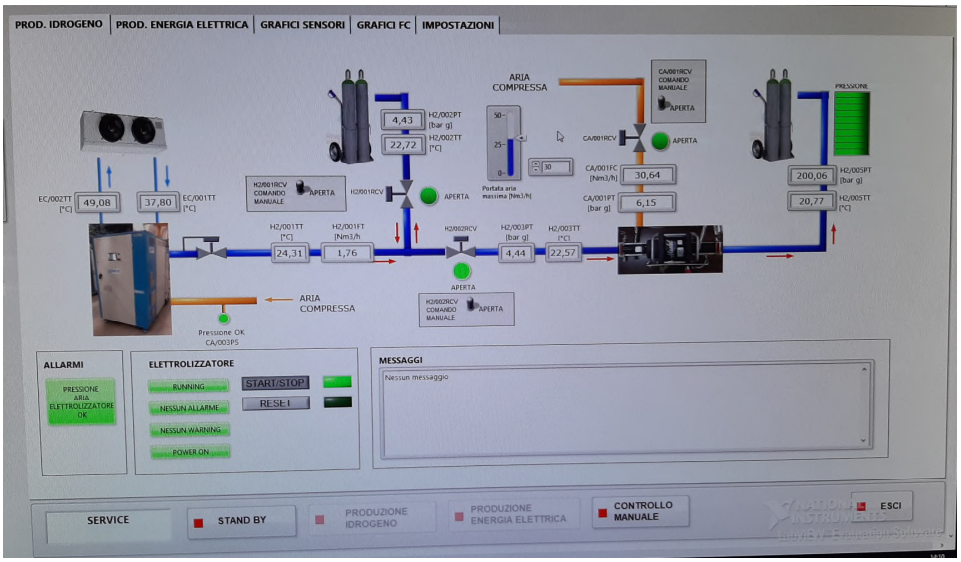

Figure 135. Hydrogen production and storage plant with storage system @ 200 bar g. Photo by the author.

The plots overtime of the hydrogen flow rate processed by the booster and its driving-air flow rate, for the booster running at 44 cycles per minute, are shown in Figure 136 and Figure 137.
When the electrolyser hydrogen output flow rate is considered (Figure 136), it can be noticed that this is reduced if compared to the test on the electrolyser as a stand-alone unit and working at the same

output pressure. This depends on the processing capability limits of the booster. The already described fluctuations of the hydrogen flow from the electrolyser due to the internal recirculation for filter cleaning can be noticed as well [62].

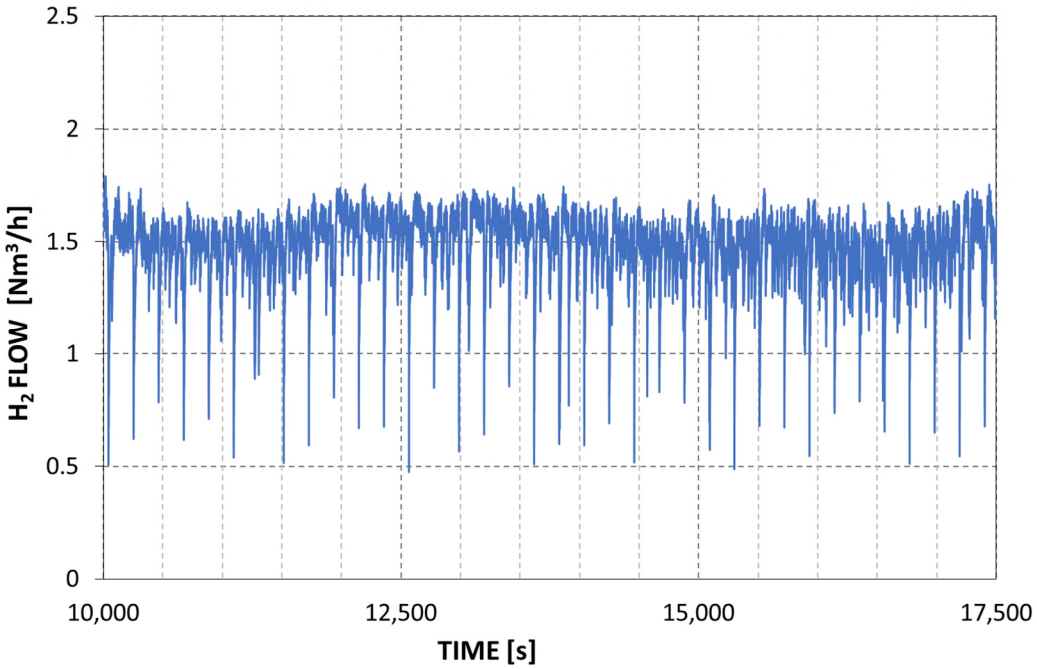

Figure 136. Plot over time of the hydrogen flow from the electrolyser during the test with hydrogen booster running at 44 cycles per minute. [62]

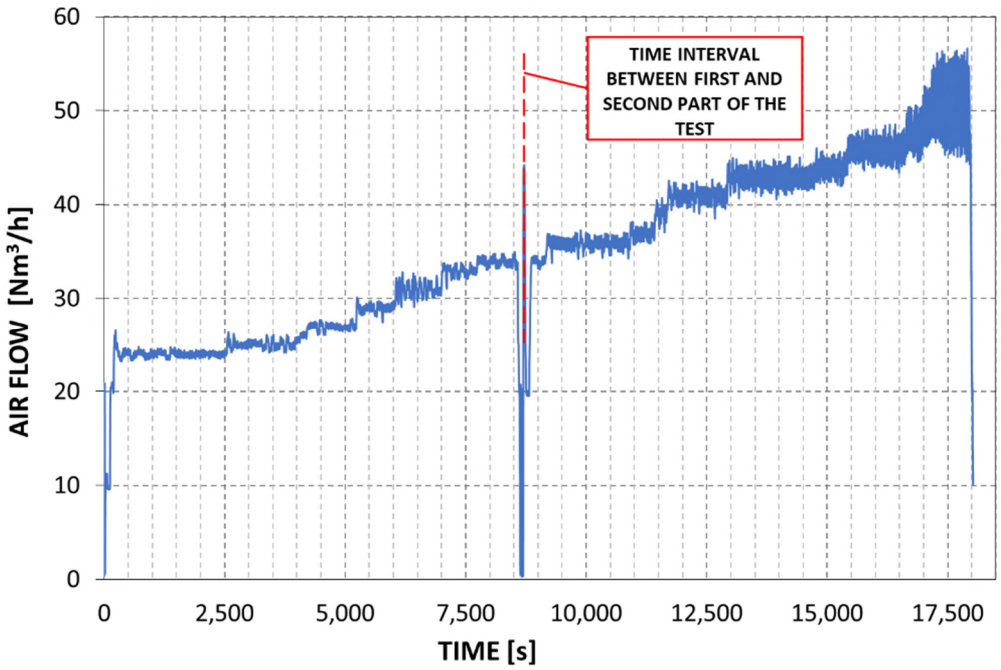

Figure 137. Plot over time of the booster driving-air flow rate during the test with hydrogen booster running at 44 cycles per minute. [62]

From Figure 137 it can be noticed that the booster driving-air flow rate is progressively increased in steps by the automation control system, in order to keep the compressor speed constant at 44 cycles per minute as the pressure in the storage system increases.

To evaluate the specific energy required by the hydrogen booster, the following quantities are calculated:

- the energy associated with the isentropic air compression process required to produce the compressed air is calculated. This air is the one required to drive the hydrogen booster for the entire storage process;
- the energy content of the mass of hydrogen stored is quantified.

The specific energy required by the hydrogen booster is then calculated as the ratio between energy associated to compress air and that of the hydrogen stored. The calculated specific energy of the hydrogen booster for compression from 4.6 bar g (pressure at suction sisde of the booster) to 200 bar g (final pressure in the storage system) is equal to 15 kWh/kgH_2.
It could be interesting to compare this value with other data, but literature on these types of boosters, as already highlighted in paragraph 4.3.3.1, is scarce. Moreover, using this approach to assess the efficiency implies that the operating conditions must be the same (initial pressure and final pressure). Therefore, it is difficult to make a comparison with the tested system and other data.
As already pointed out in paragraph 4.3.3.1, the specific energy consumption of an air-driven hydrogen booster can vary from 4.4 to 9.3 kWh/kgH_2 with an inlet pressure decreasing from 200 to 120 bar g and outlet pressure of the storage of 450 bar g [71].
These values, although lower, are comparable with the ones referred to the hydrogen booster used in the experimental test rig [62].

7.3.3 Test results: Hydrogen pressure variation with time

The plots overtime of the hydrogen pressure measured on the hydrogen low-pressure buffer and on the high-pressure storage during the test with the electrolyser working at output nominal pressure of 4.6 bar g and the hydrogen booster running at 44 cycles per minute are shown in Figure 138 and Figure 139.

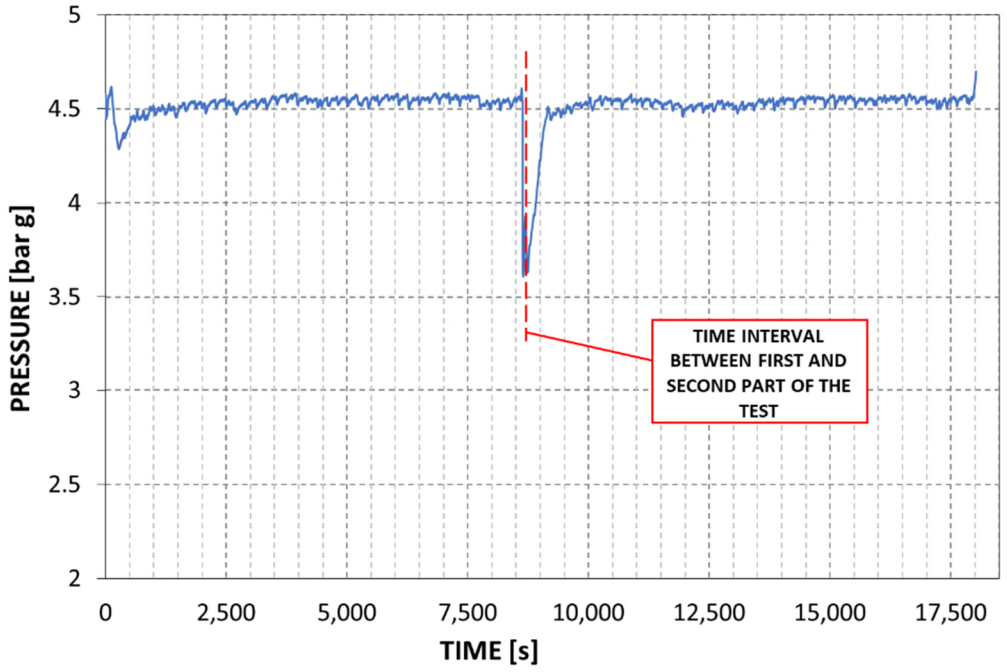

Figure 138. Plot over time of the hydrogen pressure in the low-pressure buffer during the test with hydrogen booster running at 44 cycles per minute. [62]

As shown in Figure 138, the hydrogen pressure in the low-pressure buffer is almost constant during the test. In both figures it is also evident the interruption of the test during the first and dhe second part of the test (at a time of approx. 8500 s).

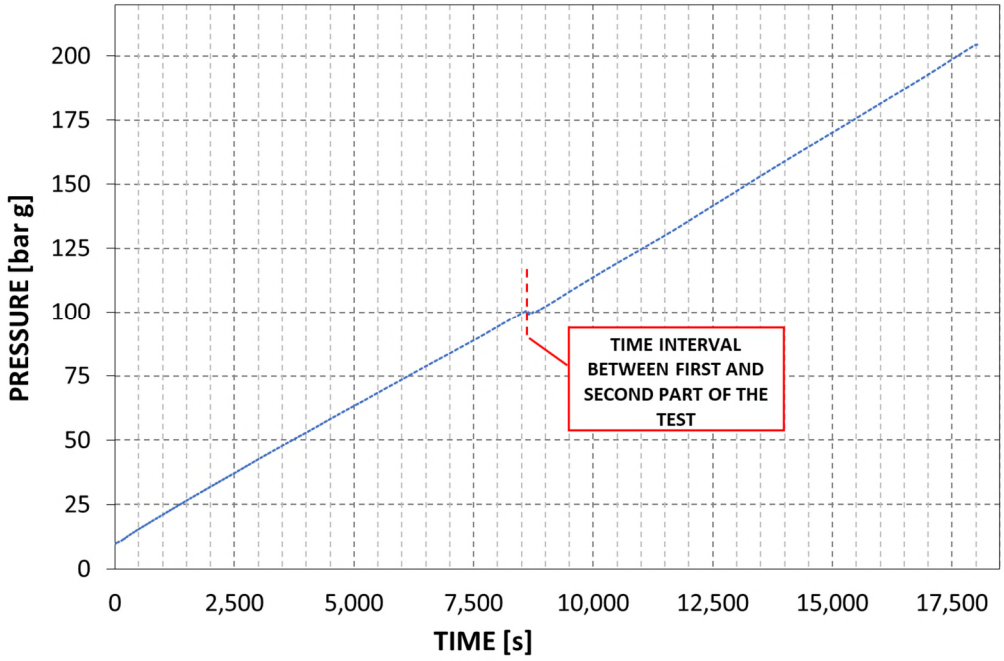

Figure 139. Plot over time of the hydrogen pressure on the hydrogen storage during the test with hydrogen booster running at 44 cycles per minute. [62]

7.3.4 Test results: Booster running at 35 cycles per minute

A similar storage system filling test was then performed with the electrolyser operating at rated output pressure (4.6 bar g), but with the booster running at a reduced speed of 35 cycles per minute. As in the previous case, the test was divided into two steps. With reference to the pressure in the storage system, in the first step of the test, the pressure was raised from 0 to 172 bar g and, in the second step from 172 to 200 bar g. In this case, the overall filling time was about 6 and a half hours. Plots of booster hydrogen flow rate and hydrogen storage pressure variations with time were similar in trend to those recorded in the previous test and are shown in Figure 138 and Figure 139 [62].
Figure 140 shows the variation of the storage pressure over time on the high-pressure storage during the test. In the same figure thered vertical line indicates the interruption between the first and second part of the test.
In the second part of the test a further interruption occurred due to the filling of the demineralized water tank completely emptied. The green vertical line in Figure 140 identifies the moment in which the level in the demineralized water tank of the electrolyser falls below the minimum allowed level.

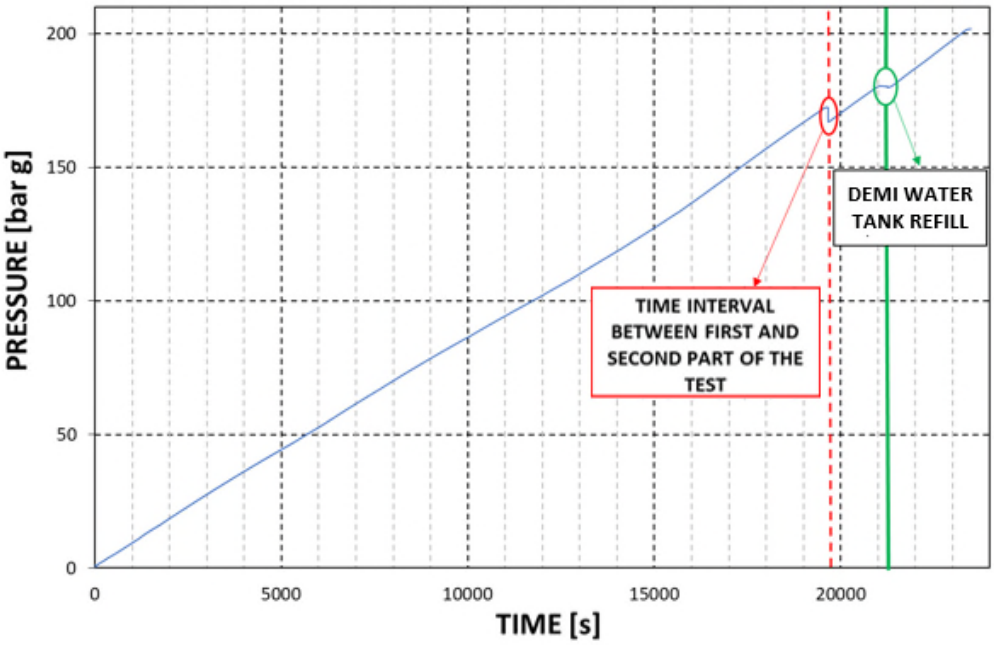

Figure 140. Plot over time of the hydrogen pressure on the hydrogen storage during the test with hydrogen booster running at 35 cycles per minute.

7.3.5 Test results: Production and storage specific energy consumption consideration

Table 48 shows the mean values calculated from the data collected with the electrolyser operating at output nominal pressure and booster running at 44 cycles per minute

Quantity	Unit	From 10 to 100 bar g	From 100 to 200 bar g	Overall Process: from 10 to 200 bar g
Electrolyser H_2 outlet flow rate (average)	[Nm^3/h]	1.54	1.43	1.51
Electrolyser H_2 outlet pressure (average)	[bar g]	4.6	4.6	4.6
Electrolyser power consumption (average)	[kW]	21.2	21.2	21.2
Air compressor power consumption (average)	[kW]	8	9.7	8.85
Peak air compressor power consumption	[kW]	12.4	12.7	-
Peak H_2 compressor driving air flow rate	[Nm^3/h]	35	56.5	-
Storage initial pressure	[bar g]	10	99.3	-
Storage final pressure	[bar g]	100	204.5	-
Buffer pressure (average)	[bar g]	4.53	4.51	4.52
H_2 compressor booster speed	[cycles/min]	44	44	44

Table 48. Test results for tests with electrolyser operating at 4.6 bar g and hydrogen booster running at 44 cycles per minute. [62]

Based on these data and considering the electricity required to compress the air for driving the booster, it is possible to define the storage-specific energy consumption as the overall energy required to compress 1 kg of hydrogen from 4.6 to 200 bar g.
For the considered case, a 65 kWh/kgH_2 value has been calculated. This value is significantly higher than the air driven booster specific energy consumption previously stated (15 kWh/kgH_2) and it is higher than figures found in literature for the considered pressure range (4.6 to 200 bar g): in paragraph 4.3.3.1, a value of about 10 kWh/kgH_2 [72] is reported.
It must be however highlighted that this specific energy consumption is related to an electric-driven hydrogen booster. Such a solution is intrinsically more efficient since the conversion from electricity to compressed air is not required. Moreover, the air compressor used in the presented test to drive the hydrogen booster is a constant-speed electric screw compressor.
This type of compressor, once the set pressure is reached, does not switch off the electric motor, and keeps operating in the so-called "unload mode". When operating in this mode, power adsorbed can reach 50% of the full load without producing any useful effect (compressed air). This behaviour of the air compressor is illustrated in Figure 141, where the air compressor's electrical power consumption is shown for different booster output pressure. Figure 141a shows the air compressor electrical power consumption when the booster works at low hydrogen outlet pressure (abt. 10 bar g), whereas Figure 141b shows the air compressor electrical power consumption when the booster works at high hydrogen outlet pressure (abt. 200 bar g).
The electrical consumption peaks shown in Figure 141a and b correspond to the air compressor "load mode" (compressor feeding the air storage while the electrical consumption valleys correspond to the "unload mode".
Comparing Figure 141a and b it is also possible to observe that the electrical energy adsorbed when the compressor is in "unload mode" is higher when the hydrogen outlet pressure is low.

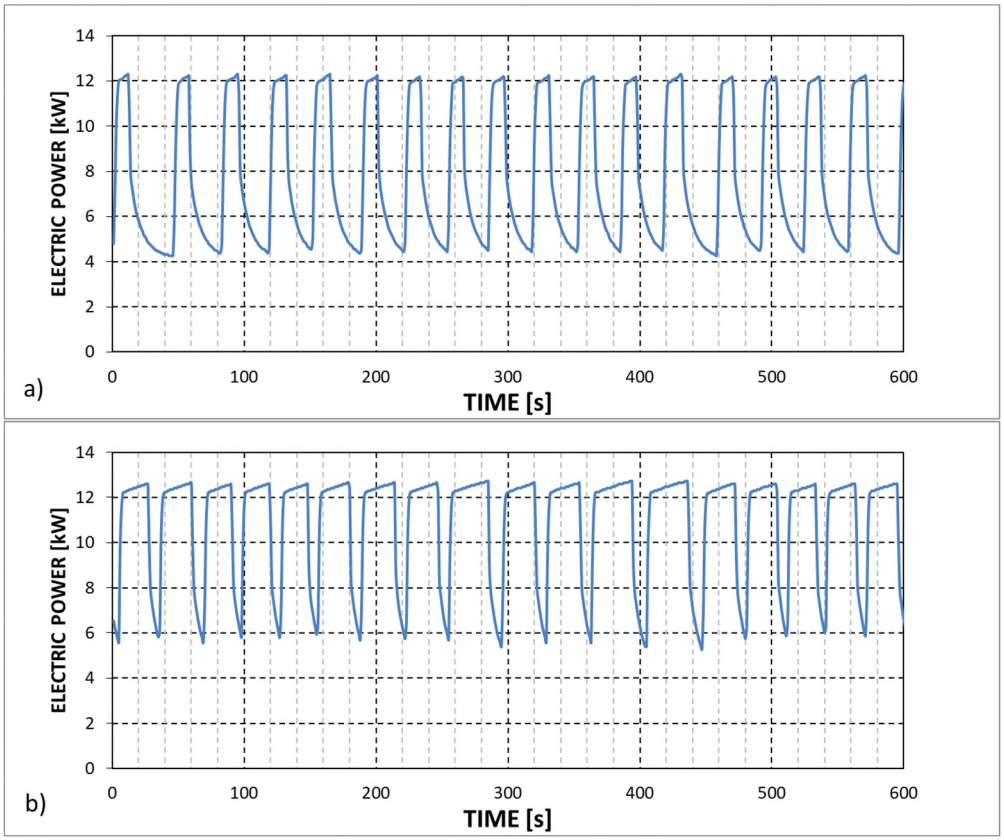

Figure 141. Electric power consumption of the air compressor in an interval of 10 min. respectively: (a) with a hydrogen outlet pressure of abt. 10 bar g; (b) with a hydrogen outlet pressure of abt. 200 bar g. [62]

Based on the measured data, considering the electrolyser working at a design flow rate (77 kWh/kgH_2 at 5.53 Nm3/h) and a hypothetical compressor able to elaborate this hydrogen flow with the same specific energy consumption as the one installed in the test rig (65 kWh/kgH_2), the production and storage required specific energy would be 142 kWh/kg.
Table 49 summarizes the results obtained with the electrolyser operating at output nominal pressure (4.6 bar g) and booster running at a reduced speed of 35 cycles per minute. Slowing down the hydrogen booster, the processed hydrogen flow rate is further decreased to an average value of 1.19 Nm3/h. The electrolyser and booster efficiencies are reduced as well. These data show that, for achieving high production and storage efficiencies, it is important to choose the right match of system components. For example, when the electrolyser is considered, its efficiency is severely affected when operated at partial load [62].

Quantity	Unit	From 0 to 172 bar g	From 172 to 200 bar g	From 0 to 200 bar g
Electrolyser H_2 outlet flow rate (average)	[Nm^3/h]	1.26	1.12	1.19
Electrolyser H_2 outlet pressure (average)	[bar g]	4.6	4.6	4.6
Electrolyser power consumption (average)	[kW]	21.2	21.2	21.2
Air compressor power consumption (average)	[kW]	8	9.4	8.7
Peak air compressor power consumption	[kW]	12.7	12.7	-
Peak H_2 compressor driving air flow rate	[Nm^3/h]	35.7	43.7	-
Storage initial pressure	[bar g]	0	167	-
Storage final pressure	[bar g]	172	202	-
Buffer pressure (average)	[bar g]	4.58	4.46	4.52
H_2 compressor booster speed	[cycles/min]	35	35	35

Table 49. Test results for tests with electrolyser operating at 4.6 bar g and hydrogen booster running at 35 cycles per minute. [62]

7.4 Electrolyser purge gas (nitrogen) consumption evaluation

The purpose of the test was to evaluate the nitrogen consumption during the startup, shutdown and hydrogen production phases of the electrolyser.

7.4.1 Test Procedure

The procedure followed to determine the electrolyser nitrogen consumption is hereiafter described.
Nitrogen cylinder is connected to the electrolyser and the nitrogen pressure, measured through the analogue pressure gauge of the pressure reducer is recorded.
All the auxiliaries necessary for the operation of the electrolyser such as the compressed air package and the electrolyser external water treatment system are then started.
As soon as the auxiliaries are ready, the electrolyser is started the electrolyser is turned on and automatically heated and pressurized by the internal control logics.

At the end of the electrolyser automatic startup sequence, the pressure inside the nitrogen cylinder is again recorded.
The hydrogen production phase is then started and during this operation, the nitrogen cylinder pressure is recorded at regular intervals.
The electrolyser is then stopped, and the automatic shutdown sequence is performed by the internal control logics.
The pressure inside the nitrogen cylinder is recorded for the last time.

7.4.2 Test results

The measurement of nitrogen consumption took place at the same time as the tests described in paragraph 7.3. As expected, no nitrogen consumption was detected as this is used only if there is the need to remove any internal accumulation of condensate or in case of maintenance. These conditions never occurred in the execution of the tests.

Figure 142. Electrolyser demineralized water tenk (left) and nitrogen cylinder (right). Photo by the author.

7.5 Electrolyser demineralized water consumption evaluation

The purpose of the test was to evaluate the consumption of demineralized water by the electrolyser during the different phases of its operation: startup, hydrogen production and shutdown.

7.5.1 Test Procedure

The procedure followed to determine the electrolyser water consumption is hereiafter described.
The initial water level in the external storage tank FZ/001WT and survey time are recorded. All the auxiliaries necessary for the operation of the electrolyser such as the compressed air package and the electrolyser external water treatment system are then started.
As soon as the auxiliaries are ready, the electrolyser is started the electrolyser is turned on and automatically heated and pressurized by the internal control logics.
At the end of the electrolyser automatic startup sequence, the water level in the external storage tank FZ/001WT and initial survey time are recorded.
The hydrogen production phase is then started and during this operation, the water level in the external storage tank FZ/001WT and survey time are recorded at regular intervals.
The electrolyser is then stopped, and the automatic shutdown sequence is performed by the internal control logics.
The water level in the external storage tank FZ/001WT survey time are recorded for the last time.

7.5.2 Test results

During the operation of the electrolyser, it was observed that:

- the electrolyser automatically loads the demineralized water necessary for its operation by taking it from the water treatment system external storage tank FZ/001WT;
- deionized water loads are characterized by non-constant volumes and are not related to a specific operating phase of the electrolyser;
- it is assumed that the electrolyser is equipped with an internal tank which is filled as needed.

As regards the hydrogen production phase, during the efficiency tests of the plant in paragraph 7.3.4, a water consumption of 5.5 liters was observed in a time of 5 h and 19 min. Table 50 reports the volume of deionized water consumed, the average flow rate of hydrogen produced during the test, the water consumption test time duration and the and the specific deionized water consumption defines as the kg of deionized water consumed on average per kg of hydrogen produced.

Deionized water consumption [l]	Average hydrogen flow [Nm^3/h]	Water consumption test time duration [s]	Deionized water specific consumption [kg_{H2O}/kg_{H2}]
5,5	1,25	19140	9,2

Table 50. Volume of water consumed, flow rate of hydrogen produced, operation time and ratio of water consumed per kg of hydrogen produced during the test described in paragraph 7.3.4.

8 Experimental characterization of the electrical power production plant

This chapter summarizes the tests carried out for the experimental characterization of the test rig electrical power production plant. Considering the state of the art of the regulatory framework and the most recent literature available, the experimental characterization has been carried out following test methods and procedures which are currently not used for marine applications, bringing a useful contribution to a possible wider use of PEM fuel cells and hydrogen on board ships. More specifically, the plant testing procedure has been developed followed the recognised international standard IEC 62282-3-200 [18] and the European Community testing procedure document Test Module PEFC ST 5-3 [19].
The characterization tests performed on the plant are listed in Table 51.

Test	Scope
Fuel cell generator	
Fuel cell and system electrical efficiency evaluation	Fuel cell generator gross and net efficiency evaluation during operation at 50% and 100% rated load
Fuel cell heat recovery efficiency evaluation	Fuel cell heat recovery efficiency evaluation during operation at 50% and 100% rated load
Fuel cell polarization curve plotting	Plotting of of fuel cell generator graph of its current–voltage characteristics.
System startup and shutdown characterization	Evaluation of fuel cell generator energy and fuel consumption during startup and shutdown phases
Discharge water quality test	Assessment of the quality of process water discharged from the fuel cell generator
Fuel cell electric load response analysis	Evaluatio of the fuel cell generator response time following connected load variations with supercapacitors connected and disconnected.
Load cycle test	Evaluation of the dynamic response of the fuel cell generator when following a continuously variable load
DC/AC converter	
Supercapacitors charging process characterization	Evaluation of supercapacitors voltage and and fuel cell voltage and current variation with time during supercapacitor charging.
Converter efficiency evaluation	Power converter efficiency evaluation in different operating conditions
System current and voltage behaviour at different power factors	System response evaluation under real operating conditions when a reactive electrical load component is present

Table 51. Electrical power production plant. Experimental characterization test list.

8.1 Field instrumentation

The characterization of the plant was carried out using part of the instrumentation part of the field instrumentation installed on the test rig and described in the prvious chapter (paragraph 6.5).
Additional instrumentation has been included by manufacturer on the fuel cell generator output for the monitoring of the fuel cell output voltage and current (marked as V and A on Figure 143).
The electrical power measurements on the load bank have been performed trough the embedded monitoring software, whereas measurements of the balance of plant power consumption have been carried out by connecting a portable network analyser to the dedicated feeding lines form the test rig electric board.

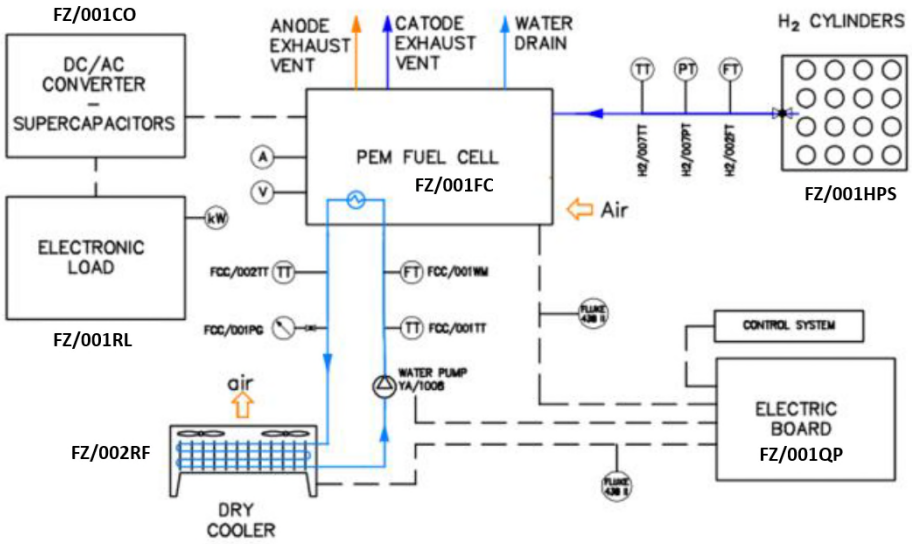

Figure 143. Overview of the field instrumentation for the experimental characterization of the electrical power production plant. [5]

8.1.1 Instrumentation on hydrogen lines

Instrumentation providing analog input to the automation controller has been installed on the fuel cell generator hydrogen supply line (piping ramp 1). Hydrogen pressure and temperature have been monitored trough dedicated transmitters.
These instruments are indicated with suffix PT (Pressure Transmitter) and TT (Temperature Transmitter –IEC751 class A Pt100 sensors) in the P&I diagram of the investigated system of Figure 143. Hydrogen flowrate have been monitored through dedicated flowmeter, marked with tag FT (Flow Transmitter) on Figure 143.

8.1.2 Instrumentation on cooling circuit piping

Fuel cell cooling circuit piping is provided with dedicated pressure gauge FCC/001PG and is interfaced with the automation system for temperature and flow monitoring via temperature transmitters FCC/001TT and FCC/002TT, and flowmeter FCC/001WM. In addition to the above, as already described in paragraph 6.5.2.3, in electrical power production mode, the automation system:

- adjusts the rotation speed of the circulation pump of the fuel cell cooling circuit,
- adjusts the rotation speed of the dry cooler fans.

8.1.3 Instrumentation metrological characteristics

Table 52 summarizes the list of the field instruments used in the characterization of the plant with indication of their location on the hydrogen lines (piping ramp 1) and on the fuel cell cooling circuit.

Sensor/ device Piece mark	Measure quantity Or check carried out	Sensor/device Type	Signal type
Piping ramp 1			
H2/004RCV	Open/close	Solenoid valve	Digital output
H2/002FT	H_2 flowrate	Flowmeter	Analog input 4...20 mA
H2/007TT	H_2 temperature	Temperature sensor	PT 100
H2/007PT	H_2 pressure	Pressure transmitter	Analog input 4...20 mA
Fuel cell cooling circuit			
FCC/001TT	Cooling water temperature	Temperature sensor	PT 100
FCC/002TT	Cooling water temperature	Temperature sensor	PT 100
FCC/001WM	Cooling water flowrate	Flowmeter	Analog input 4...20 mA
YE/1008_CTR	Circulation pump inverter control	Circulation pump inverter status	Output analogico 4...20 mA
YE1008_PO	Circulation pump inverter power output	Circulation pump inverter status	Analog input 4...20 mA
YE1008_RUN	Circulation pump inverter running	Circulation pump inverter status	Digital input
YE1008_FAIL	Circulation pump inverter failure	Circulation pump inverter status	Digital input
FCC/001DC	Fuel cell dry cooler fans speed	Controllo dry cooler	Analog output 4...20 mA converted in 0-10 V signal through signal converter installed iside automation cabinet
FCC/001DC_S	Fuel cell dry cooler fans CBs status	Fuel cell dry cooler power circuit stats	Digital input

Table 52. Electrical power production plant characterization. Field sensors/devices list.

The accuracy of the main instruments (fixed and portable) used is plant characterization presented in Table 53.

Component	Feature	Value
Hydrogen flowmeter (H2/002FT)	Accuracy Repeatability	±0.5% Rd plus ± 0.1% FS <0.2% Rd
Hydrogen pressure transmitter (H2/007PT)	Accuracy Repeatability	±0.50% FS <0.1% FS
Fuel cell voltage	Accuracy	< 1%
Fuel cell current	Precision class	1
Fuel cell cooling water flowmwter (CA/001FC)	Accuracy Repeatability	±0.3% of actual flow 0.1%
Portable network analyzer	Voltage accuracy Ampere accuracy	0.1% of V_{nom} ± (0.5% Rd plus 5% counts)

Table 53. Electrical power production plant characterization. Main metrological characteristics of the instrumentation.

During the tests, the environmental parameters (ambient temperature and pressure) were monitored by means of a dedicated weather station installed in the test rig room.

8.2 Fuel cell and system performance characterization

8.2.1 Fuel cell and system electrical efficiency evaluation

8.2.1.1 Test procedure

Once the fuel cell has been started and the heating phase completed in accordance with the procedures described in its operating manual, the load was connected to the power converter, and the data listed in Table 54 were recorded.

Quantity	Unit	Instrument	P&I Reference
Fuel cell generator hydrogen inlet flow	[Nm³/h]	Flow meter	H2/002FT
Fuel cell generator hydrogen inlet pressure	[bar g]	Pressure transmitter	H2/007PT
Fuel cell generator hydrogen inlet temperature	[°C]	Temperature sensor	H2/007TT
Fuel cell generator air inlet temperature	[°C]	Weather station	-
Fuel cell generator air inlet pressure	[hPa]	Weather station	-
Fuel cell generator BoP power consumption	[kW]	Network analyzer	-
Fuel cell generator external cooling pump power consumption	[kW]	Network analyzer	-
Fuel cell dry cooler fans power consumption	[kW]	Network analyzer	-
Fuel cell generator output voltage	[V]	Transducer on fuel cell generator	V
Fuel cell generator output current	[A]	Transducer on fuel cell generator	A
DC/AC power converter output power	[kW]	Electronic load bank	kW
Cooling water flow	[l/min]	Flowmeter	FCC/001WM
Fuel cell cooling water inlet temperature	[°C]	Temperature sensor	FCC/001TT
Fuel cell cooling water outlet temperature	[°C]	Temperature sensor	FCC/002TT
Cooling water pressure	[bar g]	Pressure gauge	FCC/001PG
Ambient temperature	[°C]	Weather station	-
Ambient pressure	[hPa]	Weather station	-

Table 54. Quantities measured during the fuel cell and system electrical efficiency evaluation with unit of measurement, instrument used for the survey and P&I diagram refernce.

8.2.1.2 Fuel cell and system efficiency calculation

Fuel cell gross electrical efficiency has been calculated according to formula (31) :

$$\eta_{FC\_gross} = \frac{P_{elFC}}{P_{in}} \cdot 100 = [\%] \quad (31)$$

Fuel cell net electrical efficiency has been calculated according to the formula (32) indicated in IEC 62282-3-200:

$$\eta_{FC\_net} = \frac{P_{elFC} - P_{elin}}{P_{in}} \cdot 100 = [\%] \quad (32)$$

Similarly, the system gross and net electrical efficiencies have been defined as:

$$\eta_{el\_gross} = \frac{P_{elSYS}}{P_{in}} \cdot 100 = [\%] \quad (33)$$

$$\eta_{el\_net} = \frac{P_{elSYS} - P_{elin}}{P_{in}} \cdot 100 = [\%] \quad (34)$$

The average power associated with thefuel cell hydrogen inlet flow (P_{in}) was calculated with equation (35):

$$P_{in} = \rho_{H_2} \times \frac{\dot{V}}{3600} \times LHV \times 1000 \quad [\text{kW}] \quad (35)$$

The meaning of the quantities shown in the above formulas, the corresponding unit of measurement, and the methodology used to calculate them are summarized in Table 55.

Table 55. Quantities used for the calculation of thefuel cell and system electrical efficiency, unit of measurement and methodology used for the calculation.

Quantity	Unit	Formula, Calculation Method or Value
P_{in}	[kW]	Power associated with hydrogen inlet flow. Equation (35)
LHV	[MJ/kg]	120 [1]
$\dot{V}$	[Nm^3/h]	Flow rate measured by the H2/002FT flowmeter referred to normal conditions: 101.325 Pa, 0 °C
ρ_{H_2}	[kg/m^3]	0.0899 [2]
P_{elFC}	[kW]	Average fuel cell generator DC output power obtained from the recorded fuel cell output voltage and current data
P_{elin}	[kW]	Average power consumption of the fuel cell generator BoP and ancillaries (circulation pump and cooler fans) from data recorded with portable network analyzer
P_{elSYS}	[kW]	Average system AC power output from the recorded load bank power absorbed data

[1] IEC 62282-3-200–Stationary fuel cell power systems–Performance test method. [115]
[2] National Institute for Standards and Technology (NIST)–Reference Fluid Thermodynamic and Transport properties Database (REFPROP). [116]

8.2.1.3 Test results

The Fuel Cell and system electrical efficiencies have been calculated at 100% and 50% nominal power (100kWel DC) referring to hydrogen Lower Heating Value (LHV) equal to 120 MJ/kg.
Table 56 reports the average values of the quantities measured during the efficiency test carried out at the nominal power of the fuel cell: 100 kWel and Table 57 reports the values at the power of 50 kWel.

Quantity	Average value	Unit of measure
Fuel cell generator hydrogen inlet flow	59.26	Nm^3/h
Fuel cell generator BoP power consumption	7.75	kW
Fuel cell generator external cooling pump power consumption	2.20	kW
Fuel cell dry cooler fans power consumption	2.40	kW
Fuel cell generator output voltage	405.48	V
Fuel cell generator output current	241.17	A
Fuel cell generator output power	97.78	kW
DC/AC power converter output power	93.00	kW
Cooling water flow	73.25	l/min
Fuel cell cooling water inlet temperature	31.47	°C
Fuel cell cooling water outlet temperature	50.59	°C
Cooling water pressure	3.00	bar g

Table 56. Electrical power production plant effciency evaluation. Average values of recored quantities with fuel cell operating @ 100 kWel output.

Quantity	Average value	Unit of measure
Fuel cell generator hydrogen inlet flow	29.46	Nm^3/h
Fuel cell generator BoP power consumption	5.17	kW
Fuel cell generator external cooling pump power consumption	2.2	kW
Fuel cell dry cooler fans power consumption	2.4	kW
Fuel cell generator output voltage	441.24	V
Fuel cell generator output current	117.07	A
Fuel cell generator output power	51.66	kW
DC/AC power converter output power	49.13	kW
Cooling water flow	35.05	l/min
Fuel cell cooling water inlet temperature	29.86	°C
Fuel cell cooling water outlet temperature	48.27	°C
Cooling water pressure	3.00	bar g

Table 57. Electrical power production plant effciency evaluation. Average values of recored quantities with fuel cell operating @ 50 kWel output.

Table 58 shows gross and net FC and system electrical efficiency at 100% and 50% nominal power.

FC power	FC gross el. eff.	FC net el. eff.	System gross el. eff.	System net el. eff.
100%	54,5 %	47,8 %	52,2 %	45,3 %
50%	58,5 %	47,5 %	56,6 %	45,6 %

Table 58. System efficiency test: gross and net fuel cell and system electrical efficiency at 100% and 50% fuel cell nominal power. [5]

Fuel cell electrical efficiency is in line with data declared by other stationary systems fuel cell producers. The difference between the FC gross and net electrical efficiency is higher at 50% nominal power output. This is due to the BOP and built-in ancillaries power consumption, which increases less than linearly with respect to the FC power output [5].

8.2.2 Fuel cell heat recovery efficiency evaluation

8.2.2.1 Test procedure

The calculation of the thermal efficiency of the fuel cell generator was performed at the same time as the tests carried out for the calculation of the fuel cell and system electrical efficiency described in paragraph 8.2.1 using the same recorded data.

8.2.2.2 Fuel cell heat recovery efficiency calculation

The fuel cell heat recovery efficiency has been calculated, following the international standard IEC 62282-3-200 [115], with the following formula (36) :

$$\eta_{th} = \frac{P_{HR}}{P_{in}} \cdot 100 = [\%] \quad (36)$$

where P_{HR} is the recovered thermal power output in kW and P_{in} is the fuel power input referred to the hydrogen LHV calculated with formula (35). The Power absorbed by the BOP and built-in ancillaries is not considered in the formula. As already mentioned, in the investigated system, the thermal power has been dissipated by means of a dedicated dry cooler. For this reason, the fuel cell recovered thermal power required by the calculation has been replaced with the heat dissipated by the dry cooler. Such thermal power is in fact potentially available for on board low temperature thermal users. The average thermal power dissipated by the fuel cell dry cooler wass calculated with the formula (37).

$$P_{HR} = Q_{HR} / t \quad (37)$$

Where Q_{HR} is the thermal energy dissipated during the test t and is the duration of the test. Dividing the duration of the test into a suitable number of time intervals, the dissipated thermal energy can be calculated with the following approximated formula (38) .

$$Q_{HR} = \sum [(T_{HR1} - T_{HR2}) * q_{VHR*}\rho_{HR} * t_{dur} * c_{HR}] \quad (38)$$

The meaning of the quantities shown in the above formulas, the corresponding unit of measurement, and the methodology used to calculate them are summarized in Table 59.

Quantity	Unit	Formula, Calculation Method or Value
P_{HR}	[kW]	Fuel cell recovered thermal power. Equation (37)
P_{in}	[kW]	Power associated with hydrogen inlet flow. Equation (35)
Q_{HR}	[kJ]	Thermal energy dissipated during the test. Equation (38)
T_{HR1}	[°C]	Fuel cell cooling water outlet temperature during considered time interval from temperature sensor
T_{HR2}	[°C]	Fuel cell cooling water inlet temperature during considered time interval from temperature sensor
q_{VHR}	[m^3/s]	Cooling water flow during considered time interval from flowmeter
ρ_{HR}	[kg/m3]	Cooling water/glycol mixture density
t_{dur}	[s]	Diration of the considered time interval
c_{HR}	[kJ/(kg*k)]	Cooling water/glycol mixture specific heat

Table 59. Quantities used for the calculation of the fuel cell thermal efficiency efficiency, unit of measurement and methodology used for the calculation.

8.2.2.3 Test results

Fuel cell heat recovery efficiencies have been calculated at 100% and 50% nominal power output and are shown in Table 60.

FC power	P_{HR}	FC heat recovery eff.
100%	98.7 kW	55.6 %
50%	45.4 kW	51.5 %

Table 60. Fuel cell heat recovery test: heat recovery at 100% and 50% fuel cell nominal power. [5]

The fuel cell generator high efficiency value is essentially due to two main reasons: the choice of referring to the hydrogen LHV and the fact that, as already mentioned, the calculation proposed by the international standard IEC 62282-3-200 does not consider the energy consumed by the internal auxiliaries of the generator.

Figure 144. Fuel cell generator during electrical power plant characterization tests. Photo by the author.

8.2.3 Fuel cell polarization curve plotting

8.2.3.1 Test procedure

FC polarization curve has been plotted following the guidelines included in the European Community Joint Research Centre test module PEFC ST 5-3 [117].
Before starting the polarization plotting procedure, it was first necessary to charge the supercapacitors and then warm the fuel cell until it reached its operating temperature. Figure 145. Fuel cell and system power output versus time.
On the left side of Figure 145 it is possible to observe the peak power delivered by the fuel cell to charge the supercapacitors. Then the fuel cell heats up delivering about 40 kWel DC power. Fuel cell system warming phase lasts about 25 minutes.

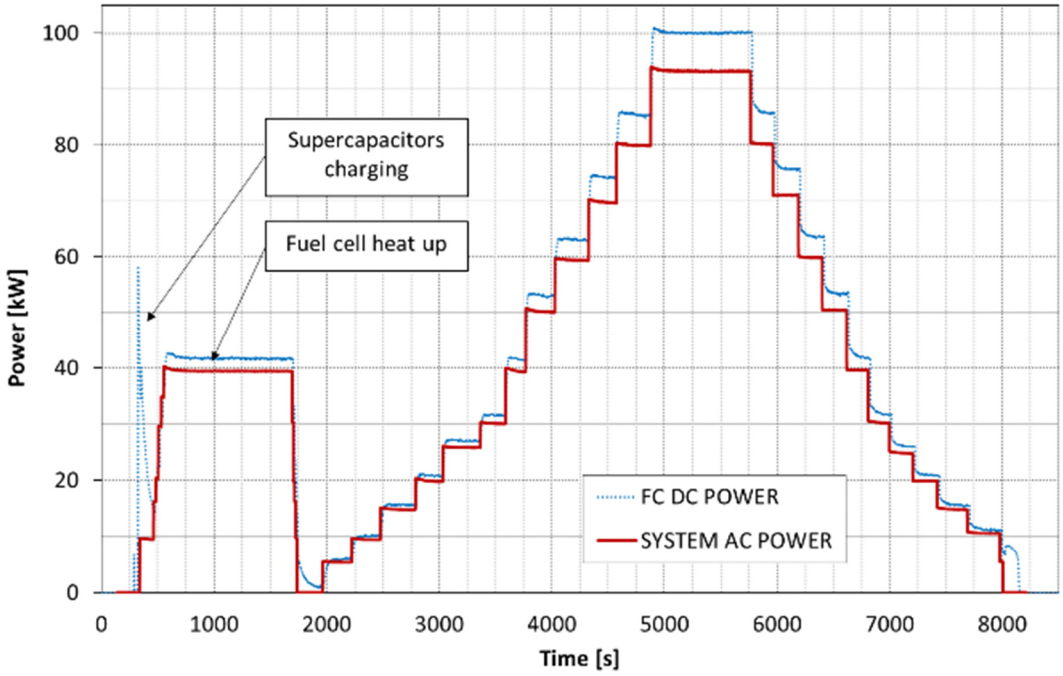

Figure 145. Fuel cell and system power output versus time. [5]

After the fuel cell has warmed up, the polarization curve plotting procedure is started by increasing first (from step 1 to step 12) and then decreasing (from step 12 to step 1) the power absorbed by the load bank in steps, as indicated in Table 61.

Set point number	Load bank power kW_{el}	Set point number	Load bank power kW_{el}
1	5	**7**	40
2	10	**8**	50
3	15	**9**	60
4	20	**10**	70
5	25	**11**	80
6	30	**12**	93

Table 61. Load bank power set point imposed for measuring the fuel cell polarization curve. [5]

At each load step the quantities listed in Table 54 are recorded.

8.2.3.2 Test results

Figure 146 shows the fuel cell polarization curve recorded during the test. In the same figure the fuel cell DC power variation with current is presented. Fuel cell polarization curve is in line with producer's data. Nominal power is delivered at about 250 A.
At this operating point, considering that the fuel cell system consists of 2 strings connected in parallel each composed by 6 stacks in series, and that the total number of cells is 1152, the single cell voltage is about 0.7 V. The set of data recorded for the polarization curve plotting allowed to also calculate the FC and system electrical efficiency at different FC operating point [5].

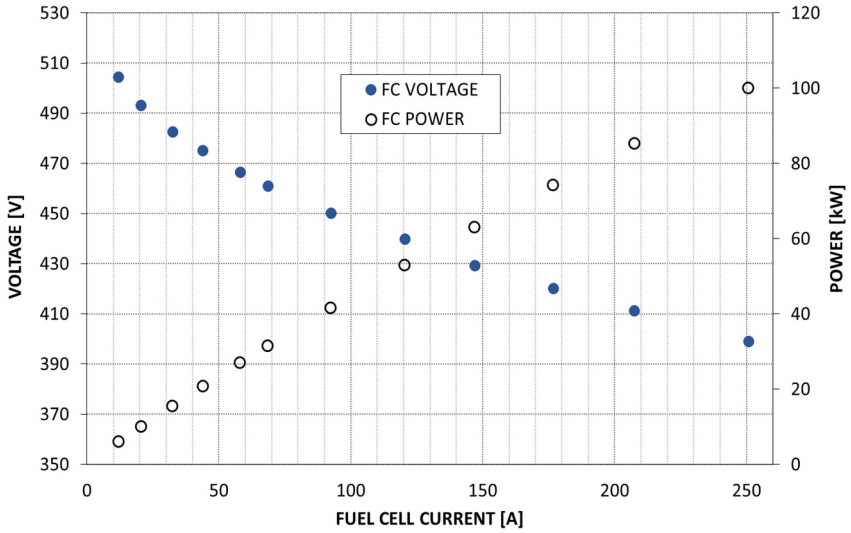

Figure 146. Fuel cell voltage and power variation with current. [5]

Figure 147 shows FC and system gross and net electrical efficiencies variation at different FC power. It is possible to observe that FC and system gross electrical efficiencies decrease as power increase while FC and system net electrical efficiencies increase with power. As already mentioned in 8.2.1, this behaviour is due to the higher influence of BOP power consumption at low loads.
The highest FC gross electrical efficiency (about 60%) is reached at 30% nominal load. System net electrical efficiency remains almost constant from about 60% to 100% fuel cell power [5].

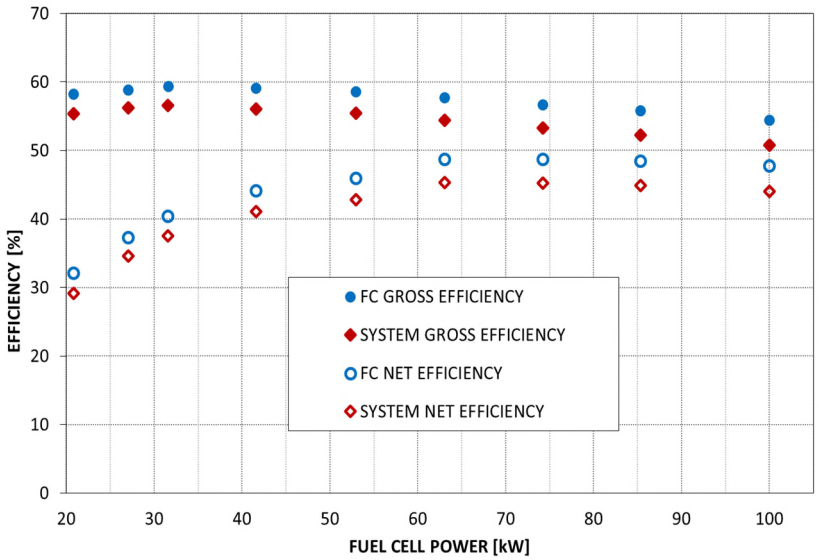

Figure 147. Fuel cell and system gross and net electrical efficiency. [5]

8.2.4 System startup and shutdown characterization

The system startup and shutdown characterization test has been developed to investigate energy and fuel consumption during these operational phases. To improve fuel cell expected life, the system is flushed with hydrogen every time it is started or shutdown. In both cases hydrogen is discharged in atmosphere. An evaluation of the discharged hydrogen volume is essential to allow the calculation of the extension of any dangerous areas onboard, as required by Classification Societies. This parameter is also fundamental for the proper sizing of the hydrogen storage system [5].

8.2.4.1 Test procedure

During startup and shutdown of the fuel cell generator, the quantities listed in Table 54 were recorded. For the purpose of the test, the startup period has been considered as the time interval between the issuing of the start signal and the reaching of a stable 15 kWel AC power output. Similarly, the shutdown period has been considered as the time interval between load disconnection and the interruption of hydrogen consumption [5].

8.2.4.2 Test results

In Table 62 and Table 63 hydrogen consumption, average and peak BOP electric power consumption and BOP electric energy demand at system startup and shutdown are recorded. Total hydrogen consumption at startup is 0.33 Nm3, while hydrogen consumption at shutdown is 0.24 Nm3. Maximum recorded peak BOP consumption is equal to 10 kWel.

	Unit of measure	Value
Time	s	120
Hydrogen consumption	Nm^3	0.33
Average BOP consumption	kW_{el}	3.3
Peak BOP consumption	kW_{el}	10
BOP electric energy demand	kWh_{el}	0.11

Table 62. Hydrogen consumption, average and peak BOP electric power consumption and BOP electric energy demand at system startup. [5]

	Unit of measure	Value
Time	s	175
Hydrogen consumption	Nm^3	0.24
Average BOP consumption	kW_{el}	3.8
Peak BOP consumption	kW_{el}	9.6
BOP electric energy demand	kWh_{el}	0.19

Table 63. Hydrogen consumption, average and peak BOP electric power consumption and BOP electric energy demand at system shutdown. [5]

Figure 148 and Figure 149 show hydrogen flow rate variation at startup and shutdown, respectively. It is possible to observe that the highest peak flow rate was measured at system shutdown and is higher than 25 Nl/min.

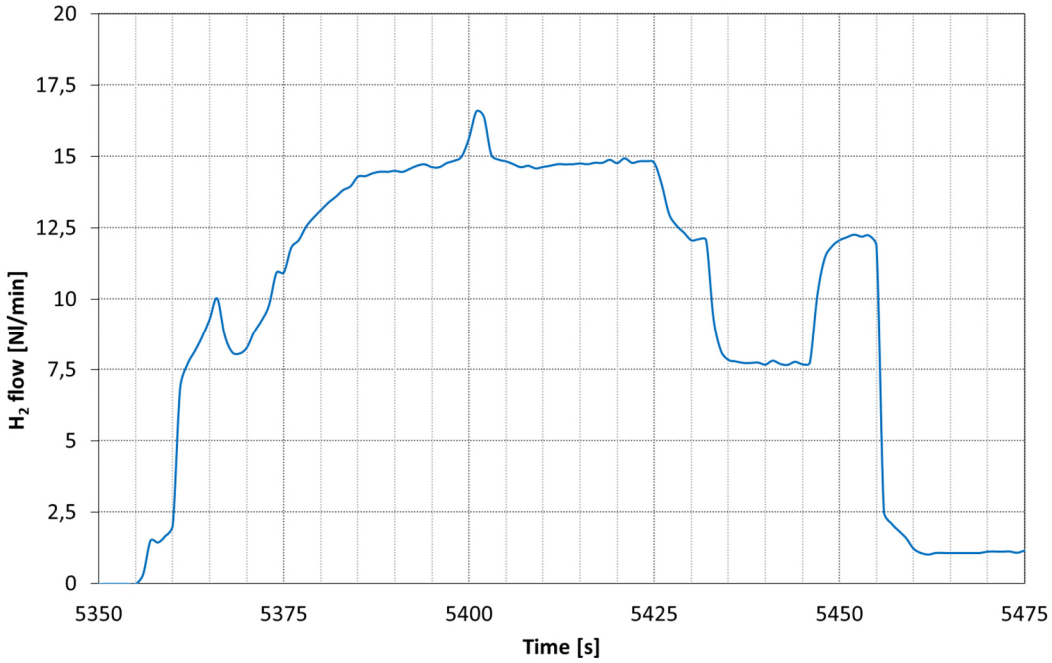

Figure 148. System startup: hydrogen flow rate variation with time. [5]

Hydrogen flow peaks shown in Figure 149 are due to the fuel cell manufacturer's control strategy that aims to remove every unwanted residue from the anode side before the fuel cell shuts down [5].

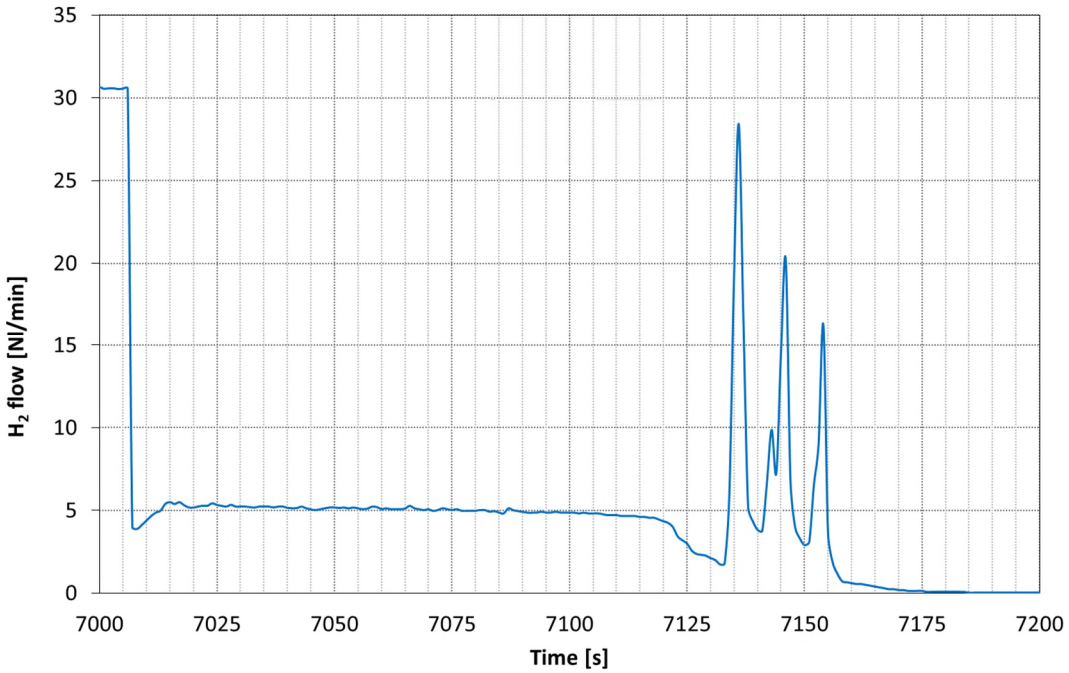

Figure 149. System shutdown: hydrogen flow rate variation with time at system shutdown. [5]

8.2.5 Discharge water quality test

This test has been performed for assessing the quality of water discharged from the fuel cell to verify the possibility to collect the excess of product water into the onboard grey water collecting system.

8.2.5.1 Test procedure

The international standard IEC 62282-3-200 requires the analysis to be carried out on water samples collected during the operation of the fuel cell generator in operation. However, since the test rig PEMFC generator is powered by pure hydrogen, the product water is expected to be pure and similar in composition to demineralized water. It is therefore believed that there can be no significant variations in the composition of the process water during the various operating phases of the generator and for this reason, the sampling was carried out with the machine stopped, drawing directly from the internal tank of the generator.

8.2.5.2 Test results

As expected, the water analysis has shown that the fuel cell produced water can be considered demineralized water except for the presence of negligible quantities of iron, lead, zinc and nickel, probably originating from the cooling system pipes materials. Concentration of such contaminants is lower than the values given in a study focused on the impact of grey water discharge in the Baltic Sea [118] and others stated in a document issued by the United States Environmental Protection Agency [119].

Figure 150. Fuel cell generator. Internal water tank (bottom left). Photo by the author.

8.2.6 Fuel cell electric load response analysis

This test has been performed for measuring the FC power response time, which is defined as the time interval necessary to reach a FC electric power output steady-state value starting from the moment in which a change of electric power output is started. The test has been carried out both with supercapacitor storage system connected and disconnected.
For the purpose of the test, it has been chosen not to apply a load power increase higher that 30 kWel in order to preserve system integrity.

8.2.6.1 Test procedure

Once the fuel cell has been started and the heating phase completed in accordance with the procedures described in its operating manual, the supercapacitors were charged. With supercapacitors charged the load load cycle described in Table 64 was repeated for four consecutive cycles. At each load bank power step, the data listed in Table 54 were recorded.

Load bank power setting [kW]	Duration [s]
15	30
45	30
75	30
93	30
33	30
15	30

Table 64. Fuel cell electric load response analysis. Load cicle set on load bank for testing purpose.

The procedure and date recording were again repeated for four consecutive cycles with supercapacitors disconnected from the DC/AC converter.

8.2.6.2 Test results

Table 65. FC electrical load response time and FC delivered power for different load power variations. Supercapacitors connected. and Table 66 show the FC electrical load response time and the FC delivered power with supercapacitor storage system connected and disconnected, respectively.

Load bank power variation		FC response time	FC delivered power
from kW	to kW	s	kW
0	15	-	17.80
15	45	19	47.75
45	75	15	79.92
75	93	10	99.09
93	33	18	38.79
33	15	21	20.12
15	45	10	47.76
45	75	15	79.66
75	93	9	98.94
93	33	20	40.22
33	15	24	20.16
15	45	10	47.77
45	75	15	78.96
75	93	10	99.07

Load bank power variation		FC response time	FC delivered power
from kW	to kW	s	kW
93	33	20	40.23
33	15	22	20.29
15	45	9	46.63
45	75	17	79.66
75	93	11	100.4
93	33	21	38.98
33	15	23	20.23

Table 65. FC electrical load response time and FC delivered power for different load power variations. Supercapacitors connected. [5]

Load bank power variation		FC response time	FC delivered power
from kW	to kW	s	kW
0	15	-	15.84
15	45	≤ 1	47.21
45	75	2	80.78
75	93	≤ 1	99.65
93	33	≤ 1	33.34
33	15	≤ 1	15.83
15	45	2	48.13
45	75	≤ 1	80.32
75	93	≤ 1	99.27
93	33	≤ 1	34.48
33	15	≤ 1	15.83
15	45	2	48.10
45	75	≤ 1	80.36
75	93	≤ 1	99.26
93	33	2	34.50
33	15	≤ 1	15.82
15	45	≤ 1	48.13
45	75	2	80.22
75	93	≤ 1	99.24
93	33	≤ 1	34.52
33	15	≤ 1	15.80

Table 66. FC electrical load response time and FC delivered power for different load power variations. Supercapacitors disconnected. [5]

With supercapacitors connected, the longest FC response time was 24 seconds with a step load reduction from 33 to 15 kWel. The shortest FC response time was 9 seconds, and it was recorded with a step load increase from 15 to 45 kWel and from 75 to 93 kWel.
With supercapacitors disconnected, the longest FC response time was about 2 seconds. Figure 151 and Figure 152 show the fuel cell power variation during the FC electric load response test with supercapacitor storage system connected and disconnected, respectively.
Comparing Figure 151 and Figure 152 it is evident how the supercapacitor energy storage system integrated in the DC/AC converter smoothens the FC delivered power output [5].

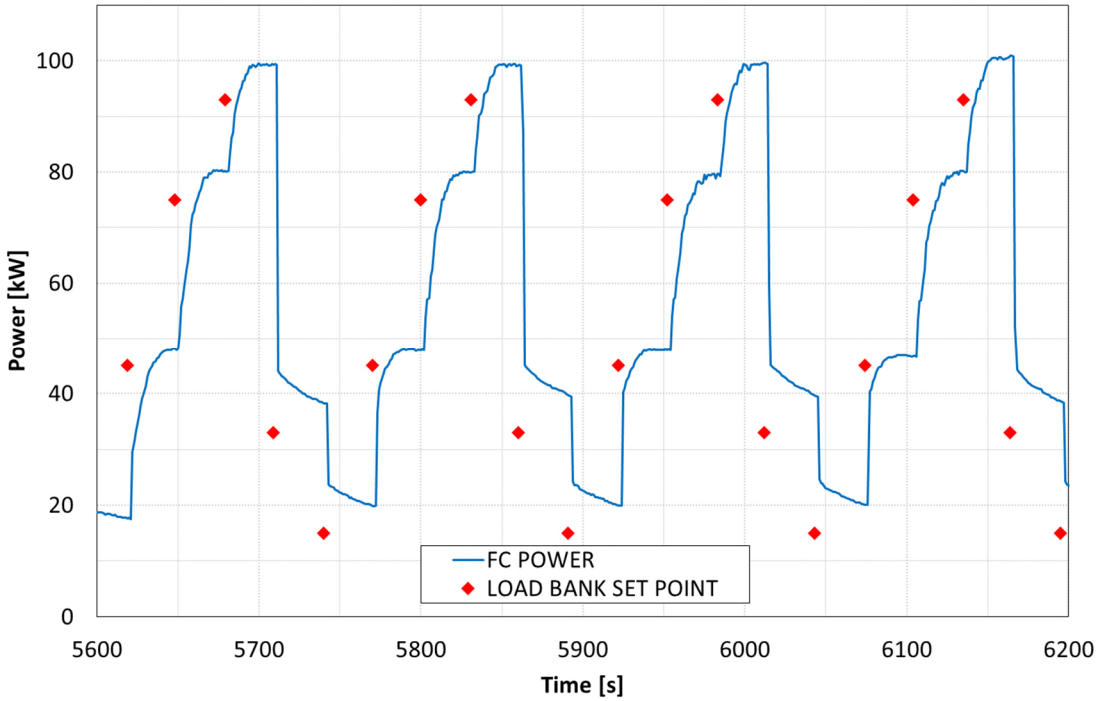

Figure 151. Fuel cell power variation for the FC electrical load response time test with supercapacitor storage system. [5]

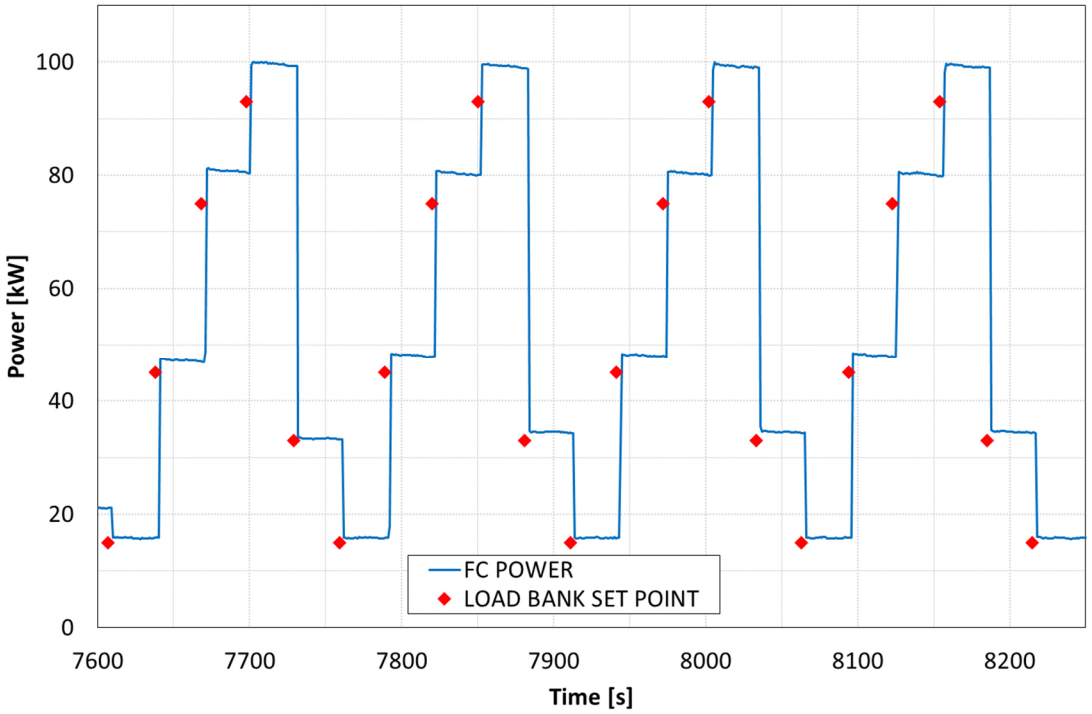

Figure 152. Fuel cell power variation for the FC electrical load response time test without supercapacitor storage system. [5]

8.2.7 Load cycle test

A load cycle test consisting of a periodical changing of the power required from the generator has been performed to evaluate the dynamic response of the generator when following a continuously variable load, i.e., a load cycle. The test has been carried out with the supercapacitors in operation.

8.2.7.1 Test procedure

The load profile applied at the load bank had a triangular shape, with power output varying from a minimum value of 19 kWel up to the load bank rated power (93 kWel), as shown in Figure 153.

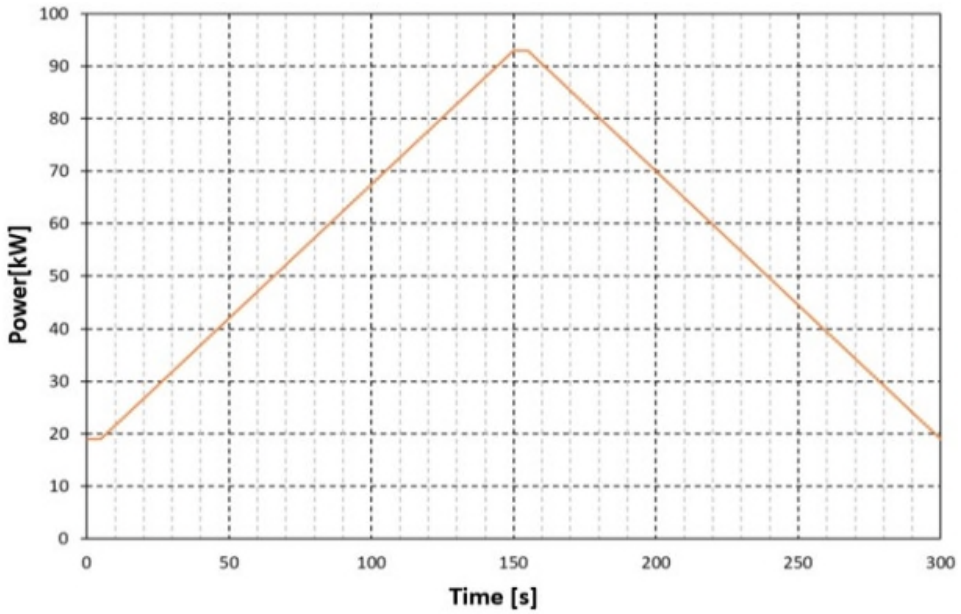

Figure 153. Load cycle test: load profile applied at the load bank. [5]

The load cycle had a period of 5 minutes. Once the fuel cell has been started and the heating phase completed in accordance with the procedures described in its operating manual, the supercapacitors were charged.
With supercapacitors charged the load load cycle described in Figure 153 was repeated for five consecutive cycles. At each load bank power step, the data listed in Table 54 were recorded.

8.2.7.2 Test results

Figure 154 shows the fuel cell delivered power variation during the load cycle test. The system can follow the proposed triangular-shaped load cycle without any issue.

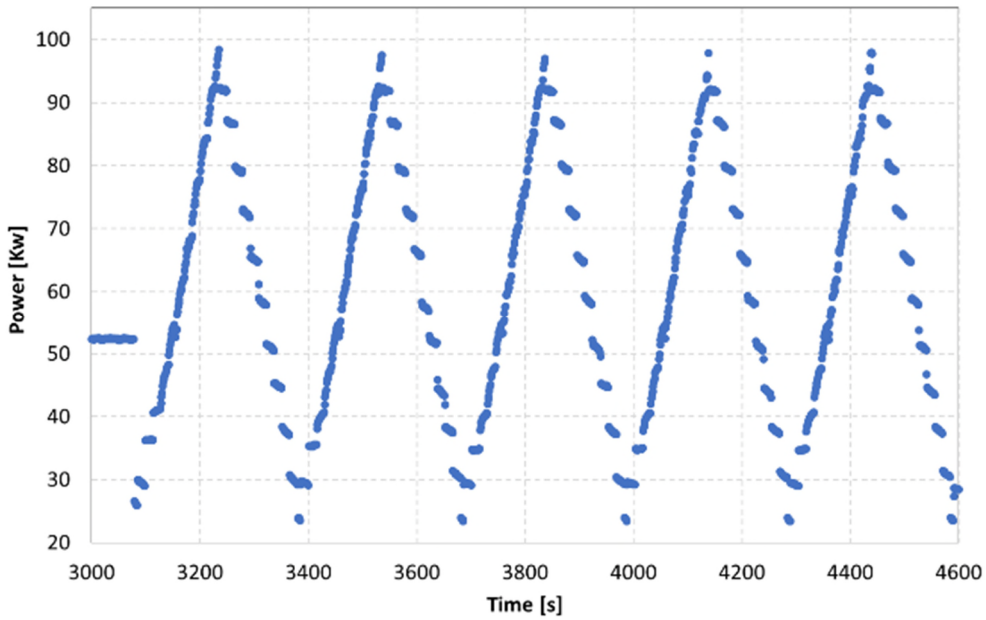

Figure 154. Fuel cell delivered power variation during the load cycle test. [5]

To evaluate fuel cell degradation over time, authors are aware that further tests should be performed when a variable load is applied over a longer period, as it could happen on board of a ship in operation. Currently, the literature available on PEM durability and performance degradation prediction focus mostly on the automotive application of this technology. Thanks to the wide availability of data recorded both during tests carried out in the lab and in the actual operation of road vehicles, for such application several predictive models and theories have been developed.
As an example, among the literature available on this topic, the study [120] proposes an accelerated method for the evaluation of automotive PEM fuel cell lifetime based on data collected on at least 300 h test time in laboratory.
Study [121], instead, proposes an experimental-based algorithm for the prediction of the loss of performance of the fuel cell catalyst layer during cyclical load variations.
More recently, in [122] a semi-empirical model for the evaluation of the loss of PEM fuel cell Electro-Chemically active Surface Area (ECSA) in automotive operating conditions has been developed.
In the automotive sector, the use of the fuel cell as a propulsion system makes it possible to well define load profiles typically including starting, acceleration, high power operation, deceleration, stopping and idling periods. As regards the specific application of PEM fuel cells on the maritime sector and, especially, on board of cruise ships, typical load profiles will be essentially influenced by their intended use (propulsive, for hotel load supply or both). In order to develop effective predictive models for PEM fuel cell maritime generators, the experiences and knowledge developed for the automotive sector will have to be adapted to the real load profiles recorded onboard [5].

8.3 DC/AC converter characterization

8.3.1 Supercapacitors charging process characterization

The characterization of the supercapacitor charging process aimed to evaluate the supercapacitors voltage variation with time, the time required for charging them and the current and voltage at the fuel cell output during such process.

8.3.1.1 Test procedure

After having completely discharged the supercapacitors, the fuel cell generator was started. At the end of the heating phase of the generator, carried out in accordance with the procedures described in its operating manual, the supercapacitors were charged by applying an increasing load in three steps through the load bank. At the beginning of the supercapacitors charging process the fuel cell delivered approximatively 20 kWel.
The charging process was considered completed when the power delivered by the fuel cell is equal to the final setting point of the load bank and the voltage reading across the supercapacitors was constant. During the charging proess, the the data listed in Table 54 were recorded.

8.3.1.2 Test results

In Figure 156 is shown the measured supercapacitors voltage variation with time. In the same figure, the theoretical supercapacitors voltage variation with time of the DC/AC converter internal resistor-capacitor (RC) circuit is also plotted. The parameters of the DC/AC internal RC circuit are reported in Figure 155.

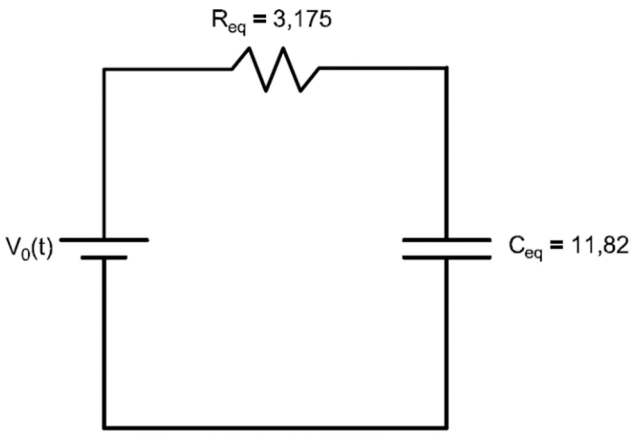

Figure 155. Test rig DC/AC power converter supercapacitor charging equivalent RC internal circuit.

In Figure 156 it is possible to observe a good correspondence between the experimental and the theoretical curves. It has been observed that the overall charging process takes about 175 s. The final supercapacitors voltage is 470 V [5].

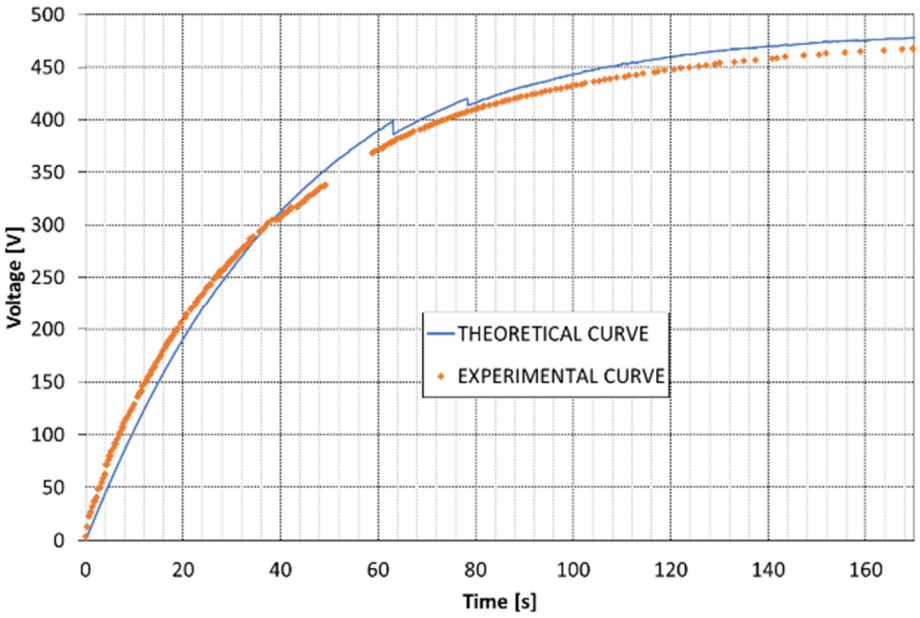

Figure 156. Experimental and theoretical supercapacitors voltage variation with time. [5]

Figure 157 shows fuel cell current and voltage variation with time during the supercapacitors charging period. Fuel cell voltage initially increases, then becomes stable at 470 V. Instead, the fuel cell current decreases as supercapacitors charge. It is also possible to notice two discontinuities in the fuel cell current and voltage curves. These are due to the adopted supercapacitors charging strategy. If the external connected load is not modified, as the charge of the energy storage system progresses, the power delivered by the fuel cell would tend to decrease progressively with the consequent increase in its output voltage. In order to prevent fuel cells from operating at high potential, which in the long term accelerates their degradation and negatively affects their performance, the external load is increased in steps during the supercapacitors charging period [5].

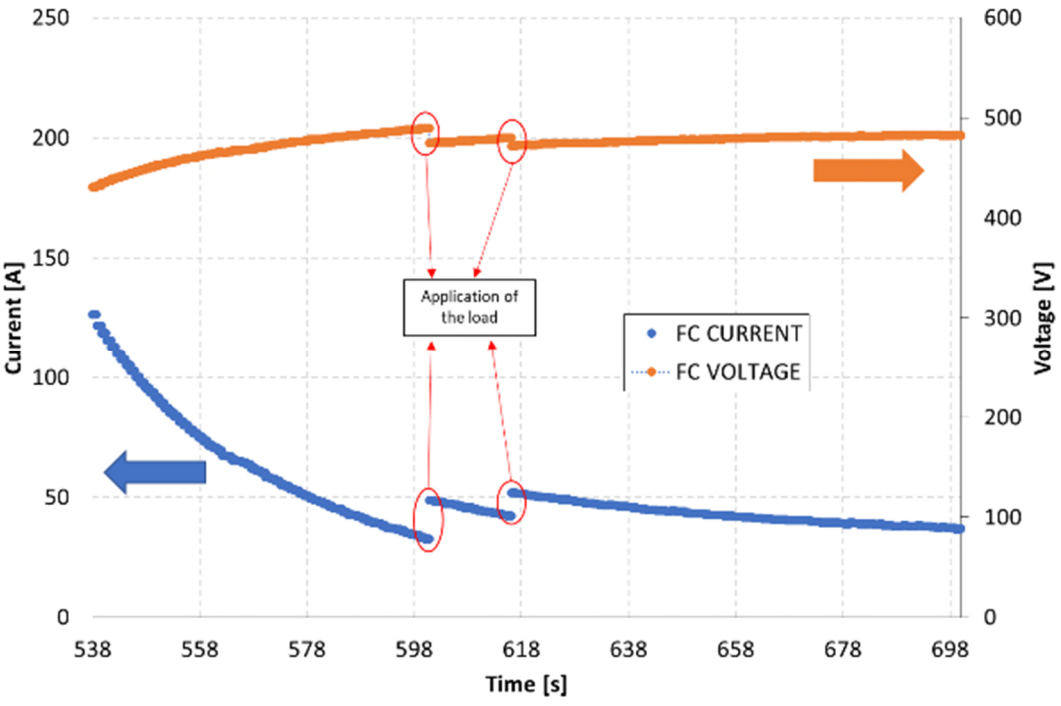

Figure 157. Fuel cell current and voltage behaviour during the supercapacitors charging period. [5]

8.3.2 Converter efficiency evaluation

8.3.2.1 Test procedure

Once the supercapacitors have been loaded, the electrical power absorbed by the load bank was first set and maintained at a value corresponding to the delivery by the fuel cell generator of about 50% of the nominal power and, subsequently, it was increased and maintained constant to a value corresponding to the output from the generator of a power close to its ratedl power.
At each power step the the data listed in Table 54 were recorded.

8.3.2.2 Test results

In Table 67 conversion efficiency, converter average power and FC average power at two different load bank set points (45 kWel and 80 kWel) are presented. Average values are calculated on a 10-minute basis.

Load bank set point kWel	Average FC power kWel	Converter average power kWel	Conversion efficiency %
45	46.9	45.1	96.2
80	85.5	81.2	94.9

Table 67. Conversion efficiency, converter and FC average power at different load bank set point. [5]

Results show that the maximum conversion efficiency is reached at 45 kWel output and is equal to 96.2 %. Considering that the DC/AC converter is a prototypal unit, this value could be further improved [5].

8.3.3 System current and voltage behaviour at different power factors

A power factor variation test has been also performed to evaluate the response of the system under real operating conditions when a reactive electrical load component is present.

8.3.3.1 Test procedure

At the end of the test performed to determine the efficiency of the power converter, the power on the load bank was set again to a value corresponding to the output by the fuel cell generator of 50% of its nominal power (50 kWel). Keeping the active power absorbed by the load bank constant, the power factor was first reduced in steps up to an inductive value of 0.8 and was subsequently brought back in steps to 1 (purely resistive load).
During the test, the data listed in Table 54 were recorded for each variation of the power factor. The influence of the power factor variation on the power generation system behaviour has been evaluated by measuring the consequent variations in the reactive power delivered by the converter and in the power delivered by the fuel cell.

8.3.3.2 Test results

Figure 158 shows the converter reactive power output variation as power factor changes: converter reactive power increases up to 38.9 kvar as the power factor decreases from 1 to 0.8.

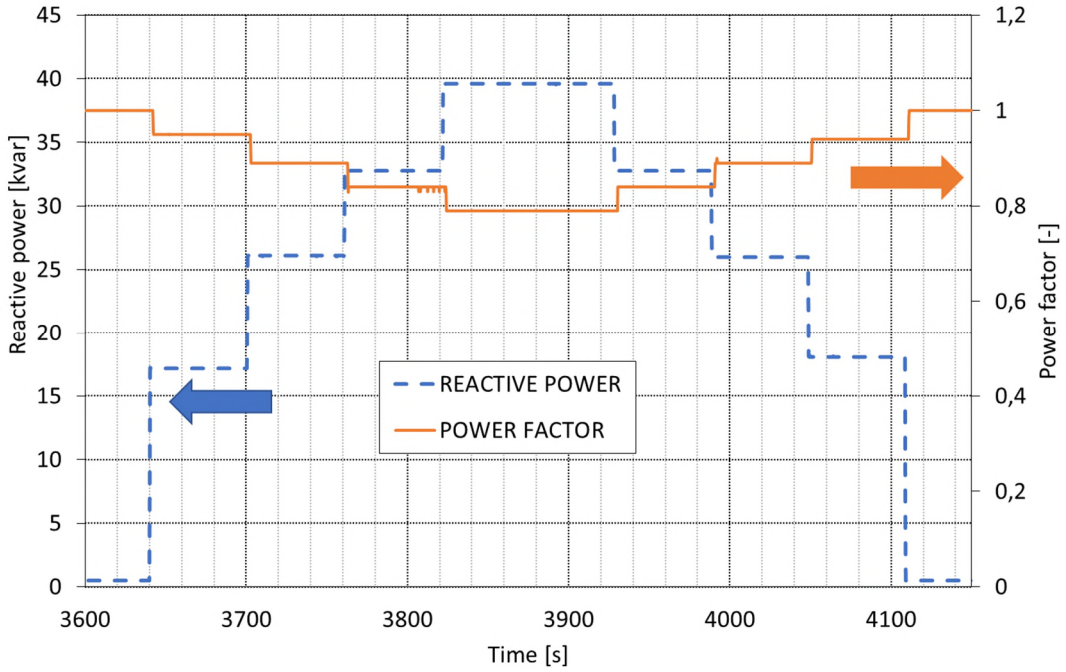

Figure 158. Converter reactive power output variation as load bank power factor changes. Considered system load: 50 kWel. [5]

Figure 159 shows FC power output and load bank power factor variation with time: as the power factor varies, the effect on the fuel cell is negligible, with small oscillations of the produced output power [5].

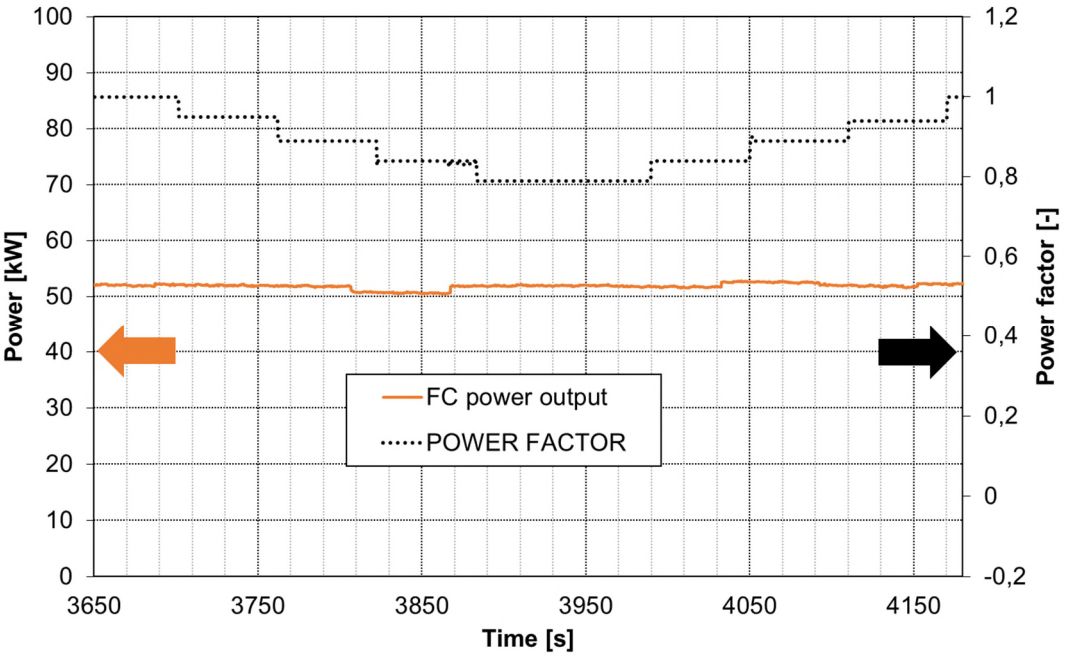

Figure 159. FC power output and load bank power factor variation with time. [5]

9 Onboard installation and scale-up perspectives

This last chapter chapter dedicated to the description of the short and medium-term developments of the hydrogen production and compression and power generation plants assessed and characterized on the test rig:

- in the short term, the test rig plants have been installed as a demonstrator aboard an operational cruise ship;
- in the medium term on the other hand, as soon as the regulatory framework relating to bunkering and the management of hydrogen on board the ship is defined, the goal is to upgrade the generation plant to provide first the supply of hotel electrical loads of a cruise ship and then, at a later stage, also feed the propulsion system.

The open technological challenges are in fact many and a fuel cell zero emission cruise ship is not feasible at the current technology's state of the art. A strong opportunity for the future is the implementation of a hybrid solution on board, which will encompass normal or dual fuel ICE, fuel cells and accumulators like batteries or supercapacitors. This solution will affect cruise ship's power plant and their general arrangement [1].
The on-board installation of fuel cell generators and energy storage systems will also affect the architecture of the electrical distribution systems with the introduction of DC networks and the adoption of technical paradigms and solutions already successfully used in terrestrial applications that may also be advantageous in the maritime sector, first of all, the microgrid concept.
Such a paradigm, while implying a complete re-design of the currently adopted shipboard electrical power systems, is gaining importance since it allows an increase of efficiency, a reduction of polluting emissions, a high reliability and resilience, and a better quality of service on board [123].
In the last decade, the advantages of DC distribution of electrical power have been widely discussed and assessed in terms of both energy efficiency and simplification of the electrical architecture.
The recognized advantages of DC power distribution are numerous, for example:

- simplification of electrical equipment connection to the power grid;
- elimination of power transformers;
- possibility to optimize the generation system by using high speed generators;
- reduction of fuel consumption by optimizing the operating points of the gensets' prime movers;
- elimination of voltage drop due reactive power;
- elimination of the need for power factor correction [124].

9.1 Demonstrator plant onboard a cruise ship

In parallel with the design of the test rig, the possibility of integrating the same systems tested ashore on board a medium-sized luxury cruise ship was verified. The goal was to develop the detailed project of a demonstration plant composed of the same main elements of the test rig and working at the same design pressures, analyze its suitability for installation onboard in terms of space availability and arrangement onboard, assess the system safety and then proceed with its installation on board.
The block diagram of the onboard demonstrator plant is shown in Figure 160.

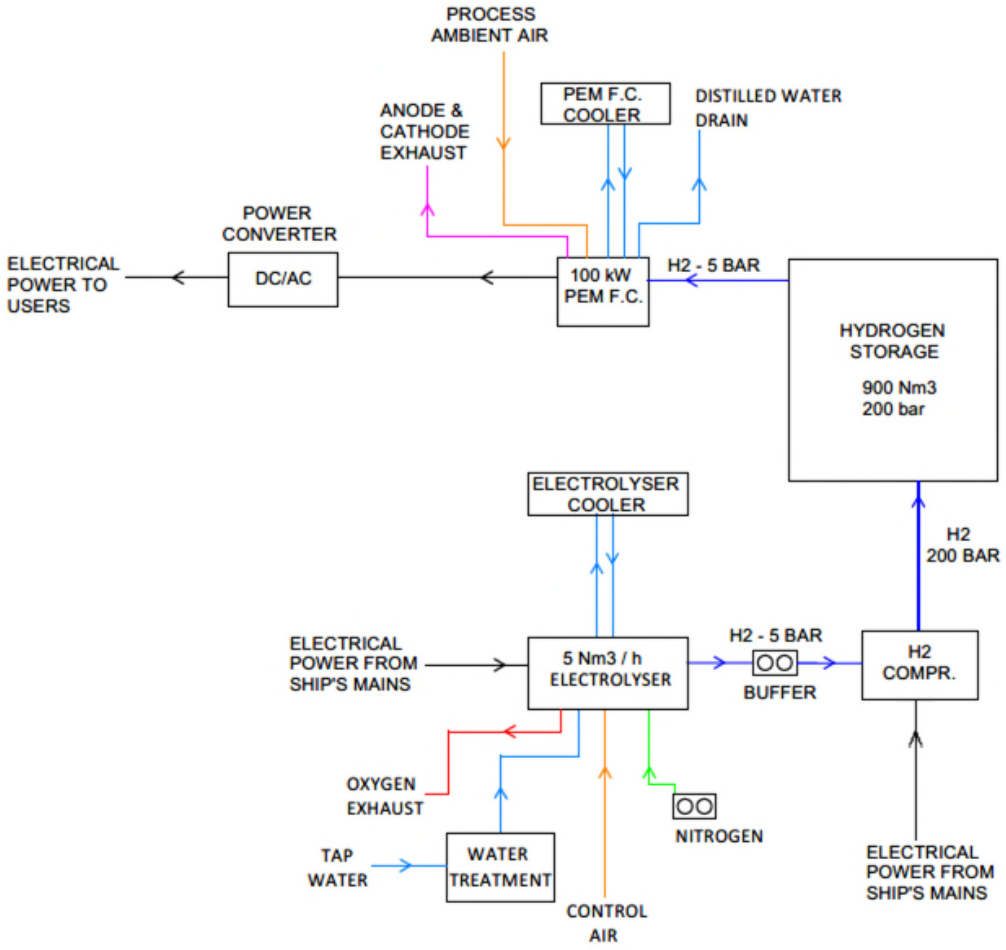

Figure 160. Demonstrator plant for onboard instllation. Block diagram.

The two plants installed and tested in the test rig can be easily recognized on the block diagram of the demonstrator. The hydrogen generation and compression plant with the alkaline electroliser and the hydrogen booster is represented in the lower part of the block diagram, whereas the electrical power porducrion plant with tht fuel cell generator and the DC/AC power converter is repressnted on the top part of the diagram.
The operating modes of the systems that make up the on-board demonstrator are the same as those already described in paragraph 6.5 in which the automation and control system of the test rig was described. For safety reasons, the two systems are interlocked so that they can never operate simultaneously.

The expected operation of the onboard demonstrator plant is as follows:

- in harbour or in navigation, the stored hydrogen is used to produce electrical power with the fuel cell generator and feed the connected electrical users through the DC/AC power converter. Electrical power is generated at zero-emissions.
- During navigation electrical power form ship's mains is used to integrate the consumed hydrogen by producing it from tap water with the electrolyser. Hydrogen is compressed and stored for later use.

Working functionality of the demostrator plant is summarized in Figure 161

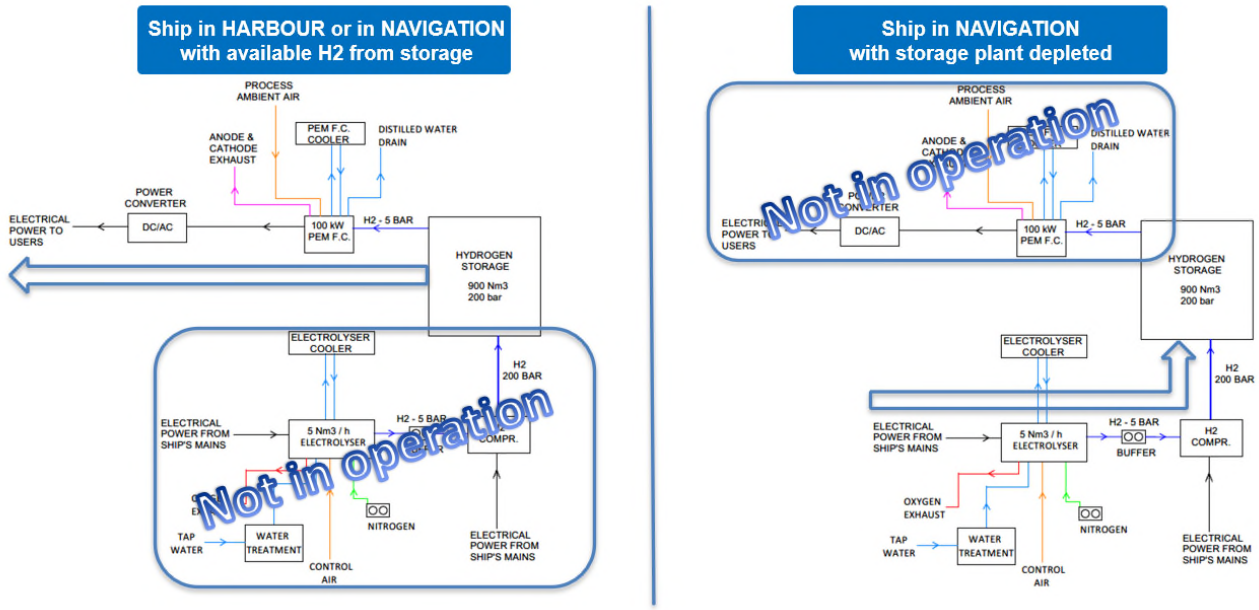

Figure 161. Onboard demonstrator plant. Operation summary.

The monitoring and control of the plants in the demonstrator are carried out through the on-board automation system in which the dedicated pages developed for the land-based test rig have been suitably adapted.
As already mentioned, the on-board demonstrator uses the same main components as the test rig (electrolyser, fuel cell generator and converter). The fuel cell generator radiator and its external cooling circuit circulation pump have been specifically purchased for onboard installation were certified for marine use. The test rig and the onboard demonstrator plants essentially differ in the type of hydrogen booster (on board it is electrically powered while on the ground it was powered by compressed air) and in the volume and type of cylinders of the hydrogen storage system. The gas cylinders used for the onboard installation were large diameter seamless steel pipes of the same type as those shown in Figure 162.
The main characteristics of the onboard high pressure storage system are summarized in

Onboard demonstrator high pressure storage	
Storage pressure	200 bar g
Cylinder external diameter	559 mm
Cylinder lenght	7400mm
Number of cylinders	4

Table 68. Onboard demonstrator. High pressure storage cylinders.

Figure 162. Large diameter seamless steel cylinders. [125]

The storage plant has been sized with a capacity of about 900 Nm3 as the best compromise between

- service autonomy
- recharge time

The autonomy of the onboard plant at full power (100 kWe) is about 10 hours in both winter and summer outside air temperatures. Considering the connected power, the type of users fed and their daily load profile, the quantity of hydrogen should be enough to supply the connected load during a stop in port or in navigation for days.
As regards the charging times of the storage system, in order not to increase consumption and emissions during navigation, the hydrogen generation and compression system has been sized to ensure the recharging of the completely emptied storage system in about 6-8 days both in winter and in summer.
The analysis of the general arrangement plans of the cruise ship selected for the demonstrator installation has led to the identification of the deckhouse located in the aft part of the ship, as the most suitable area for the plant. In order to allow the arrangement of the system, during the design stage the following modifications were foreseen for the area:

- widening of the deckhouse on port and starboard sides;
- creation of the new fuel cell space on port side with dedicated ventilation system;
- creation of an isolated fuel cell auxiliary space on port side;
- creation of a new storeroom on starboard side to replace the current one located on port side;
- loss of toilet on the port side and relocation of the starboard side one;
- provision of new pipes for the supply of water to the electrolyser and for the drainage of distilled water from fuel cells;
- relocation of the deckhouse stair door from the starboard side to the forward side of the deckhouse;
- raising the roof of the deckhouse;
- positioning of hydrogen pressure cylinders and exhaust fans on the roof of the deckhouse.

The main area layout modifications are shown in Figure 163.
The fuel cell room and the areas where the plant components are located have been equipped with safety systems such as: fire detection and extinguishing, gas detection and safety shutdowns.

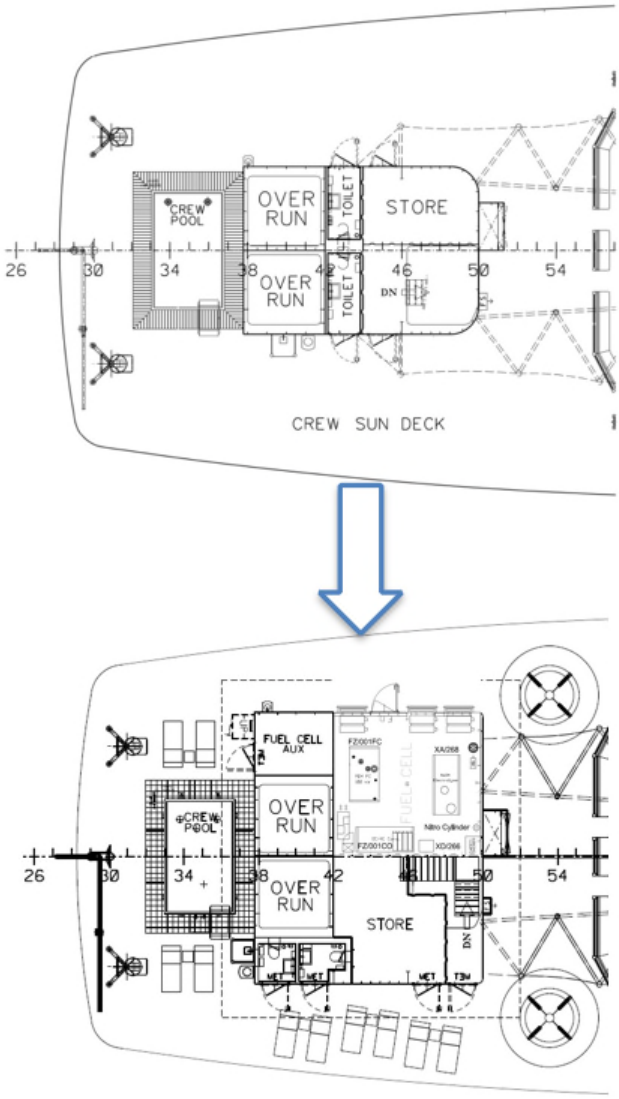

Figure 163. Onboard demonstrator. Ship's layout modification.

Except for the hydrogen cylinders, hydrogen compressor, equipment coolers and exhaust fans, placed on the roof of the deckhouse, the remaining components of the plant are arranged in the same space, thus making the fuel cell plant self-contained.
In agreement with the Owner, the plant onboard provide alternative power supply to the houselighting dimmers serving the ship's main public areas. Dimmers are provided with automatic changeover to feed them from mains supply when the fuel cell plant is not in operation.

9.1.1 The preliminary HAZID study

To assess the safety of the system, the preliminary project of theonboard demonstrator plant was subject to apreliminary Hazard Identification (HAZID) study which followed a Structured What-If? (SWIFT) and checklist technique based on the following standards [126]:

- HAZID, Guide to Best Practice, 2nd Edition. IChemE (2008);
- BS ISO 31000: 2009, Risk Management – Principles and Guidelines;
- BS ISO 31010: 2010, Risk Management – Risk Assessment Techniques.

The objectives of the HAZID workshop were to identify:

1. hazards and how they can be realised (i.e., the accident scenarios – what can go wrong and how?);
2. the consequences that may result;
3. existing measures/safeguards that minimise leaks, ignition and potential consequences, and maximise spill containment and
4. recommendations to eliminate or minimise safety risks.

The HAZID technique adopted involved the definition of discrete process sections, termed “Nodes”, and the application of a checklist to these Nodes to identify deviations that may lead to a safety or operational problems [126].

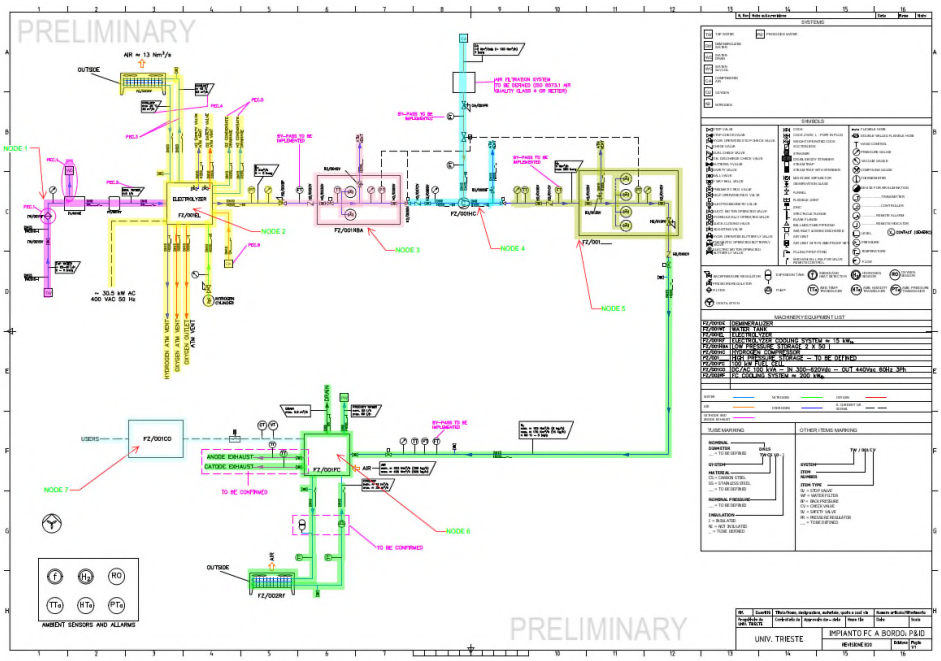

Figure 164. Onboard demonstrator. Preliminary HAZID nodes identified by dufferent colors. [126]

Nodes provisionally identified for the study were:

1. water feed system to the electrolyser;
2. the electrolyser;
3. the low-pressure hydrogen storage;
4. the hydrogen compression system;
5. the high-pressure hydrogen storage;
6. the fuel cell generator;
7. the DC/AC power converter.

To ensure maximum accuracy in each Node analysis, the preliminary HAZID study was attended by the main component manufacturers.
The HAZID process did not lead to the identification of unacceptable risks associated with the design of the on-board demonstrator system, as shown in the HAZID Severity/Likelihood matrix of Figure 165.

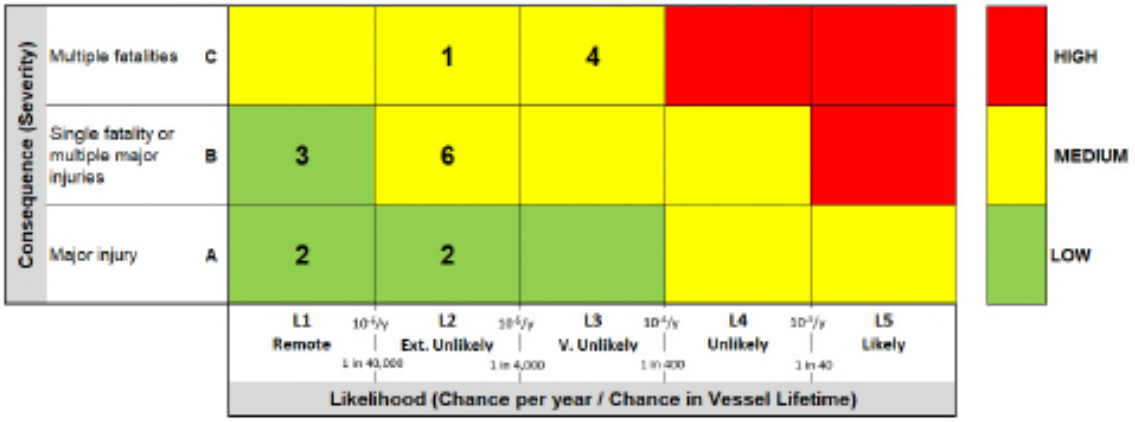

Figure 165. Preliminary HAZID study. Severity/likelihood matrix. [126]

Based on the observations and comments that emerged in the preliminary HAZID study, some changes were made to the initial design to mitigate the danger of possible failure scenarios and further studies necessary to complete the risk analysis of the plant were launched. The main changes made to the plant concerned:

- the installation of heat detectors where hydrogen could be ignited;
- the modification of the equipment installed on the hydrogen pipeline. In detail: some valves have been added, others have been removed, a new pressure transducer has been implemented and new piping purge points have been added to facilitate maintenance operations, nitrogen and air purge has been added hydrogen booster;
- the installation of a water-fog cooling system for the high-pressure hydrogen storage cylinders;
- the maximization of the mutual spacing of the hydrogen and oxygen vents;
- the installation of a visual alarm system activated in case of a low concentration of the oxygen level in the fuel cell room;
- the installation on the ceiling of the fuel cell room of ATEX certified equipment (lighting fixtures and and fire detectors) and of fire extinguishing systems that do not act as an ignition source by accumulation of stati charges;
- the relocation of the hydrogen booster low pressure storage cylinders and of all the high-pressure hydrogen piping outside the fuel cell room.

From the preliminary HAZID of the measurement plant, the need emerged to simulate, using Computational Fluid Dynamics (CFD) software, the worst-case hydrogen leakage scenarios inside and outside the fuel cell room, to identify the extension of areas in which potentially explosive concentrations are built-up and the presence and location of possible gas pockets where to install the hydrogen detectors. The purpose of the CFD study was also the classification of hazardous areas as required by the international standard IEC 60079-10-1.

9.1.2 The CFD Study

The CFD analysis performed on the demonstrator plant has been divided into three tasks aimed at analyzing:

- the ventilation system effectiveness in normal operating conditions, without any gas leakage in the room;
- the effect of the worst-case hydrogen leak inside the fuel cell room;
- the effect of the worst-case hydrogen leak outside the fuel cell room.

To carry out the CFD calculation, a detailed 3D model of the fuel cell room and deckhouse roof was first developed starting from the drawings of the hull structure, those of the installed equipment and those of the entire piping part with the relative accessories (connections, instruments, and valves).

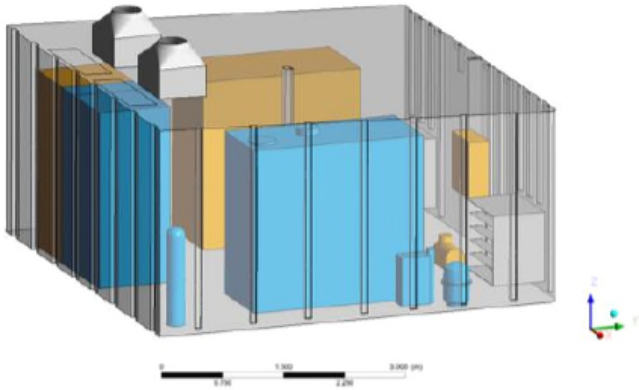

Figure 166. Fuel cell room model for CFD study. [127]

After generating the computational grid, the fuel cell room ventilation analysis has been carried out in normal operating conditions, reproducing numerically the airflows generated by the ventilation system inside the room, without introducing any gas leakage in the room. Computations aimed at estimating the release characteristic have been performed to analyse results according to the the international standard IEC 60079-10-1 and evaluate if the air velocity due to the ventilation is sufficient to guarantee the desired degree of dilution in case of hydrogen leakage.
The CFD analysis demonstrated the effectiveness of the ventilation system: within the fuel cell room there are no low dilution regions in the, while medium and high dilution regions are both always present in different percentages depending on the ventilating machine in service.

Figure 167. Fuel cell room ventilation. Visualization of airflow path trough velocity streamlines. [127]

The results of the CFD analysis for the worst-case internal leakage scenario showed that:

- H_2 concentrations within the flammable limits (LFL 4% - UFL 77% in volume) are localised very close to the hydrogen leakage source (less than 40cm downstream the leakage point).
- The hydrogen quantity in the room is very low, with an average mass concentration in the room of 5e-5 kg/m3, resulting in a total H_2 mass in the room of less than 3 grams.
- H_2 accumulation regions are confined in the medium dilution region, while high dilution regions are well washed by the ventilation system.

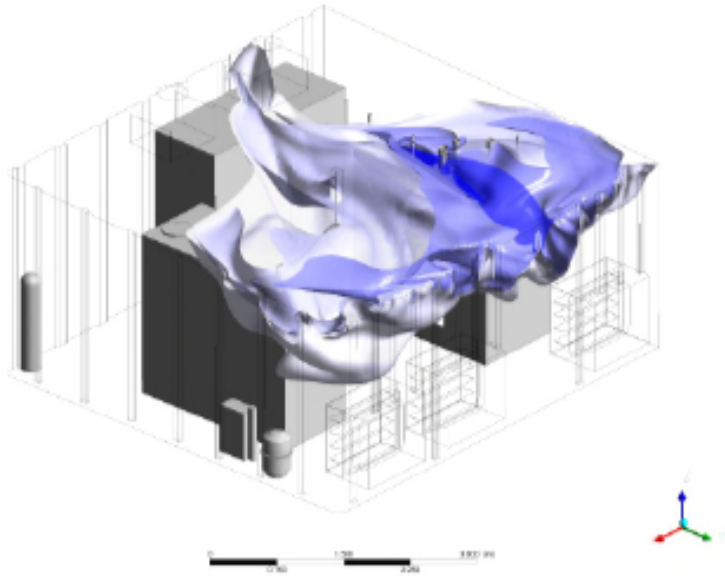

Figure 168. Fuel cell room internal leakage. Isosurfaces of H2 volume percentage at the end of the simulation. [127]

Also, the CFD study relating to the worst-case scenario of leakage in the external area did not highlight areas of hydrogen stagnation and confirmed the presence of a high degree of dilution on the entire surface of the deckhouse and in the areas surrounding the structure.

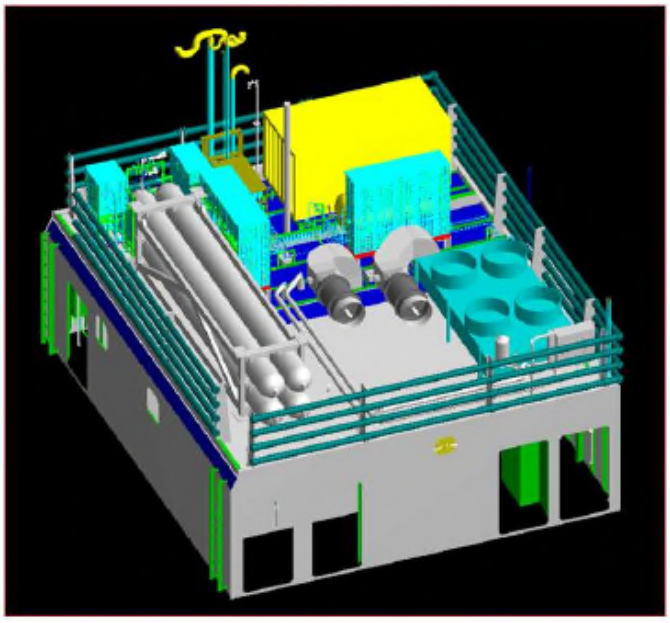

Figure 169. Demonstrator plant. Preliminary arrangement of deckhouse roof [128].

9.1.3 The HAZID review and HAZOP study

After implementing the design changes that emerged in the first HAZID study and after starting the CFD study, the implant was subjected to a HAZID study review conducted in a similar manner on the same Nodes identified in the preliminary study. The main component manufacturers also participated in this second HAZID study.
The results of the second HAZID study, although developed on a much more detailed design basis, confirmed the results of the perliminal study and did not lead to the identification of unacceptable risks for the installation on board of the demonstrator. The Severity/Likelihood matrix of the HAZID review is reported in Figure 170 in which no high risks, 22 medium risks and 36 low risks are indicated.
No additional comment or reccommendation emerged from the plant HAZID review.

				Consequence		
				A	B	C
				Major injury	One fatality or multiple major injuries	Multiple Fatalities
Likelihood	L5	Likely	$\leq 10^{-2}$ to 10^{-3}			
	L4	Unlikely	$\leq 10^{-3}$ to 10^{-4}			
	L3	Very Unlikely	$\leq 10^{-4}$ to 10^{-5}	24	5	3
	L2	Extremely Unlikely	$\leq 10^{-5}$ to 10^{-6}	8	10	4
	L1	Remote	$\leq 10^{-6}$		4	

Intolerable risk
Tolerable risk - ALARP
Broadly acceptable

Figure 170. Demonstrator plant HAZID review. Severity/likelihood matrix. [129]

Prior to its commissioning, the demonstrator underwent a dedicated HAZard and OPerability (HAZOP) study to identify how the process could deviate from design intent creating risks to personnel, equipment, or operability issues. The stydy was aimed at [130]:

- Identify possible hazards associated with the operation of the electrolyser, hysdrogen storage system and fuel cell generator,
- Understand reasonably foreseeable consequences of these hazards.
- Review system safeguards/control measyres to ensure suitability and understand what nmeasures could be taken to eliminate, reduce /minimize the risk levels .
- Record actions/safety recommendations.

9.2 Scaling up of the plant: PEM-based distributed generation and LVDC shipboard microgrids

The adoption of the microgrid paradigm for shipboard electrical systems is one of the key steps for achieving the goals of efficiency and environmental sustainability imposed to the shipping sector and described in chapter 1.
The practical setup of microgrids onboard, in fact, implies the development and the introduction in the shipping sector of various technological approaches and solutions, e.g., distributed electricity generation on board, including the use of fuel cells as decentralized generation (DG) units, the integration of energy storage systems and their coordination with DGs, the pervasive use of power electronic converters, the use controllers and energy management systems for optimal operation of the on-board electrical system, and, the use of direct current (DC) electrical distribution systems [131].
The purpose is to overcome the traditional concept of power generation with installation of a superior number of smaller generating elements properly distributed on board and integrated each other through an appropriate electrical distribution grid. This design philosophy increases the system's flexibility, reliability and it can prevent the energy black-out on board also in emergency events like flooding and fire. This new design approach is applicable to highly specialized types of ships that require a large amount of electrical power nearly continuously available, as large passenger ships or ferry. [132]
Consequently, the traditional configuration of the power distribution system should be reviewed in order to maximize the benefits of the Distributed Energy Resources (DER) approach. In this context, a novel configuration of the grid can be selected instead of the traditional one (e.g., radial). The traditional radial configuration is characterized by a centralized generation system in high voltage (HV), a MV primary distribution system from the main buses to the power transformers (e.g., which are installed in each hotel and galley substation) and a secondary distribution network in low voltage (LV) to feed the distributed loads on board the ships. Each substation is a single branch of the network, powered by the primary distribution system through the substation transformer, as proposed in Figure 171. Being designed for a centralized power generation system, this configuration is well-suited for traditional applications. [133]

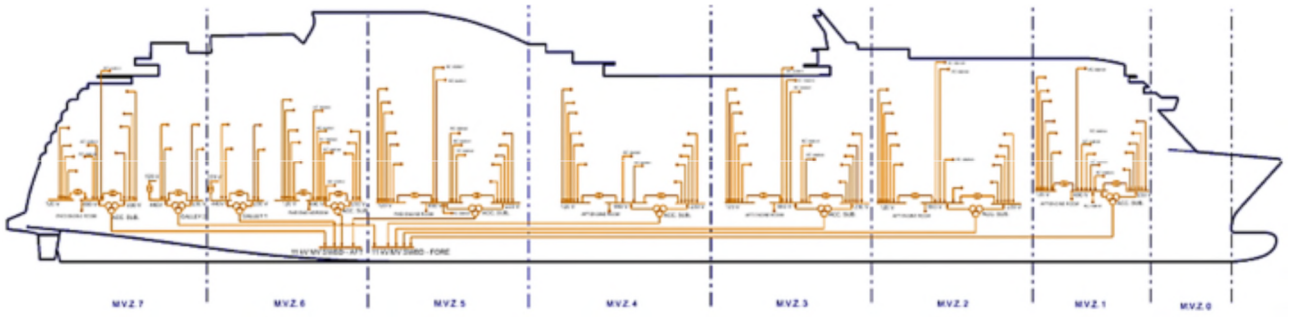

Figure 171. Traditional radial distribution system configuration for a cruise ship. [133]

Figure 172 shows a conceptual scheme of the main technologies and solutions enabling the implementation of the microgrid paradigm on board.

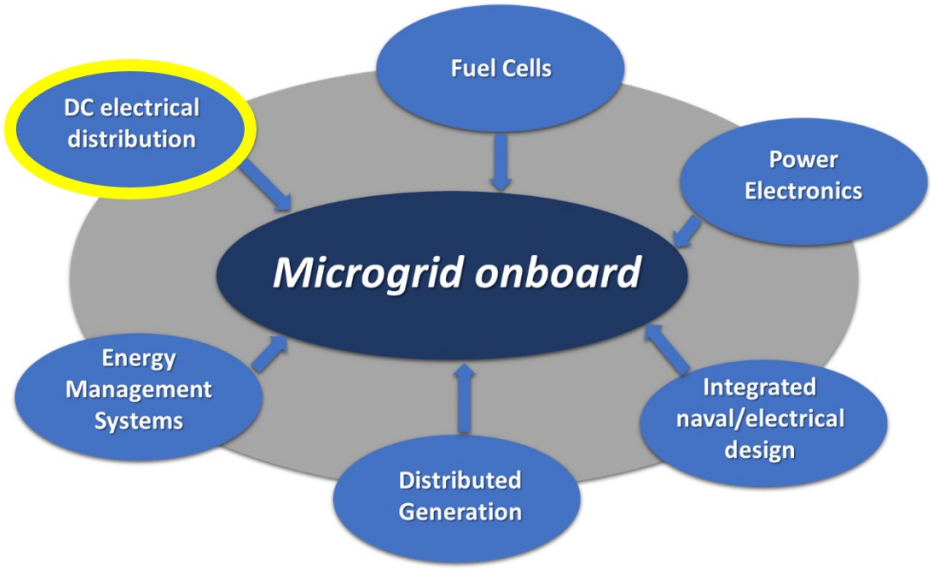

Figure 172. Technologies and solutions involved in the implementation of the microgrid paradigm on board. [131]

As far as the use of DC distribution on board is concerned, the expected advantages of such an approach have made it one of the highly rated emerging applications in the shipping industry. DC distribution is suited to shipboard power systems since they are inherently islanded systems typically compatible with DC generation units. Furthermore, DC distribution systems have emerged in the last decades thanks to their higher power density, design simplicity, efficiency, and power quality, in comparison to conventional AC distribution systems [131].
The high voltage DC (HVDC) concept, i.e., the distribution of electricity on-board through a common DC bus at high voltage (up to 35 kV), is considered a promising solution for coping with the increasing power demand and overcoming many of the limitations due to the privileged use of alternating current (AC). But currently, this approach has not been applied on board yet due to the lack of suitable industrial equipment and protection devices [131].
In the pathway toward the on-board implementation of fully DC electrical distribution systems, hybrid AC/DC architectures represent a viable solution. Specifically, technical literature exhibits a simpler but still innovative and advantageous approach consisting in the use of low voltage DC (LVDC) for on-board secondary power distribution, coupled to a conventional HV AC main distribution system. Such a hybrid approach allows obtaining some of the advantages of HVDC distribution, making it possible the integration of a zonal distribution for improved dependability and power quality [131].
In this area, [124] proposes a novel AC/DC electrical architecture for LV electrical power distribution in ships, highlighting its advantage in terms of an increased payload of the vessel, obtained thanks to the volume and weight saving compared to the previous configuration. Reference paper [134] proposes a technique for selecting the most appropriate voltage level of an LVDC distribution grid used to replace an AC counterpart in a passenger ship. Besides, an overview of hybrid shipboard microgrids is provided in [135], including a discussion on the energy management systems needed for controlling, monitoring, and optimizing the microgrid performance under different mission profiles. Ultimately, the setup of suitable electrical architectures for increased efficiency and sustainability of ships, in compliance with the essential requirements of safety and reliability is a topic of pivotal importance. This is particularly true for cruise ships, whose impact on environmental pollution is huge in almost all eurpean countries [131].

One of the foremost enabling technologies for implementing DC distribution is power electronics, which, although being a quite mature technology, has further room for improvements thanks to achievements on new static device materials and new converter topologies.
The advantages of DC-based power systems are numerous. The use of a DC and power electronics-based shipboard electrical system allows a straightforward and flexible integration of several electrical generators, such as batteries, fuel cells shaft generators and variable-speed gensets, well supporting the distributed generation paradigm. For gensets, the reduction of fuel consumption by optimizing the operating points of the prime movers is a major advantage of DC distribution. The specific fuel oil consumption (SFOC) of a diesel engine with a fixed rotational speed (corresponding to conventional AC distribution) is indeed higher than the SFOC obtained with a variable rotational speed which is compatible with the DC distribution solution [131].
The possibility to operate on-board electrical drives at variable speed, also embedding loss minimization-based control techniques, enables regulation of motors, which represent a significant share of the on-board power loads. This has a beneficial impact on the drives' efficiency and, therefore, on the overall power system efficiency, as well [136].
Shipboard DC power systems could help in making more flexible the shore connection; in fact, if shore connection is realized on the DC side, the local grid frequency becomes irrelevant and adaptation to different frequency values is no longer an issue. An additional advantage of the DC systems is the improved power quality mainly due to the absence of voltage distortion; voltage drop caused by reactive power, and the need for power factor correction.
A DC-based power system with massive use of power electronic converters also provides a suitable technical platform for implementing solutions for on board energy management, e.g., monitoring, control, and optimization of the power system performance [123].
Finally, a great advantage of shipboard DC power systems consists in a relevant reduction of volume and weight of the electrical plant. This is due to the possibility to eliminate power transformers, and to reduce the number of power conversion stages onboard. This reduction is estimated to be of the order of about 30%. Moreover, distributing electrical power in DC leads to a reduction of needed cables. A 1 kV DC distribution system used instead of the conventional 690 VAC allows the need for cables to be reduced by as much as about 40%, also and permitting the use of lower-cost cables [131].
In [131], after outlining the ensemble of opportunities and the most significant open challenges tied to shipboard DC distribution, two specific hybrid AC/DC schemes for the LV electrical distribution on cruise ships have been investigated, to assess their impact on volumes and weights of the overall electrical plant. The first proposed configutation relays on the centralized ship generation, whereas the second is relays on a decentralized generation, based on PEM fuel cell generators and batteries.
In [131] the advantages of using shipboard LVDC distribution, in terms of the electrical components' volume and weight reduction, are demonstrated with reference to a real-world cruise ship, assumed as the case study. The considered electrical hybrid configurations embedding LVDC have been compared with the currently used electrical architecture and between each other. Quantitative results coming from the volume/weight evaluations and comparisons have been given, together with a discussion on pros and cons of the considered electrical schemes. In the next pparagraphs an pverview of the case staudy and of the results relative to the proposed architecture based on distributed PEM fuel cell generators and batteries are given.

9.2.1 The case study

The case study considered by [131] for the investigation is a cruise ship having a tonnage of about 48,000 GRT, a maximum speed of 20 knots, and a total installed electric power of about 23,500 kW. The ship is propelled by two propulsion drives with twin induction motors (IMs) having a rated power of around 7.250 kW.
The electrical plant of the ship under study is a typical integrated power system (IPS) with an AC 6.6 kV primary distribution and an AC 690/220 V secondary LV distribution supplying accommodation zones, galleys, and auxiliary services. Specifically, the ship includes four accommodation substations (ACC1-4) and two galleys which are operated under a single HV/LV power transformer.
The main features of the ship are summarized in Table 69.

Case study Cruise ship	
Gross tonnage	48,000 GRT
Length (overall)	230 m
Breadth	29 m
Draught (design)	6.5 m
Service speed	17 kn
Maximum speed	20 kn
Propulsion electric motors	2 x 7,250 kW
Diesel generators	2 x 5,000 + 2 x 6,700 kW
Max persons on board	1,400

Table 69. Case study cruise ship main data. [131]

Figure 173 shows a scheme of the LV distribution, downstream of a substation transformer; this is the electrical power system level on which the presented analysis is focused. The LV electric distribution systems considered in [131] are, in fact, those located downstream of the substation transformers supplying the ship's main vertical zones; they are prevalently devoted to ship's hotel services (such as passengers' cabins, air conditioning, local entertainment areas, etc.) and each of them involves an installed power of about 1,000 kW.

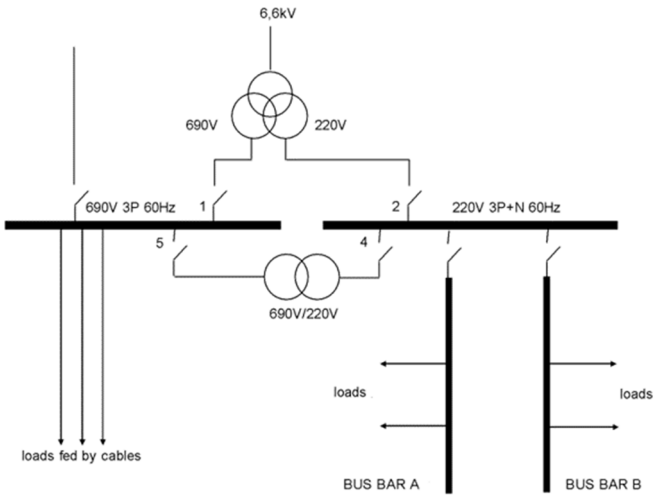

Figure 173. Sample LV distribution scheme downstream of a MV/LV substation. [131]

9.2.2 Hybrid AC/DC architecture: PEMFC and battery

The proposed topology based on distributed PEM fuel cell generators and batteries is shown in Figure 174.

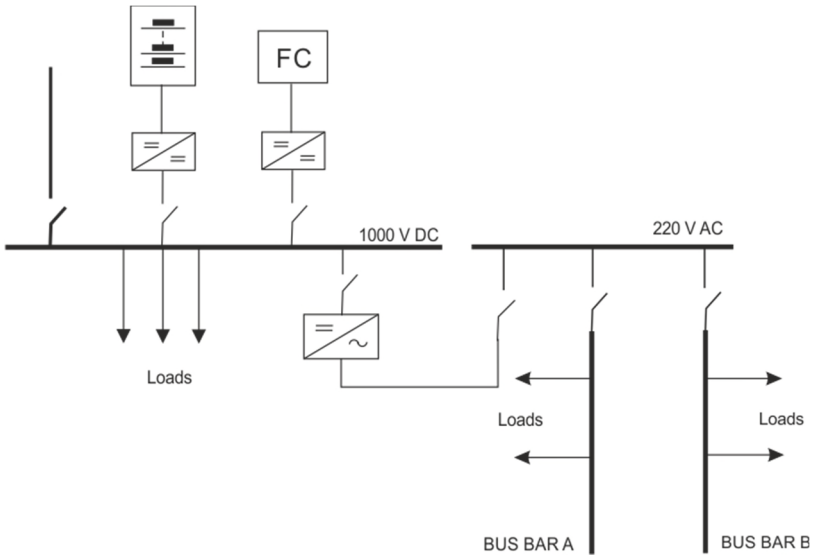

Figure 174. Hybrid AC/DC LV distribution scheme encompassing FC and battery. [131]

In the proposed topology, the electrical load of each substation is supplied exclusively by a decentralized PEMFC-based generator coupled with a batteryenergy storage system (BESS); each source is used as a grid-forming generator and contributes to establishing the 1000 V DC bus (used in place of the 690 VAC bus of the original configuration) by a DC/DC power electronic converter; connection with the main switchboard is limited to an emergency back-up line between the 100 V DC bus and the engine room substation provided for redundancy, thus each hybrid AC/DC LV distribution system is operated as an isolated microgrid. In such a system, the FC is designed to provide the load peak power, but it is operated to supply the average load power for increased efficiency and lifetime of the generator; the battery, on the other hand, is designed to cope with power demand fluctuation around the average value.
The main features of the FC and battery for each hybrid AC/DC LV distribution system are given in Table 70.

FC		**Battery**	
Technology	PEM	**Technology**	$LiFePO_4$
Power	600 kW	**Capacity**	360 kWh
Power converter	Half-bridge DC/DC	**Power converter**	Half-bridge DC/DC

Table 70. Main features of FC and Battery. [131]

In the proposed topology, all the MV/LV and LV power transformer are eliminated to partially compensate for the increased volume and weight of the electrical plant equipment due to the introduction of the FC, the battery and the respective power converters.
On the other hand, the supply of the cruise ship's hotel loads (whose maximum value is generally about 10% of the total installed power) by means of decentralized "green" power sources has a beneficial impact on the ship's carbon footprint and, more in general, on its environmental sustainability [131].

9.2.3 Evaluation of electrical system weight/volume reduction

For evaluating to what an extent the use of the considered hybrid architecture affects the reduction of the electrical plant equipment's volume and weight, a simplified equivalent representation of the LV distribution systems has been used, as described in [124]; this approach also allows performing comparisons among the considered architectures. To reach the equivalent schemes, starting from the original electrical configuration, a suitable aggregation of electrical loads has been considered. Moreover, for each aggregate of loads (e.g., pool machinery, HVAC, generic power panels, loads supplied by transformers, etc.), the formation and equivalent length of the feeding cables have been defined, according to the aggregate loads' installed power [124].
The comparisons among the different topologies have been performed by considering, both separately and globally, the electrical plant equipment having a greater impact on volume/weight, i.e., electrical cables and the combination of power transformers (P-TR), decentralized generation (DG) units, and power converters (PC). It is worth considering that the analysis refers only to electrical plant equipment, therefore, no FCs' auxiliaries, e.g., reforming systems, fuel storage and distribution systems are accounted for.
With the proposed topology based on distributed PEM fuel cell generators and batteries a weight saving of around 17% and a volume saving of 24% are obtained compared to the current distributiuon configration. The result of the global comparison is summarized in table

Current topology (AC)			**Hybrid AC/DC: PEMFC and BESSS**		
Equipment	Weight [kg]	Volume [m^3]	Equipment	Weight [kg]	Volume [m^3]
P-TR	34,114	60.98	P-TR, DG, PC	38,594	47.1
Cables	60,712	19,74	Cables	40,384	14.51
Total	**94,826**	**80.72**	**Total**	**78,978**	**61.61**
Δ (%)	**-**	**-**	**Δ (%)**	**-16.7%**	**-23.7%**

Figure 175. Global comparison of electrical plant weight and volume. [131]

9.2.4 Open technical challenges

The microgrid of the proposed topology is a weak electrical system, since it comprises only a PEM type FC-based generator, a storage system based on lithium batteries and a set of passive loads. The absence of rotating generators in the system leads to the absence of a rotating reserve and consequently to low inertia of the microgrid. As a result, the microgrid could be more prone to instability problems. Moreover, in such a configuration the design of a suitable protection system is a critical task.
As far as stability is concerned, critical elements of shipboard DC microgrids are the so-called constant power loads (CPL), i.e., electrical drives or loads with tightly regulated controllers that can be modeled, through a negative incremental resistance. The presence of CPLs in DC microgrids introduces instability in the voltage regulation system so that, if the main controller is not properly designed, it can trigger substantial voltage fluctuations or shutdown of the system itself.
Aside from CPLs, uncontrolled or closed-loop controlled loads with small bandwidth should be properly considered, as well. This type of loads, indicated as dynamic loads, has a significant impact on the stability of the DC microgrids. Specifically, dynamic loads, unlike CPLs, can dramatically affect the stability margin of the overall system in low power conditions [131].

Additionally, the design and implementation of an appropriate protection system for DC microgrids with pervasive use of power electronics still pose several technological challenges in both terrestrial and naval applications.
In general, the fault current in the event of a short circuit can increase very rapidly up to 100 times the rated current at steady state without a natural zero-crossing; this phenomenon also applies to DC/DC converters, where the discharge of the output capacitor can flow through uncontrolled and undesired paths [131].
In particular, the implementation of shipboard DC distribution will not only require a re-design of the protection devices (e.g., through the introduction of novel DC circuit breakers with very high speed, high reliability and power density features), but also implies the need to completely reconsider the existing protection strategies, including methods for fault current calculations, grounding systems, fault detection techniques, and coordination/selectivity strategies to accomplish suitable reliability and safety requirements [131].
All the described issues are today the subject of intensive studies whose advances are paving the way for the massive use of shipboard distributed generation based on distributed PEM fuel cell generators, batteries and LVDC electrical systems.

10 Conclusions and future developments

As stated in Chapter 2, the aim of this doctoral work was to investigate and identify through an experimental approach which are the main issues and the real prospectives for the use of hydrogen fed PEMFC generators on board cruise ships. Through the design and characterization of the test rig and the subsequent installation of the system on board an operating cruise ship, all the research questions have been addressed and the project objectives have all been achieved. In particular:

- The activities carried out during the project have in fact made it possible to verify that PEMFC and hydrogen are in all respects suitable for use on board cruise ships, although the main obstacle to their large-scale application on board is still today represented by the lack of specific rules governing the matter. In addition to regulatory issues, the open technological challenges are still many, and a fuel cell zero emission cruise ship is not feasible at the current technology's state of the art. A strong opportunity for the future is the implementation of a hybrid solution on board, which will encompass normal or dual fuel ICE, fuel cells and energy storage systems such as batteries or supercapacitors;
- With the design of the experimental test rig, it was possible to develop an innovative PEMFC generator for marine applications integrating automation and control systems. In the design both in the test rig and in the onboard installation, only industry standard components suitable for marine applications with the highest degree of technological readiness and directly available on the market have been used. Furthermore, the fuel cell generator and the DC/AC power converter have been specially designed by the manufacturers to meet the specific needs of the plant. In designing the test rig, particular care and attention was paid to developing a system suitable for installation on board a cruise ship, i.e., characterized by a reduced number of interfaces with the existing onboard systems and and with completely independent cooling and ventilation systems with no impact on the systems serving the engine rooms and other machinery spaces;
- The integration of a gaseous hydrogen generation and compression plant into the test rig not only allowed experimental research to be carried out on a first example of a plant of this type designed for a specific naval application, but also made the on-board system self-sufficient regarding hydrogen production and strategically allowed to embark and actively use the experimental test rig on an operational cruise vessel despite the absence of rules and regulations for hydrogen bunkering on board ships. This installation, the first ever in the cruise industry, is essential in determining how hydrogen can be used on a larger scale in future newbuilds. In fact, it will allow the development of technological devices and will be a reference for the development of rules and regulations for the use of hydrogen on board cruise ships.

The characterization activities carried out on the hydrogen production and compression plants and on the electricity production plant with PEMFCs integrated in the test rig are summarized below. Despite the difficulties encountered in identifying recognized international test standards, dedicated test procedures have been developed for both hydrogen and electricity production plants for the characterization of their efficiency, consumption and for verifying compliance with the performance requirements. For each activity, following information are given:

- A summary of the main experimental results;
- The original contribution provided by the experimental activity to the increase of knowledge in the specific technology;
- The limitation encountered and suggestion for further improvement;
- Possible future developments.

Regarding the hydrogen production and compression plant, this work presents the experimental data acquired in the characterization of a small hydrogen production and storage system, based on an alkaline electrolyser and an air-driven hydrogen booster.
The experimental activity on this plant, beyond the project objectives, has contributed to increasing the amount of experimental data available on small capacity hydrogen production and storage plants (5 Nm3/h of hydrogen, storage at 200 bar g). In the future, this size of plants could become commercially acttractive, allowing domestic applications and small or medium-sized industries to store the renewable energy they produce when it is not immediately used [62].
The recorded experimental data show that the electrolyser efficiency is in line with the manufacturer specifications. This reaches 36% (93 kWh/kgH_2) at a reduced flow rate (pressure 4.6 bar g) and increases up to 43% (77 kWh/kgH_2) at a design flow rate (4.2 bar g). Post-processing of the plant experimental data has clarified that the great difference in efficiency is essentially due to the large increase of the hydrogen flow between the first and second operating condition.
Although the data available in the literature for similar electrolysers show an average specific energy consumption of 57.6 kWh/kgH_2, it should be anyway remembered that part of the hydrogen generated by the tested electrolyser is used for the regeneration of the cartridges of the integrated hydrogen purification system. Considering this peculiar feature of the tested system, it is possible to conclude that the experimental value of the efficiency can be considered in line with the values available in the literature.
On the other hand, instead, the power absorbed by the compressed air hydrogen booster was high in comparison with other data available in the literature. The calculated specific energy required by the test rig hydrogen booster for a complete compression cycle from 4.6 bar g up to 200 bar g is 15 kWh/kgH_2 when referring to compressed air consumption only. If, on the other hand, the energy consumption of the air compressor is also considered in the calculation, the specific energy required by the booster increases up to 65 kWh/kgH_2 [62].
The analysis of the experimental activity made it possible to identify three possible actions aimed at increasing the overall efficiency of the plant, namely:

- The replacement of the hydrogen booster with a multistage unit capable of processing a higher flow rate;
- The modification of the electrolyser unit in order to avoid using hydrogen to regenerate the filter cartridges;
- The increase of the electrolyser output pressure.

In order to identify the most effective course of action, it would therefore be necessary to carry out, as a possible future development of the experimental activity already carried out, an in-depth analysis aimed at identifying, among the proposed solutions, the best compromise in terms of technical, economic and safety requirements [62].
On the onboard demonstration plant, the problem of the low efficiency of the hydrogen compressor was addressed exclusively from a technical point of view. For the onboard demonstrator, it was decided to replace the compressed air-driven hydrogen booster used for the test rig with an electrically driven one capable of processing the electrolyser nominal flow rate. No modifications were instead applied to the electrolyser.

As regards the test rig power plant, this was designed, built, and experimentally characterized with the aim of contributing to expanding the knowledge and experimental data available in the literature on marine-ready PEM fuel cells-based systems and in order to ease the approval process for on board installation and the integration with the ship electrical system [5].
It should be in fact remembered that that in the past years PEM fuel cell-based systems have been limited to only niche vessels, like inland small passenger vessels or naval submarines. In literature still very little experimental data is available especially for seagoing vessel or cruise ships.

The obtained data demonstrate that plant efficiency is comparable with commercial heavy-duty systems for land-based applications. It has been also observed that, as expected, the system load response time is noticeably improved by the supercapacitors-based energy storage that, at the same time reduces the stress on the fuel cell generator. Nevertheless, the PEM fuel cell generator still shows good response time even when supercapacitors are not activated.
The analysis on the fuel cell startup and shutdown procedures highlighted also that some hydrogen was used by the gernerator to flush the fuel cells internal channels is discharged into the atmosphere. The largest volume of hydrogen is flushed at system startup and is about 0.33 Nm^3.
This amount of released gas must be considered to calculate the extension of any dangerous area that can arise at fuel cell anode exhaust on board of a ship, as required by Classification Societies. Moreover, hydrogen leaks must be monitored in view of the recent concerns over indirect hydrogen greenhouse effect.
The DC/AC power converter and system startup analysis showed that the time to recharge the supercapacitors is about 175 s (about 3 minutes) and that the time to warm up the fuel cell system is about 25 minutes. A BOP peak power of about 10% of the plant nominal power should be made available for the startup.
The load cycle test performed on the test rig confirmed the capability of the system to follow a cyclical load variation. However, further tests should be done to evaluate fuel cell degradation when a variable load is applied over a longer period, as it could happen on board of a ship in operation [5].
To this proposal, it should also be remembered that, according to IMO SOLAS convention (chapter 1, regulation 10 a [137]), each passenger ship must undergo two inspections of the hull in dry dock in any five-years period, at intervals not exceeding 36 months.
For this reason, in order to be an effective alternative to internal combustion engines, in addition to having higher efficiency and ensuring the absence of greenhouse gas emissions, PEM fuel cell generators for marine application should guarantee stack replacement and refurbishment action at least after every 26.000- 30.000 running hours and a lifetime equal to a multiple of a dry dock interval. For the fuel cell generator used in the project, anyway, the manufacturer already guarantees stack replacement and refurbishment actions every 24.000 running hours [5].
The test campaign made it also possible to identify some possible system design improvements. During system warm-up with supercapacitors fully discharged, it was observed in fact that the fuel cell output current exceeded (although for a short period of time) the current limit value suggested by the manufacturer.
To avoid exceeding fuel cell current limit at system warm-up, the plant control logic should:

- Allow the fuel cell to charge the supercapacitors when the generator has reached its operational temperature or manage their charging trough the onboard network;
- Be provided with a power management system impeding the generator startup in case the available load is outside the limits required for proper system warm-up.

Another plant design remark emerged from the experimental activities is related to the fuel cell external cooling system. The fuel cell cooling system used in the test rig was based on a commercially available dry cooler characterized by a large heat transfer surface. A large surface is required as the temperature difference between the fuel cell system and the ambient air is limited. This is especially true when the ambient temperature is high, such as when the ship sails in tropical zones.
Should the ship have some installation constraint, a specifically designed dry cooler should be considered in order to reduce the cooling system size. Indeed, more benefits could rise if the heat recovered from the fuel cell could be used for low temperature on board applications, such as, for example, the heating of a swimming pool water on a cruise ship [5].

The experimental activity conducted at the test rig gave an essential contribution to complete the resolution of technical and regulatory issues related to the installation of the system on board a newly built cruise ship through the development of detailed HAZID, HAZOP and CFD studies.
The onboard system, the first ever of its kind to be installed aboard an operating cruise ship, was successfully commissioned in November 2022 to provide alternative power supply to houselighting dimmers serving the main public areas of the vessel. The Owner is currently using the small system as a test to determine how hydrogen fuel could be used on a larger scale in future new builds. As soon as the regulatory framework relating to bunkering and the management of hydrogen on board the ship is defined, the goal is to upgrade the electrical power geneation plant to provide first the supply of hotel electrical loads of a cruise ship and then, at a later stage, also feed the propulsion system.

Figure 176. Onboard demonstrator. Fuel cell rom. Photo by the author.

Figure 177. Onboard Demonstrator.The author (left) and Prof.R. Taccani (2022/11/04). Photo by the author.

References

[1] M. Gianni, A. Pietra e R. Taccani, «Outlook of future implementation of PEMFC and SOFC onboard cruise ships,» in *E3S Web of Conference 238*, DOI: 10.1051/e3sconf/202123804004, 2021.

[2] UNCTAD, «Review Of Maritime Transport,» 2018. [Online]. Available: https://unctad.org/webflyer/review-maritime-transport-2018.

[3] E. Niemi, «Sustainable Maritime Power Alternatives for Cruise Business,» Metropolia University of Applied Sciences, 2021.

[4] J. Kizielewicz, «Eco-Trends in Energy Solutions on Cruise Ships,» *Energies, 14, 3746, https://doi.org/10.3390/en14133746,* 2021.

[5] A. Pietra, M. Gianni, Z. Nicola e S. Malabotti, «Experimental characterization of a PEM fuel cell for marine power generation,» in *ES3 Web Conf. Volume 334 EFC21-European Fuel Cells and Hydrogen Piero Lunghi Conference*, https://doi.org/10.1051/e3sconf/202233405002, 2022.

[6] IMO, "International Convention for the Prevention of Pollution from Ships (MARPOL)," [Online]. Available: https://www.imo.org/en/About/Conventions/Pages/International-Convention-for-the-Prevention-of-Pollution-from-Ships-(MARPOL).aspx. [Accessed June 2022].

[7] A. P. Karanasiou, "Cruise shipping and emissions in Mediterranean ports," University of Piraeus, 2021.

[8] DNV-GL, «Global Sulphur cap 2020,» 2020. [Online]. Available: https://safety4sea.com/wp-content/uploads/2016/11/DNV-GL-Global-sulphur-cap-2020-2016_11.pdf.

[9] J. Tae-Hwan, K. Seong-Gil, L. Jong-Kap e A. Junkeon, «The IMO initial strategy for reducing Greenhouse Gas(GHG) emissions, and its follow-up actions towards 2050,» *Journal of International Maritime Safety, Environmental Affairs, and Shipping (https://doi.org/10.1080/25725084.2019.1707938),* vol. 4, n. 1, pp. 1-7, 2020.

[10] IRENA, "A pathway to decarbonize the shipping sector by 2050," 2021. [Online]. Available: https://www.irena.org/publications/2021/Oct/A-Pathway-to-Decarbonise-the-Shipping-Sector-by-2050. [Accessed June 2022].

[11] S. H. Ltd., "MARPOL Annex VI - EEDI & SEEMP," [Online]. Available: https://www.marpol-annex-vi.com/eedi-seemp/. [Accessed June 2022].

[12] DNV-GL, "Maritime Forecast to 2050 - Energy Transition Outook 2019," 2019. [Online]. Available: https://sustainableworldports.org/wp-content/uploads/DNV-GL_2019_Maritime-forecast-to-2050-Energy-transition-Outlook-2019-report.pdf. [Accessed June 2022].

[13] DNV, «CII – Carbon Intensity Indicator - FAQs,» [Online]. Available: https://www.dnv.com/maritime/insights/topics/CII-carbon-intensity-indicator/answers-to-frequent-questions.html. [Consultato il giorno June 2022].

[14] DNV, «CII – Carbon Intensity Indicator - Implementation,» 2022. [Online]. Available: https://www.dnv.com/maritime/insights/topics/CII-carbon-intensity-indicator/implementation.html. [Consultato il giorno June 2022].

[15] Dromon Bureau of Shipping, "EEDI & CII Explanatory guidance," 2021. [Online]. Available: https://www.dromon.com/wp-content/uploads/2021/09/Dromon-TP-on-EEDI-CII.pdf. [Accessed June 2022].

[16] UNCTAD, "Review of Maritime Transport," 2021. [Online]. Available: https://unctad.org/webflyer/review-maritime-transport-2021.

[17] Ricardo Energy & Environment, «Technological, Operational and Energy Pathways for Maritime Transport to Reduce Emissions Towards 2050,» 2022. [Online]. Available: https://www.concawe.eu/wp-content/uploads/Technological-Operational-and-Energy-Pathways-for-Maritime-Transport-to-Reduce-Emissions-Towards-2050.pdf.

[18] Hidrogen Europe, "Hydrogen - a carbon-free energy carrier and commodity," 2021. [Online]. Available: https://hydrogeneurope.eu/wp-content/uploads/2021/11/2021.11_Hydrogen-as-a-carbon-free-energy-carrier-and-commodity_clean.pdf. [Accessed June 2022].

[19] DNV-GL for EMSA, "Study On The Use Of Fuel Cells In Shipping," 2017. [Online]. Available: http://emsa.europa.eu/csn-menu/download/4545/2921/23.html. [Accessed July 2019].

[20] Cruise Market Watch, "Growth of the Ocean Cruise Line Industry," [Online]. Available: https://cruisemarketwatch.com/growth/. [Accessed June 2022].

[21] Nedstack, "PEM-FCS Stack Technology," [Online]. Available: https://nedstack.com/en/pem-fcs-stack-technology. [Accessed June 2022].

[22] L. Cindrella, A. M. Kannan, J. F. Lin, K. Saminathan, Y. Ho, C. W. Lin and J. Wertz, "Gas diffusion layer for proton exchange membrane fuel cells—A review," *Journal of Power Sources (https://doi.org/10.1016/j.jpowsour.2009.04.005),* vol. 194, no. 1, , pp. 146-160, 2009.

[23] F. Barbir, PEM Fuel Cells: Theory and Practice, Elsevier Academic Press, 2005.

[24] J. Larminie and A. Dicks, Fuel Cell Systems Explained, John Wiley & Sons Ltd., 2003.

[25] X.-Z. Yuan and H. Wang, "PEM Fuel Cell Fundamentals," in *PEM Fuel Cell Electrocatalysts and Catalyst Layers*, Springer, 2008, pp. 1-87.

[26] I. M. Saleh, R. K. Calay e R. Ali, «Modelling and Examining Open Circuit Voltage for PEM Fuel Cells,» *Journal of Electrical Engineering (https://www.researchgate.net/publication/274564761),* pp. 140-146, 2013.

[27] R. O'Hayre, S.-W. Cha, W. G. Colella e F. B. Prinz, Fuel Cell Fundamentals, John Wiley & Sons, Inc., 2016.

[28] J. M. Correa, F. A. Farret, L. N. Canha and M. G. Simoes, "An electrochemical-based fuel-cell model suitable for electrical engineering automation approach," *IEEE Transactions on Industrial Electronics (10.1109/TIE.2004.834972),* vol. 51, no. 5, pp. 1103-1112, 2004.

[29] D. Bonanno, F. Genduso, R. Miceli and C. Rando, “Main Fuel Cells mathematical models: Comparison and analysis in terms of free parameters,” in *The XIX International Conference on Electrical Machines - ICEM 2010 (doi: 10.1109/ICELMACH.2010.5608225.)*, Rome, 2010.

[30] V. P. McConnell, “Now, voyager? The increasing marine use of fuel cells,” *Fuel Cells Bulletin,* no. 5, May 2010, pp. 12-17, 2010.

[31] France Hydrogène, “L'enciclopedie H2 - 9.4.2 Applications marines et sous-marines des piles à combustible,” [Online]. Available: https://www.france-hydrogene.org/fiches-techniques/?fwp_paged=7. [Accessed June 2022].

[32] Fincantieri, “Submarine U212A Todaro Class,” [Online]. Available: https://www.fincantieri.com/globalassets/prodotti-servizi/navi-militari/m-06-16_u212a_todaroclass_f.pdf. [Accessed June 2022].

[33] Siemens AG Indistry Sector Marine & Shipbuilding, *SINAVY PEM Fuel Cell for submarines,* 2013.

[34] T. Sawa, T. Aoki, I. Yamamoto, S. Tsukioka, H. Yoshida, T. Hyakudome, S. Ishibashi, T. Inada, T. Kabeno, R. Sasamoto and Y. Nasuno, "Performance of the fuel cell underwater vehicle URASHIMA," *Acoustical Science and Technology,* vol. 26, no. 3, pp. 249-257, 2005.

[35] T. Maeda, K. Yokoyama, N. Hisatome, S. Ishiguro, K. Irokawa and T. Tani, "Fuel Cell AUV "URASHIMA"," *Mitsubishi Heavy Industries, Ltd. Technical Review,* vol. 43, no. 1, 2006.

[36] T. Aoki, T. Hyakudome, T. Murashima, S. Tsukioka, H. Nakajoh, T. Maeda, K. Hirokawa and S. Ishibashi, "Cruising Autonomous Underwater Vehicle URASHIMA," *Journal of the Society of Mechanical Engineers (DOI:http://dx.doi.org/10.1299/jsmemag.108.1039_454),* vol. 108, 2005.

[37] Yacht Club de Monaco, "Presentation-Yacht-Club-Monaco," 22 September 2020. [Online]. Available: https://yacht-club-monaco.mc/wp-content/uploads/2020/09/Presentation-Yacht-Club-Monaco-ind-4.pdf. [Accessed June 2022].

[38] J. Pratt, "Considerations for On-Board Hydrogen Fuel Cells, Golden Gate Zero Emission Marine," 12 October 2019. [Online]. Available: https://www.energy.gov/sites/prod/files/2019/10/f68/fcto-h2-at-ports-workshop-2019-iv1-pratt.pdf. [Accessed June 2022].

[39] Hydrogen House, "HYDROGEN FUEL CELL DUFFY-HERRESHOFF WATERTAXI," [Online]. Available: https://hydrogenhouseproject.org/duffy-herreshoff-watertaxi.html#. [Accessed June 2022].

[40] N. Carlos , “Development of Business Cases for Fuel Cells and Hydrogen Applications for European Regions and Cities,” 2017. [Online]. Available: https://www.fch.europa.eu/sites/default/files/FCH%20Docs/171121_FCH2JU_Application-Package_WG3_Boats%20%28ID%202910572%29%20%28ID%202911658%29.pdf. [Accessed Jume 2022].

[41] “The Energy Observer Fuel Cell,” Energy Observer, [Online]. Available: https://www.energy-observer.org/innovations/energy-observer-fuel-cell. [Accessed June 2022].

[42] FUEL CELLS and HYDROGEN 2 JOINT UNDERTAKING, “Addendum to the Multi-Annual Work Plan 2014–2020,” Fuel Cells and Hydrogen Joint Undertaking (FCH JU), Brussel, 2018.

[43] D. Bouix, “Hybrid PEMFC System Experimentation in the Sailboat Zero CO2,” in *Fuel Cells and Hydrogen for Maritime and Harbour Applications FCH Vorkshop*, Venice 14 June 2013, 2013.

[44] E4tech, “Clean Maritime Clusters Research Study,” April 2020. [Online]. Available: https://www.u-mas.co.uk/wp-content/uploads/2021/06/E4Tech-UMAS-2021-Clean-Maritime-Clusters-Research-Study.pdf. [Accessed June 2022].

[45] C. Dall'Armi, D. Micheli and R. Taccani, “Comparison of different plant layouts and fuel storage solutions for fuel cells utilization on a small ferry,” *International Journal of Hydrogen Energy (https://doi.org/10.1016/j.ijhydene.2021.02.138),* vol. 46, no. 26, pp. 13878-13897, 2021.

[46] J. Markowski and I. Pielecha, “The potential of fuel cells as a drive source of maritime,” in *IOP Conference Series: Earth and Environmental Science, Volume 214 - International Conference on the Sustainable Energy and Environmental Development*, Krakow, 2019.

[47] R. Taccani, F. Ustolin, N. Zuliani, S. Pinamonti and A. Pietra, “Fuel Cells and Shipping Emissions Mitigation,” in *NAV 2018 - 19th International Conference on Ship & Maritime Research*, Trieste, DOI:10.3233/978-1-61499-870-9-885, 2018.

[48] D. Madouch and A. Colavitto, “Zero-Emission research vessel,” *Electric & Hybrid,* pp. 42-43, April 2021.

[49] N. Gray, S. McDonagh, R. O'Shea, B. Smyth and J. D. Murphy, “Decarbonising ships, planes and trucks: An analysis of suitable low-carbon fuels for the maritime, aviation and haulage sectors,” *Advances in Applied Energy (https://doi.org/10.1016/j.adapen.2021.100008),* vol. 1, 2021.

[50] ARUP, “Hydrogen Transport - Fuelling the Future,” [Online]. Available: https://www.arup.com/perspectives/publications/research/section/the-future-of-energy-green-hydrogen-transport. [Accessed June 2022].

[51] J. Depken, A. Dyck, L. Roß and S. Ehlers, “Safety Considerations of Hydrogen Application in Shipping in Comparison to LNG,” *ENERGIES (https://doi.org/10.3390/en15093250),* vol. 15, no. 9, 2022.

[52] HySafe, “Physical Properties Of Hydrogen,” [Online]. Available: http://www.hysafe.net/wiki/BRHS/PhysicalPropertiesOfHydrogen. [Accessed June 2022].

[53] American Bureau of Shipping, «Hydrogen as a marine fuel,» June 2021. [Online]. Available: https://maritimecyprus.com/wp-content/uploads/2021/06/ABS-hydrogen-as-marine-fuel.pdf. [Consultato il giorno June 2022].

[54] Pacific Northwest National Laboratory, “H2 Hydrogen Tools - Hydrogen Compared with Other Fuels,” [Online]. Available: https://h2tools.org/bestpractices/hydrogen-compared-other-fuels. [Accessed June 2022].

[55] L. E. Klebanoff, J. W. Pratt and C. B. LaFleur, “Comparison of the safety-related physical and combustion properties of liquid hydrogen and liquid natural gas in the context of the SF-BREEZE high-speed fuel-cell ferry,” *International Journal of Hydrogen Energy (https://doi.org/10.1016/j.ijhydene.2016.11.024),* vol. 42, no. 5, pp. 757-774, 2017.

[56] E. a. M. National Academies of Sciences, Emergency and Continuous Exposure Guidance Levels for Selected Submarine Contaminants (https://doi.org/10.17226/12032), Washington, DC: The National Academies Press, 2008.

[57] M. Balat, "Potential importance of hydrogen as a future solution to environmental and transportation problems," *International Journal of Hydrogen Energy (doi:10.1016/j.ijhydene.2008.05.04),* vol. 33, no. 15, pp. 4013-4029, 2008.

[58] S. Milojević, "RECONSTRUCTION OF EXISTING CITY BUSES ON DIESEL FUEL FOR DRIVE ON HYDROGEN," *Applied Engineering Letters - Journal of Engineering and Applied Sciences,* vol. 1, no. 1, pp. 16-23, 2016.

[59] Shell Deutschland Oil GmbH, SHELL hydrogen study - Energy of the future? - Sustainable Mobility through Fuel Cells and H2, Hamburg, 2017.

[60] International Renewable Energy Agency (IRENA), Hydrogen from Renewable Power, 2018.

[61] NCE Maritime CleanTech, Norwegian future value chains for liquid hydrogen, 2016.

[62] A. Pietra, M. Gianni, N. Zuliani, S. Malabotti e R. Taccani, «Experimental Characterization of an Alkaline Electrolyser and a Compression System for Hydrogen Production and Storage,» *Energies (https://doi.org/10.3390/en14175347),* vol. 14, 2021.

[63] F. Gambou, D. Guilbert, M. Zasadzinski and H. Rafaralahy, "A Comprehensive Survey of Alkaline Electrolyzer Modeling: Electrical Domain and Specific Electrolyte Conductivity," *Energies (https://doi.org/10.3390/en15093452),* vol. 15, no. 9, 2022.

[64] S. K. Mazloomi and N. Sulaiman, "Influencing factors of water electrolysis electrical efficiency," *Renewable and Sustainable Energy Reviews,* vol. 16, no. 6, pp. 4257-4263, 2012.

[65] I. A. Hassan, H. S. Ramadan, M. A. Saleh and D. Hissel, "Hydrogen storage technologies for stationary and mobile applications: Review, analysis and perspectives," *Renewable and Sustainable Energy Reviews (https://doi.org/10.1016/j.rser.2021.111311),* vol. 49, 2021.

[66] G. Sdanghi, G. Maranzana, A. Celzard and V. Fierro, "Review of the current technologies and performances of hydrogen compression for stationary and automotive applications," *Renewable and Sustainable Energy Reviews,* vol. 102, pp. 150-170, 2019.

[67] C. Sánchez and D. González, "Experimental characterization of a grid-connected hydrogen energy buffer: Hydrogen production," *International Journal of Hydrogen Energy,* vol. 38, no. 23, pp. 9741-9754, 2013.

[68] S. M. Riedl, "Development of a Hydrogen Refueling Station Design Tool," *International Journal of Hydrogen Energy,* vol. 45, no. 1, pp. 1-9, 2020.

[69] G. Saur, S. Sprik, J. Kurtz, S. Onorato, S. Gilleon and E. Winkler, "Hydrogen Station Data Collection and," in *DOE Hydrogen and Fuel Cells Program - 2019 Annual Merit Review and Peer Evaluation Meeting*, Washington, DC, 2019.

[70] Y. Ligen, H. Vrubel, J. Arlettaz and H. Girault, “Experimental correlations and integration of gas boosters in a hydrogen refueling station,” *International Journal of Hydrogen Energy,* vol. 45, no. 33, pp. 16663-16671, 2020.

[71] C. Sánchez-Diaz, J. Monrabal, D. González, D. Alfonso and E. Peñalvo-López, “Experimental results of the hydrogen production control of a hydrogen energy buffer,” *International Journal of Hydrogen Energy,* vol. 40, no. 15, pp. 5013-5024, 2015.

[72] A. J. Cornish, “Hydrogen Fueling Station Cost Reduction Study,” Engineering, Procurement & Construction, LLC, Lakewood, CO, 2011.

[73] H. Barthélémy, “Hydrogen storage – Industrial prospectives,” *International Journal of Hydrogen Energy,* vol. 37, no. 22, pp. 17364-17372, 2012.

[74] JEC Group, “Korea in the mood for composites,” 2021. [Online]. Available: https://www.jeccomposites.com/news/korea-in-the-mood-for-composites/. [Accessed June 2022].

[75] Toyota, “Outline of the Mirai,” [Online]. Available: https://www.toyota-europe.com/download/cms/euen/Toyota%20Mirai%20FCV_Posters_LR_tcm-11-564265.pdf. [Accessed June 2022].

[76] L. Van Hoecke, L. Laffineur , R. Campe , P. Perreault , S. W. Verbruggen and S. Lenaerts , “Challenges in the use of hydrogen for maritime applications,” *Energy & Environmental Science (https://doi.org/10.1039/D0EE01545H),* no. 2, 2021.

[77] K. Reddi, A. Elgowainy, N. Rustagi and E. Gupta, “Impact of hydrogen SAE J2601 fueling methods on fueling time of light-duty fuel cell electric vehicles,” *International Journal of Hydrogen Energy,* vol. 42, no. 26, pp. 16675-16685, 2017.

[78] ITM power, “Feasibility of Hydrogen Bunkering,” 2019. [Online]. Available: https://northsearegion.eu/media/9385/feasibility-of-hydrogen-bunkering-final-080419.pdf. [Accessed June 2022].

[79] J. E. Fesmire and A. Swanger, “Overview of the New LH2 Sphere at NASA Kennedy Space Center,” 2021. [Online]. Available: https://www.energy.gov/sites/default/files/2021-10/new-lh2-sphere.pdf. [Accessed June 2022].

[80] BMW Group, “PRESSCLUB ITALIA · ARTICLE - La BMW Hydrogen 7,” 21 November 2006. [Online]. Available: https://www.press.bmwgroup.com/italy/article/detail/T0019005IT/la-bmw-hydrogen-7?language=it. [Accessed June 2022].

[81] HySTRA, “News - The SUISO FRONTIER to begin her maiden voyage,” 20 May 2021. [Online]. Available: https://www.hystra.or.jp/en/gallery/article.html. [Accessed June 2022].

[82] Kawasaki, “World's First Liquefied Hydrogen Carrier SUISO FRONTIER Launches Building an International Hydrogen Energy Supply Chain Aimed at Carbon-free Society,” 11 December 2019. [Online]. Available: https://global.kawasaki.com/en/corp/newsroom/news/detail/?f=20191211_3487&wovn=it. [Accessed June 2022].

[83] DNV, “HANDBOOK FOR HYDROGEN-FUELLED VESSELS,” 2021.

[84] Bureau Veritas, “REPORT OF CCC 7 MEETING - 6 TO 9TH SEPTEMBER 2021,” 28 September 2021. [Online]. Available: https://marine-offshore.bureauveritas.com/newsroom/report-ccc-7-meeting-6-9th-september-2021. [Accessed JUne 2022].

[85] United States Maritime Resource Center, “Flammable Cryogenic Liquid Carriers,” 2016. [Online]. Available: https://marinechemistassociation.com/wp-content/uploads/2018/09/06%20MCA%20FCLC%20LNG%20Fuel%20Tanks%20and%20Safety%20Systems.pdf. [Accessed June 2022].

[86] IMO, “Resolution A.716(17),” 6 November 1991. [Online]. Available: https://wwwcdn.imo.org/localresources/en/KnowledgeCentre/IndexofIMOResolutions/AssemblyDocuments/A.716(17).pdf. [Accessed June 2022].

[87] IACS, “About IACS,” [Online]. Available: https://iacs.org.uk/about/. [Accessed June 2022].

[88] IACS, “IACS PROCEDURES - Volume 1: IACS GENERAL PROCEDURES,” 16 July 2021. [Online]. Available: https://iacs.org.uk/download/1788. [Accessed June 2022].

[89] Bureau Veritas, *Ships using Fuel Cells - Rule Note NR 547 DT R01 E,* 2022.

[90] DNV, *Rules for Classification of Ships - Pt. 6, Ch.2, Sect. 3 - Fuel cell installations - FC,* 2019.

[91] Korean Register of Shipping, *Guidance for Fuel Cell Systems on Board of Ships,* 2015.

[92] Lloyd's Register, *Rule Proposal 2021-ENG007 - Rules for fuel cell installations,* 2021.

[93] RINA, *Rules for the Classification of,* 2022.

[94] Cenergy, *600 Fuel Cell, Basovizza laboratory photo gallery,* 2020.

[95] A. Pietra, «From GEI project to on-board application. The Trieste laboratory experience.,» 2020.

[96] Pure Energy Centre, *Hydrogen Production System Operation Manual,* 2020.

[97] IACS, *Test Specification for Type Approval IACS Req. 1991/Rev.7,* 2018.

[98] Pure Energy Centre, “P1085 -2019 Inclination test procedure,” 2019.

[99] Pure Energy Centre, "Vibration Test Report, Document: STDC1085," 2019.

[100] Haskel, *Operating and maintenance manual, model number 86990.*

[101] Kaeser Kompressoren , *Manuale di servizio, compressore a vite, Tipo: SK 19/10 bar..*

[102] Kaeser Kompressoren, *Manuale di servizio, essicatore a ciclo frigorifero, modello TCH.*

[103] Fincantieri, *Fuel Cell System Technical Specification for Suppply,* 2019.

[104] Nedstack, “PemGen MT-FCPI-100,” 2021. [Online]. Available: https://nedstack.com/sites/default/files/2021-02/mt-fcpi-100-datasheet.pdf. [Accessed June 2022].

[105] Nedstack, *RFI Response Memo rev.3.0,* 2019.

[106] Fincantieri, *Skid del circolatore per il radiatore delle Fuel Cell, Specifica di Fornitura,* 2019.

[107] Gianneschi pumps and blowers, *Centrifugal el/pump CG 40/16C, drawing 01FCG40161,* 2019.

[108] Gianneschi pumps and blowers, *Confronto curve,* 2019.

[109] Fincantieri, *Scambiatore di calore per sistema Fuel Cell, Specifica di fornitura,* 2019.

[110] Nedstack, "MT-FCPP-100 Factory Approval Test," 2020.

[111] CEG, "Power Converter for Fuel Cell System 100 kVA p.f.1 440 VCA 3F 60 Hz - Manuale Operativo," 2020.

[112] Fincantieri, *Power Converter fo Fuel Cell System Technical Specification for Supply,* 2019.

[113] CEG, "Test Report - Convertitore DC/AC 100kVA per Fuel cell (6361-20-01-01)," 2020.

[114] ASCO Power Technologies, *6000 Series Data Sheet, Model 6045,* 2019.

[115] International Electrotechnical Commission, *IEC 62282-3-200:2015 Fuel cell technologies - Part 3-200: Stationary fuel cell power systems - Performance test methods,* 2015.

[116] National Institute of Standards and Technology, "Thermodynamic and Transport Properties Database (REFPROP)".

[117] European Commission Joint Research Centre, *PEFC power stack performance testing procedure. Measuring voltage and power as function of current density. Polarisation curve test method Test Module PEFC ST 5-3,* 2013.

[118] E. Ytreberg, M. Eriksson, I. Maljutenko, J.-P. Jalkanen, L. Johansson, I.-M. Hassellöv and L. Granhag, "Environmental impacts of grey water discharge from ships in the Baltic Sea," *Marine Pollution Bulletin (https://doi.org/10.1016/j.marpolbul.2020.110891),* vol. 152, 2020.

[119] Environmental Protection Agency (EPA), "Graywater Discharges from Vessels," Washington, DC, 2011.

[120] P. Pei, Q. Chang and T. Tang, "A quick evaluating method for automotive fuel cell lifetime," *International Journal of Hydrogen Energy (https://doi.org/10.1016/j.ijhydene.2008.04.048),* vol. 33, no. 14, pp. 3829-3836, 2008.

[121] J. Moein-Jahromi, M. J. Kermani and S. Movahed, "Degradation forecast for PEMFC cathode-catalysts under cyclic loads," *Journal of Power Sources,* vol. 359, pp. 611-625, 2017.

[122] A. Kneer and N. Wagner, "A Semi-Empirical Catalyst Degradation Model Based on Voltage Cycling under Automotive Operating Conditions in PEM Fuel Cells," *Journal of The Electrochemical Society (DOI: 10.1149/2.0641902jes),* vol. 166, no. 2, 2019.

[123] G. La Tona, M. Luna, M. C. Di Piazza and A. Pietra, "Energy Management System for Efficiency Increase in Cruise Ship Microgrids," in *IECON 2019 - 45th Annual Conference of the IEEE Industrial Electronics Society (DOI: 10.1109/IECON.2019.8927314)*, Lisbon, Portugal, 2019.

[124] M. C. Di Piazza, M. Luna, G. La Tona, A. Accetta, M. Pucci and A. Pietra, "A mixed DC/AC low voltage electrical distribution architecture for increasing payload on ships.," in *Technology and Science for the Ships of the Future - Proceedings of NAV 2018: 19th International Conferrence on Ship & Maritime Technology*, Trieste, 2018.

[125] Tenaris, "Cylinders for high pressure gases," Aprile 2014. [Online]. Available: https://www.tenaris.com/umbraco/surface/downloads/pdf?url=%2Fmedia%2Fetphnr5o%2Fcylinders-for-high-pressure-gases-eng-28-03-2014.pdf. [Accessed June 2022].

[126] Lloyd's Register Consulting, "PEM Fuel Cell System HZID report," 2020.

[127] CETENA, "CFD simulation of ventilation and leakage. Activity 1 - CFD simulation of ventilation," 2021.

[128] Fincantieri, *Fuel Cell System Description,* 2022.

[129] Lloyd's Register Consulting, "HAZID Study. Fuel Cell Installation Final Report," 2022.

[130] Lloyd's Register EMEA, «HAZOP Study 2201-0047 Report 2,» 2022.

[131] M. C. Di Piazza, M. Luna, G. La Tona, A. Accetta, M. Pucci and A. Pietra, "Shipboard microgrids: comparison of solutions based on LVDC distribution on cruise ships," in *2021 IEEE International Conference on Environment and Electrical Engineering and 2021 IEEE Industrial and Commercial Power Systems Europe (EEEIC / I&CPS Europe)*, Bari (doi: 10.1109/EEEIC/ICPSEurope51590.2021.9584742), 2021.

[132] G. Fiore, D. Negroni, T. Lamberti, P. Gualeni, L. Magistri, F. Silvestro and A. Pietra, "Distributed Energy Resources On-Board Cruise Ships: Integration into the Ship Design Process," in *Technology and Science for the Ships of the Future - Proceedings of NAV 2018: 19th International Conference on Ship & Maritime Technology*, Trieste, 2018.

[133] A. Boveri, M. Maggioncalda, D. Rattazzi, P. Gualeni, P. Magistri, L. Magistri, F. Silvestro and A. Pietra, "Innovative Energy Systems: Motivations, Challenges and Possible Solutions in the Cruise Ship Arena," in *Technology and Science for the Ships of the Future - Proceedings of NAV 2018: 19th International Conferrence on Ship & Maritime Technology*, Trieste, 2018.

[134] M. C. Di Piazza, M. Luna , G. La Tona, A. Pucci and A. Pietra, "A New Method for Selecting the Voltage Level for an Advantageous Transition to DC Distrbution in Ships," in *IEEE International Conference on Electrical Systems for Aircraft, Railway, Ship Propulsion and Road Vehicles & International Transportation Electrification Conference (ESARS-ITEC) (https://doi.org/10.1109/ESARS-ITEC.2018.8607438)*, Nottingham, UK, 2018.

[135] M. Othman, A. Anvari-Moghaddam and J. M. Guerrero, "Hybrid shipboard microgrids: System architectures and energy management aspects," in *IECON 2017 - 43rd Annual Conference of the IEEE Industrial Electronics Society (DOI:10.1109/IECON.2017.8217188)*, Beijing, China, 2017.

[136] M. Pucci, A. Accetta, M. C. Di Piazza, M. Luna, G. La Tona and A. Pietra, "Electric Ship Propulsion Improvement by Increasing Efficiency of Adjustable-Speed Motor Drives," in *IEEE International*

Conference on Environment and Electrical Engineering and 2018 IEEE Industrial and Commercial Power Systems Europe (EEEIC / I&CPS Europe) (DOI: 10.1109/EEEIC.2018.8494207), Palermo, Italy, 2018.

[137] International Maritime Organization, International Convention for the Safety of Life at Sea (SOLAS) - Consolidated Edition, 2020.

[138] European Commission, "Departments and executive agencies, Joint Research Centre," [Online]. Available: https://ec.europa.eu/info/departments/joint-research-centre_en#latest. [Accessed June 2022].

[139] A. Andronie, I. Stamatin, V. Girleanu, V. Ionescu and N. Buzbuchi, "Simplified Mathematical Model for Polarization Curve Validation and Experimental Performance Evaluation of a PEM Fuel Cell System," *Procedia Manufacturing (https://doi.org/10.1016/j.promfg.2019.02.289),* pp. 810-819, 2019.

Annex A: international standards on hydrogen and fuel cell

International hydrogen standards

Hydrogen has been used for a long time around the world, as an industrial gas and in the space aerospace industry. Standardization activities related to the use of hydrogen as a fuel in the land transport sector are more recent and mainly focus on the development of standards for hydrogen filling stations and for FC hydrogen vehicles.
Some of the standards and codes in force, especially those concerning the industrial use of hydrogen, may also be relevant to the use of hydrogen as a fuel on board ships.
In the United States, for example, industry standards developed by the American Society of Mechanical Engineers (ASME) and the American Petroleum Institute (API) are alreadi widely used for maritime applications.
In other geographic areas, other national or international industry standards on hydrogen may also be adopted in the maritime sector. In the EU context, for example, reference could be made to EU directives and standards.
Internationally, industry standards relevant to the introduction of hydrogen as a fuel for ships are those developed by leading global standards development organizations such as the International Organization for Standardization (ISO) and the International Electrotechnical Commission (IEC). In line with their mission, the ISO and IEC mainly focus on the development of generic component standards and protocols.
The international standards for components developed in the hydrogen sector by ISO and IEC aim to eliminate global trade barriers. In this way, a component for a hydrogen system (such as a pipe, a valve, or a safety device) or an assembly (such as a reformer or a refueling station) can be designed and manufactured anywhere in the world following the same criteria of design and test, and therefore can be marketed anywhere without additional requirements.
The installation requirements for hydrogen components or assemblies may then vary according to the specific applicable regulations [83].
Since the ISO and IEC standards are developed by international stakeholders, these are to be considered as "super" standards and therefore, should replace any other national standard relating to the same components. This consideration has the following implications:

- National component standards, including those that have served as reference documents for the development of international standards, must harmonize their design and test requirements with adopted international standards. The only allowable deviations should be those relating to references to specific relevant national standards and regulations and, if applicable, to specific climatic conditions.
- National legislation and installation codes should include international standards or their harmonized national adoptions in the only/preferred list of standards for component certification.
- National installation codes should remove any references to design requirements and refer explicitly for such requirements only to available international component standards or their harmonized national versions.

The following paragraphs list the main international standards for hydrogen useful for the development of the regulatory framework for the use of hydrogen on board ships.

ISO standards

ISO is an independent, non-governmental international organization with a membership of 167 national standards bodies.
The ISO standards relevant to the use of hydrogen on board ships are those developed by the following technical committees (TC):

- ISO TC 197: standardization in the field of systems and devices for the production, storage, transport, measurement and use of hydrogen;
- ISO TC 67: standardization of the materials, equipment and offshore structures used in the drilling, production, transport by pipelines and processing of liquid and gaseous hydrocarbons within the petroleum, petrochemical and natural gas industries.

The most significant standards for the maritime sector developed by the two technical committees are those listed in Table 71.

Standard	Title	Description
ISO/TR 15916:2015	Basic considerations for the safety of hydrogen systems	The standard provides guidelines for the use of hydrogen in its gaseous and liquid forms as well as its storage in either of these or other forms (hydrides). It identifies the basic safety concerns, hazards and risks, and describes the properties of hydrogen that are relevant to safety.
ISO 19880-3:2018	Gaseous hydrogen- Fuelling stations- Part 3: Valves	This document provides the requirements and test methods for the safety performance of high-pressure gas valves that are used in gaseous hydrogen stations of up to the H70 designation. This document covers the following gas valves: • check valves; • excess flow valves; • flow control valves; • hose breakaway devices; • manual valves; • pressure safety valves; • shut-off valves.

Standard	Title	Description
ISO 26142:2010	Hydrogen detection apparatus-Stationary applications	This International Standard defines the performance requirements and test methods of hydrogen detection apparatus that is designed to measure and monitor hydrogen concentrations in stationary applications. The provisions in this International Standard cover the hydrogen detection apparatus used to achieve the single and/or multilevel safety operations, such as nitrogen purging, or ventilation and/or system shut off corresponding to the hydrogen concentration. The requirements applicable to the overall safety system, as well as the installation requirements of such apparatus, are excluded. This International Standard sets out only the requirements applicable to a product standard for hydrogen detection apparatus, such as precision, response time, stability, measuring range, selectivity and poisoning. This International Standard is intended to be used for certification purposes.
ISO 15649:2001	Petroleum and natural gas industries-Piping	This standard specifies the requirements for design and construction of piping for the petroleum and natural gas industries, including associated inspection and testing. The standard is applicable to all piping within facilities engaged in the processing or handling of chemical, petroleum, natural gas or related products. The standard is not applicable to transportation pipelines and associated plant.
ISO 19882:2018	Gaseous hydrogen — Thermally activated pressure relief devices for compressed hydrogen vehicle fuel containers	This document establishes minimum requirements for pressure relief devices intended for use on hydrogen fuelled vehicle fuel containers. The scope of this document is limited to thermally activated pressure relief devices installed on fuel containers used with fuel cell grade hydrogen according to SAE J2719 or ISO 14687 for fuel cell land vehicles, and Grade A or better hydrogen according to ISO 14687 for internal combustion engine land vehicles. This document also contains requirements for thermally activated pressure relief devices acceptable for use on-board light duty vehicles, heavy duty vehicles and industrial powered trucks such as forklifts and other material handling vehicles

Table 71. ISO hydrogen standards.

IEC standards

Founded in 1906, the International Electrotechnical Commission (IEC) is the world's leading organization for the preparation and publication of International Standards for all electrical, electronic, and related technologies. The most important IEC standard relating to the use of hydrogen on board ship is the IEC 60079-10-1 developed by subcommittee 31J (SC31J) of the Technical Committee 31 (TC31). The scope of IEC SC31J is to prepare and maintain international standards relating to the use of equipment including area classification, the selection and installation, inspection and maintenance, repair, overhaul and reclamation of equipment where there is a hazard due to the possible presence of explosive atmospheres of gases, vapours, mists or combustible dusts.
Standard IEC 60079-10-1 is already considered a reference document by most of the classification societies that adopt it in their Rules and Regulations for the classification of hazardous areas.

Standard	Title	Description
IEC 60079-10-1:2020	Explosive atmospheres - Part 10-1: Classification of areas - Explosive gas atmospheres	The standard is concerned with the classification of areas where flammable gas or vapour hazards may arise and may then be used as a basis to support the proper design, construction, operation and maintenance of equipment for use in hazardous areas.

Table 72. IEC hydrogen standards.

American Society of Mechanical Engineeers (ASME) standards

The American Society of Mechanical Engineers (ASME) is a not-for-profit professional organization developing standards and publications promoting knowdlege sharing and skill development across the different engineering disciplines. The most relevant ASME standards for the use of hydrogen in the maritime sector are those listed in Table 73.

Standard	Title	Description
B31.12 - 2019	Hydrogen Piping and Pipelines	It suggests standards for suitable materials, welding, inspection and testing, operations and maintenance, and quality programmes for piping. General considerations are expected to be applicable and transferrable to maritime use but will need validation. The code is applicable to piping in gaseous and liquid hydrogen service, and to pipelines in gaseous hydrogen service up to and including the joint connecting the piping to the associated pressure vessels/equipment; but it is not applicable to the vessels and equipment. It is also applicable to the location and type of support elements, but not to the structure to which the support elements are attached.
B31.3 - 2020	Process Piping	This standard contains requirements for piping including piping that interconnects pieces or stages within a packaged equipment assembly. It covers materials and components, design, fabrication, assembly, erection, examination, inspection and testing of piping.

Table 73. ASME hydrogen standards.

Compressed Gas Association (CGA) standards

The Compressed Gas Association (CGA) is the American trade association of industrial and medical gas suppliers. The CGA publishes standards and practices that codify industry practices. Where there is no specific government regulation, CGA documents are considered authoritative. The following CGA standards may be particularly relevant for the design of hydrogen systems on ships:

Standard	Title	Description
CGA G-5-2017	Hydrogen	This publication provides information on the physical and chemical properties of hydrogen and proper handling and use. It is intended to provide background information for personnel involved in the manufacture, distribution, and use of hydrogen)
CGA G-5.4-2019	Standard for Hydrogen Piping Systems At User Locations	This standard describes the specifications and general principles recommended for piping systems for gaseous (Type I) or liquid (Type II) hydrogen. The standard applies to hydrogen piping in a supply system (to the source valve) and to customer piping from the source valve to the point of use. For the purposes of this standard, high pressure is defined as gaseous hydrogen at service pressures equal to or greater than 3000 psi (20 680 kPa).
CGA G-5.5-2014	Hydrogen Vent Systems	This publication presents design guidelines for hydrogen vent systems used in gaseous and liquid hydrogen systems at user sites and provides recommendations for safe operation of these vents.
ANSI/CGA H-5-2020	Bulk Hydrogen Supply Systems	This standard contains minimum requirements for locating/siting, selecting equipment, installing, starting up, maintaining, and removing bulk hydrogen supply systems.
CGA P-50-2014	Site Security Standard	This publication provides instruction to the industrial gas industry for assessing security risks and identifying and implementing preventive security measures at fixed sites. It is intended as a resource to help managers at individual facilities make security decisions based on risk.
CGA P-74-2019	Standard For Tube Trailer Supply Systems At Customer Sites	This standard contains minimum requirements for high pressure tube trailers that store compressed gases and serve as supply systems at customer locations. It details requirements for locating/siting, selecting equipment, installing, starting up, maintaining, and removing tube trailer supply systems.

Table 74. CGA hydrogen standards.

Additional international codes and standards on hydrogen

Additional international standards that may be useful in the development of the regulatory framework for the use of hydrogen onboard ships are listed in Table 75.

Standard	Title	Description
EN 13480:2002	Metallic industrial piping	Standard EN 13480:2002 is divided in seven parts providing the rules for the design, fabrication, and inspection of metallic industrial piping. It is a standard for cryogenic vessels developed for land-based application.
Directive, 2014/34/EU	Apparatus and protection systems intended for use in potentially explosive atmospheres (ATEX)	Thie Directive 2014/34/EU covers: • equipment and protective systems intended for use in potentially explosive atmospheres; • safety, control and regulating devices intended for use outside potentially explosive atmospheres, but necessary or useful for the safe operation of equipment and protective systems with respect to explosion risks; • components intended to be incorporated into equipment and protective systems. The document provides key definitions and sets the boundary conditions for ATEX zoning.
Directive 2014/68/EU	Pressure Equipment Directive (PED)	The (2014/68/EU) applies to the design, manufacture and conformity assessment of stationary pressure equipment with a maximum allowable pressure greater than 0,5 bar. The Pressure Equipment Directive aims to guarantee free movement of the products in its scope while ensuring a high level of safety.
NFPA 2.	Hydrogen Technologies Code	This publication by the US National Fire Protection Association (NFPA) provides fundamental safeguards for the generation, installation, storage, piping, use, and handling of hydrogen in compressed gas (GH_2) form or cryogenic liquid (LH_2) form.

Table 75. Additional international codes and standards on hydrogen.

International standards on fuel cell

Key international standards considered applicable for FC installations in ships are those listed in Table 76:
Most of the listed standards were developed by the IEC (TC) IEC/TC 105 Fuel Cells Technical Committee. The purpose of the committee is to develop international standards regarding fuel cell technologies of all types and various associated applications such as stationary FC power systems for distributed power generators and combined heat and power systems, FCs for transportation such as propulsion systems, range extenders, auxiliary power units, portable FC power systems, micro FC power systems, reverse operating FC power systems, and general electrochemical flow systems and processes. [83].
Other relevant standards listed in Table 76 are developed by the American National Standars Institute (ANSI), ISO and by the Eureopean Commission Joint Research Centre (JRC). The Joint Research Centre is the Commission's science and knowledge service. The JRC employs scientists to carry out research in order to provide independent scientific advice and support to EU policy [138].

Standard	Title	Description
ANSI/CSA FC 1-2014	Fuel Cell Technologies - Part 3-100: Stationary Fuel Cell Power Systems - Safety (Adopted IEC 62282-3-100:12, First Edition, 2012-02 With U.S. Deviations)	The standard is an adoption with U.S. deviations of the identically titled IEC (International Electrotechnical Commission) Standard 62282-3-100 (first edition, 2012-02)
IEC 60050-485:2020	International Electrotechnical Vocabulary (IEV) - Part 485: Fuel cell technologies	The standa gives the general terminology used in fuel cell technologies, as well as general terms pertaining to specific applications and associated technologies.
IEC 62282-2-100:2020	Fuel cell technologies - Part 2-100: Fuel cell modules - Safety	The standardprovides safety related requirements for construction, operation under normal and abnormal conditions and the testing of fuel cell modules. This document deals with conditions that can yield hazards to persons and cause damage outside the fuel cell modules. Protection against damage inside the fuel cell modules is not addressed in this document, provided it does not lead to hazards outside the module.
IEC 62282-3-100:2019	Fuel cell technologies - Part 3-100: Stationary fuel cell power systems - Safety	The standard applies to stationary packaged, self-contained fuel cell power systems or fuel cell power systems comprised of factory matched packages of integrated systems which generate electricity through electrochemical reactions. This document is applicable to stationary fuel cell power systems intended for indoor and outdoor commercial, industrial and residential use in non-hazardous areas.

Standard	Title	Description
IEC 62282-3-200:2015	Fuel cell technologies - Part 3-200: Stationary fuel cell power systems - Performance test methods	The standard covers operational and environmental aspects of the stationary fuel cell power systems performance. The test methods apply as follows: • power output under specified operating and transient conditions; • electrical and heat recovery efficiency under specified operating conditions; • environmental characteristics; for example, exhaust gas emissions, noise, etc. under specified operating and transient conditions This standard does not apply to small stationary fuel cell power systems with electric power output of less than 10 kW which are dealt with in IEC 62282-3-201.
IEC 62282-3-300:2012	Fuel cell technologies - Part 3-300: Stationary fuel cell power systems - Installation	The standard provides minimum safety requirements for the installation of indoor and outdoor stationary fuel cell power systems in compliance with IEC 62282-3-100 and applies to the installation of the following systems: • intended for electrical connection to mains directly or with a readily accessible, manually operable switch or circuit-breaker; • intended for a stand-alone power distribution system; • intended to provide AC or DC power; • with or without the ability to recover useful heat.
IEC TS 62282-7-1:2017	Fuel cell technologies - Part 7-1: Test methods - Single cell performance tests for polymer electrolyte fuel cells (PEFC)	The standard covers cell assemblies, test station setup, measuring instruments and measuring methods, performance test methods, and test reports for PEFC single cells. This document is used for evaluating: • the performance of membrane electrode assemblies (MEAs) for PEFCs in a single cell configuration; • materials or structures of PEFCs in a single cell configuration; or • the influence of impurities in fuel and/or in air on the fuel cell performance.
IEC 62282-7-2:2021	Fuel cell technologies - Part 7-2: Test methods - Single cell and stack performance tests for solid oxide fuel cells (SOFCs)	The standardapplies to SOFC cell/stack assembly units, testing systems, instruments and measuring methods, and specifies test methods to assess the performance of SOFC cells and stacks. This document is not applicable to small button cells that are designed for SOFC material testing and provide no practical means of fuel utilization measurement. It is to be used for data exchanges in commercial transactions between cell manufacturers and system developers

Standard	Title	Description
IEC 60079-10-1:2020	Explosive atmospheres - Part 10-1: Classification of areas - Explosive gas atmospheres	The standard is concerned with the classification of areas where flammable gas or vapour hazards may arise and may then be used as a basis to support the proper design, construction, operation and maintenance of equipment for use in hazardous areas.
IEC 60068-2-6:2007	Environmental testing - Part 2-6: Tests - Test Fc: Vibration (sinusoidal)	The standard gives a method of test which provides a standard procedure to determine the ability of components, equipment and other articles, hereinafter referred to as specimens, to withstand specified severities of sinusoidal vibration.
ISO 14687-3:2014	Hydrogen fuel- Product specification- Part 3: Proton exchange membrane (PEM) fuel cell applications for stationary appliances	The standard specifies the quality characteristics of hydrogen fuel in order to ensure uniformity of the hydrogen product for utilization in stationary proton exchange membrane (PEM) fuel cell power systems.
ISO 16110-1:2007	Hydrogen generators using fuel processing technologies- Part 1: Safety	The standard applies to packaged, self-contained or factory matched hydrogen generation systems with a capacity of less than 400 m3/h at 0 °C and 101,325 kPa, intended for indoor and outdoor commercial, industrial, light industrial and residential use. It applies to hydrogen generators using one or a combination of different fuels like natural gas and other methane-rich gases, fuels derived from oil refining, fossil fuel sources (e.g., methanol) and gaseous mixtures containing hydrogen gas.
JRC Test module PEFC ST-5-3: 2010	PEFC power stack performance testing procedure. Measuring voltage and power as function of current density. Polarisation curve test method.	The scope of the test module is the characterization of the performance of PEFC stacks in terms of stack voltage and power as a function of current density (polarisation curves) under constant operating conditions. The module has no target application. It is a general characterization method used in research & development (R&D) of PEFC stacks.
JRC Test Module TM SOFC ST M21:2010	Testing the voltage and power as function of the current density. Polarisation curve for a SOFC Stack	The scope of the module is the characterization of the performance of SOFC stacks in terms of voltage and power as a function of current density (polarisation curves) under constant operating conditions. The module has no target application. It is a general characterization method used in research & development (R&D) of SOFC.

Table 76. International standards on fuel cell.

Annex B: test rig P&I diagrams

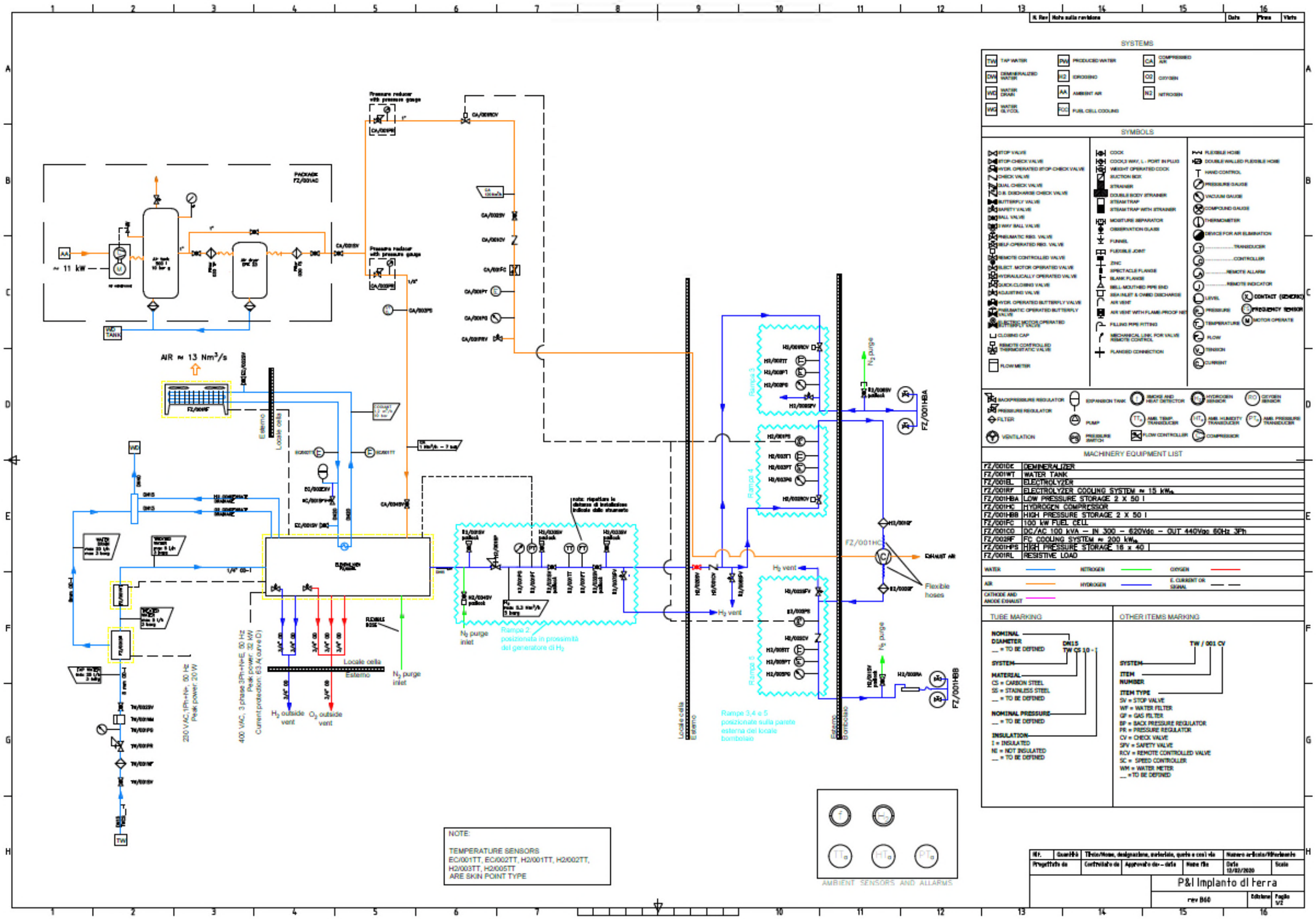
N. Rev
Note sulla revisione
Data
Firma
Visto
SYSTEMS
TW TAP WATER
DW DEMINERALIZED WATER
WC WATER CRAIN
WG WATER GLYCOL
PW PRODUCED WATER
IG IDROGENO
AA AMBIENT AIR
FCC FUEL CELL COOLING
CA COMPRESSED AIR
OG OSSIGENO
NG NITROGEN
SYMBOLS
MACHINERY EQUIPMENT LIST
FZ/001DE DEMINERALIZER
FZ/001WT WATER TANK
FZ/001EL ELECTROLYZER
FZ/001RF ELECTROLYZER COOLING SYSTEM ≈ 15 kWth
FZ/001HBA LOW PRESSURE STORAGE 2 X 50 l
FZ/001HC HYDROGEN COMPRESSOR
FZ/001HBB HIGH PRESSURE STORAGE 2 X 50 l
FZ/001FC 100 kW FUEL CELL
FZ/001CD DC/AC 100 kVA – IN 300 – 620Vdc – OUT 440Vac 60Hz 3Ph
FZ/002RF FC COOLING SYSTEM ≈ 200 kWth
FZ/001HPS HIGH PRESSURE STORAGE 16 x 40 l
FZ/001RL RESISTIVE LOAD
TUBE MARKING
OTHER ITEMS MARKING
NOMINAL DIAMETER
SYSTEM
MATERIAL
NOMINAL PRESSURE
INSULATION
ITEM NUMBER
ITEM TYPE
AIR ≈ 13 Nm³/s
~ 11 kW
PACKAGE FZ/001AC
Pressure reducer with pressure gauge
Flexible hoses
Locale cella
Esterno
Locale cella Esterno
Rampa 3
Rampa 4
Rampa 5
Rampa 2 posizionata in prossimità del generatore di H2
Rampe 3,4 e 5 posizionate sulla parete esterna del locale bombolaio
H2 vent
N2 purge
N2 purge inlet
H2 outside vent
O2 outside vent
400 VAC, 3 phase 3Ph+N+E, 50 Hz Peak power: 32 kW Current protection: 63 A (curve D)
230 VAC, 1Ph+N+, 50 Hz Peak power: 20 W
AMBIENT SENSORS AND ALLARMS
NOTE:
TEMPERATURE SENSORS EC/001TT, EC/002TT, H2/001TT, H2/002TT, H2/003TT, H2/005TT ARE SKIN POINT TYPE
P&I Impianto di terra
rev B60

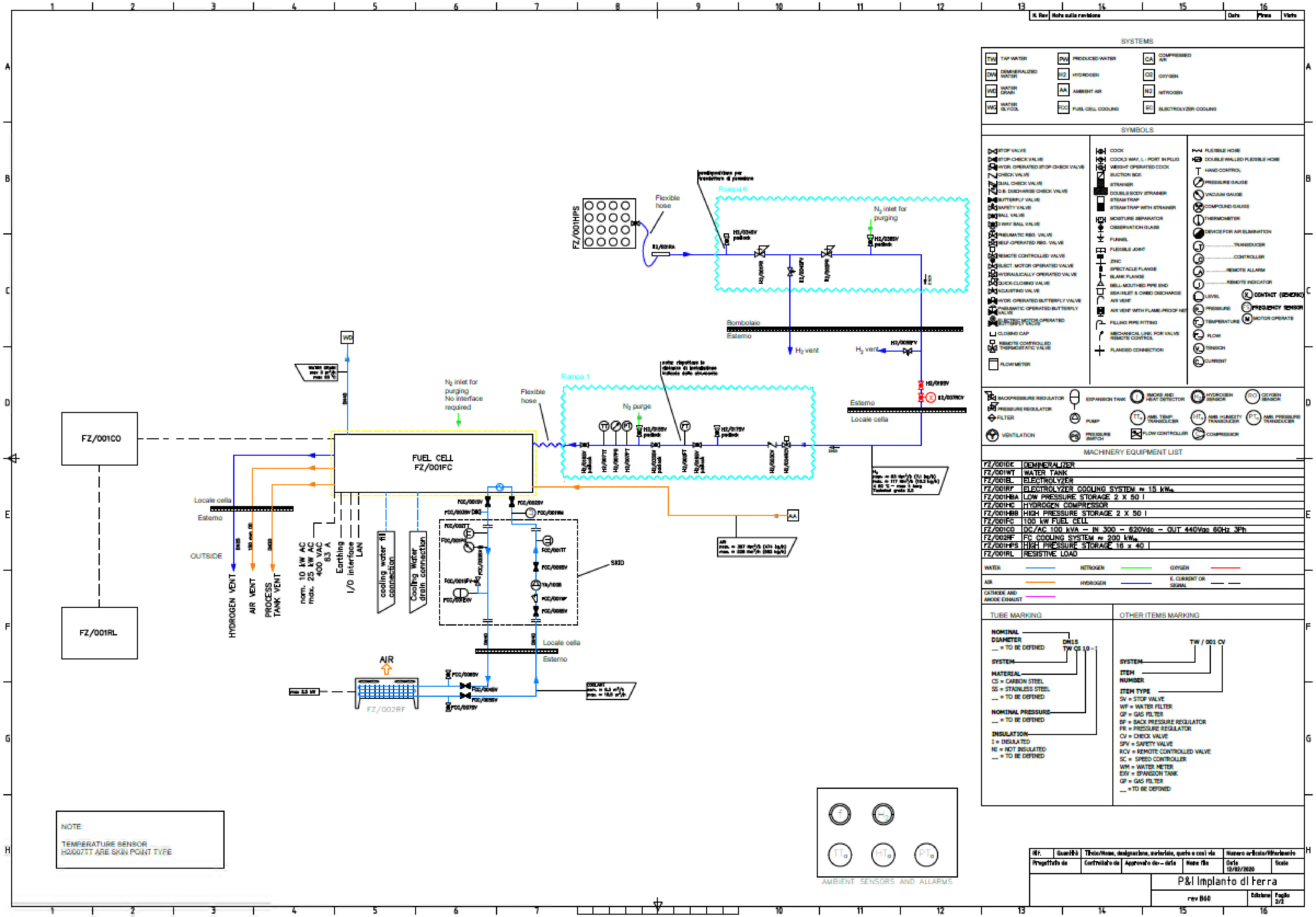
SYSTEMS
SYMBOLS
MACHINERY EQUIPMENT LIST
FZ/001DE DEMINERALIZER
FZ/001WT WATER TANK
FZ/001EL ELECTROLYZER
FZ/001RF ELECTROLYZER COOLING SYSTEM ≈ 15 kW
FZ/001HBA LOW PRESSURE STORAGE 2 X 50 l
FZ/001HC HYDROGEN COMPRESSOR
FZ/001HBB HIGH PRESSURE STORAGE 2 X 50 l
FZ/001FC 100 kW FUEL CELL
FZ/001CO DC/AC 100 kVA – IN 300 – 620Vdc – OUT 440Vac 60Hz 3Ph
FZ/002RF FC COOLING SYSTEM ≈ 200 kW
FZ/001HPS HIGH PRESSURE STORAGE 16 x 40 l
FZ/001RL RESISTIVE LOAD
WATER
NITROGEN
OXYGEN
AIR
HYDROGEN
E. CURRENT OR SIGNAL
CATHODE AND ANODE EXHAUST
TUBE MARKING
OTHER ITEMS MARKING
FZ/001HPS
Flexible hose
Rampa 6
Rampa 1
Bombolaio
Esterno
Locale cella
OUTSIDE
FUEL CELL
FZ/001FC
FZ/001CO
FZ/001RL
AIR
FZ/002RF
SKID
HYDROGEN VENT
AIR VENT
PROCESS TANK VENT
Earthing
I/O interface
LAN
cooling water fill connection
Cooling Water drain connection
N2 purge
NOTE:
TEMPERATURE SENSOR
H2/007TT ARE SKIN POINT TYPE
AMBIENT SENSORS AND ALLARMS
P&I Implanto di terra
rev B60

Annex C: test rig site layout

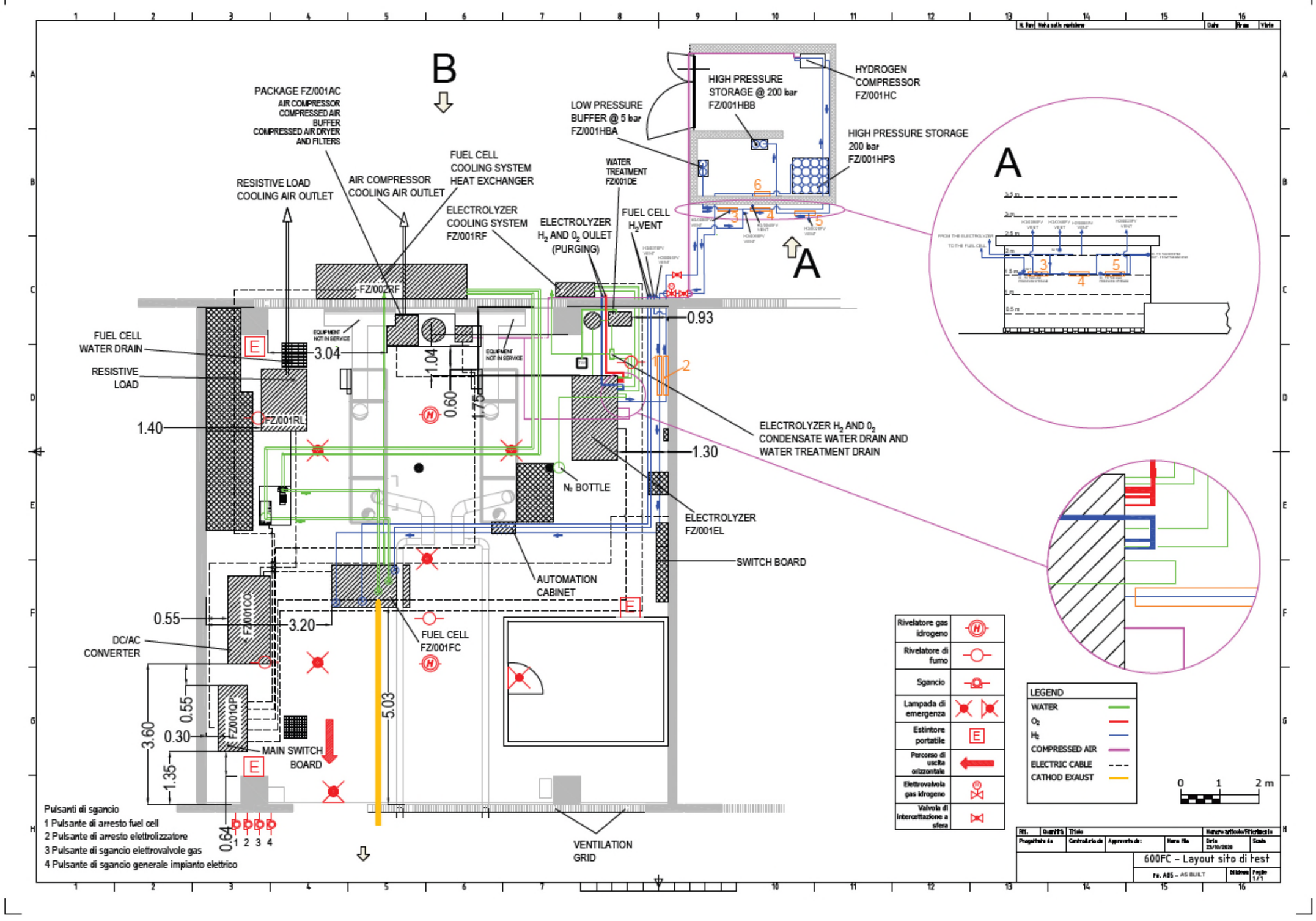
B
A
PACKAGE FZ/001AC
AIR COMPRESSOR
COMPRESSED AIR BUFFER
COMPRESSED AIR DRYER AND FILTERS
RESISTIVE LOAD COOLING AIR OUTLET
AIR COMPRESSOR COOLING AIR OUTLET
FUEL CELL COOLING SYSTEM HEAT EXCHANGER
ELECTROLYZER COOLING SYSTEM FZ/001RF
ELECTROLYZER H2 AND 02 OULET (PURGING)
WATER TREATMENT FZ/001DE
FUEL CELL H2 VENT
LOW PRESSURE BUFFER @ 5 bar FZ/001HBA
HIGH PRESSURE STORAGE @ 200 bar FZ/001HBB
HYDROGEN COMPRESSOR FZ/001HC
HIGH PRESSURE STORAGE 200 bar FZ/001HPS
FZ/002RF
FUEL CELL WATER DRAIN
RESISTIVE LOAD
FZ/001RL
ELECTROLYZER H2 AND 02 CONDENSATE WATER DRAIN AND WATER TREATMENT DRAIN
N2 BOTTLE
ELECTROLYZER FZ/001EL
SWITCH BOARD
AUTOMATION CABINET
FUEL CELL FZ/001FC
DC/AC CONVERTER
FZ/001CO
FZ/001QP
MAIN SWITCH BOARD
VENTILATION GRID
0.93
3.04
1.04
0.60
1.75
1.40
1.30
0.55
3.20
5.03
0.55
0.30
3.60
1.35
0.64
Pulsanti di sgancio
1 Pulsante di arresto fuel cell
2 Pulsante di arresto elettrolizzatore
3 Pulsante di sgancio elettrovalvole gas
4 Pulsante di sgancio generale impianto elettrico
Rivelatore gas idrogeno
Rivelatore di fumo
Sgancio
Lampada di emergenza
Estintore portatile
Percorso di uscita orizzontale
Elettrovalvola gas idrogeno
Valvola di intercettazione a sfera
LEGEND
WATER
O2
H2
COMPRESSED AIR
ELECTRIC CABLE
CATHOD EXAUST
0 1 2 m
600FC – Layout sito di test
Fz. ABS – AS BUILT

A

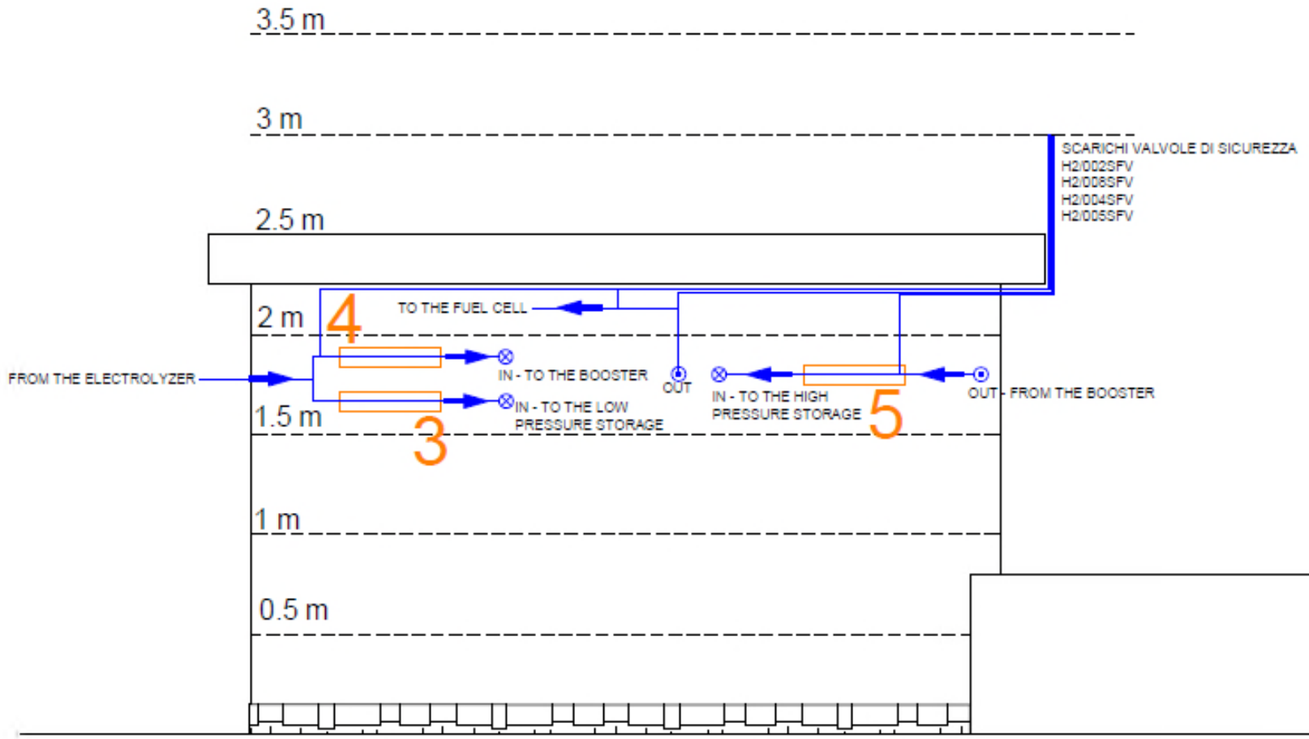

Particolare A

B

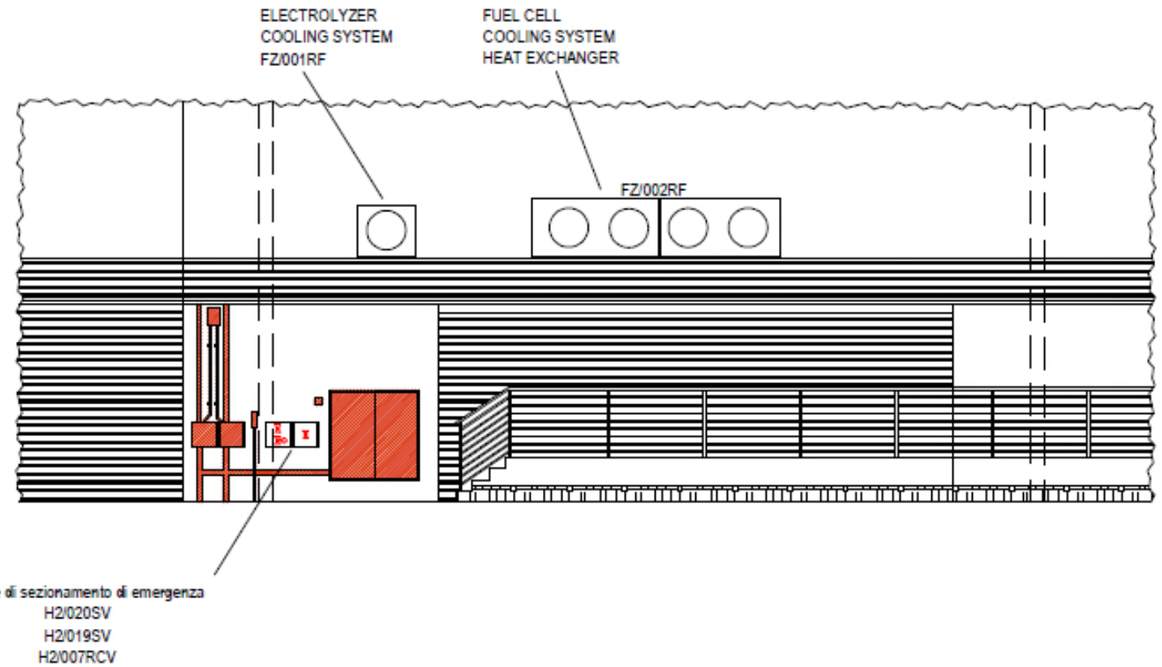

Particolare A

Annex D: test rig automation functional diagram

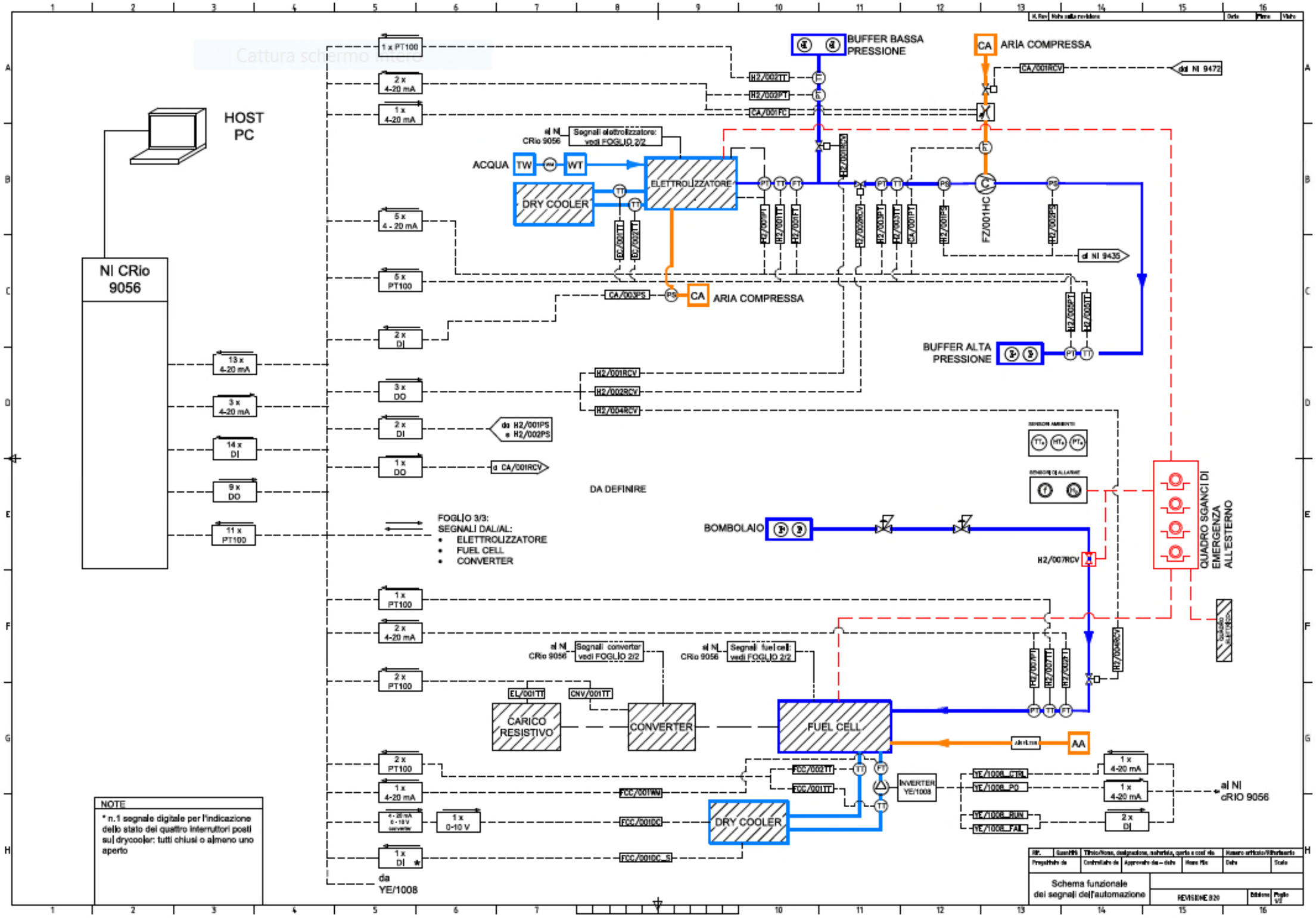
HOST PC
NI CRio 9056
1 x PT100
2 x 4-20 mA
1 x 4-20 mA
5 x 4 - 20 mA
5 x PT100
2 x DI
13 x 4-20 mA
3 x 4-20 mA
14 x DI
9 x DO
11 x PT100
3 x DO
2 x DI
1 x DO
da H2/001IPS e H2/002PS
da CA/001RCV
DA DEFINIRE
FOGLIO 3/3:
SEGNALI DAL/AL:
• ELETTROLIZZATORE
• FUEL CELL
• CONVERTER
1 x PT100
2 x 4-20 mA
2 x PT100
2 x PT100
1 x 4-20 mA
1 x 0-10 V
1 x DI ★
da YE/1008
al NI CRio 9056
Segnali elettrolizzatore: vedi FOGLIO 2/2
Segnali converter vedi FOGLIO 2/2
Segnali fuel cell: vedi FOGLIO 2/2
ACQUA
TW
WT
DRY COOLER
ELETTROLIZZATORE
BUFFER BASSA PRESSIONE
BUFFER ALTA PRESSIONE
CA ARIA COMPRESSA
CA/001RCV
da NI 9472
H2/002TT
H2/002PT
CA/001FC
H2/002RCV
H2/001PT
H2/001TT
H2/001FT
H2/001RCV
H2/003PT
H2/003TT
CA/001PT
H2/001PS
FZ/001HC
H2/003PS
al NI 9435
CA/003PS
H2/004PT
H2/004TT
H2/002RCV
H2/004RCV
BOMBOLAIO
H2/007RCV
QUADRO SGANCI DI EMERGENZA ALL'ESTERNO
EL/001TT
CNV/001TT
CARICO RESISTIVO
CONVERTER
FUEL CELL
AA
FCC/002TT
FCC/001TT
FCC/001WI
FCC/001DC
FCC/001DC_S
INVERTER YE/1008
YE/1008_CTRL
YE/1008_PO
YE/1008_RUN
YE/1008_FAIL
1 x 4-20 mA
1 x 4-20 mA
2 x DI
al NI cRIO 9056
NOTE
* n.1 segnale digitale per l'indicazione dello stato dei quattro interruttori posti su| drycooler: tutti chiusi o almeno uno aperto
Schema funzionale dei segnali dell'automazione
REVISIONE 820

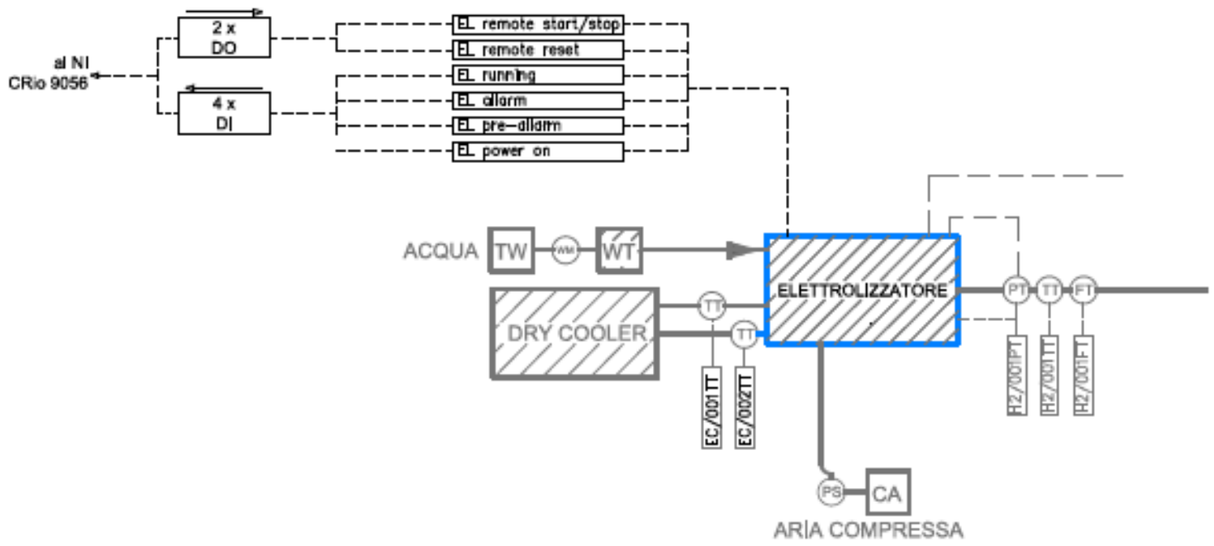
al NI
CRio 9056
2 x
DO
4 x
DI
EL remote start/stop
EL remote reset
EL running
EL allarm
EL pre-allarm
EL power on
ACQUA
TW
WM
WT
DRY COOLER
TT
TT
ELETTROLIZZATORE
PT
TT
FT
EC/001TT
EC/002TT
HZ/001IPT
HZ/001TT
HZ/001FT
PS
CA
ARIA COMPRESSA

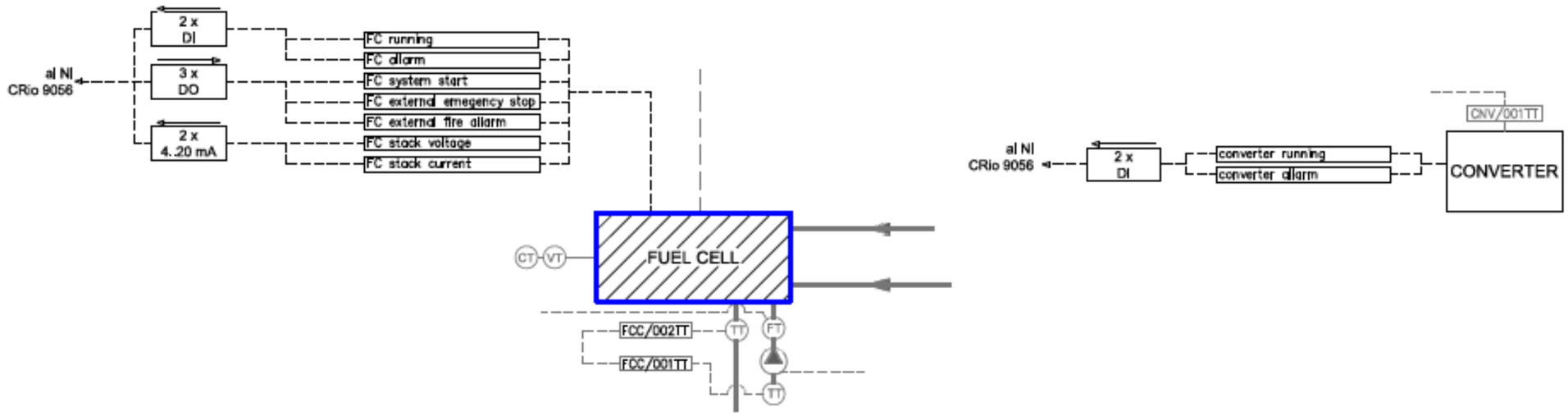
al NI
CRio 9056
2 x
DI
3 x
DO
2 x
4..20 mA
FC running
FC allarm
FC system start
FC external emegency stop
FC external fire allarm
FC stack voltage
FC stack current
CT
VT
FUEL CELL
FCC/002TT
FCC/001TT
TT
FT
TT
al NI
CRio 9056
2 x
DI
converter running
converter allarm
CNV/001TT
CONVERTER
Schema funzionale
dei segnali dell'automazione
REVISIONE 820